International linear collider reference design report — **Source link**

G. Aarons

Related papers:

- Design of a High Luminosity 100 TeV Proton Antiproton Collider

- CLIC, a 0.5-TeV to 5-TeV e+- compact linear collider

- Status of the SLC

- Luminosity upgrade of CLIC-LHC ep/γp collider

- High energy muon colliders

INTERNATIONAL LINEAR COLLIDER

REFERENCE DESIGN REPORT

2007

APRIL, 2007

LIST OF CONTRIBUTORS

Gerald Aarons[60], David Adey[68], Chris Adolphsen[60], Ilya Agapov[58], Jung-Keun Ahn[56], Mitsuo Akemoto[24], Maria del Carmen Alabau[37], Michael Albrecht[79], David Alesini[38], Jim Alexander[15], Wade Allison[81], John Amann[60], Shozo Anami[24], Terry Anderson[21], Michael Anerella[3], Deepa Angal-Kalinin[12,6], Sergie Antipov[2], Claire Antoine[8,21], Rob Appleby[12,76], Sakae Araki[24], Tug Arkan[21], Ned Arnold[2], Ray Arnold[60], Xavier Artru[28], Alexander Aryshev[24], Fred Asiri[60], David B. Augustine[21], Derek Baars[45], Nigel Baddams[11], Ian R. Bailey[12,75], N. I. Balalykin[35], Jean-Luc Baldy[11], Maurice Ball[21], Philip Bambade[37], Syuichi Ban[24], Karl Bane[60], Bakul Banerjee[21], Serena Barbanotti[27], Desmond P. Barber[18,12,75], D. Yu. Bardin[35], Barry Barish[5,22], Roger Barlow[12,76], Maura Barone[21,22], Yuri Batygin[60], D. Elwyn Baynham[7], Carl Beard[12,6], Leo Bellantoni[21], Paul Bellomo[60], Lynn D. Bentson[60], Martin Berndt[60], Simona Bettoni[38], Vinod Bharadwaj[60], Marica Biagini[38], Wilhelm Bialowons[18], Thomas Bieler[45], John Bierwagen[45], Alison Birch[12,6], Victoria Blackmore[81], Grahame Blair[58], Christian Boffo[21], Courtlandt Bohn[50], V. I. Boiko[35], Eduard N. Bondarchuk[16], Roberto Boni[38], Stewart Boogert[58], Gary Boorman[58], Alessio Bosco[58], Pierre Bosland[8], Angelo Bosotti[27], Gordon Bowden[60], Gary Bower[60], Axel Brachman[60], Tom W. Bradshaw[7], Hans Peter Brasser[1], James Brau[80], Steve Bricker[45], Craig Brooksby[41], Timothy A. Broome[7], James H. Brownell[17], Mélanie Bruchon[8], Heiner Brueck[18], Amanda J. Brummitt[7], Yu. A. Budagov[35], Karsten Buesser[18], Eugene Bulyak[48], Adriana Bungau[12,76], Craig Burkhart[60], Philip Burrows[81], Graeme Burt[12], David Burton[12,39], Yunhai Cai[60], Ofelia Capatina[11], Ruben Carcagno[21], F. Stephen Carr[7], Harry F. Carter[21], John Carter[58], John Carwardine[2], Richard Cassel[60], Giorgio Cavallari[8], Brian Chase[21], Robert Chehab[37], Stéphane Chel[8], Chiping Chen[44], Jian Cheng[31], M. Chevallier[28], William Chickering[70], Jin-hyuk Choi[53], Glenn Christian[81], Mike Church[21], Gianluigi Ciovati[62], Christine Clarke[81], Don G. Clarke[6], James A. Clarke[12,6], Elizabeth Clements[21,22], Paul Coe[81], John Cogan[60], Chris Compton[45], Ed Cook[41], Peter Cooke[12,75], Laura Corner[81], Clay Corvin[60], Curtis Crawford[15], James A. Crittenden[15], Hamid Dabiri Khah[81], Olivier Dadoun[37], Chris Damerell[7], Michael Danilov[32], Ken P. Davies[6], Antonio de Lira[60], Stefano De Santis[40], Laurence Deacon[58], Jean-Pierre Delahaye[11], Nicholas Delerue[81], Olivier Delferriere[8], Yu. N. Denisov[35], Christopher J. Densham[7], Guillaume Devanz[8], Amos Dexter[12], Sudhir Dixit[81], Ralph Dollan[26], George Doucas[81], Robert Downing[57], Eric Doyle[60], Alessandro Drago[38], Alex Dragt[77], Alexandr Drozhdin[21], Gerald Dugan[15], Viktor Duginov[35], Helen Edwards[21], Heiko Ehrichmann[18], Michael Ehrlichman[78], Peder Eliasson[11], George Ellwood[12,6], Eckhard Elsen[18], Louis Emery[2], Kazuhiro Enami[24], Kuninori Endo[24], Atsushi Enomoto[24], Fabien Eozénou[8], Roger Erickson[60], Karen Fant[60], Alberto Fasso[60], John Fehlberg[54], John Ferguson[11], J. Luis Fernandez-Hernando[12,6], Ted Fieguth[60], Mike D. Fitton[7], Mike Foley[21], Richard Ford[21], Brian Foster[81], Horst Friedsam[2], Josef Frisch[60], Masafumi Fukuda[24], Shigeki Fukuda[24], Yoshisato Funahashi[24], Warren Funk[62], Kazuro Furukawa[24], Fumio Furuta[24], Karsten Gadow[18], Wei Gai[2], Fred Gannaway[81], Jie Gao[31], Peter Garbincius[21], Luis Garcia-Tabares[10], Terry Garvey[37], Edward Garwin[60], Martin Gastal[11], Lixin Ge[60], Zheqiao Geng[31], Lawrence Gibbons[15], Allan Gillespie[72], Peter Gladkikh[48],

George D. Gollin[74], Erik Gottschalk[21], Philippe Goudket[12,6], Filimon Gournaris[66], Justin Greenhalgh[12,6], Terry Grimm[45], Jeff Gronberg[41], Susanna Guiducci[38], Andy Haase[60], Lars Hagge[18], Larry Hammond[21], Louis Hand[15], Kazufumi Hara[24], Anthony Hartin[81], Walter Hartung[45], Carsten Hast[60], Claude Hauviller[11], Hitoshi Hayano[24], Samuel Heifets[60], Richard Helms[15], Norio Higashi[24], Yasuo Higashi[24], Toshiyasu Higo[24], Michael D. Hildreth[79], Thomas Himel[60], Koichiro Hirano[34], Tachishige Hirose[84], Hiromi Hisamatsu[24], Chit Thu Hlaing[70], Yousuke Honda[24], Hiroyuki Honma[24], Kenji Hosoyama[24], David Howell[81], Maxine Hronek[21,22], Jung-Yun Huang[53], Emil Huedem[21], Peter Huggard[7], Youngseok Hwang[9], Hitoshi Inoue[24], Youichi Inoue[63], Katerina Ioakeimidi[60], V. V. Ivanov[35], Valentin Ivanov[21], Yury Ivanyushenkov[7], Yoshihisa Iwashita[30], Frank Jackson[12,6], Steven Jamison[12,6], Ron Jedziniak[21], Leo J. Jenner[12,75], Chris Jensen[21], David R. Jensen[60], Hairong Jiang[45], R. Keith Jobe[60], Matt Johnson[45], Michael Johnston[81], Paul Joireman[21], James Jones[12,6], Roger Jones[12,76], Erik Jongewaard[60], Jin-Young Jung[40], Eiji Kako[24], Alexander Kalinin[12,6], Takuya Kamitani[24], Yoshio Kamiya[84], Yukihide Kamiya[24], Ken-ichi Kanazawa[24], Heung-sik Kang[53], Pavel Karataev[58], Vladimir Kashikhin[21], Shigeru Kashiwagi[52], Paul Kasley[21], Hiroaki Katagiri[24], Takashi Kato[49], Sergei Kazakov[24], V. D. Kekelidze[35], Lewis Keller[60], Kurt Kennedy[40], Robert Kephart[21], Oleg Khainovski[70], Mitsuo Kikuchi[24], Eun San Kim[9], Guinyun Kim[9], Hongjoo Kim[9], Hyoungsuk Kim[9], Hyun-Chui Kim[56], Jonghoon Kim[60], Kwang-Je Kim[2], Seunghwan Kim[53], Maurice Kimmitt[73], Robert Kirby[60], François Kircher[8], Arkadiy L. Klebaner[21], Peter Kneisel[62], In Soo Ko[53], Kwok Ko[60], Nobuko Kobayashi[24], Yuuji Kojima[24], Yury G. Kolomensky[70], Sachio Komamiya[33], Shane Koscielniak[65], Sergey Kostromin[35], Anatoly Krasnykh[60], Dirk Kruecker[18], Nicholas A. Krumpa[6], Kiyoshi Kubo[24], Vic Kuchler[21], Noboru Kudoh[24], Masayuki Kumada[47], Tatsuya Kume[24], German Kurevlev[12,76], Yoshimasa Kurihara[24], Masao Kuriki[24], Shigeru Kuroda[24], Sharon Lackey[21], Thomas W. Lackowski[21], Briant Lam[60], David Larbalestier[83], Ray Larsen[60], Andrea Latina[11], Lisa Laurent[60], Paul Lebrun[21], Jerry Leibfritz[21], Frank Lenkszus[2], Jim Lewandowski[60], Greg Leyh[60], S. Li[31], Xiaoping Li[31], Zenghai Li[60], Lutz Lilje[18], Andrew J. Lintern[7], Sheng-Guang Liu[24], Wanming Liu[2], Weibin Liu[31], Pavel V. Logatchev[4], Thomas Lohse[26], Peter Loveridge[7], Tracy Lundin[23], Michel Luong[8], Alexey Lyapin[66], Lili Ma[12,6], Allan MacLeod[67], David MacNair[60], Bino Maiheu[66], Stephen Malton[66], Oleg B. Malyshev[12,6], Larisa I. Malysheva[12,75], John Mammosser[62], Fabio Marcellini[38], Tom Markiewicz[60], Steve Marks[40], Andrew Marone[3], Felix Marti[45], Takashi Maruyama[60], Mika Masuzawa[24], Hiroshi Matsumoto[24], Shuji Matsumoto[24], Toshihiro Matsumoto[24], Thomas Mattison[69], Patricia McBride[21], Douglas McCormick[60], Kirk T. McDonald[55], Mike McGee[21], Peter McIntosh[12,6], Bobby McKee[60], Mandi Meidlinger[45], Bob Meller[15], Adam Mercer[12,76], I. N. Meshkov[35], Paolo Michelato[27], Shinichiro Michizono[24], Daniel Mihalcea[50], Takanori Mihara[36], Alexander A. Mikhailichenko[15], Catia Milardi[38], David J. Miller[66], Roger J. Miller[60], Toshihiro Mimashi[24], Shekhar Mishra[21], Chad Mitchell[77], Takako Miura[24], Klaus Moenig[18], Ken Moffeit[60], Nikolai Mokhov[21], Stephen Molloy[60], Laura Monaco[27], Paul R. Monasterio[70], Gudrid A. Moortgat-Pick[12,20], Yoshiyuki Morita[24], Youhei Morita[24], Yuichi Morita[33], Nikolai Morozov[35], Yuichi Morozumi[24], Sekazi Mtingwa[44], Alex Mueller[28], Wolfgang Mueller[29], Morrison Munro[60], Toshiya Muto[64], Ganapati Rao Myneni[62], Segei Nagaitsev[21], Takashi Naito[24], Hirotaka Nakai[24], Hiromitsu Nakajima[24], Tomoya Nakamura[82], Tsutomu Nakanishi[46], Katsumi Nakao[24], Noriaki Nakao[21], Sang Nam[53], Yoshihito Namito[24], Chris Nantista[60], Olivier Napoly[8],

Janice Nelson[60], Michael Neubauer[60], Myriam Newman[81], Oleg Nezhevenko[21],
Cho-Kuen Ng[60], Mihn Nguyen[60], Jim Niehoff[21], Tomohiro Nishitani[34], Shuichi Noguchi[24],
John Noonan[2], Yuri Nosochkov[60], Mitsuaki Nozaki[24], Joseph O'Dell[12,6], Kazuhito Ohmi[24],
Yukiyoshi Ohnishi[24], Satoshi Ohsawa[24], Norihito Ohuchi[24], Katsunobu Oide[24],
Takahiro Okamura[24], Toshiyuki Okugi[24], Shoji Okumi[46], Jeff Olsen[60], A. G. Olshevsky[35],
Tsunehiko Omori[24], Will Oren[62], Toyoko J. Orimoto[70], Masahiro Oroku[82],
Francois Ostiguy[21], Brian Ottewell[81], Hasan Padamsee[15], Carlo Pagani[27],
Mark A. Palmer[15], Nicola Panzeri[27], Rocco Paparella[27], Brett Parker[3], Vittorio Parma[11],
Ralph Pasquinelli[21], Ewan Paterson[60], Jim Patrick[21], Ritchie Patterson[15],
Vince Pavlicek[21], Jacques Payet[8], John Pedersen[11], Guoxi Pei[31], Gregory Penn[40],
Colin Perry[81], Franz Peters [60], Thomas Peterson[21], Howard Pfeffer[21], Phil Pfund[21],
Jonathan Phillips[72], Nan Phinney[60], Paolo Pierini[27], W. Thomas Piggott[41],
Phillippe Piot[50], Mauro Pivi[60], Dave Plate[40], Michael Poehler[11], Matthew Poelker[62],
Igor Pogorelsky[3], Freddy Poirier[18], Ronald Poling[78], John Popielarski[45], Miro Preger[38],
Richard Prepost[83], Michael Price[58], Dieter Proch[18], Jean-Pierre Quesnel[11],
Pantaleo Raimondi[38], Kirti Ranjan[21], Alessandro Ratti[40], Tor Raubenheimer[60],
Bill Rease[43], Charles E. Reece[62], Kay Rehlich[18], Ina Reichel[40], Armin Reichold[81],
John Reid[21], Ron Reid[12,6], François Richard[37], Sabine Riemann[19], Louis Rinolfi[11],
James H. Rochford[7], Ponciano Rodriguez[60], Martin Roeben[41], Marc Ross[21], Allan Rowe[21],
Perrine Royole-Degieux[37,22], David Rubin[15], Ingo Ruehl[11], Robert Ruland[60],
Brian Rusnak[41], Sun-Young Ryu[56], Gian Luca Sabbi[40], Takayuki Saeki[24], David Sagan[15],
Kenji Saito[24], Kiwamu Saito[24], Shogo Sakanaka[24], Kazuyuki Sakaue[84], Zen Salata[60],
Toshiya Sanami[24], John Santic[21], Tomoyuki Sanuki[33], Noboru Sasao[36], Kotaro Satoh[24],
Claude Saunders[2], Laura Saxton[45], Andreas Schälicke[19], Sebastien Schaetzel[18],
Glenn Scheitrum[60], Markus Schlösser[18], Ross D. Schlueter[40], Peter Schmid[19],
Heinz-Juergen Schreiber[18], K. Peter Schuler[18], Daniel Schulte[11], Duncan J. Scott[12,6],
David Seidman[51], Sergei Seletskiy[60], Rohan Senanayake[81], Daniele Sertore[27],
Andrei Seryi[60], Nicholas Shales[12,39], G. A. Shelkov[35], John C. Sheppard[60], Ci Tu Shi[31],
Tetsuo Shidara[24], Yeo-Jeong Shim[56], Hirotaka Shimizu[25], Seunghwan Shin[9],
Grigori Shirkov[35], Toshio Shishido[24], Claire Simon[8], Stefan Simrock[18], Nikolai Sinev[80],
A. N. Sissakian[35], N. B. Skachkov[35], Alexander Skrinsky[4], Mark Slater[71], A. Smith[78],
Brian J. Smith[7], Jeff Smith[15], Jonathan Smith[12,39], Steve Smith[60], Tonee Smith[60],
W. Neville Snodgrass[6], Young-uk Sohn[53], Nikolai Solyak[21], Dongchul Son[9],
Andre Sopczak[12,39], V. Soskov[42], Cherrill M. Spencer[60], Panagiotis Spentzouris[21],
Daryl Sprehn[60], Steve St. Lorant[60], Richard P. Stanek[21], Werner Stein[41], Matt Sternberg[80],
Mark Stockton[68], John Strachan[6], V. Strakhovenko[4], Sergei I. Striganov[21],
Gennady Stupakov[60], Taikan Suehara[82], Yusuke Suetsugu[24], Ryuhei Sugahara[24],
Yipeng Sun[31], Peter Sutcliffe[12,75], Tsuyoshi Suwada[24], Chihiro Suzuki[46], Richard Swent[60],
Christina Swinson[81], E. M. Syresin[35], Tohru Takahashi[25], Mikio Takano[59],
Fumihiko Takasaki[24], Seishi Takeda[24], Tateru Takenaka[24], Masami Tanaka[24],
Takashi Taniguchi[24], Sami Tantawi[60], Michael A. Tartaglia[21], Toshiaki Tauchi[24],
Laurent Tavian[11], Hiroko Tawara[24], Peter Tenenbaum[60], Akio Terashima[24],
Nobuhiro Terunuma[24], Jay Theilacker[21], Mark Thomson[71], Jeff Tice[60], Maury Tigner[15],
Nobu Toge[24], N. A. Tokareva[35], John Tompkins[21], Dragan Toprek[12,76], Fernando Toral[10],
Eric Torrence[80], G. V. Trubnikov[35], Kiyosumi Tsuchiya[24], Akira Tsunumi[61],
Robin Tucker[12,39], Kenji Ueno[24], Kensei Umemori[24], Junji Urakawa[24], Jeremy Urban[15],
Didier Uriot[8], David Urner[81], Andrei Ushakov[19], Linda Valerio[21], Alex Valishev[21],

Gary Van Zandbergen[21], Alessandro Variola[37], Marco Venturini[40], Bernard Visentin[8], Michele Viti[18], S. B. Vorozhtsov[35], Margaret Votava[21], Masayoshi Wake[24], Roman Walczak[81], Nicholas J. Walker[18], Sean Walston[41], Dieter Walz[60], Faya Wang[60], Haitao Wang[2], Jiuqing Wang[31], Juwen Wang[60], Lanfa Wang[60], Rainer Wanzenberg[18], David Ward[71], Barbara Warmbein[18,22], David W. Warner[13], Masakazu Washio[84], Ken Watanabe[24], Yuichi Watanabe[24], Nigel Watson[68], Harry Weerts[2], Thomas Weiland[29], Hans Weise[18], John Weisend[60], Manfred Wendt[21], Steve Wesseln[21], Glen R. White[60], William Willis[14], Matthew Wing[66], Brian D. Wirth[70], Stephen A. Wolbers[21], Dan Wolff[21], Andrzej Wolski[12,75], Mark D. Woodley[60], Michael Woods[60], Michael L. Woodward[7], Guoxing Xia[18], Aimin Xiao[2], Liling Xiao[60], Vitaly Yakimenko[3], Hitoshi Yamamoto[64], Masahiro Yamamoto[46], Naoto Yamamoto[46], Yasuchika Yamamoto[24], Takashi Yamanaka[82], Hiroshi Yamaoka[24], Satoru Yamashita[33], Yoshiharu Yano[24], Hakutaro Yoda[82], Kaoru Yokoya[24], Hirokazu Yokoyama[36], Richard C. York[45], Mitsuhiro Yoshida[24], Andrew Young[60], Igor Zagorodnov[18], Jijiu Zhao[31], Feng Zhou[60], Frank Zimmermann[11], Michael S. Zisman[40], Fabian Zomer[37].

[1] *Amberg Engineering AG, Trockenloostr. 21, P.O.Box 27, 8105 Regensdorf-Watt, Switzerland*

[2] *Argonne National Laboratory, 9700 S. Cass Avenue, Argonne, IL 60439, USA*

[3] *Brookhaven National Laboratory, P.O.Box 5000, Upton, NY 11973-5000, USA*

[4] *Budkar Institute for Nuclear Physics, 630090 Novosibirsk, Russia*

[5] *California Institute of Technology, 1200 East California Blvd, Pasadena, CA 91125, USA*

[6] *CCLRC Daresbury Laboratory, Daresbury, Warrington, Cheshire WA4 4AD, UK*

[7] *CCLRC Rutherford Appleton Laboratory, Chilton, Didcot, Oxton OX11 0QX, UK*

[8] *CEA Saclay, DAPNIA, F-91191 Gif-sur-Yvette, France*

[9] *Center for High Energy Physics (CHEP) / Kyungpook National University, 1370 Sankyuk-dong, Buk-gu, Daegu 702-701, Korea*

[10] *Centro de Investigaciones Energéticas, Medioambientales y Technológicas, CIEMAT, Avenia Complutense 22, E-28040 Madrid, Spain*

[11] *CERN, CH-1211 Genève 23, Switzerland*

[12] *Cockcroft Institute, Daresbury, Warrington WA4 4AD, UK*

[13] *Colorado State University, Fort Collins, CO 80523, USA*

[14] *Columbia University in the City of New York, 2960 Broadway, New York, NY 10027-6902, USA*

[15] *Cornell University, Ithaca, NY 14853, USA*

[16] *D.V. Efremov Research Institute, 'SINTEZ', 196641 St. Petersburg, Russia*

[17] *Dartmouth College, Hanover, NH 03755, USA*

[18] *DESY Hamburg, Deutsches Elektronen-Synchrotoron in der Helmholtz-Gemeinschaft, Notkestrasse 85, 22607 Hamburg, Germany*

[19] *DESY Zeuthen, Deutsches Elektronen-Synchrotoron in der Helmholtz-Gemeinschaft, Platanenallee 6, D-15738 Zeuthen, Germany*

[20] *Durham University, South Rd., Durham DH1 3LE, UK*

[21] *Fermi National Accelerator Laboratory, FNAL, P.O.Box 500, Batavia, IL 60510-0500, USA*

[22] *Global Design Effort*

[23] *Hanson Engineering*

[24] *High Energy Accelerator Research Organization, KEK, 1-1 Oho, Tsukuba, Ibaraki 305-0801, Japan*

[25] *Hiroshima University, 1-3-1 Kagamiyama, Higashi-Hiroshima 739-8526, Japan*

[26] *Humboldt-Universität zu Berlin, Unter den Linden 6, 10099 Berlin, Germany*

[27] *INFN Milano, LASA, Via Fratelli Cervi 201, 20090 Segrate, Italy*

[28] *Institut de Physique Nucléaire, F-91406 Orsay, France*

[29] *Institut für Theorie Elektromagnetischer Felder (TEMF), Technische Universität Darmstadt, Schloßgartenstr. 8, D-64289 Darmstadt, Germany*

[30] *Institute for Chemical Research, Kyoto University, Gokasho, Uji, Kyoto 611-0011, Japan*

[31] *Institute for High Energy Physics, IHEP, P.O.Box 918, Beijing 100039, China*

[32] *Institute of Theoretical and Experimetal Physics, B. Cheremushkinskawa, 25, RU-117259, Moscow, Russia*

[33] *International Center for Elementary Particle Physics, University of Tokyo, Hongo 7-3-1, Bunkyo Dist., Tokyo 113-0033, Japan*

[34] *Japan Atomic Energy Agency, 4-49 Muramatsu, Tokai-mura, Naka-gun, Ibaraki 319-1184, Japan*

[35] *Joint Institute for Nuclear Research, Joliot-Curie 6, Moscow Region, RU-141980 Dubna, Russia*

[36] *Kyoto University, Kitashirakawa-Oiwakecho, Sakyo-ku, Kyoto 606-8502, Japan*

[37] *Laboratoire de l'Accélérateur Linéaire, Université Paris-Sud 11, Bâtiment 200, 91898 Orsay, France*

[38] *Laboratori Nazionali di Frascati, INFN, Via E. Fermi, 40 Frascati, Italy*

[39] *Lancaster University, Lancaster LA1 4YB, UK*

[40] *Lawrence Berkeley National Laboratory, 1 Cyclotron Rd, Berkeley, CA 94720, USA*

[41] *Lawrence Livermore National Laboratory, Livermore, CA 94551, USA*

[42] *Lebedev Physical Institute, Leninsky Prospect 53, RU-117924 Moscow, Russia*

[43] *Los Alamos National Laboratory, P.O.Box 1663, Los Alamos, NM 87545, USA*

[44] *Massachusetts Instite of Technology, 77 Massachusetts Ave., NW16, Cambridge, MA 02139, USA*

[45] *Michigan State University, East Lansing, MI 48824, USA*

[46] *Nagoya University, Furo-cho, Chikusa-ku, Nagoya, Aichi 464-8602, Japan*

[47] *National Institute of Radiological Sciences, 4-9-1 Anagawa, Inaga, Chiba 263-8555, Japan*

[48] *National Science Center Kharkov Institute of Physics and Technology, 1, Akademicheskaya St., Kharkov, 61108, Ukraine*

[49] *Nikken Sekkai Ltd., 2-18-3 Iidabashi, Chiyoda Dist., Tokyo 102-8117, Japan*

[50] *Northern Illinois University, DeKalb, Illinois 60115-2825, USA*

[51] *Northwestern University, 633 Clark St., Evanston, IL 60208, USA*

[52] *Osaka University, 1-1 Machikaneyama, Toyonaka, Osaka 560-0043, Japan*

[53] *Pohang Accelerator Laboratory (POSTECH), San-31 Hyoja-dong, Nam-gu, Pohang, Gyeongbuk, 790-784, Korea*

[54] *PRIMERA*

[55] *Princeton University, Princeton, NJ 08542-0708, USA*

[56] *Pusan National University, Busan, 609-735 Korea*

[57] *R. W. Downing, Inc.*

[58] *Royal Holloway, University of London, Egham, Surrey TW20 0EX, UK*

[59] *Saube Ltd., Tsukuba, Ibaraki, Japan*

[60] *Stanford Linear Accelerator Center, SLAC, 2575 Sand Hill Road, Menlo Park, CA 94025, USA*

[61] *Sumitomo Heavy Industries Ltd*

[62] *Thomas Jefferson National Accelerator Facility, 12000 Jefferson Avenue, Newport News, VA 23606, USA*

[63] *Tohoku Gakuin University, 1-13-1 Chuo, Tagajo, Miyagi 985-8537, Japan*

[64] *Tohoku University, Aoba Dist., Sendai, Miyagi 980-8578, Japan*

[65] *TRIUMF, 4004 Wesbrook Mall, Vancouver, BC V6T 2A3, Canada*

[66] *University College of London, Gower Street, London WC1E 6BT, UK*

[67] *University of Abertay Dundee, Bell St, Dundee, DD1 1HG,*

[68] *University of Birmingham, Edgbaston, Birmingham B15 2TT, UK*

[69] *University of British Columbia, 6224 Agricultural Rd., Vancouver, BC V6T 1Z1, Canada*

[70] *University of California, Berkeley, Berkeley, CA 94720, USA*

[71] *University of Cambridge, Cavendish Laboratory, J J Thomson Avenue, Cambridge CB3 0HE, UK*

[72] *University of Dundee, Nethergate, Dundee, DD1 4HN, Scotland, UK*

[73] *University of Essex, Wivenhoe Park, Colchester CO4 3SQ, UK*

[74] *University of Illinois at Urbana-Champaign, 1110 W. Green St., Urbana, IL 61801-3080, USA*

[75] *University of Liverpool, Liverpool L69 7ZE, UK*

[76] *University of Manchester, Manchester M13 9PL, UK*

[77] *University of Maryland, College Park, MD 20742, USA*

[78] *University of Minnesota, 148 Tate Lab. Of Physics, 116 Church St. S.E., Minneapolis, MN 55455, USA*

[79] *University of Notre Dame, Notre Dame, IN 46556, USA*

[80] *University of Oregon, Eugene, OR 97403, USA*

[81] *University of Oxford, Wellington Square, Oxford OX1 2JD, UK*

[82] *University of Tokyo, 7-3-1 Hongo, Bunkyo Dist., Tokyo 113-0033, Japan*

[83] *University of Wisconsin, Madison, WI 53706-1390, USA*

[84] *Waseda University, Advanced Research Institute for Science and Engineering, Shinjuku, Tokyo 169-8555, Japan*

CONTENTS

CONTENTS

CONTENTS

LIST of FIGURES

LIST OF FIGURES

LIST of TABLES

CHAPTER 1

RDR Process

1.1 INTRODUCTION

In August 2004, the International Technology Recommendation Panel (ITRP) recommended [1] that the International Linear Collider (ILC) should be based on superconducting RF accelerating technology. The recommendation was subsequently endorsed by the International Committee for Future Accelerators (ICFA). Shortly thereafter, the international Linear Collider community began the task of developing a single design for the superconducting ILC, as a truly global project. The first steps in this challenging effort were taken at the First International Linear Collider Workshop, held in KEK, Tsukuba, Japan in November, 2004.

Approximately six-months after the first workshop, the Global Design Effort (GDE) was formally created at the Second International Linear Collider Workshop, held in parallel with the Americas Linear Collider Physics Group (ALCPG) workshop at Snowmass, Colorado, in July 2005. The 2nd workshop built on the foundations laid at the KEK meeting, and was paramount in making many basic fundamental design choices for the ILC, including among others the choice of operating accelerating gradient. These decisions were then iterated over the next months, resulting in the ILC Baseline Configuration Document (BCD), which was officially accepted and adopted at the first GDE meeting held at INFN, Frascati, Italy in December 2005. An equally important component of the BCD is a catalogue of important *alternative* design options, which, although considered currently too immature for the Baseline cost estimate, may eventually prove beneficial in either cost and/or performance.

At the same meeting at INFN, the process of organising the global effort to produce the detailed ILC Reference Design and associated cost estimate began. The GDE structure (Figure 1.1-1) consisted of the following entities:

- An Executive Committee (EC), chaired by the GDE Director, who were responsible for all major decisions and overall GDE management. The committee membership included the three Regional GDE Directors and the three Accelerator Leads (one from each region).
- Three Cost Engineers, one from each region, who were responsible for coordinating the cost effort, defining and maintaining the Work Breakdown Structure (WBS) and its associated dictionary, and ultimately assembling and reviewing the cost estimate.
- A Design and Cost Board (DCB), charged with defining the costing methodology and reviewing the progress of the ILC design and costs. The board membership was made up of the three Cost Engineers and additional GDE members.

- A Change Control Board (CCB), responsible for implementing Change Control for the BCD as the design developed. Membership was drawn from the GDE.
- A Global R&D Board (RDB), charged with defining, monitoring and reviewing the global ILC R&D programmes. The board was chaired by the GDE R&D Coordinator with members drawn from the GDE.
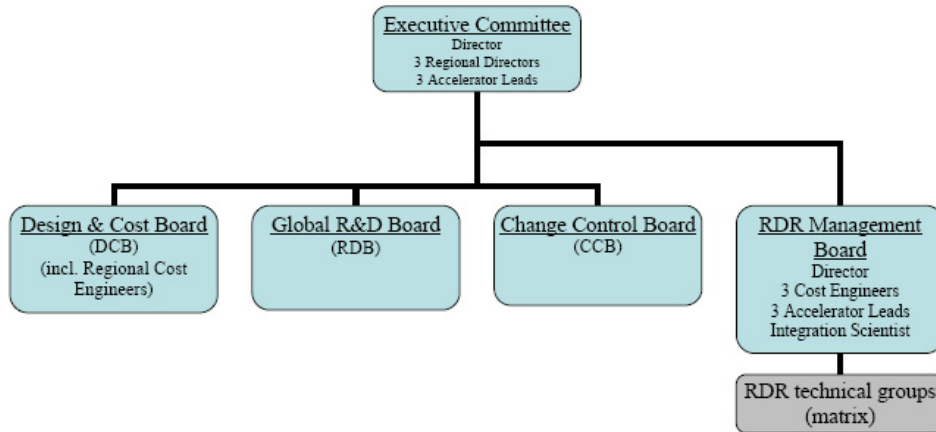
FIGURE 1.1-1. GDE structure for producing the ILC Reference Design and Cost.

1.2 TECHNICAL DESIGN AND COSTING

The actual technical work of producing the conceptual design and associated cost estimate was implemented using the matrix approach shown in Figure 1.2-2.

FIGURE 1.2-2. Organizational structure for the Reference Design technical design and costing.

The design of the machine was geographically broken down into the Area Systems (represented in Figure 1.2-2 as the columns of the matrix). At least two coordinators were assigned to each Area System from different regions. Critical systems such as the Main Linac, Damping Rings and Beam Delivery System were assigned coordinators from all three regions. In all cases, a lead contact coordinator was identified.

The Area Systems coordinators were given the following responsibilities:

- produce the detailed design and requirements for the layout and components of their sub-systems;

- coordinate cost- and performance- driven design modifications, and submit the associated formal Change Requests to the Change Control Board;
- roll-up and maintain the cost estimates for their specific Area System, and supply that information to the Cost Engineers.

While it was the job of the Area Systems to define the scope and technical requirements for their respective systems, the Technical and Global systems (represented by the rows in Figure 1.2-2) were primarily responsible for component design and producing the unit cost estimates:

- **Technical Systems** are generally associated with specific accelerator components found in nearly all the Area Systems: Magnets (conventional and superconducting), Power Supplies and Supports; Vacuum systems, including insulating vacuum for the cryogenic systems as well as beamline UHV; Instrumentation, including beam position, profile, length and loss monitoring; dumps and collimators were responsible for low- and high-powered beam dumps, and numerous collimator systems throughout the machine; RF power sources supplied klystrons, modulators and waveguide distribution systems design and cost estimates (dominated by the Main Linac RF unit); Cryomodule and Cavity Package are special cases, both being focused on the Main Linac superconducting RF. However, these systems were also responsible for warm RF sections in the source capture sections, as well as the superconducting RF for the Damping Rings.
- **Global Systems**, as the name suggests, represent more global aspects of the machine design which are not directly related to specific areas. Of these, Civil Construction and Siting (CFS) is by far the largest system (cost driver). Others include cryogenics, controls, availability and operations (which includes Machine Protection) and installation.

Each Technical/Global system was assigned a coordinator from each region (considered important for maintaining cost input information from all regions). Points of contact between Technical/Global and Area systems were identified to enable exchange of information between the two. The responsibilities for the Technical/Global Systems coordinators were to:

- Obtain and consolidate lists of components and their requirements from the Area System Coordinators;
- produce cost estimates of the components/systems, using a suitably justifiable method (e.g. comparison to existing machines, bottoms-up approximate designs, in-house estimate or direct industrial quotes);
- iterate design considerations, where either the technical feasibility of the requirements is not practical, or an alternative, more cost effective solution may exist;
- supply the cost information to the relevant Area Systems, and ultimately to the Cost Engineers for review.

Overall day-to-day coordination of the design and costing process was provided by the **RDR Management Board** (RDR MB), comprised of the GDE Director, the Cost Engineers and Accelerator Leads, and an overall Integration Scientist responsible for global layout and integration issues. The RDR MB had primary responsibility for the technical activities (e.g. schedules and milestones, organizing review meetings, monitoring progress across the RDR technical groups), and reported directly to the GDE Executive Committee.

1.3   CHANGE CONTROL

The important concept of Change Control was implemented early in the history of the ILC design effort, as a mechanism of maintaining a history of the baseline design, as well as reviewing the cost/performance trade-off of any proposed modification. Change Control was formally implemented via the GDE Change Control Board (CCB), whose regionally-balanced membership was taken from accelerator expertise within the GDE.

The CCB designated the following levels of Change Control Request depending on the estimated cost impact:

- Class 0: minor modifications (mostly to documentation) with no cost impact.
- Class 1: modifications to the Baseline Configuration with a net expected impact on cost of <100 M$.
- Class 2: modifications to the Baseline Configuration with a net expected impact of cost of >100 M$.

Differing formal review procedures have been implemented depending on the class (severity) of the change request. Class 0 and Class 1 modifications can be formally accepted and implemented by the CCB, while major (Class 2) requests are ultimately decided by the GDE Director and the Executive Committee based on recommendations from the CCB.

The CCB also played an important role in facilitating interactions to the World Wide Study (WWS) and the physics and detector groups, who were actively encouraged to participate in the Change Request review process, especially when that request was of relevance to the physics goals or the detector.

1.4   CRITICAL MILESTONES AND SCHEDULE FOR THE RDR

The detailed design work and cost estimation began shortly after the Baseline Configuration was agreed upon at the Frascati GDE meeting (November 2005). The effort that followed can be loosely split into two half-year periods:

- **Frascati GDE Meeting (Dec. 2005) – Vancouver GDE Meeting (July 2006)** Consolidation of the detailed Baseline Design; production of component specifications and requirements for Technical/Global Systems; Area/Technical/Global Systems preparation of a first estimate of total project cost for review at the Vancouver meeting.
- **Vancouver GDE Meeting (July 2006) - Valencia GDE Meeting (Nov. 2006)** Cost-driven iteration of Baseline Design (Area Systems) and technical component costs. Re-evaluation of (bottoms-up) cost estimate of the final RDR design. This phase saw a re-evaluation of the Frascati Baseline Design, resulting in several significant cost-driven machine layout modifications.

Figure 1.4-3 shows a more detailed schedule, identifying the critical interim milestones in the process.

1.5   GLOBAL ORGANIZATION ISSUES

Although the RDR design and cost estimate for the ILC is in itself a significant challenge, the global nature of the project has raised additional challenges and complications, which

FIGURE 1.4-3. Milestones in producing the Reference Design Report, including costs.

in many ways equal the technical issues and design decisions for the machine itself. The geographically distributed groups have had to learn to remotely work together; the lack of a "geographically centralized group" has required additional formality and discipline to the way the work has been organized.

While examples of international projects do exist, the GDE has been learning during the RDR process how best to organize itself. Significant use has been made of teleconferencing facilities and web-based conferencing tools (e.g. WebEx) where possible. Several "global" teleconferences including all three regions (and therefore all time-zones) were scheduled each week, especially for the various GDE and RDR Management boards. Area, Technical and Global Systems organized themselves, again primarily using remote conferencing facilities. A primary communication tool was the Web and email, without which the RDR would not have been possible. Use of a centralized wiki site for all technical information (on http://www.linearcollider.org/wiki/) also greatly facilitated the distribution of key information between the RDR groups.

CHAPTER 2

Accelerator Description

2.1 BEAM PARAMETERS

The International Linear Collider (ILC) is designed to achieve the specifications listed in the ILCSC Parameter Subcommittee Report [5]. The three most important requirements are: (1) an initial center-of-mass (cms) energy up to 500 GeV with the ability to upgrade to 1 TeV, (2) an integrated luminosity in the first four years of 500 fb^{-1} at 500 GeV cms or equivalent at lower energies, and (3) the ability to scan in energy between 200 and 500 GeV cms.

The ILC Reference Design Report describes a collider that is designed to meet these requirements. The installed RF system is capable of accelerating beams for collisions at 500 GeV cms. The peak luminosity of $2 \times 10^{34} \, \mathrm{cm}^{-2}\mathrm{s}^{-1}$ at 500 GeV and a collider availability of 75% should enable the delivery of 500 fb^{-1} in the first four years of physics operation assuming an annual physics run of 9 months. The energy flexibility has been a consideration throughout the design and essential items to facilitate a future upgrade to 1 TeV, such as the length of the beam delivery system and the power rating of the main beam dumps, have been incorporated.

2.1.1 Collider and Beam Parameters

The ILC is based on 1.3 GHz superconducting RF cavities operating at a gradient of 31.5 MV/m. The collider operates at a repetition rate of 5 Hz with a beam pulse length of roughly 1 msec. The site length is 31 km for a cms energy of 500 GeV; the site would have to be extended to reach 1 TeV. The beams are prepared in low energy damping rings that operate at 5 GeV and are 6.7 km in circumference. They are then accelerated in the main linacs which are ~11 km per side. Finally, they are focused down to very small spot sizes at the collision point with a beam delivery system that is ~2.2 km per side. To attain a peak luminosity of $2 \times 10^{34} \, \mathrm{cm}^{-2}\mathrm{s}^{-1}$, the collider requires ~230 MW of electrical power. A summary of the overall collider parameters appears in Table 2.1-1.

The beam parameters to reach a peak luminosity of $2 \times 10^{34} \, \mathrm{cm}^{-2}\mathrm{s}^{-1}$ are listed in Table 2.1-2. The table lists a set of nominal parameters and three other sets that define a 'parameter plane'. The collider has been designed to the nominal parameter set which was optimized considering aspects of the whole accelerator system such as: the beam instabilities and kicker hardware in the damping rings, the beam current and the pulse length in the linacs, and the kink instability and background in the final focus system. The parameter plane establishes

TABLE 2.1-1

Global Accelerator Parameters for 500 GeV cms.

Parameter	Value	Units
Center-of-mass energy	500	GeV
Peak luminosity	2×10^{34}	cm^{-2}s^{-1}
Availability	75	%
Repetition rate	5	Hz
Duty cycle	0.5	%
Main Linacs		
Average accelerating gradient in cavities	31.5	MV/m
Length of each Main Linac	11	km
Beam pulse length	1	ms
Average beam current in pulse	9.0	mA
Damping Rings		
Beam energy	5	GeV
Circumference	6.7	km
Length of Beam Delivery section (2 beams)	4.5	km
Total site length	31	km
Total site power consumption	230	MW
Total installed power	~300	MW

a range of operating parameters that represent slightly different tradeoffs between these considerations. Experience with past accelerators indicates that there will be operational difficulties, which will be eased by modifying the beam parameters. The parameter plane provides flexibility to cope with such problems without sacrificing performance. It can also be useful during collider commissioning and when tuning the luminosity characteristics for different measurements and particle physics detectors.

2.1.2 The Nominal Parameter Set

The main linac RF system is designed to accelerate beam at a gradient of 31.5 MV/m. The nominal beam current is 9.0 mA and the beam pulse length is 970 μs so that the RF pulse length (including the fill time of the cavities) is 1.56 ms. The optimal single bunch charge is a balance between effects at the IP and in the damping ring; the choice of 2×10^{10} is similar to that specified in the TESLA TDR [2] and the US Technical Options Study [3].

The normalized vertical emittance at the IP is chosen to be 4×10^{-8} m·rad. This corresponds to a geometric emittance of ~ 2 pm from the damping rings (5 GeV) and assumes 100% emittance growth during the transport to the IP. This damping ring emittance is slighty lower than what has already been achieved but is thought to be well within the present technology. The 100% emittance growth estimate is based on calculations made during the ILC Technical Review Report [4].

TABLE 2.1-2
Beam and IP Parameters for 500 GeV cms

Parameter	Symbol/Units	Nominal	Low N	Large Y	Low P
Repetition rate	f_{rep} (Hz)	5	5	5	5
Number of particles per bunch	N (10^{10})	2	1	2	2
Number of bunches per pulse	n_b	2625	5120	2625	1320
Bunch interval in the Main Linac	t_b (ns)	369.2	189.2	369.2	480.0
in units of RF buckets		480	246	480	624
Average current in the Main Linac	I_{ave} (mA)	9.0	9.0	9.0	6.8
Normalized emittance at IP	$\gamma\epsilon_x^*$ (mm·rad)	10	10	10	10
Normalized emittance at IP	$\gamma\epsilon_y^*$ (mm·rad)	0.04	0.03	0.08	0.036
Beta function at IP	β_x^* (mm)	20	11	11	11
Beta function at IP	β_y^* (mm)	0.4	0.2	0.6	0.2
R.m.s. beam size at IP	σ_x^* (nm)	639	474	474	474
R.m.s. beam size at IP	σ_y^* (nm)	5.7	3.5	9.9	3.8
R.m.s. bunch length	σ_z (μm)	300	200	500	200
Disruption parameter	D_x	0.17	0.11	0.52	0.21
Disruption parameter	D_y	19.4	14.6	24.9	26.1
Beamstrahlung parameter	Υ_{ave}	0.048	0.050	0.038	0.097
Energy loss by beamstrahlung	δ_{BS}	0.024	0.017	0.027	0.055
Number of beamstrahlung photons	n_γ	1.32	0.91	1.77	1.72
Luminosity enhancement factor	H_D	1.71	1.48	2.18	1.64
Geometric luminosity	$\mathcal{L}_{geo}$ 10^{34}/cm^2/s	1.20	1.35	0.94	1.21
Luminosity	$\mathcal{L}$ 10^{34}/cm^2/s	2	2	2	2

2.1.3 Parameter Plane

The parameter sets labeled 'Low N' (low number of particles per bunch), 'Large Y' (large vertical emittance) and 'Low P' (low beam power) in Table 2.1-2 are representative points in the parameter plane. These parameter sets deliver essentially the same luminosity $2 \times 10^{34}\,\mathrm{cm}^{-2}\mathrm{s}^{-1}$ at 500 GeV but with different values for the specific beam parameters. The collider subsystems have been designed such that any point in the parameter plane is attainable. At present, it is not believed that there is a large cost impact of maintaining the parameter plane and there is a significant gain in operational flexibility; this will need to be examined again during the next phase of design optimization.

Low N

The bunch population of 2×10^{10} may lead to problems such as microwave instabilities in the damping rings, single bunch wakefield emittance dilutions, or a large disruption parameter at the IP which can cause a kink instability and may make the IP feedback difficult. In such cases, it could be desirable to reduce the bunch population.

The Low N parameter set addressed these possible difficulties with a reduced single bunch

charge and reduced bunch length. Halving the bunch population with fixed current (twice the number of bunches and half the bunch interval) reduces the luminosity but this is compensated by focusing more tightly at the IP. These parameters also have lower beamstrahlung and possibly lower backgrounds in the particle physics detectors at the IP which may be desirable for some measurements. All these changes are beneficial, however, the Low N parameter set is more demanding in terms of the damping ring kicker, the bunch compressor, and the multi-bunch collective effects in the damping rings.

Large Y

The vertical emittance at the IP of 4×10^{-8} m·rad may not be achieved due to tuning difficulties in the damping rings and beam delivery system or wakefield effects in the linac. The Large Y parameters assume a vertical emittance that is twice the design and the luminosity is recovered by focusing more tightly in the horizontal at the IP and using a longer bunch to reduce the increased beamstrahlung. Unfortunately, the disruption parameter at the interaction point is increased and kink instability may be more pronounced.

Low P

Another condition that may arise are limitations due to the beam current or beam power. These may arise in the injector systems, damping rings, main linacs or beam delivery system. In this case, the collider could be optimized in the direction of the Low P parameters where the beam current is reduced by 30% and the beam power is reduced by a factor of two. Again, the luminosity is recovered with increased focusing at the IP in the horizontal plane. In this case, the beamstrahlung cannot be reduced by increasing the bunch length because of the tight focusing in the vertical plane. This results in a beamstrahlung that is roughly double that in the nominal parameters and this may limit the performance of the particle physics detector and the beam delivery extraction line.

2.1.4   Range of Parameters

The parameter plane described above defines a range of parameters as shown in Table 2.1-3. Note, however, the parameters, when they are varied, are correlated. For example, the shortest bunch length is required only when the bunch population is low.

TABLE 2.1-3
Range of parameters

Parameter	Symbol	min		nominal		max	Units
Bunch population	N	1	-	2	-	2	$\times 10^{10}$
Number of bunches	n_b	1320	-	2625	-	5120	
Linac bunch interval	t_b	189	-	369	-	480	ns
Bunch length	σ_z	200	-	300	-	500	μm
Vertical emittance	$\gamma\epsilon_y^*$	0.03	-	0.04	-	0.08	mm·mrad
Beta function at IP	β_x^*	11	-	20	-	20	mm
	β_y^*	0.2	-	0.4	-	0.4	mm

2.1.5   Bunch Spacing and Path Length Considerations

In order to extract the bunches in the damping ring one by one and inject into the main linac there are certain constraints to satisfy among the DR circumference, number of bunches, RF frequencies and bunch distances in the DR and main linac. The present beam parameters do not meet all of the constraints needed to best facilitate injection and extraction from the damping rings [6]. The parameters will continue to be optimized during the next design phase to better satisfy the constraints, and it is expected that the damping ring circumference and linac bunch spacing will change by small amounts.

In addition, there is another another constraint due to the fact that the positrons are generated by electrons on the previous pulse. For flexible operation, it is highly desireable that the sum of certain beamline lengths such as the main linac and the transport lines be a multiple of the DR circumference. Because of this constraint, the exact location of the injector complex and the layout of the transport lines is a subject that can be fixed only after the final component lengths and the site are decided.

2.2 ELECTRON SOURCE

2.2.1 Overview

The ILC polarized electron source must produce the required train of polarized electron bunches and transport them to the Damping Ring. The nominal train is 2625 bunches of 2.0×10^{10} electrons at 5 Hz with polarization greater than 80%. The beam is produced by a laser illuminating a photocathode in a DC gun. Two independent laser and gun systems provide redundancy. Normal-conducting structures are used for bunching and pre-acceleration to 76 MeV, after which the beam is accelerated to 5 GeV in a superconducting linac. Before injection into the damping ring, superconducting solenoids rotate the spin vector into the vertical, and a separate superconducting RF structure is used for energy compression. A third polarized electron source (500 MeV) drives the Positron Keep Alive Source (KAS). Polarization is not required in the baseline, but will be required for either the e^--e^- or γ-γ options.

The SLC polarized electron source already meets the requirements for polarization, charge and lifetime. The primary challenge for the ILC source is the long bunch train, which demands a laser system beyond that used at any existing accelerator, and normal conducting structures which can handle high RF power. Both R&D developments are considered manageable.

2.2.2 Beam Parameters

The key beam parameters for the electron source are listed in Table 2.2-1.

TABLE 2.2-1
Electron Source System Parameters

Parameter	Symbol	Value	Units
Electrons per bunch (at gun exit)	n_e	3×10^{10}	Number
Electrons per bunch (at DR injection)	n_e	2×10^{10}	Number
Number of bunches	N_e	2670	Number
Bunch repetition rate	$F_{\mu b}$	3	MHz
Bunch train repetition rate	F_{mb}	5	Hz
Bunch length at source	Δt	1	ns
Peak current in bunch at source	I_{avg}	3.2	A
Energy stability	S	<5	% rms
Polarization	P_e	80 (min)	%
Photocathode Quantum Efficiency	QE	0.5	%
Drive laser wavelength	Λ	790±20 (tunable)	nm
Single bunch laser energy	E	5	μJ

2.2.3   System Description

Figure 2.2-1 depicts schematically the layout of the polarized electron source. Two independent laser systems are located in a surface building. The light is transported down an evacuated light pipe to the DC guns. The beam from either gun is deflected on line by a magnet system which includes a spectrometer, and it then passes through the normal-conducting subharmonic bunchers, traveling wave bunchers and pre-accelerating sections. This is followed by the 5 GeV superconducting linac. The Linac-to-Ring transfer line that brings the beam to the damping rings contains the spin rotators and energy compression.
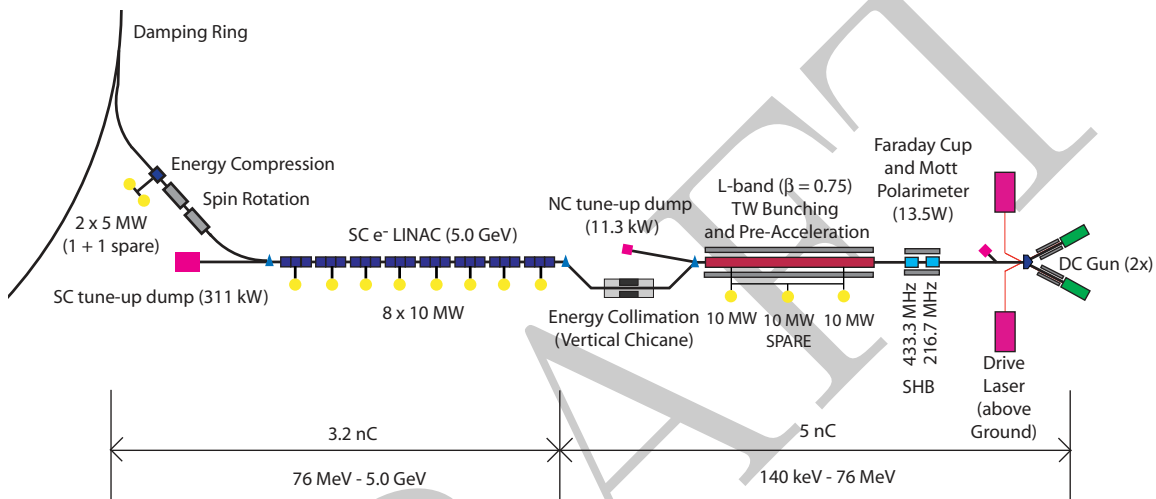
FIGURE 2.2-1. Schematic View of the Polarized Electron Source

2.2.3.1   Photocathodes for Polarized Beams

Photocathode materials have been the subject of intense R&D efforts for more than 15 years. The most promising candidates for the ILC polarized electron source are strained GaAs/GaAsP superlattice structures (see Figure 2.2-2). GaAs/GaAsP superlattice photocathodes routinely yield at least 85% polarization with a maximum QE of 1% (routinely 0.3 to 0.5%) [7, 8]. The present cathodes consist of very thin quantum well layers (GaAs) alternating with lattice-mismatched barrier layers (GaAsP). Each layer of the superlattice (typically 4 nm) is considerably thinner than the critical thickness ($\sim$10 nm) for the onset of strain relaxation, while the transport efficiency for elec relaxation, while the transport efficiency for electrons in the conduction band still can be high. The structures are p-doped using a high-gradient doping technique, consisting of a thin (10 nm), very highly doped (5×10^{19} cm^{-3}) surface layer with a lower density doping (5×10^{17} cm^{-3}) in the remaining active layer(s). A high surface doping density is necessary to achieve high QE while reducing the surface-charge-limit problem. A lower doping density is used to maximize the polarization. With bunch spacing of $\sim$300 ns, the surface-charge-limit problem for the ILC is not expected to be a major issue. The optimum doping level remains to be determined. An alternative under study is the InAlGaAs/GaAs strained superlattice with minimum conduction band offset where a peak polarization of 91% has been observed [9]. Research continues on various cleaning and surface preparation techniques. Atomic hydrogen cleaning (AHC) is a

well-known technique for removing oxides and carbon-related contaminants at relatively low temperatures [10] and will be further explored in the near future.
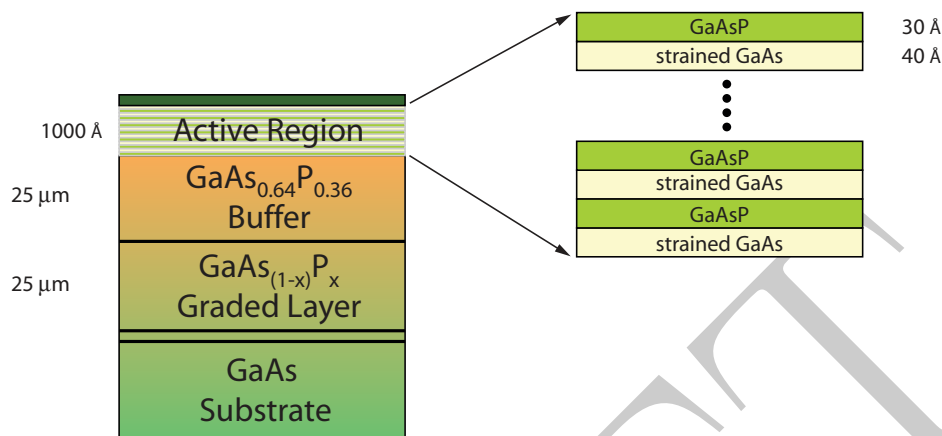
FIGURE 2.2-2. Structure of a Strained GaAs/GaAsP Superlattice Photocathode for Polarized Electrons

2.2.3.2 Polarized Electron Gun

The ILC polarized electron gun is a DC gun based on the design of the gun used for the SLC [11]. However, DC gun technology for polarized sources has evolved considerably, [12] and technological advances will be incorporated into the ILC gun design. The ILC gun will be optimized for a space charge limited peak current of 4.5-5 A (4.5-5 nC/1ns). This provides overhead to compensate for losses that occur primarily through the bunching system. The gun power supply provides a cathode bias of -140 to -160 kV. An ultrahigh vacuum system with a total pressure $\leq 10^{-12}$ Torr (excluding H_2) is required to maintain the negative electron affinity (NEA) of the cathode. An SF_6/dry air gas system is used to maintain a high dielectric gun environment to avoid HV breakdown between ground and HV components. During HV operation the electric field on the cathode surface must be kept below 7 MeV/m to ensure low dark current ($<$ 25 nC). Excessive dark current will lead to field emission resulting in molecular desorption from nearby surfaces. This process leads to deterioration of the gun vacuum and is destructive to the cathode's NEA surface.

The gun area will be equipped with a Mott polarimeter to measure polarization and a Faraday cup to measure the charge. Several Residual Gas Analyzers (RGAs) characterize the vacuum near the gun. Other special diagnostics for the DC gun include means to measure the quantum efficiency of the cathode (a cw diode laser integrated into the gun) and a nano-ammeter for dark current monitoring.

An NEA cathode requires periodic cesiation. Cesiator channels are located near the cathode to allow in situ cesiation of the photocathode. An improvement of the current SLC gun design will be to locate the cesiation channels behind a retractable photocathode. This will eliminate the deposition of Cesium on electrode surfaces, thereby reducing the dark current of the gun. The SLC and subsequent polarized beam experiments at SLAC have demonstrated the operation of an efficient and highly automated cesiation system with minimal source downtime. The gun will have an integrated cathode preparation chamber and load-lock system. The activation chamber will be semi-permanently attached to the gun and both volumes will be semi-permanently maintained under high vacuum. The preparation

chamber will allow the option of local cathode cleaning and activation as well as storage of spare cathodes. Cathodes may be rapidly exchanged between the gun and preparation chamber. The load-lock consists of a small rapidly-pumped vacuum chamber for transferring cathodes from an external atmospheric source into or out of the preparation chamber without affecting the latter's vacuum.

The dominant source of intensity variations and timing jitter is the laser system. A secondary source for intensity variations is the gun power supply and beam dynamics influenced by space charge forces within the gun and the low energy sections of the injector.

2.2.3.3 ILC Source Laser System

A conceptual layout schematic of the laser system is depicted in Figure 2.2-3. To match the bandgap energy of GaAs photocathodes, the wavelength of the laser system must be 790 nm and provide tunability (±20 nm) to optimize conditions for a specific photocathode. Therefore, the laser system is based on Ti:sapphire technology.
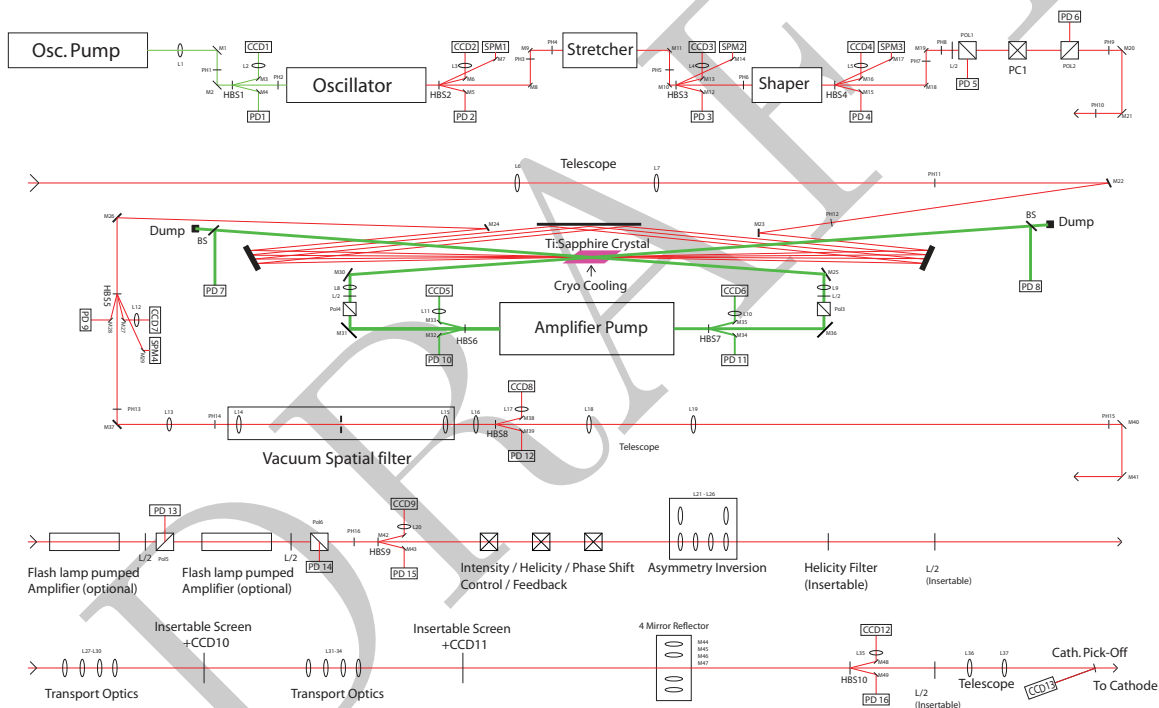
FIGURE 2.2-3. Schematic View of Source Drive Laser System

The 3 MHz pulse train is generated by a cavity-dumped mode-locked oscillator. After diffractive pulse stretching to 1 ns and temporal pulse shaping, the bunch train is amplified using a multi-pass Ti:sapphire amplifier. The amplifier crystal must be cryogenically cooled to facilitate power dissipation and minimize instabilities caused by thermal lensing induced by the high power amplifier pump. A cw frequency-doubled Nd:YAG (or similar such as Nd:vanadate) diode pumped solid state (DPSS) laser provides the pump power for the Ti:sapphire amplifier. Additional amplification can be supplied by one or multiple flash-lamp pumped Ti:sapphire stages. Final laser pulse energy and helicity control is achieved by electro-optical techniques. This system can also be used as a feed-back device to compensate for the QE decay of the photocathode between cesiations, to remove slow intensity drifts of

laser and/or electron beam, and to maintain the circular polarization state of the laser beam. Various optical techniques are used to cancel systematic effects caused by an asymmetric laser beam profile or effects associated with the sign of the helicity of the laser light.

2.2.3.4 Bunching and Pre-Acceleration

The bunching system compresses the 1 ns micro-bunches generated by the gun down to ∼20 ps FWHM. It includes two subharmonic bunchers (SHBs) and a 5 cell traveling wave β=0.75 L-band buncher. The SHB cavities operate at 216.7 MHz and 433.3 MHz, respectively. Together they compress the bunch to ∼200 ps FWHM. The L-band bunching system is a modification of the TESLA Test Facility [13] design with a traveling wave buncher to maximize capture efficiency. The buncher has 5 cells with β=0.75 and a gradient of 5.5 MV/m and compresses the bunch to 20 ps FWHM. The buncher and the first few cells of the following TW pre-accelerator are immersed in a 660 G solenoidal field to focus the beam. Two 50 cell β=1 normal conducting (NC) TW accelerating sections at a gradient of 8.5 MV/m increase the beam energy to 76 MeV. These structures must withstand very high RF power for the duration of the very long pulse but they are identical to those being developed for the positron source. Further details of the bunching system are summarized in reference [14].

2.2.3.5 Chicane, Emittance Measurement and Matching Sections

Immediately downstream of the NC pre-acceleration a vertical chicane provides energy collimation before injection into the SC booster linac. The chicane consists of four bending magnets and several 90° FODO cells. The initial dipole at the chicane entrance can be used as a spectrometer magnet (see Figure 2.2-1). A short beam line leads to a diagnostic section that includes a spectrometer screen. The injector beam emittance is measured by conventional wire scanners downstream of the chicane. Two matching sections combine the chicane and emittance measurement station with the downstream SC booster linac.

2.2.3.6 The 5 GeV Superconducting Pre-Acceleration (Booster) Linac

Twenty-one standard ILC-type SC cryomodules accelerate the beam to 5 GeV,and typical FODO cells integrated into the cryomodules transversely focus the beam. An additional string of three cryomodules is added to provide redundancy (total of 24 cryomodules). The booster linac consists of two sections. In the first section, the e$^-$ beam is accelerated from 76 MeV to 1.7 GeV in cryomodules with one quadrupole per module. In the second section, the e$^-$ beam is accelerated to the final 5 GeV in cryomodules with one quadrupole every other module.

2.2.3.7 Linac to Damping Ring Beamline and Main e$^-$ Source Beam Dump

The Linac To Ring (LTR) beam line transports the beam to the damping ring injection point and performs spin rotation and energy compression. The 5 GeV longitudinally polarized electron beam is first bent through an arc. At 5 GeV, the spin component in the plane normal to the magnetic field precesses 90° in that plane for every n × 7.9° (n: odd integer) of rotation of momentum vector. An axial solenoid field integral of 26.2 T-m rotates the spin direction into the vertical [15]. A 5 GeV beam dump is installed near the LTR. To dump the 5 GeV beam, the first bend of the LTR is turned off, and the dump bend downstream energized. The dump drift is ∼12 m.

2.2.4   Accelerator Physics

Simulations indicate that >95% of the electrons produced by the DC gun are captured within the 6-D damping ring acceptance: $\gamma(A_x+A_y) \leq$ 0.09 m and ΔE x $\Delta z \leq (\pm 25$ MeV) x $(\pm 3.46$ cm). The starting beam size diameter at the gun is 2 cm, and this is focused to a few mm diameter before it is injected into the DR. Calculations in the low energy regions of the injector ($\leq$76 MeV) include space charge effects and use PARMELA [16]. The beam propagation through the superconducting booster linac and LTR beam line has been optimized using MAD [17] and tracked by the ELEGANT code [18].
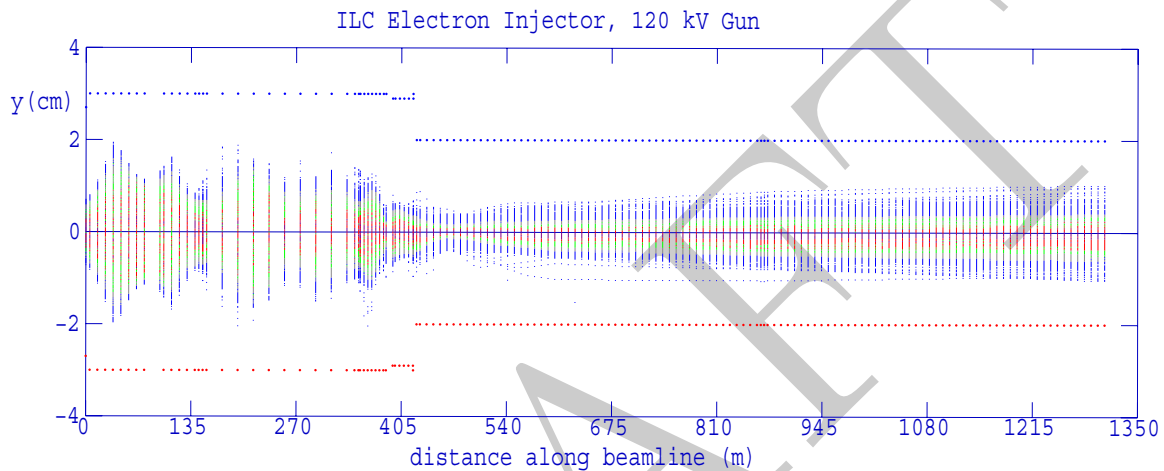
FIGURE 2.2-4. Beam Envelope along the 76 MeV Injector

2.2.4.1   DC Gun and Bunchers

The DC gun creates a 140-160 keV electron beam with a bunch charge of 4.5-5 nC with a bunch length of 1 ns and an unnormalized transverse edge emittance at the gun exit of 70 mm-mrad. To minimize longitudinal growth of the bunch it is desirable to locate the first subharmonic buncher as close to the gun as possible. However, the beam lines needed to combine both guns require a distance of $\sim$1-1.5 m between gun and first SHB. The SHBs capture almost 100% of the electrons generated at the gun. The beam parameters at 76 MeV are summarized in Table 2.2-2. A plot of the beam envelope from gun up through the bunching system is given in Figure 2.2-4.

TABLE 2.2-2
76 MeV Beam Parameters for the NC Bunching and Pre-Accelerating Electron Source

Parameters	$\beta = 0.75$ TW Buncher Design
Initial charge	4.5 - 5 nC
Transmitted charge	92%
Phase extension FWHM	9 deg L-band
Energy spread FWHM	<100 keV
Normalized rms emittance	70 μm-rad

2.2.4.2   The 5 GeV Booster Linac and Linac to Damping Ring Line (eLTR)

The optics of the superconducting booster linac are shown in Figure 2.2-5.
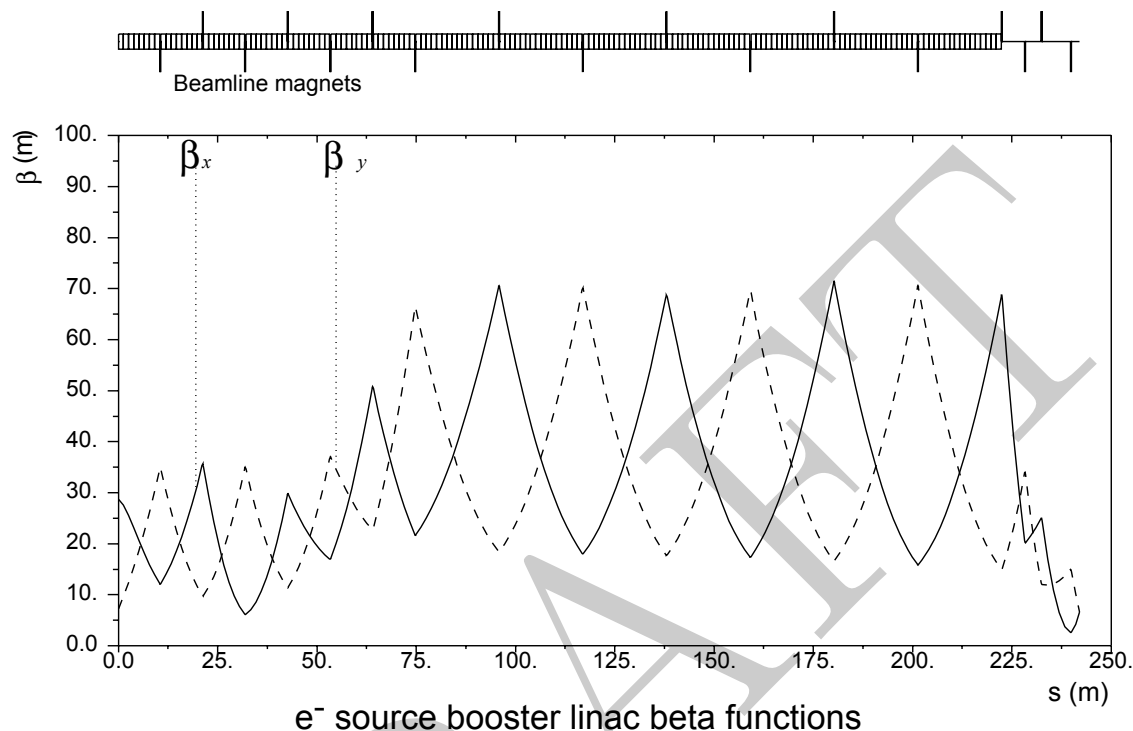
FIGURE 2.2-5. Optics of the SC Electron Booster Linac

At the dump window, the e-edge beam size σ_x/σ_y is 0.72 cm/1.4 cm and 13.9 cm/1.4 cm for 0% and ±10% energy spread, respectively. These beam sizes are within the dump window specifications. At the monitor location the dispersion dominates the beam size and thus the dump also serves as an energy spectrometer with 0.1% resolution.

The LTR arc consists of four FODO cells with eight bends. The total arc bending angle is $7 \times 7.9°$. The R_{56} (path length energy correlation) is adjustable (86 ±40 cm). The arc is followed by the solenoid sections and RF unit, which occupy 5.5 m and 8.32 m, respectively. There are three PPS stoppers with 1 m space in the LTR arc. Two FODO cells upstream of the LTR arc have laser wire emittance measurement stations. The optics of the LTR system are shown in Figure 2.2-6.

The arc of the eLTR is designed to rotate the spin vector by 90 degrees from longitudinal into a horizontal position before injection into the damping ring and to provide the R56 necessary for energy compression. For a n × 90° of spin rotation, an arc angle of n × 7.9° is required. A 8.3-m-long superconducting solenoid with 3.16 T magnetic field solenoid rotates the spin vector into a vertical orientation. After the bunch is decompressed by the arc, an RF voltage of 180 MV provided by a 9-m-long 6-cavity superconducting linac, rotates the electrons in longitudinal phase space to match with longitudinal DR acceptance. The LTR also includes an additional 34.5° horizontal bend, a matching section with 4 quadrupoles and a double bend achromat to match Twiss parameters at the DR injection line [19].
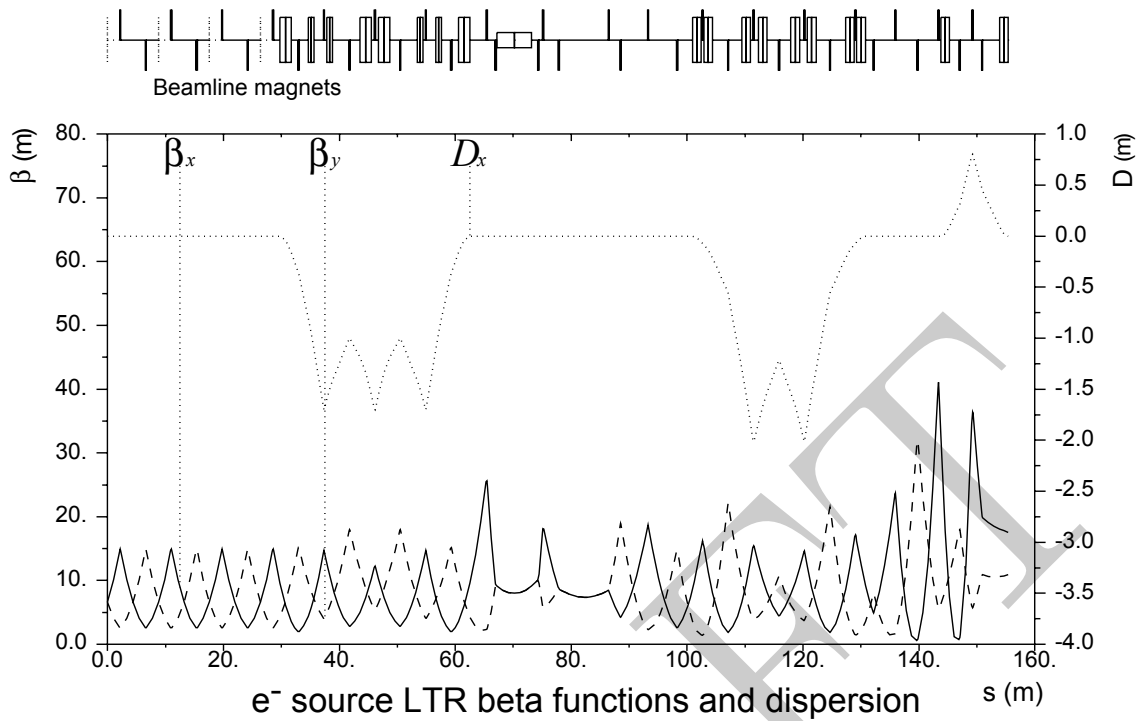
FIGURE 2.2-6. Optics of the LTR

2.2.5 Accelerator Components

2.2.5.1 Table of Parts Count

Table 2.2-3 lists the major components of the ILC electron source and Table 2.2-4 the lengths of the various electron source beamlines.

TABLE 2.2-3
Total number of components for the polarized electron source.

Magnets		Instrumentation		RF	
Bends	25	BPMs	100	216.7 SHB Cavity	1
Quads (NC)	76	Wirescanners	4	433.3 SHB Cavity	1
Quads (SC)	16	Laserwires	1	5 Cell L-band buncher	1
Solenoids(NC)	12	BLMs	5	L-band TW structure	2
Solenoids(SC)	2	OTRs	2	1.3 GHz cryomodules	25
Correctors(SC)	32	Phase monitors	2	L-band klystrons/modulators	13

TABLE 2.2-4
System lengths for the e- source beamlines.

Beam Line Section	Length
Gun area	7 m
NC beam lines	14 m
Chicane + emittance station	54 m
SC beam lines	245 m
eLTR	157 m
Dumplines	12 m
Total beam line length	489 m
Total tunnel length	505 m

2.3 POSITRON SOURCE

2.3.1 Overview

The ILC Positron Source uses photoproduction to generate positrons. The electron main linac beam passes through a long helical undulator to generate a multi-MeV photon beam which then strikes a thin metal target to generate positrons in an electromagnetic shower. The positrons are captured, accelerated, separated from the shower constituents and unused photon beam and then are transported to the Damping Ring. Although the baseline design only requires unpolarized positrons, the positron beam produced by the baseline source has a polarization of $\sim 30\%$, and beamline space has been reserved for an eventual upgrade to $\sim 60\%$ polarization.

The positron source must perform three critical functions:

- generate a high power multi-MeV photon production drive beam in a suitable short period, high K-value helical undulator;
- produce the needed positron bunches in a metal target that can reliably deal with the beam power and induced radioactivity;
- capture and transport the positron bunch to the ILC Damping Rings with minimal beam loss.

In addition, the Positron Source requires sufficient instrumentation, diagnostics and feedback (feedforward) systems to ensure optimal operation of the source and ILC.

2.3.2 Beam Parameters

The key parameters of the Positron Source are listed in Tables 2.3-1, 2.3-4, 2.3-5. The source is required to deliver 2×10^{10} positrons per bunch at the IP with the nominal ILC bunch structure and pulse repetition rate. The source target system is designed with a 50% overhead and can deliver up to 3×10^{10} positrons per bunch to the 400 MeV point. There is sufficient RF power to accelerate 2.5×10^{10} to the damping ring within the 0.09 m-rad transverse dynamic aperture.

2.3.3 System Description

Figure 2.3-1 shows the layout of the ILC electron side and the relative positions of the major systems of the positron source. Figure 2.3-2 shows the major elements of the positron source. The positrons are produced, separated and accelerated to 400 MeV in the *Undulator* area of Fig. 2.3-1. They are then transported to the e^+ *Booster* area where they are further accelerated to the positron damping ring injection energy. The important lengths and distances associated with the positron source are summarized in Table 2.3-2.

Positrons are produced in electromagnetic showers when a multi-MeV photon beam impinges on a metal target. The photon beam is produced by passing the main electron linac beam through a long undulator. This photon beam is transported ~ 500 meters to the positron source target hall where it hits a 0.4 radiation length thick Ti-alloy target producing showers of electrons and positrons. The resulting beam is captured using an optical matching device (OMD) and normal conducting (NC) L-band RF with solenoidal focusing and accelerated to 125 MeV. The electrons and remaining photons are separated from the positrons and

TABLE 2.3-1
Nominal Positron Source Parameters († upgrade values)

Beam Parameters	Symbol	Value	Units
Positrons per bunch at IP	n_b	2×10^{10}	number
Bunches per pulse	N_b	2625	number
Pulse repetition rate	f_{rep}	5	Hz
Positron energy (DR injection)	E_0	5	GeV
DR transverse acceptance	$\gamma(A_x+A_y)$	0.09	m-rad
DR energy acceptance	δ	$\pm\,0.5$	%
DR longitudinal acceptance	A_l	$\pm3.4\times\pm25$	cm-MeV
Electron drive beam energy	E_e	150	GeV
Electron beam energy loss in undulator	ΔE_e	3.01	GeV
Positron polarization †	P	$\sim$60	%
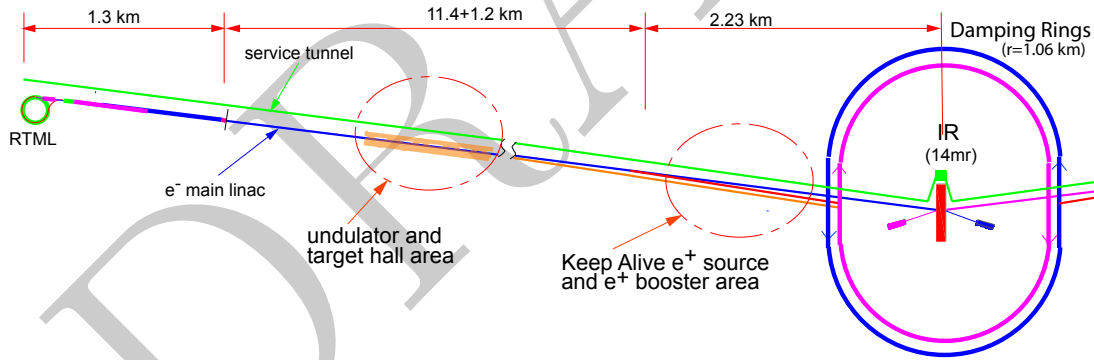
FIGURE 2.3-1. Positron Source Locations within the ILC Complex

dumped. The positrons are accelerated to 400 MeV in a NC L-band linac with solenoidal focusing. They are transported $\sim$5 km to the central damping ring complex, where they are boosted to 5 GeV in a linac using superconducting (SC) L-band RF and injected into the positron damping ring.

The positron source system also includes a Keep Alive Source to generate a low intensity positron beam that can be injected into the SC L-band linac. This allows various beam feedbacks to remain active if the main electron beam, and hence the undulator based positrons, is lost. ILC availability studies (see Section 2.9.1) show that the Keep Alive Source makes a significant improvement in accelerator uptime and delivered luminosity. This source uses a 500 MeV electron drive beam impinging on a tungsten-rhenium target to produce positrons which are then captured and accelerated to 400 MeV similar to the main positron source.
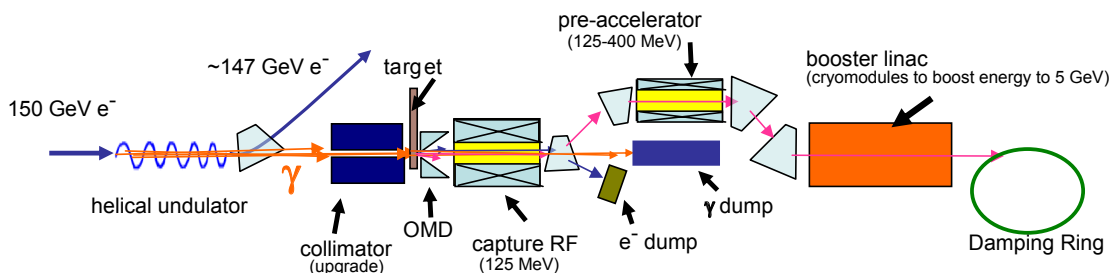
FIGURE 2.3-2. Overall Layout of the Positron Source

The Keep Alive Source is designed to produce 10% bunch intensity for the full 2625 bunch ILC pulse train at 5 Hz.

2.3.3.1   Photon Production

The positron source relies upon an intense beam of high energy photons impinging upon a metal target. The photons must be of sufficient energy, typically of order 10 MeV, to generate electron-positron pairs that can escape from the target material and be captured and accelerated. The photons are generated by the radiation from relativistic electrons as they pass through the periodic, helical, magnetic field of the undulator. Details of the undulator are provided in Section 2.3.5.1. To generate the required photon energy, very high energy electrons are required. To avoid the expense of a dedicated electron beam, the undulator is installed part way along the electron main linac, where the electron energy has reached 150 GeV. After passing through the undulator the electrons continue through the remainder of the main electron linac, gaining energy up to 250 GeV. The first harmonic cut-off energy for the photon spectrum is 10 MeV.

A helical undulator generates twice the synchrotron radiation power per period than the equivalent planar undulator, enabling the overall undulator to be shorter for the same number of positrons. The helical device also produces circularly polarized light which in turn generates longitudinally polarized positrons.

2.3.3.2   Positron Production and Capture

The positron production, capture and transport to the damping rings are shown in Figure 2.3-2. The photon beam generated by the helical undulator is incident on the rim of a 0.4 X_0

TABLE 2.3-2
Positron Source Beamline Lengths

Area	Length (meters)
Undulator chicane insert	1257
Undulator center to target	500
Undulator insert length	200
Target Hall length	150
400 MeV long transport line	5032
Total RF acceleration length	350
Damping Ring injection line	431
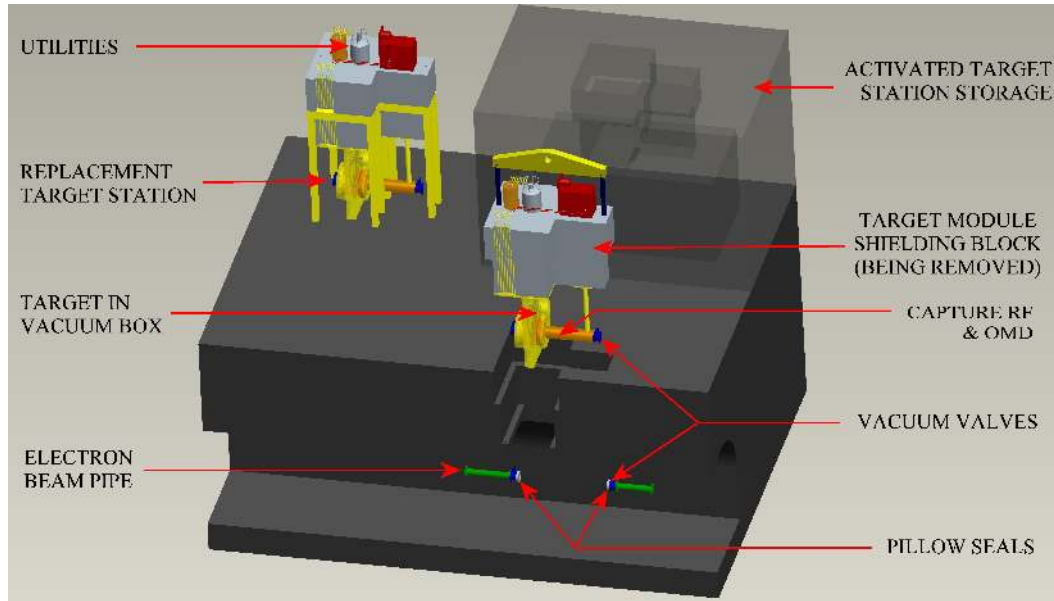
FIGURE 2.3-3. Target Removal Scheme (5-spoke target wheel, OMD and first RF section is seen being removed from the beamline)

thick rotating target (see Section 2.3.5.2) contained in a vacuum vessel. The photon beam has a transverse size of ∼1 mm rms and deposits ∼10.5 kW of power in the target. Photons up to the 8th harmonic contribute to the positron generation. The particles emerging from the downstream side of the target are captured in the 0.09 m-rad transverse dynamic aperture defined by the positron damping ring. The energy of the beam coming out of the target is 3 - 55 MeV. The target is followed by the tapering magnetic field of an Optical Matching Device (OMD) (see Section 2.3.5.3) which has a field which decays from 5 - 0.5 T over 20 cm. The OMD matches the beam phase space from the target into the capture L-band RF which accelerates the beam to 125 MeV. The RF cavities have an average gradient of 8 MV/m and are located inside 0.5 Tesla solenoids which provide beam focusing. Details of the RF are given in Section 2.3.5.4.

The target and equipment immediately downstream are expected to become highly activated. A remote-handling system is used to replace the target, OMD and 1.3 meter NC RF cavities. Due to the underground location, the activated equipment needs to be removed vertically from the target vault. Figure 2.3-3 shows the conceptual design of such a system, where the target wheel, OMD and the first 1.3 meter NC RF cavity is shown being removed. This design does require special vacuum seals to enable speedy removal from the beam line, as the power deposition from the beam does not allow for windows in these lines.

2.3.3.3 Low Energy Positron Transport

Downstream of the capture RF, the positrons are separated from electrons and photons in an achromatic dogleg which horizontally deflects the positron line by 2.5 m. A set of collimators remove positrons with large diverging angles and large energy offsets. Normal conducting L-band RF structures embedded in a constant solenoid field of 0.5 T accelerate the positrons from 125 MeV to 400 MeV. The accelerating gradient is ∼8 MV/m and the length is 34.6 m.

A dogleg deflects the beam 5 m horizontally to the electron main linac tunnel and 2 m vertically to position the long positron transport line above the electron main linac. This

beamline carries the positrons 4.09 km to the end of the main linac tunnel, then 941 m to the positron booster linac in a separate tunnel.

2.3.3.4 Keep Alive Source

The Keep Alive Source (KAS) is designed to deliver a low intensity (~10%) beam of positrons at 400 MeV to the positron booster linac in case the primary positron beam is unavailable. It occupies ~500 meters of tunnel just before the booster linac. A 500 MeV electron beam impinges on a tungsten-rhenium target to produce positrons. The electron drive beam is similar to the main electron source. The KAS positron target has a simpler design because of the lower incoming beam power, but still requires remote handling. The positrons are captured, separated and accelerated to 400 MeV using the same system as for the primary positron beam.

2.3.3.5 5-GeV SC Booster Linac

The SC booster linac accelerates the beam from 400 MeV to 5 GeV in three sections of periodic FODO lattice. The first section up to 1083 MeV has four non-standard cryomodules, each containing six 9-cell cavities and six quadrupoles. The quad field strength ranges from 0.88-2.0 T. The second section up to 2626 MeV has six non-standard cryomodules, each containing eight 9-cell cavities and two quadrupoles . The quad strength ranges from 0.62-1.3 T. Finally, the positrons are accelerated to 5 GeV using twelve standard ILC-type cryomodules, each with eight 9-cell cavities and one quadrupole with strength ranging from 0.95-1.63 T.

2.3.3.6 Linac to Damping Ring Beam Line

The Linac to Ring (LTR) brings the positrons from the booster linac to the Damping Ring (DR) injection line. In addition, the LTR orients the beam polarization and compresses the beam energy to improve acceptance into the DRs. The LTR design is the same as for the electron source LTR described in 2.2.4.2. The longitudinal polarization of the positrons from the target is preserved to the LTR. If polarization is needed at the IP it must be preserved through the DR. This is achieved by rotating the spin to vertical before injection into the DR. The LTR contains bending magnets which rotate the spin vector from longitudinal to horizontal, followed by solenoids, if turned on, that rotate from horizontal to vertical. At 5 GeV, the total bending angle must be an odd integer multiple of 7.9° to produce a net 90° of spin rotation. 26.23 T-m of solenoidal field is required to produce the horizontal-to-vertical spin rotation which is provided by two 2.5 meter 5.2 T solenoids.

2.3.4 Accelerator Physics Issues

2.3.4.1 Photon Drive Beam

The photon drive beam is generated by passing the main electron beam through a long, small-aperture undulator which sits in the middle of a magnetic chicane. The design of this system has to ensure that this does not compromise the main electron beam quality, and hence the ILC luminosity. In addition the undulator system and the main linac downstream of the undulator need to be protected from any beam failures.

The electron beam transport through the complete undulator system is based upon a simple FODO arrangement with quadrupole spacing of ~12 m (in the room temperature

section). There are beam position monitors (BPM) at every quadrupole and horizontal and vertical corrector magnets in each cryomodule. A recent study [20] indicated that a quadrupole to BPM misalignment of 10 μm leads to a vertical emittance growth of less than 2%, due to the quadrupole mislignment rather than the undulator. The undulator increases the energy spread of the electron beam from 0.16% to 0.23%.

The baseline pressure requirement of 10^{-8} torr has been set to avoid fast ion instability problems. Vacuum calculations confirm that the cryopumping will be adequate provided that photons with energy >10 eV are intercepted by absorbers spaced approximately every 12 m to shadow the cold vessel surfaces. These absorbers are in room temperature sections.

To protect the undulator and downstream linac from beam failure, there is a fast extraction system before the chicane that can dump the main electron beam into a full power beam dump. A collimator in front of the undulator can intercept a few bunches before the dump system fires.

2.3.4.2 Positron Generation

The primary issue for positron production is to efficiently capture the positrons which are produced with a small spatial extent and large angles. Point-to-parallel focusing immediately after the target increases the positron capture. An optical matching device (OMD) placed immediately after the target produces a longitudinal field that decays from 5 Tesla to 0.5 Tesla in $\sim$ 20 cm. Calculations show a factor of two improvement in positron capture from the OMD.

2.3.4.3 Beam Transport

The positron beam transport must efficiently bring the large emittance beam from the target through several km of beamline. The beam at damping ring injection must match the damping ring phase space to avoid beam losses in the damping ring. Beam outside the acceptance must be absorbed on collimators to localize radioactivation.

The linac transfer line that takes the 400 MeV positron beam from the target hall to the booster linac has 16.8 m long FODO cells with 90 degree phase advance per cell and $\sim$28.5 m maximum β-function. It follows the earths curvature as does the linac tunnel. The vertical dogleg which brings the positron beam 8 m vertically from the linac tunnel to the booster tunnel, has at each end a double bend achromat to provide 17.1 mrad of bending angle. Four quads are inserted in between two bends to create 180° phase advance between the two bends and cancel the dispersion. The last section connects to the positron booster linac.

In order to match the positron beam into the longitudinal acceptance of the damping ring, the beam energy spread is reduced from $\pm$2.8% to $\pm$0.5%. The energy compression and spin rotation take place in four FODO-like cells with 8 bends in the first arc of the LTR. The total bending angle is 55.5°. The nominal momentum compaction, R_{56}, is 86 cm but it is adjustable. After the bunch decompression, a standard 12 m superconducting cryomodule at an RF voltage of 180 MV rotates the positrons in longitudinal phase space to match the DR acceptance. The rest of the LTR includes a section with an additional 34.5° horizontal bend, a matching section with 4 quadrupoles and a double bend achromat used to match into the DR injection line. The geometry is shown in Figure 2.3-4.

Multi-particle tracking has been performed from the target to the DR injection. The ELEGANT code [?] was chosen to track the positron beam with large angular divergence and long low-energy tails. The LTR energy compression was optimized to maximize the
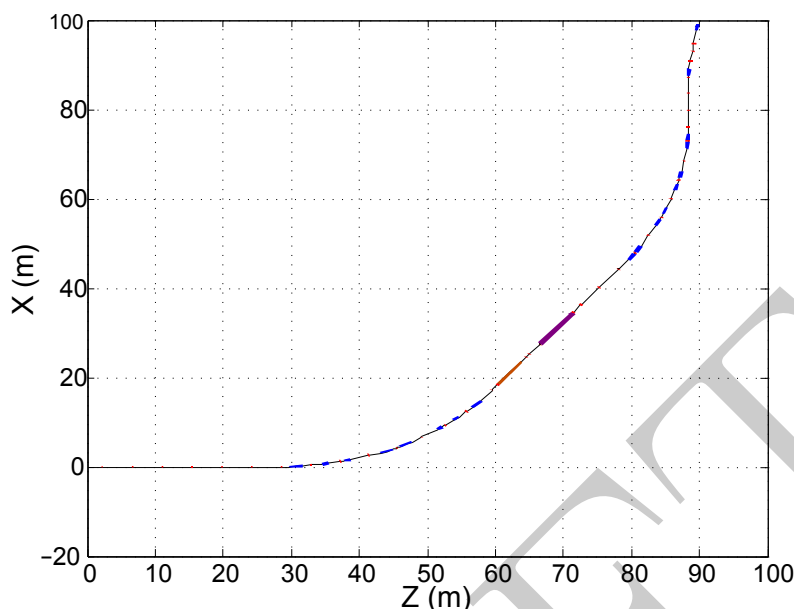
FIGURE 2.3-4. Optics of the LTR Beamline (Matching happens from 1-25 meters and DR injection is at z=90meters)

positron beam within the 6-dimensional acceptance in the DR equal to $\gamma(A_x + A_y) < 0.09$ m and $(\pm 25$ MeV$) \times (\pm 3.46$ cm$)$. Of the positrons from the target, 55% survive the transport through the complete beamline based on the physical apertures of the beam pipes [21] and $\sim 50\%$ of the positrons are within the DR 6-dimensional acceptance. An energy collimator in the LTR second arc reduces the number of unwanted particles reaching the DR from 5.6% to 1.1%. Additional betatron and energy collimators may be required to collimate the rest of the unwanted 1.1% of particles, 0.8% of which are outside of the transverse DR acceptance. Tracking with realistic magnet errors shows similar results after orbit correction. Figure 2.3-5 shows the positron yield in various parts of the ILC Positron Source.
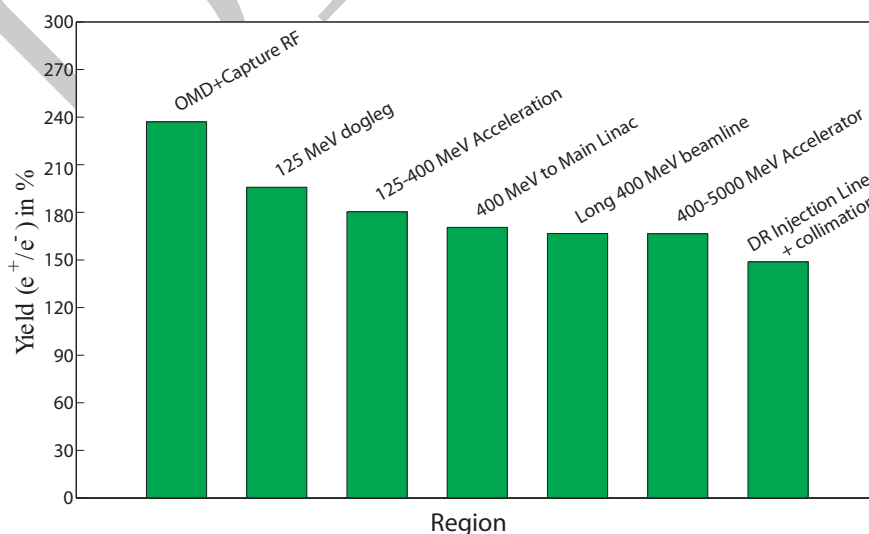
FIGURE 2.3-5. Positron Yield in Various Parts of the Positron Source

2.3.5   Accelerator Components

Table 2.3-3 lists the components for the positron source. In addition to this there are two target stations, the first of which is the main production target and the second used in the Keep Alive Source, and their associated instrumentation. Except for the undulator, target, remote handling and the OMD, costing for the positron source system was done by the global systems groups. The undulator, target and OMD costs were estimated by the design engineers and the remote handling system costs were projected from costs associated with remote handling in other accelerator facilities.

TABLE 2.3-3
Total Number of Components in the Positron Source.

Magnets	#	Instrumentation	#
Dipoles	157	BPM x,y pairs	922
NC quads	871	BPM readout channels	922
SC quads	51	Wire scanners	29
Sextupoles	32	Beam length monitors	2
NC solenoids	38	Profile monitors	7
SC solenoids	2	Photon profile monitors	3
NC correctors	871		
SC correctors	102	RF	#
Kickers	15	NC L-band structures	30
Septa	4	1.3 GHz SC cavities	200
SC undulator cryomodules	42	1.3 GHz cryomodules	26
OMD	2	1.3 GHz klystrons/modulators	37

2.3.5.1   Undulator

The undulator must be superconducting to achieve the required parameters of high field and short period. The present baseline parameters are given in Table 2.3-4. Two interleaved helical windings of NbTi spaced half a period apart generate the transverse helical field. Figure 2.3-6 is a picture of some short sample undulator prototypes showing the forms for the helical windings. The 147 m of undulator is supplied by forty-two 4 m long cryomodules containing two separate undulators with an active undulator length per cryomodule of 3.5 m. Figure 2.3-7 shows the cryomodules with the two undulators running along the center.

The undulator vacuum chamber has a nominal inner diameter of 5.85 mm and is made of copper. The extremely high conductivity of copper at cryogenic temperatures mitigates resistive wall effects. The material between the superconducting windings is soft magnetic iron which also serves as an outer yoke to increase the field and provides additional support. Each cryomodule contains a liquid helium bath and in-situ cryocoolers are used to achieve zero liquid boil off.

Since the electron vacuum vessel is at cryogenic temperatures, each module effectively acts as a long cryopump. Roughing pumps are installed in room temperature sections between cryomodules (approximately every 12 m) but achieving UHV conditions relies upon
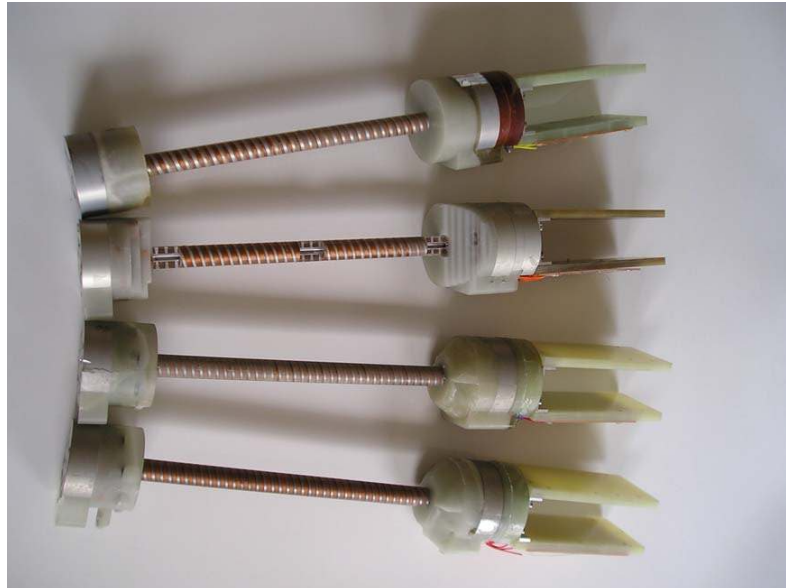
FIGURE 2.3-6. Short Sample Undulator Prototypes
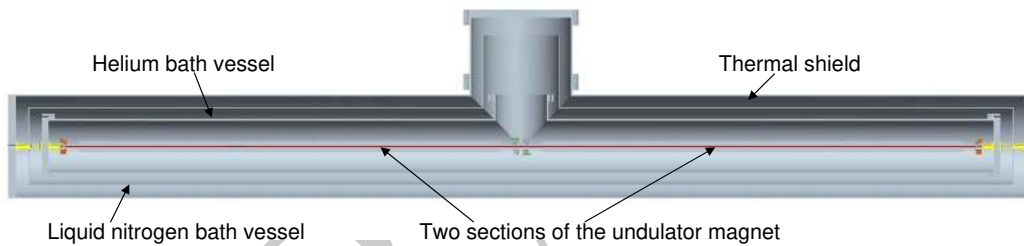
FIGURE 2.3-7. 4-meter Undulator Cryomodule

cryopumping. To achieve the baseline pressure requirement of 10^{-8} torr absorbers to prevent photons striking the cold vessel surfaces are placed every 12 meter in room temperature section.

TABLE 2.3-4
Nominal Undulator Parameters

Undulator Parameters	Symbol	Value	Units
Undulator period	λ	1.15	cm
Undulator strength	K	0.92	
Undulator type		helical	
Active undulator length	L_u	147	m
Field on axis	B	0.86	T
Beam aperture		5.85	mm
Photon energy (1$^{\text{st}}$ harmonic cutoff)	E_{c10}	10.06	MeV
Photon beam power	P_γ	131	kW

TABLE 2.3-5
Nominal Target Parameters

Target Parameters	Symbol	Value	Units
Target material		Ti-6%Al-4%V	
Target thickness	L_t	0.4 / 1.4	r.l. / cm
Target power adsorption		8	%
Incident spot size on target	σ_i	> 1.7	mm, rms

2.3.5.2 Target

The ILC positron target parameters are shown in Table 2.3-5. The positron production target is a rotating wheel made of titanium alloy (Ti-6%Al-4%V). The photon beam is incident on the rim of the spinning wheel, whose diameter is 1 m and thickness is 0.4 radiation lengths (1.4 cm). During operation the outer edge of the rim moves at 100 m/s. This combination of wheel size and speed offsets radiation damage, heating and the shock-stress in the wheel from the ~131 kW photon beam. A picture of the conceptual target layout is shown in Figure 2.3-8. A shaft that extends on both sides of the wheel with the motor mounted on one shaft end, and a rotating water union on the other end to feed cooling water. The target wheels sit in a vacuum enclosure at 10^{-8} torr (needed for NC RF operation), which requires vacuum seals to enable access to the chamber. The rotating shaft penetrates the enclosure using two vacuum pass-throughs, one on each end. The optical matching device (OMD - see Section 2.3.5.3), is mounted on the target assembly, and requires an additional liquid nitrogen cooling plant. The motor driving the target wheel is sized to overcome forces due to eddy currents induced in the wheel by the OMD.
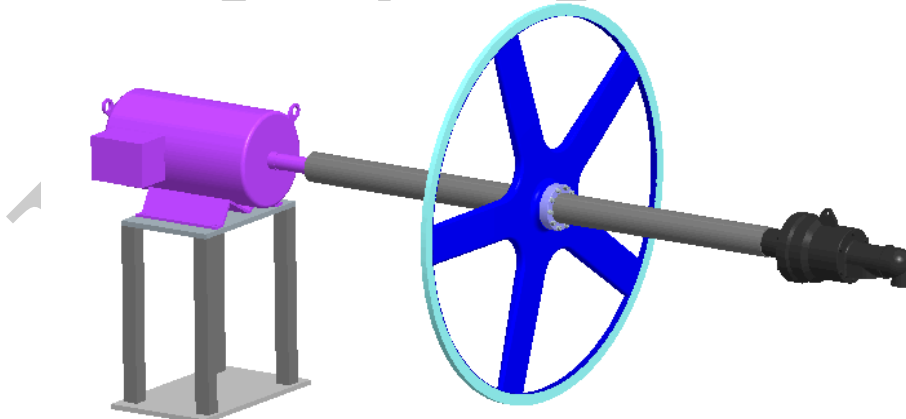
FIGURE 2.3-8. Target Station Layout

The target wheel assembly is designed for an operational life of two years. In the event that the target fails during a run, the assembly can be replaced by a new assembly in about a day using vertical remote handling.

A series of sensors provide information on the target behavior. An infrared camera tracks temperatures on the wheel, to allow for quick shutdown in the case of a cooling failure. Flowmeters monitor cooling water flow in and out of the wheel (to watch for leaks), along with thermocouples to check ingoing and outgoing flow temperature. A torque sensor is placed

on the shaft, with vibration sensors on the wheel to report mechanical behavior. Finally, the wheel's rotational speed is monitored.

2.3.5.3 Optical Matching Device

The OMD generates a solenoidal magnetic field which peaks in strength at 5 Tesla close to the target and falls off to 0.5 Tesla to match the solenoidal field at the entrance of the capture section. The OMD increases the capture efficiency by a factor of 2. The OMD is a normal conducting pulsed flux concentrator based on an extrapolation of a magnet created for a hyperon experiment [22].

The magnetic field of the OMD interacts with the spinning metal of the target to create eddy currents. The target design must accommodate this drag force which increases the average heat load and requires a stronger target drive motor. The OMD may possibly induce 5 Hz resonance effects in the target that will need to be mitigated.

2.3.5.4 Normal Conducting RF Accelerator System

Due to the extremely high energy deposition from positrons, electrons, photons and neutrons downstream of the positron target, normal conducting structures must be used up to an energy of 125 MeV. This normal-conducting section is challenging but feasible, and a prototype test structure is under construction. It must sustain high accelerator gradients during millisecond-long pulses in a strong magnetic field, provide adequate cooling in spite of high RF and particle loss heating, and produce a high positron yield with the required emittance. The design contains both standing-wave (SW) and traveling-wave (TW) L-band accelerator structures [23]. The capture region has two 1.27 m SW accelerator sections at 15 MV/m and three 4.3 m TW accelerator sections at 8.5 MV/m accelerating gradient. All accelerator sections are surrounded with 0.5 T solenoids. Figure 2.3-9 shows the schematic layout.
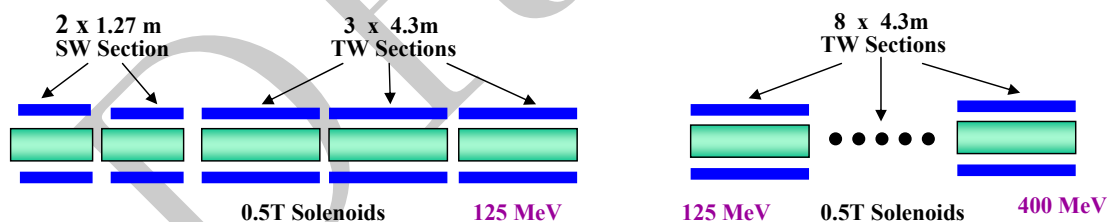
FIGURE 2.3-9. Layout of the Capture Region (left) and Pre-Accelerator Region (right)
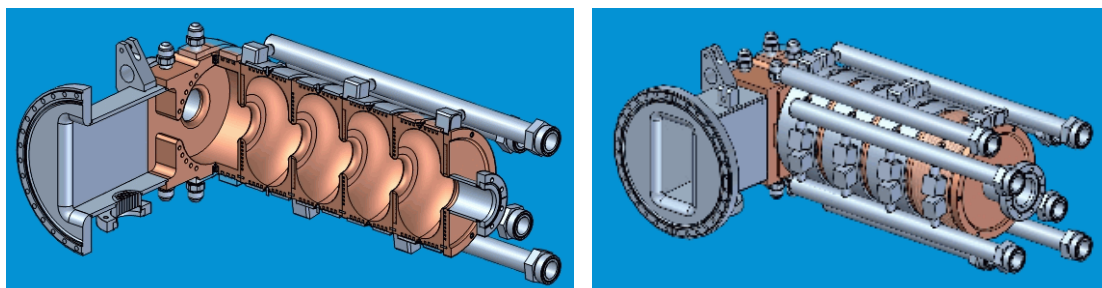
FIGURE 2.3-10. SW Structures - Cut-away and External Views

The high gradient (15 MV/m) positron capture sections are 11-cell π mode SW accelerator structures. The SW structures have a more effective cooling system and higher shunt impedance with larger aperture (60 mm) and require RF circulators to protect the klystrons from reflected power. The mode and amplitude stability under various cooling conditions for this type of structure have been theoretically verified. Figure 2.3-10 shows engineering drawings of the SW structures.

The TW sections are 4.3 m long, $3\pi/4$ mode constant gradient accelerator structures. The phase advance per cell has been chosen to optimize RF efficiency for a large aperture TW structure. The TW structures allows easy installation for long solenoids and do not need circulators. Each accelerator section has an individual 1.3 GHz RF power source.

2.3.5.5 Magnets

The Positron Source has more than 2000 magnets, see Table 2.3-3. Most of the magnet designs are quite straightforward. The large aperture DC solenoids, surrounding the L-band capture RF must be normal conducting because of the high beam losses in the target region and as such use a large amount of electrical power. In addition, there are two long high field SC solenoids for spin rotation in the LTR.

2.3.5.6 Diagnostics

The Positron Source has the normal complement of beamline instrumentation to measure orbit, emittance, charge and energy spread. Specialized diagnostics are designed into the unique positron systems, e.g. target. The major cost is in the BPM system because of the large channel count coming from the long beamlines. The number of readout channels is halved by processing only one transverse plane of the BPM x,y pair at each quadrupole. Performance specifications for the diagnostics are in most cases equal to or less than the Main Linac or RTML.

2.3.5.7 Electron and Photon Beam Dumps

There are 9 beam dumps, 16 variable aperture collimators, 1 fixed aperture collimator and 5 stoppers with burn through monitors planned for the positron source system. Three of the beam dumps must absorb sufficiently large beam power that they require dump designs with water in the path of the beam. The plumbing to cool and treat the resulting radioactive water is the dominant cost.

There is a tune-up dump at the 150 GeV pre-undulator extraction point of the electron linac. For tune-up, the number of bunches per train is limited to 100; with absorbed power of 240 kW at nominal beam parameters. This dump, roughly in line with the linac, also serves as the abort dump for up to a full train of electrons (1.35 MJ) to protect the undulator. The dump consists of a 40 cm diameter by 250 cm long stainless vessel filled with 10 mm diameter aluminum balls through which flows $\sim$30 gallons per minute of water; it is backed by a short length of peripherally cooled solid copper. The dump is shielded from the access passageway by 10 cm of steel and 40 cm of concrete. A service cavern houses a heat exchanger, pumps and a system to treat the water for hydrogen, oxygen and ^{7}Be. A second dump, technically identical (225 kW at nominal beam parameters), is located near the damping ring to tune the 5 GeV positrons before injection.

The most challenging dump in the positron production system absorbs the non-interacting undulator photons from the target. This dump must absorb up to 300 kW (upgrade value) continuously (1.9 x 10^{17} photons/sec of 10 MeV average energy). The primary absorber in this case must be water, contained in a vessel with a thin window. For a dump located 150 m downstream of the target, calculations indicate that the power density on a 1 mm Ti window is 0.5 kW/cm^2, the resultant temperature rise after the passage of one bunch train is 425°C, and in the core of the beam the rise in the water temperature is 190°C. With this geometry, a compact (10 cm diameter by 100 cm long) pressurized (12 bar) water vessel and Ti window, with a radioactive water processing system, is required. Lengthening the target to dump distance by several hundred meters would ease requirements on the dump, but incur the expense of a longer transport.

The remaining dumps and collimators in the positron system all are based on peripherally cooled solid metal construction, with the cooling water supplied directly from the accelerator low conductivity water (LCW) system and do not present technical or cost challenges.

2.4 DAMPING RINGS

2.4.1 Overview

The ILC damping rings include one electron and one positron ring, each 6.7 km long, operating at a beam energy of 5 GeV. The two rings are housed in a single tunnel near the center of the site, with one ring positioned directly above the other. The damping rings must perform three critical functions:

- Accept e- and e+ beams with large transverse and longitudinal emittances and produce the low-emittance beams required for luminosity production

- Damp incoming beam jitter (transverse and longitudinal) and provide highly stable beams for downstream systems

- Delay bunches from the source to allow feed-forward systems to compensate for pulse-to-pulse variations in parameters such as the bunch charge.

The damping ring system includes the injection and extraction systems, which themselves include sections of transport lines matching to the sources (upstream of the damping rings) and the RTML system (downstream of the damping rings).

2.4.2 Beam Parameters

The key parameters for both the electron and positron damping rings are listed in Table 2.4.3.

2.4.3 System Description

The configuration of the damping rings is constrained by the timing scheme of the main linac. In particular, each damping ring must be capable of storing a full bunch train (roughly 3000-6000 bunches) and reducing the emittances to the required level within the 200 ms interval between machine pulses. In addition, the relatively large bunch separation in the main linacs means that the damping rings must be capable of injecting and extracting individual bunches without affecting the emittance or stability of the remaining stored bunches.

Several configuration options capable of satisfying the various constraints were evaluated in 2005 on the basis of cost and technical risk, and the 6.7 km ring was selected [24]. The exact circumference has been chosen to provide flexibility in the operational timing scheme, allowing variation in the bunch charge and number of bunches per pulse, for a fixed total number of particles per pulse and constant pulse length in the linac [6]. The superconducting RF system is operated at 650 MHz. To achieve the short damping times necessary to reduce the emittances (by roughly six orders of magnitude in the case of the positron vertical emittance) within the allowed 200 ms interval, superconducting wigglers of total length roughly 200 m are used in each damping ring.

As noted in Section 2.1.5, there are significant constraints on the DR circumference, the fill patterns and the bunch spacing in the main linac. These issues will need to be optimized during the next design hase and it is likely that small changes will be made to the DR circumference and the bunch spacing.

ACCELERATOR DESCRIPTION

TABLE 2.4-1
Positron damping ring parameters. The electron damping ring is identical except for a smaller injected emittance.

Parameter	Units	Value
Energy	GeV	5.0
Circumference	km	6.695
Nominal # of bunches		2625
Nominal bunch population		2.0×10^{10}
Maximum # of bunches		5534
Bunch population at max # of bunches		1.0×10^{10}
Average current	A	0.40
Energy loss per turn	MeV	8.7
Beam power	MW	3.5
Nominal bunch current	mA	0.14
RF Frequency	MHz	650
Total RF voltage	MV	24
RF bucket height	%	1.5
Injected betatron amplitude, $A_x + A_y$	m.rad	0.09
Equilibrium $\gamma\epsilon_x$	μm.rad	5.0
Chromaticity, Ξ_x/Ξ_y		-63/-62
Partition Numbers, $J_x/J_y/J_E$		0.9998/1.0000/2.0002
h		14,516
ν_s		0.067
f_s	kHz	3.0
α_c		4.2×10^{-4}
ν_x/ν_y		52.40/49.31
σ_z	mm	9.0
σ_p/p		1.28×10^{-3}
τ_x	ms	25.7
τ_s	ms	12.9

2.4.3.1 Lattice Design Considerations

The ring lattice satisfies the basic requirements of damping time, normalized horizontal emittance and bunch length, has sufficient aperture for injecting a large emittance positron beam, and has a sufficiently large momentum compaction factor to maintain single bunch stability. However, there remains design work to be done on the lattice, for example to optimize the dynamic aperture to ensure efficient acceptance of the large emittance beam from the positron source, and to minimize sensitivity to tuning and alignment errors that could degrade the emittance.
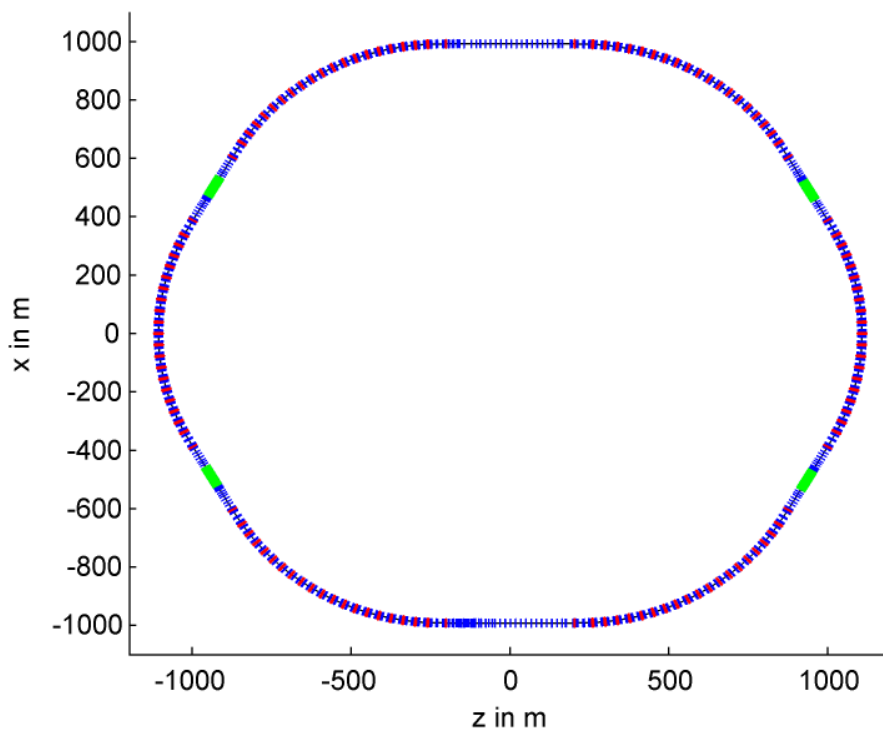
FIGURE 2.4-1. Layout of ILC Damping Ring.
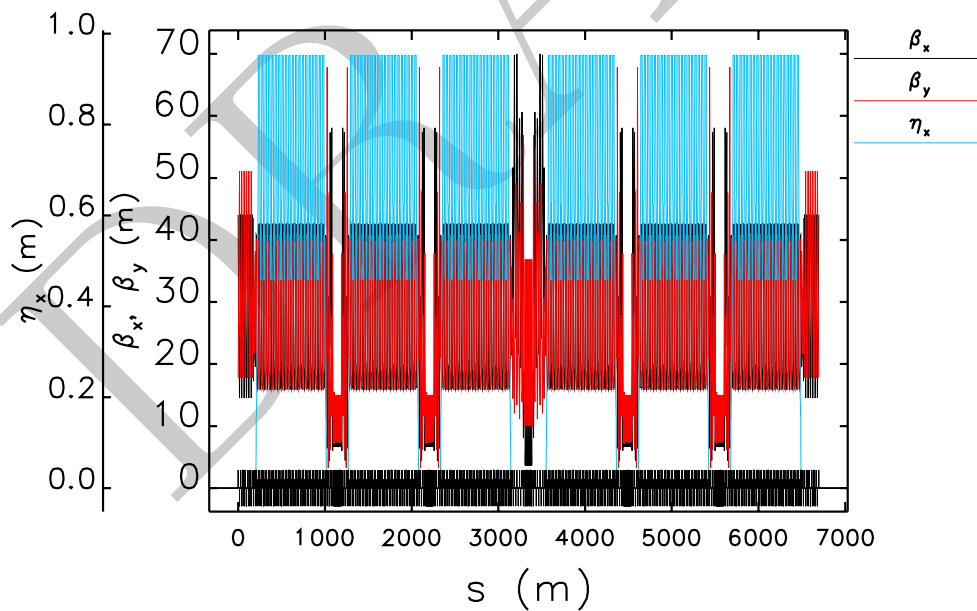
FIGURE 2.4-2. Optical functions of ILC Damping Ring.

The ring is divided into six arcs and six straight sections (see Figure 2.4-1). The arcs are composed of Theoretical-Minimum-Emittance (TME) cells to give low quantum excitation, and the straight sections are composed of FODO cells for the damping wigglers, RF cavities, and injection and extraction sections. Optical parameters are shown in Figure 2.4-2. The

parameters of the TME cells and the wigglers (peak field of 1.67 T) were selected to obtain the required damping time, momentum spread, and normalized horizontal emittance.

Two families of sextupole magnets are inserted in the TME cells for correcting the first-order chromatic effects of the linear optics. To reduce nonlinear effects of the sextupoles, the betatron phase advance of the TME cells was set to 90° in each plane. The resulting dynamic and momentum apertures (see Figure 2.4-3) were found to depend on the number of straight sections (i.e., the symmetry of the lattice) and on the betatron phase advances of the straight sections. The straight section betatron phase advances were adjusted for maximum dynamic aperture. While a larger number of straight sections was found to improve the nonlinearities, this comes at a higher cost for subsystems. A compromise configuration of six straight sections was eventually chosen for the baseline lattice.
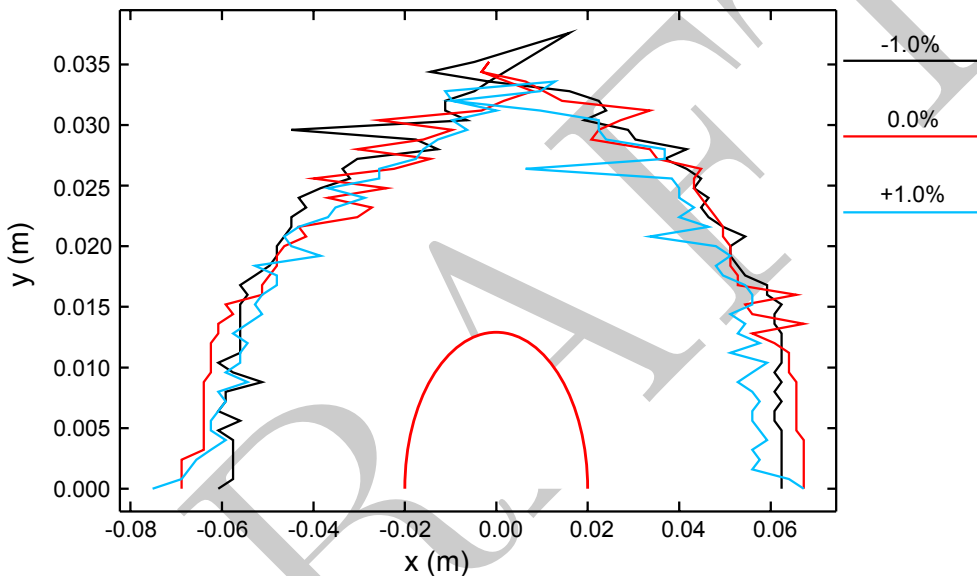
FIGURE 2.4-3. Dynamic aperture of the ILC damping ring (without field and alignment errors) for relative momentum errors of -1%, 0% and 1% at x = 44 m and y = 18 m. The thick red line represents the size of the injected positron beam.

The choice of momentum compaction factor, controlled chiefly by the total number of TME cells, results from a balance between competing requirements: single-bunch stability against the impedance of the vacuum chamber (favoring a high value of α_c) and a lower cost RF system (favoring a low value of α_c) . The value 4.2×10^{-4} is somewhat on the high side to reduce the risk of single-bunch instability. Unfortunately, a high momentum compaction factor makes it difficult to achieve a low equilibrium emittance and strong damping wigglers are required. The Twiss parameters in the wiggler region were adjusted to produce the required equilibrium emittance.

The injection/extraction sections accommodate a large number of fast stripline kickers (their large number being due to their inherent weakness). Optical functions were designed to ensure that the beam goes through the stripline kickers without hitting their apertures. For the injection section, the beam traverses the kickers at an angle but with a small trajectory offset.

2.4.3.2 Fast Ion Instability

Of significant concern to the electron damping ring is the fast ion instability. As opposed to the more familiar ion-trapping effect, where ions oscillate stably for long periods in the potential well of the stored beam, the fast ion instability is associated with ions created in the beam path by interaction with the circulating beam during a single turn. Ions created at the head of the bunch train move slowly, and remain in the beam path, influencing the motion of subsequent bunches. The resultant ion-induced beam instabilities and tune shifts are critical issues for the electron damping ring due to its ultra-low vertical emittance. A low base vacuum pressure at the 1 nTorr level is essential to reduce the number of ions formed. To mitigate bunch motion, we also employ bunch-by-bunch feedback systems with a damping time of ≈ 0.1 ms.

To further reduce the core ion density, short gaps are introduced in the electron beam bunch train by omitting a number of successive bunches. The use of such "mini-gaps" in the train significantly mitigates the fast ion instability by reducing the core ion density and by inducing tune variation along the train. Figure 2.4-4 shows the buildup of the ion cloud in the case of a particular multi-train pattern with 118 bunch trains and 49 bunches per train. In this case, the reduction in the core ion density is a factor of 60 compared with a fill consisting of a single long bunch train. It is worth pointing out that the effect of train gaps is a function of beam size, so they are less effective early in the damping cycle. The simulated growth time for the beam pattern corresponding to Fig. 2.4-4 is 280 μs.
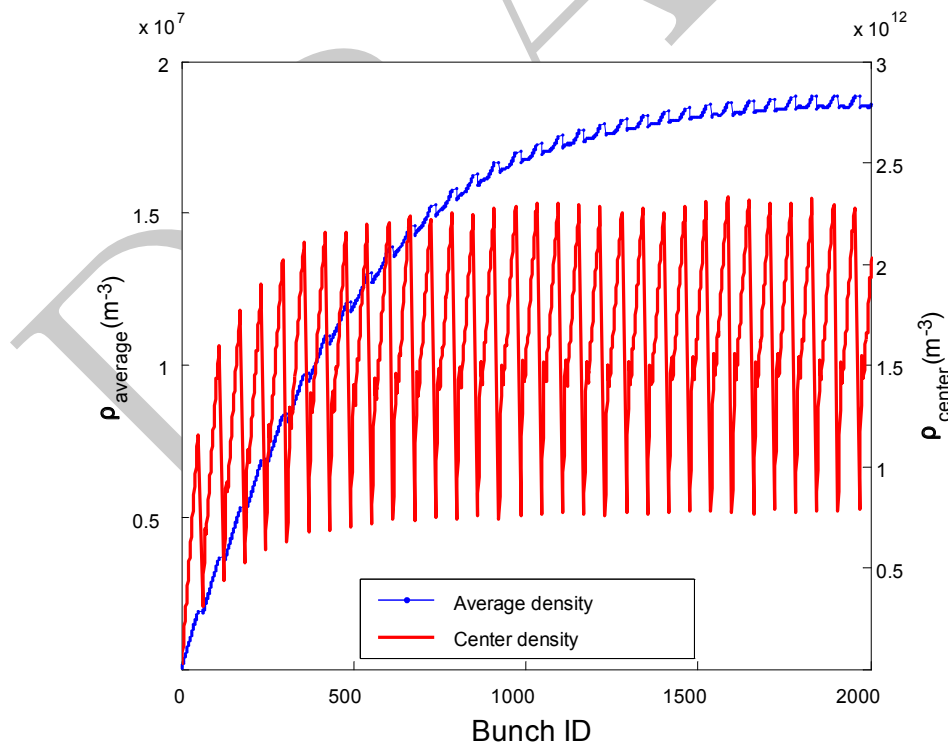
FIGURE 2.4-4. Buildup of CO^+ ion cloud at extraction. The total number of bunches is 5782 (118 trains with 49 bunches per train). The beam has a bunch separation of two RF bucket spacings, and a train gap of 25 RF bucket spacings. There are 0.97×10^{10} particles per bunch, and the partial vacuum pressure is 1 nTorr.

The tune spread due to both linear and nonlinear tune shifts provides Landau damping that helps control ion-induced instabilities [25]. With a multi-train fill pattern, the size of the ion cloud is much larger than the vertical beam size, so there is a larger tune spread. When the oscillation amplitude of the beam reaches the beam size, the nonlinearity effectively saturates the instability.

2.4.3.3   Electron Cloud Instability

Electron cloud instabilities and tune shifts are critical issues for the positron damping ring. The electron cloud develops quickly as photons striking the vacuum chamber wall knock out electrons that are then accelerated by the beam, gain energy, and strike the chamber again, producing more electrons. The peak secondary electron yield (SEY) of typical vacuum chamber materials is >1.5 even after surface treatment, leading to amplification of the cascade. Once the cloud is present, coupling between the electrons and the circulating beam can cause a single-bunch (head-tail) instability and incoherent tune spreads that may lead to increased emittance, beam oscillations, or even beam losses. Because the electron cloud is difficult to suppress in the dipole and wiggler regions of the ring, this is where its effects are expected to be most severe. A large synchrotron tune is beneficial, as it raises the threshold for the electron cloud head-tail driven instability.

Single-bunch instability simulations for the 6.7 km damping ring lattice show that the instability sets in above an average cloud density of 1.4×10^{11} e$^-$/m^3, where an incoherent emittance growth is observed, see Figure 2.4-5. Analytic calculations give higher density thresholds by roughly a factor of 4 [27, 28]. Tune shifts on the order of 0.01 are expected near threshold.
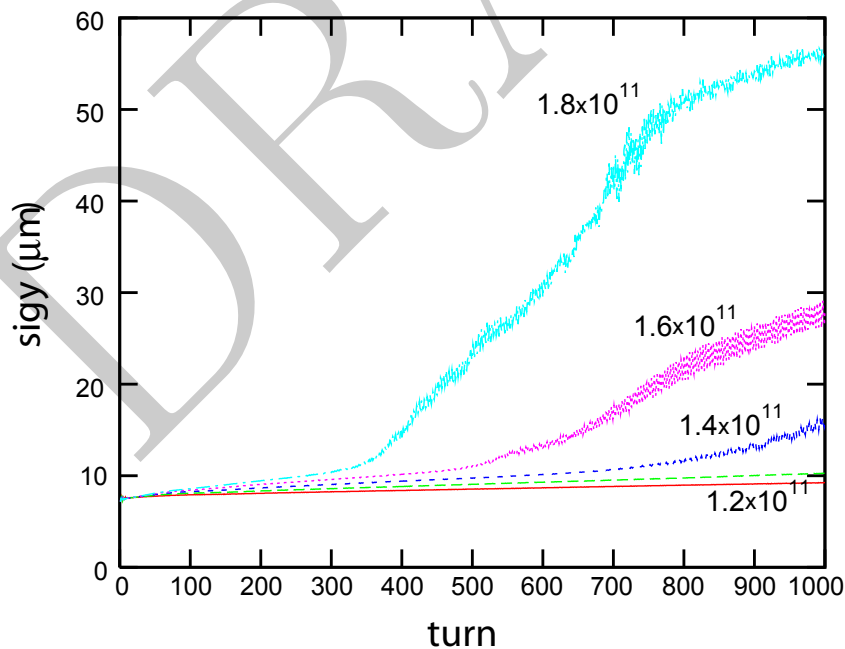
FIGURE 2.4-5. Emittance growth from single-bunch instability driven by electron cloud in the 6.7 km OCS ring. Electron cloud densities in e-/m^3 are indicated.

Simulations indicate that a peak secondary electron yield of 1.2 results in a cloud density

close to the instability threshold. Based on this, the aim of ongoing experimental studies is to obtain a surface secondary electron yield of 1.1. Simulations also indicate that techniques such as grooves in the chamber walls or clearing electrodes will be effective at suppressing the development of an electron cloud [29, 30]. Figure 2.4-6 shows the buildup of the electron cloud and the suppression effect of clearing electrodes in an arc bend of the 6.7 km ring. A clearing electrode bias potential of +100 V is sufficient to suppress the average (and central) cloud density by more than two orders of magnitude. Techniques such as triangular or rectangular fins or clearing electrodes need further R&D studies and a full demonstration before being adopted. Nonetheless, mitigation techniques appear to be sufficient to adopt a single 6.7 km ring as the baseline design for the positron damping ring.
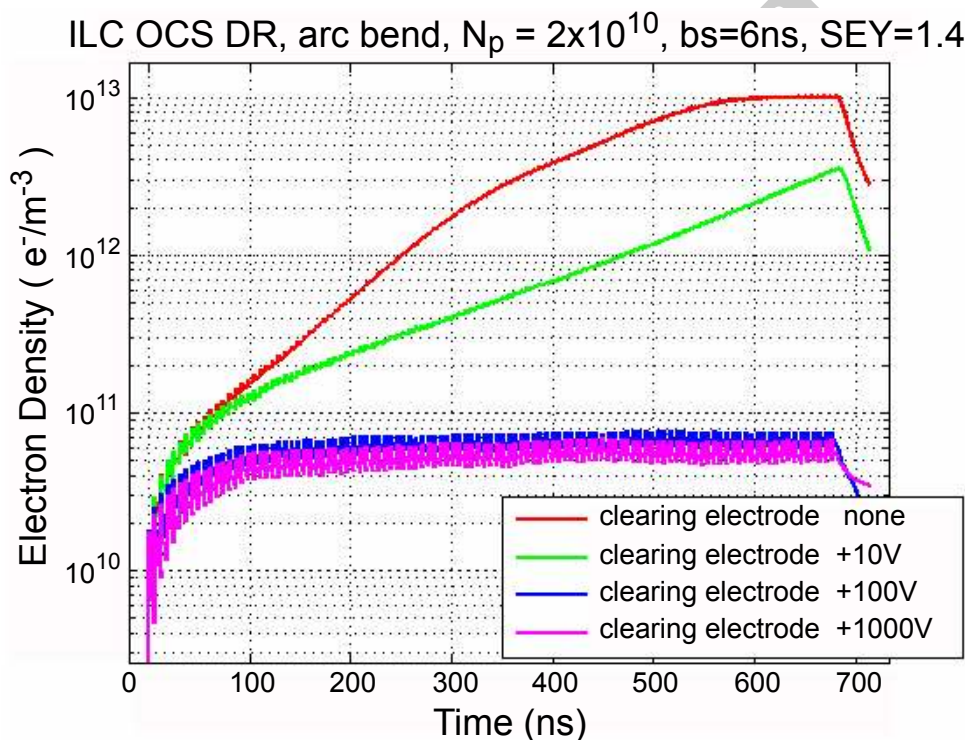
FIGURE 2.4-6. Electron cloud buildup in an arc bend of the 6.7 km ring and suppression effect of clearing electrodes biased at the indicated voltages.

2.4.3.4 Injection and Extraction

The bunch separation in the main linacs is much longer than in the damping rings, so individual bunches must be injected and extracted without affecting the emittance or stability of the remaining stored bunches. For this to be the case, the kicker field must be negligible for any stored bunch upstream or downstream of the injected or extracted bunch, requiring that the effective kicker pulse width be less than twice the bunch spacing. Injection is interleaved with extraction, to minimize excursions in beam loading of the RF system.

Extraction is located near the center of one long straight section. A set of kickers deflects a single damped bunch horizontally. A horizontally defocusing quadrupole increases the deflection. About 90° of betatron phase downstream of the kickers, the bunch passes through the bending fields of a pair of septum magnets. These deflect the trajectory further

horizontally, so it passes outside of the next focusing quadrupole and into the extraction line optics. The stored orbit is located in the nominally field-free region of the septum magnets and is not significantly affected. The extraction straight section also includes an abort dump.

Injection is located near the center of the opposite long straight section. The injection line grazes the outside of a quadrupole, and is deflected horizontally by a pair of septum bend magnets so the trajectory passes inside the aperture of the next quadrupole. This horizontally defocusing quadrupole makes the trajectory nearly parallel to the stored orbit. About 90° of betatron phase downstream from the septa, where the injection trajectory crosses the stored orbit, a set of kickers deflects the single injected bunch onto the stored orbit. As mentioned previously, the kicker is distributed into several modules at the axis-crossings of the injected trajectory, so the module aperture can be minimized.

The kicker modules are 50 Ω stripline structures inside the vacuum pipe, each 30 cm long, operating at a voltage of 22 kV, provided as +11 and -11 kV pulses on opposite electrodes. Twenty modules are required; two extra kickers are included to ensure adequate availability. The 30 cm stripline gives a 2 ns contribution to the kicker pulse width, leaving less than 10 ns for the electrical pulse width at the nominal ring bunch spacing of 6 ns. The kickers pulse about every 300 ns during the linac pulse of about 1 ms. For the low bunch charge parameters, the ring bunch spacing is 3 ns, requiring an electrical pulse width of less than 4 ns and a pulse about every 150 ns. The electrical pulser requirements are challenging, and the subject of an extensive R&D program.

Figure 2.4-7 shows beam deflection vs. kicker time measured at the ATF storage ring at KEK with 33 cm striplines and a 5 kV, 3 MHz pulser built by FID GmbH. The main pulse easily meets the width and rate requirement for 6 ns bunch spacing, although at half the desired amplitude and with undesireable structure before and after the main pulse.

The positron injection kick amplitude is $\approx 20\sigma_x$ of the damped beam, so if the extraction kick amplitude is the same, a 0.5% amplitude jitter would give a 1 σ horizontal beam jitter. This results in an extraction kicker amplitude jitter tolerance in the 10^{-3} range. A similar tolerance applies to the kicker amplitude for bunches before and after the target bunch in the ring bunch train. As a tolerance on the absolute kicker field before and after the pulse, this is very difficult to achieve and is the subject of ongoing R&D.

The septum magnets are modeled after the Argonne APS injection septa. The thin (2 mm) septum magnet has a 0.73 T field, and the thick (30 mm) septum magnet has a 1.08 T field. Each magnet has an effective length of 1 m. Both magnets are pulsed once per linac cycle to reduce power dissipation, with eddy currents in the septum shielding the circulating beam. A half-sine pulse of about 10 ms width is used, and post-regulation is required to produce a 1 ms plateau flat to 10^{-4}.

2.4.4   Accelerator Components

The damping ring has conventional electromagnets for the dipole, quadrupole, sextupole, and corrector magnets. This technology choice offers flexibility for tuning and optimizing the rings as well as for adjusting the operating beam energy by a few percent around the nominal value of 5 GeV. Superconducting wigglers based on the CESR-c design [31] provide sufficient field quality that the wigglers impose no limitation on the damping ring dynamic aperture. The large wiggler aperture improves the ring acceptance for the large injected positron beam and reduces the growth of the electron cloud in the wiggler region. Power supplies and controllers are located in alcoves at the centers of the RF-wiggler straights. Magnet counts are shown

Pulse timing v.s. kick angle(FID FPG-3000M)
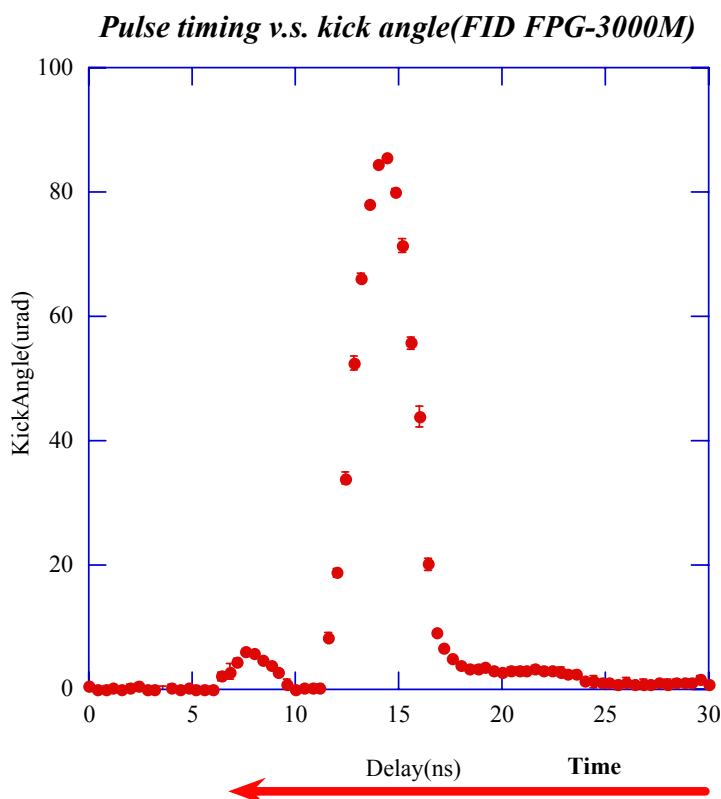
FIGURE 2.4-7. Kick angle vs. time. Note that time increases to the left here.

TABLE 2.4-2
Magnet types and counts for a single ILC Damping Ring using the OCS6 lattice. These counts do not include injection and extraction line magnets nor magnets, kickers, and septa associated with the damping ring abort beam dump. Wiggler magnets are superconducting, all others are room-temperature.

Type	Number	Power Method
Dipoles (6 m)	114	6 strings, 1 per arc
Dipoles (3 m)	12	6 strings, 1 per arc
Quadrupoles	747	Individual
Sextupoles	504	Individual
Horizontal correctors	150	Individual
Vertical correctors	150	Individual
Skew quadrupoles	240	Individual
Wigglers	80	Individual
Kickers	64	Individual
Septa	4	Individual

in Table 2.4-2. Table 2.4-3 gives the key magnet parameters and maximum higher-order harmonic content specifications.

The superconducting damping wigglers are 4.5 K devices with static heat loads of 2 W/m

TABLE 2.4-3

Target field tolerances at a reference radius of 20 mm for damping ring magnets. Magnet aperture radii are 30 mm except for the wigglers. For the wigglers, the operating field is 1.67 T and the field quality is specified by the observed roll-off for a horizontal displacement from the beam axis by the indicated distance. The maximum KL-value specifies the nominal strength of the strongest magnet of each magnet type.*(Wigglers have reference radius 20 mm (H); aperture radius 37.5 mm (H), 45 mm (V))*

Type	Max KL	L [m]	Max field error	# of types
Dipoles	0.0524	6 ; 3	2×10^{-4}	2
Quadrupoles	0.31 m^{-1}	0.3	2×10^{-4}	4
Sextupoles	0.24 m^{-2}	0.25	2×10^{-3}	1
H correctors	0.002	0.25	5×10^{-3}	1
V correctors	0.002	0.25	5×10^{-3}	1
Skew quads	0.03 m^{-1}	0.25	3×10^{-3}	1
Wigglers	–	2.5	3×10^{-3}	1

or less, based on CESR-c experience. To avoid a significant dynamic heat load, care must be taken to ensure that only tiny amounts of scattered synchrotron radiation reach the cold mass. Two of the wigglers are co-located in the damping ring straight sections with the superconducting RF cavities, where the necessary crygenic infrastructure is readily available. The other wigglers are fed by transfer lines, with a single transfer line infrastructure for both rings.

All quadrupoles, sextupoles, wigglers and corrector magnets (dipole, skew quadrupole, and possibly other multipoles yet to be specified) have individual power supplies. Individual control of the quadrupole and sextupole magnets significantly enhances the ability to tune and locally correct the machine optics in a ring with very aggressive operating parameters. Individual power supplies for the wigglers offer simplified control in the event of a magnet quench by eliminating the power system coupling between magnets. Because of the long distances between individually powered magnets and the alcoves, the power supply system uses bulk supplies located in the main alcoves that power a master "bus" from which DC-to-DC converters supply power to individual magnets. This design minimizes cable heat loads in the ring and provides a more efficient power system. For the dipole magnets, each arc section is powered separately. The pulsed power supplies for the stripline kickers require short cable runs to preserve the necessary timing synchronization, and must be located in the tunnel or in small secondary alcoves near each group of kickers.

2.4.4.1 RF System

The damping ring RF frequency of 650 MHz has a simple relationship with the main linac RF (1.3 GHz) to accommodate varying bunch patterns. While high power 650 MHz RF sources are not commercially available, several major klystron manufacturers can develop them by modifying 500 MHz klystrons of equivalent power level. Similarly, the RF cavity units can be designed by scaling from existing 500 MHz superconducting module designs currently in operation at CESR, KEK, and elsewhere. The RF cryomodule dimensions are 3.5 m in length and 1.5 m in diameter [31].

For either ring, the beam power and the total RF voltage is shared among 18 supercon-

TABLE 2.4-4
Estimated 650 MHz SC cavity parameters (scaled from 500 MHz model) for both electron and positron damping rings.

Parameter	Units	All Stations On	One Station Off
Frequency	MHz	650	
Active cavity length	m	0.23	
R/Q [Ω]		89	
Operating Temperature	K	4.5	
Standby losses at 4.5 K	W	30	
Operating SC modules per ring		18	14
Accelerating gradient	MV/m	5.8	7.5
Accelerating voltage	MV	1.33	1.72
Q_0 at operating gradient	10^9	1.0	0.9
RF cyrogenic losses per cavity	W	20	33
Total cryo losses per ring	W	900	925
Beam power per cavity	kW	194	250
Klystrons per ring		5	4
Klystron emitted power	kW	780	1000

ducting cavities. These are located in two RF straight sections roughly 40 m long. Operating 18 SC-cavity modules per ring ensures adequate energy and beam power margin in case of an RF station fault, and permits continued operation with 14 cavity modules at full performance by increasing the RF field in the remaining units. Table 2.4-4 summarizes the RF system main features and compares the parameters for the nominal case with that when one RF station is off. Parameters are scaled from the 500 MHz units developed by industry and being operated in various laboratories.

Two or three RF stations are located in each RF-wiggler straight section, as indicated schematically in Figure 2.4-8. Each klystron can feed 4 SC cavities by means of a distribution system having magic-tees for power splitting and 3-port circulators for protecting the klystron. To guarantee sufficient power margin in case of a klystron fault, the power sources are 1.2 MW CW. One "hot-spare" station in each ring is operated with only two cavities, rather than four. The stations are upstream of the wigglers at opposite ends of the straight section tunnel, with waveguides connecting them to the klystrons housed in centrally located alcoves having access shafts to the surface.

The selection of 650 MHz requires a redesign of existing 500-MHz sources, cavities and cryomodules. A critical element is the input coupler because the power handling capability must be kept at a level of about 260 kW CW, comparable to presently operating 500 MHz systems. The HOM dampers and cryostat mechanical details must also be revised.

2.4.4.2 Cryogenic Plant

The DR cavities operate at 4.5 K and the total cryogenic losses per ring are approximately 900 W with 14 modules operating in case of one klystron fault. The design has one cryogenic
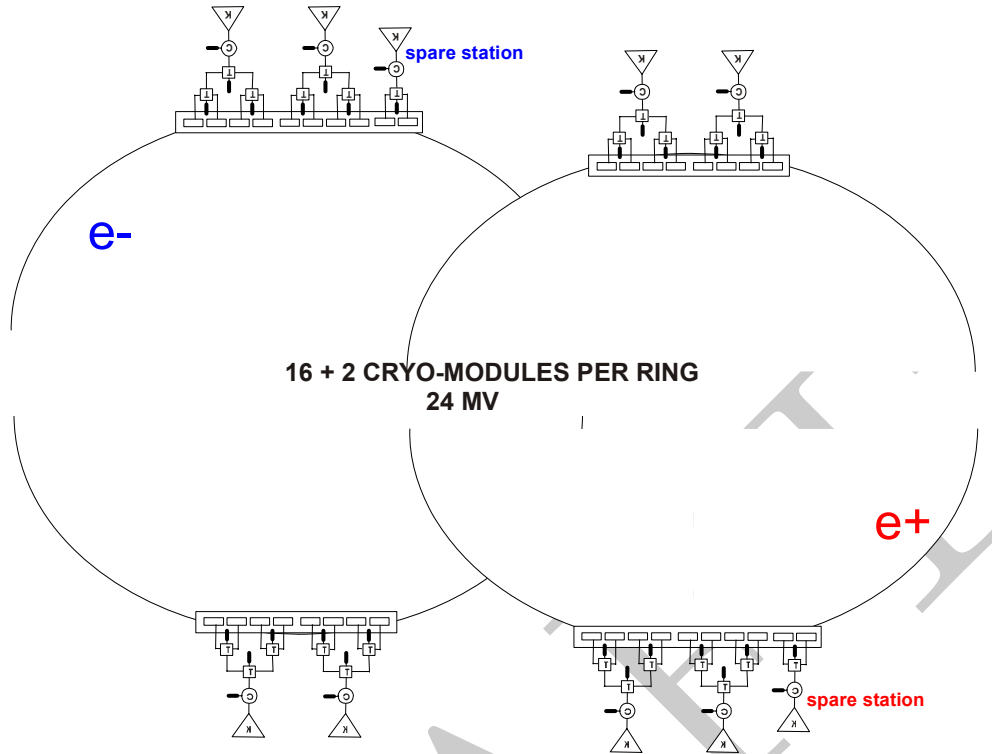
FIGURE 2.4-8. Schematic layout of DR RF systems. Each of the two RF-wiggler sections accommodates three stations from one ring, and two from the other. All stations are situated upstream of the wiggler in that ring.

plant in each RF straight section. With this choice, the helium transfer lines to the RF are not very long and do not impact the cryogenic plant cost. The cryogenic plant capability must be sufficient to handle the worst-case scenario of one klystron fault, where the cryogenic power in the other straight section could increase to a total of 925 W. With the standard refrigerator efficiency of 0.3% at 4.5 K, the total wall-plug power for each straight-section refrigerator is about 300 kW. Table 2.4-5 summarizes the specifications of the cryogenic system.

TABLE 2.4-5
Main specifications of the RF cryogenic system, with 18 modules per ring.

Parameter	Units	Value
Nominal cryogenic losses per straight section	W	900
Design cryogenic losses per straight section	W	925
Wall plug power per cryogenic plant	kW	300
Total number of cryogenic plants		2

2.4.4.3 Fast Feedback System

With thousands of bunches circulating in the ring, wakefields induced in vacuum chamber components can give rise to coupled-bunch instabilities that cause bunch jitter and/or emittance growth. To combat this, the rings have fast bunch-by-bunch feedback systems in all

three oscillation planes (longitudinal, horizontal and vertical) [33]. Modern commercial FP-GAs (Field Programmable Gate Arrays) can easily manage the requirements of the feedback systems in terms of speed and number of bunches. The bandwidth of the fast feedback system must be at least $f_{\rm RF}$ (that is, 650 MHz). This means that every block of the system must have the capability to manage the full bandwidth except for the power section (amplifiers and kickers), where half bandwidth is sufficient. The main elements of each system are the analog front end, digital processing unit, analog back end, amplifier and kicker.

The pickups are 4-button monitors (two or three for each beam line) with at least full bandwidth and adequate dynamic range. The analog front ends must be capable of extracting the oscillation signals from the monitors in each of the three planes (L, H, V) and giving them to the digital sections with a swing in the range of ∼0.5 V (typical of many analog-to-digital converters).

To minimize the quantization noise and have an adequate dynamic range, the digital units are based on a 16-bit signal processing system. The processing is able to compute the correction signal for all buckets (including the empty ones) to decouple the feedback behavior from the fill pattern. This means that all feedback systems must have the capability to process, in real time, 14,516 input/output channels, although the real bunches are in, at most, 5,534 buckets. The digital unit sampling frequency is 650 MHz. A real time FIR (finite impulse response) filter (with ≥50 taps) provides the correction synchrotron or betatron phase advance using only one pickup for each system. The feedback setup should be easily configurable using software tools. A down-sampling feature is also needed to manage very low oscillation frequencies.

The analog back-end systems adapt the output correction signals to the power section. The longitudinal kicker (a cavity) works at a frequency between 800 and 1600 MHz, whereas the transverse kickers (striplines) operate at baseband (from 10 kHz up to half the bandwidth of the fast feedback system). Each power section has four 250 W amplifiers (1 kW total), with the bandwidth required by the kicker.

2.4.4.4 Vacuum System

The vacuum design for the damping rings is similar to those for modern storage rings and synchrotron radiation sources. The need to avoid the fast ion instability leads to very demanding specifications for the vacuum in the electron damping ring: <0.5 nTorr CO-equivalent in the arc cells, <2 nTorr CO-equivalent in the wiggler cells, and <0.1 nTorr CO-equivalent in the straight sections [34]. A combination of coatings, grooved chamber profiles, and clearing electrodes is required to suppress the electron cloud in the positron damping ring. The baseline design uses a non-evaporable getter (NEG) coated aluminum tubular vacuum chamber. With NEG coating, fewer pumps with lower pumping speed are required. Issues associated with the ultimate lifetime of the NEG material, its regeneration, and the synchrotron radiation power density on the chamber walls need further study. Each of the 120 arc cells requires one sputter ion pump with an effective pumping speed of 20 L/s installed immediately downstream of the dipole. In the long straight sections, similar sputter ion pumps are required every 10 m for $0 < z < 80$ m, every 20 m for $80 < z < 160$ m, and every 40 m for $160 < z < 400$ m.

The wiggler straight section vacuum system consists of separate chambers for the wiggler and quadrupole sections. A cross section of the wiggler chamber is shown in Figure 2.4-9. The chamber is a machined and welded aluminum unit, designed as a warm-bore insert, mechanically decoupled from the wiggler and cryogenic system. A NEG pumping system

and photon absorber are incorporated in antechambers. Integral cooling is incorporated to minimize distortion of the chamber and thermal load on the wiggler cryostat during NEG regeneration. A TiZrV NEG surface coating is used on the main chamber bore to minimize secondary electron yield [35]. Clearing electrodes are also incorporated to reduce the electron cloud.
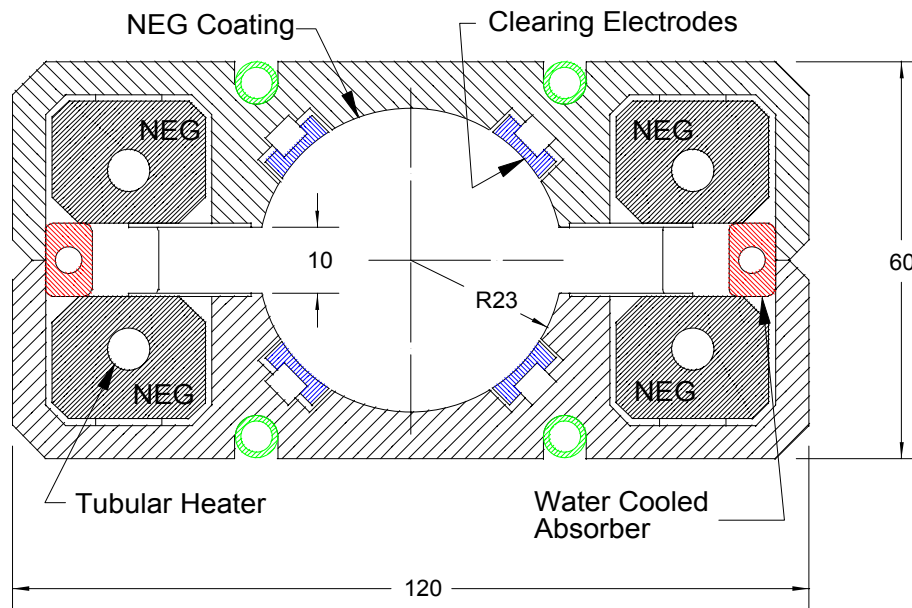
FIGURE 2.4-9. ILC damping ring wiggler chamber; dimensions in mm.

The photon absorbers are hollow water-cooled copper conductor designed to absorb photon power from upstream wigglers in the same straight section. Power radiated from the first wiggler in the straight section is intercepted initially by wiggler number three. Intercepted power increases for successive wigglers up to number nine; thereafter, a constant 3 W/mm^2 peak power density is reached. The total power absorbed per wiggler is 26 kW, that is, 13 kW per absorber.

The NEG pumping system is similar to that designed for the PEP-II B Factory. The assembly consists of NEG-coated fins and an integral heating rod for regeneration. The estimated pumping speed for CO is 1000 L/s/m. With a total incident photon flux of 2×10^{18} photons/s/m, the estimated yield of CO is 2×10^{13} molecules/s/m. This results in an equilibrium CO partial pressure of 7×10^{-10} Torr.

Between each wiggler chamber is a separate chamber for the quadrupole section. This chamber is welded aluminum, incorporating TiZrV NEG coating for secondary electron yield reduction. Bellows, a BPM assembly, and an ion pump for pumping non-reactive gases are included. The ion pump also serves as a vacuum gauge. The quadrupole chamber is completely shadowed by the wiggler chamber photon absorbers and does not absorb any of the photon power from upstream wigglers.

2.4.4.5   Cost Methodology

Several of the technical subsystems in the damping rings have specific requirements that distinguish them from corresponding subsystems in other parts of the ILC; generally, this is because of the relatively high average current and synchrotron radiation power (for the vacuum system, wigglers, and fast feedback systems), CW operation (for the RF system), or unique functionality (for the injection/extraction kickers). The cost estimates for these damping-ring-specific designs were developed by the damping ring group.

The RF system is CW and operates at 650 MHz, a different frequency from the RF systems used elsewhere in the ILC. The designs of high-power RF components, such as klystrons and circulators, were scaled from commercially available 500 MHz devices. Estimates from klystron manufacturers indicated that development costs would increase the total cost by roughly the cost of one additional unit at the standard catalog price. Manufacturing costs for the cavity cryomodules were assumed to be the same as for commercial versions of 500 MHz systems developed at Cornell and KEKB, with increased engineering effort to account for the rescaling, or in some cases redesign, of the existing subcomponents.

A preliminary design for the vacuum system was based on estimates for required vacuum levels (set by ion instabilities in the case of the electron damping ring), handling of synchrotron radiation, aperture requirements, and conditioning rates. Standard commercial component costs were used for extruded aluminum vacuum chambers, bellows, pumps, valves, and bake-out systems. Coating the chambers with NEG was assumed to be done with in-house labor. The cost estimate for the complex damping wiggler vacuum chamber was based on fabrication of similar systems for other projects.

The engineering and fabrication experience for the CESR-c wigglers were used to provide reliable cost estimates for the ILC damping wigglers, taking proper account of the well-defined differences in specification. Costs for the kicker pulser were based on a commercially available pulser (a fast ionization dynistor, or FID, device) that comes close to meeting the specifications for the damping ring injection/extraction kickers; this cost dominates the total cost of the injection/extraction system. Other components, including the stripline electrodes and the septa, are relatively conventional, and costs were based on similar existing devices.

Costs of the ILC damping ring fast feedback systems were taken directly from comparable systems in existing machines. Power amplifiers dominate the cost of the fast feedback systems. Amplifiers operating in the appropriate parameter regime are available commercially, and costs for these were obtained from an experienced manufacturer.

2.5   RING TO MAIN LINAC

2.5.1   Overview

The ILC Ring to Main Linac (RTML) is responsible for transporting and matching the beam from the Damping Ring to the entrance of the Main Linac. The RTML must perform several critical functions:

- transport of the electron and positron beams from the damping rings, at the center of the ILC accelerator complex, to the upstream ends of their respective linacs ("geometry matching");

- collimation of the beam halo generated in the damping ring;

- rotation of the spin polarization vector from the vertical to any arbitrary angle required at the IP;

- compression of the long Damping Ring bunch length by a factor of $30 \sim 45$ to provide the short bunches required by the Main Linac and the IP;

In addition, the RTML must provide sufficient instrumentation, diagnostics and feedback (feedforward) systems to preserve and tune the beam quality.

2.5.2   Beam Parameters

The key beam parameters of the RTML are listed in Table 2.5-1. Parameters are shown for the nominal configuration and for the "low charge" configuration (which requires a shorter bunch at the IP).

TABLE 2.5-1
Basic beam parameters for the RTML.

Parameter	Nominal Value	Low Charge Value
Initial energy	5.0 GeV	
Initial energy spread	0.15%	
Initial emittances	8.0μm $\times$ 20 nm	
Initial horizontal beam jitter	1 σ	
Initial bunch length	9.0 mm	
Final bunch length	0.3 mm	0.2 mm
Final energy	15.0 GeV	13.7 GeV
Final energy spread	1.5%	2.7 %
Final horizontal beam jitter	0.1σ	
ISR emittance growth	0.9 μm	0.8 μm
Emittance budget	1μm $\times$ 4 nm	

2.5.3 System Description

2.5.3.1 Layout

Figure 2.5-1 depicts schematically the layout and location of the various sub-beamlines of the RTML. The RTML includes the long low-emittance transport from the Damping Ring, followed by a 180° turn-around, the spin-rotation and two-stage bunch compression sections. The beamlines upstream of the turnaround are collectively known as the "upstream RTML," while those from the turnaround to the launch into the main linac are collectively known as the "downstream RTML." Figure 2.5-2 shows the Twiss functions of the downstream RTML. In order to accommodate the different damping ring elevations and linac lengths, the electron and positron RTMLs have slight differences in their long transport sections, but are otherwise identical.
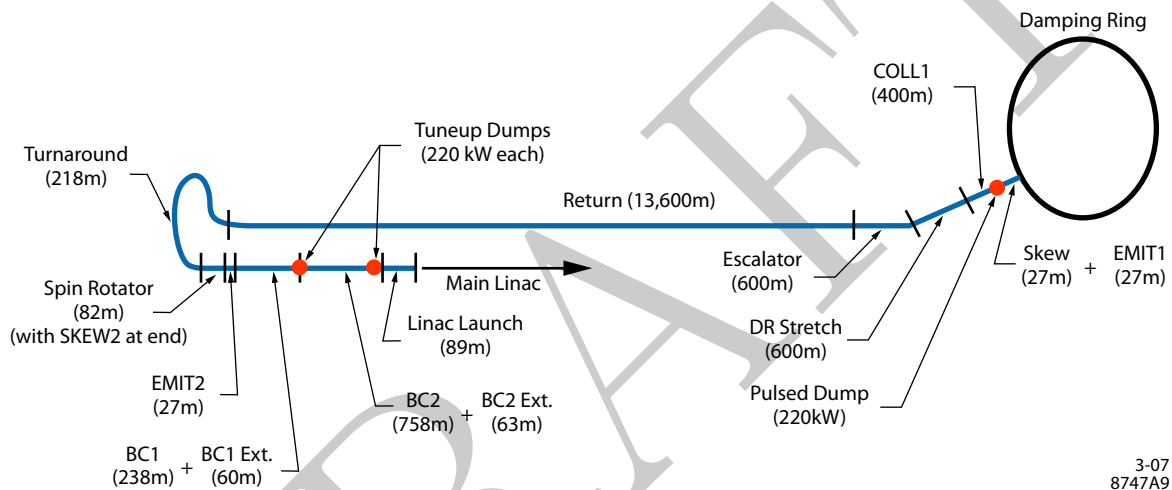
FIGURE 2.5-1. Schematic of RTML, indicating the various functions described in the text.

Each of the key functions of the RTML listed in 2.5.1 is supported by several of the sub-beamlines shown in Figure 2.5-1.

2.5.3.2 Geometry Match

Following extraction from the damping rings, the beams are brought parallel to the long axis via the 90° arcs in the Arc sections; transported from the the damping ring elevation to the main linac tunnel elevation via the vertical doglegs in the Escalator sections; transported out to their respective ends of the site via the Return lines, which are suspended from the ceiling of the main linac tunnel; and reversed in direction by the Turnaround sections. In addition, small vertical and horizontal doglegs at the upstream end of the Turnaround change the beam elevation from the ceiling of the linac tunnel to the nominal linac elevation, and adjust the horizontal position between the Return line axis and the main linac axis.

2.5.3.3 Collimation

The RTML's betatron collimation section is downstream of the damping ring extraction arc. It is constructed from two sets of thin spoiler and thick absorber pairs, placed 90° apart
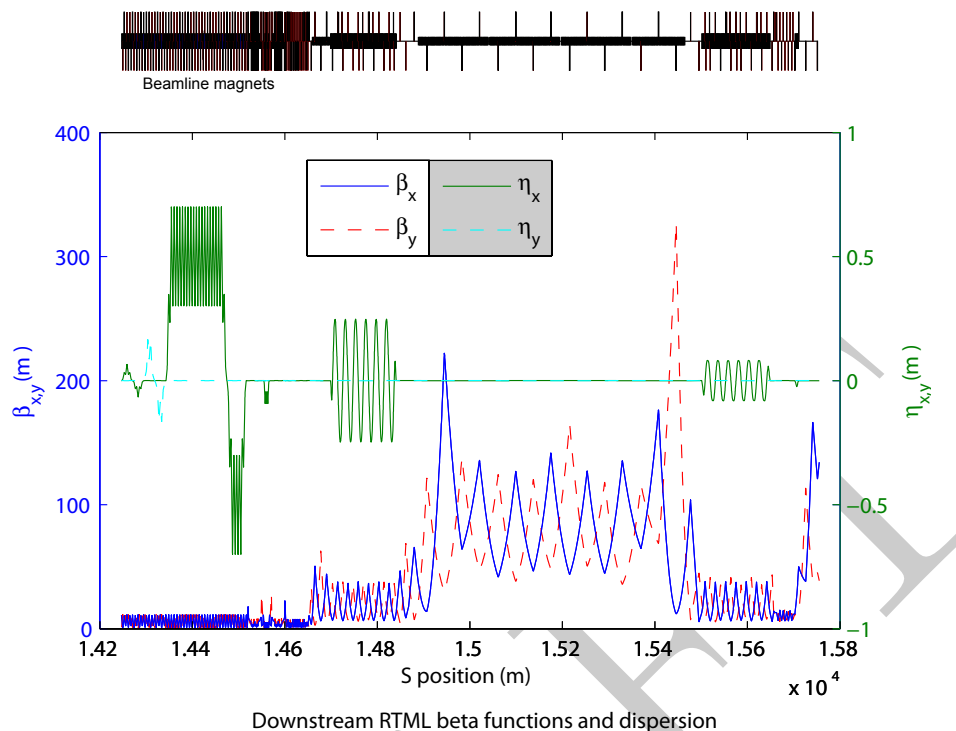
FIGURE 2.5-2. Twiss functions of the downstream RTML, from the start of the turnaround to the match into the main linac.

in betatron phase. This is considered sufficient to reduce the halo density by 3-4 orders of magnitude. The thin spoilers are needed to protect the absorbers from a direct hit from an errant beam in the event of some machine error [38]. The spoilers in the upstream section are protected by their proximity to the damping ring, which permits extraction to be halted prior to spoiler damage if the beam begins to hit the spoiler. There are additional collimators for energy collimation placed in the Turnaround, and in the wigglers of the Bunch Compressor.

2.5.3.4 Spin Rotation

The beam polarization in the damping rings is vertical, and this polarization is transported with negligible loss or precession to the end of the Turnaround. At that point it is necessary to be able to reorient the spin vector to any direction required by the experimental physicists. To achieve this, both the electron and positron RTMLs have a complete spin rotation system. Each system includes a pair of superconducting solenoids, followed by an arc with a net 7.9° bend angle, which is in turn followed by another pair of solenoids. By adjusting the excitation in the solenoid pairs, the spin vector at the end of the spin rotator can be oriented in any desired direction. In order to rotate the spin without introducing undesired x-y coupling, the solenoid-based rotators each use a pair of identical solenoids separated by a quadrupole lattice which introduces a $+I$ transformation in the horizontal plane and a $-I$ transformation in the vertical plane [39], the net effect of which is to cancel the cross-plane coupling.

2.5.3.5 Bunch Compression

In order to achieve the required bunch compression factor of 30-45, a two-stage system is adopted. A single-stage compressor would produce a beam with a relative energy-spread

TABLE 2.5-2
Key parameters for the two-stage bunch compressor in the nominal configuration, when compression to 0.3 mm RMS length is desired.

Parameter	Nominal BC1 Value	Nominal BC2 Value
Initial energy	5 GeV	4.88 GeV
Initial energy spread	0.15%	2.5%
Initial bunch length	9 mm	1.0 mm
RF voltage	448 MV	11.4 GV
RF phase	-105°	-27.6°
Wiggler R_{56}	-376 mm	-54 mm
Final energy	4.88 GeV	15.0 GeV
Final energy spread	2.5%	1.5%
Final bunch length	1.0 mm	0.3 mm

that is unacceptably high, leading to unachievable alignment tolerances in both the RTML and the early stages of the Main Linac.

Table 2.5-2 summarizes the important parameters for both the first-stage (BC1) and second-stage (BC2) compressor.

In addition to flexibility in the final bunch length, the two-stage bunch compressor allows some flexibility to balance longitudinal and transverse tolerances by adjustment of the wiggler magnet strengths, RF voltages, and RF phases. The nominal compressor configurations ease tolerances on damping ring extraction phase, damping ring bunch length, and bunch compressor phase stability, at the expense of tightening the tolerances on transverse alignment of accelerator components. There are also alternate configurations which loosen transverse alignment tolerances but tighten the longitudinal (*i.e.* phase) tolerances.

The linacs in both compressor stages use standard SCRF cryomodules and an RF power unit configuration similar to that of the Main Linac (*i.e.* one klystron driving three cryomodules). The first-stage compressor has a single RF unit with 8 cavities and one quadrupole in each of its 3 cryomodules; the second-stage compressor uses 14 RF units (plus one redundant spare) which are identical to the main linac configuration (*i.e.*, 26 cavities and 1 quad per unit, arranged in 3 cryomodules). The stronger focusing in the first stage is necessary to mitigate the higher wakefields and cavity-tilt effects resulting from the longer bunch length in the compressors. The first-stage has no spare RF unit; instead, a spare klystron and modulator are connected via a waveguide switch to provide some degree of redundancy.

Each bunch compressor stage includes a 150 m lattice of bend magnets("wiggler") which provides the momentum compaction required for bunch compression. As implied by the name, the wigglers introduce no net offset or angle to the beam.

Figure 2.5-3 shows the longitudinal phase space after compression from 9 mm to 0.3 mm RMS length.

2.5.3.6 Tuning, Correction, and Operations

The diagnostic, correction, and operational requirements of the RTML have been carefully integrated into the design of the entire beamline.

RMS = 0.30032 mm, fit = 0.29041 mm

RMS = 1.7351%, fit = 1.4126%
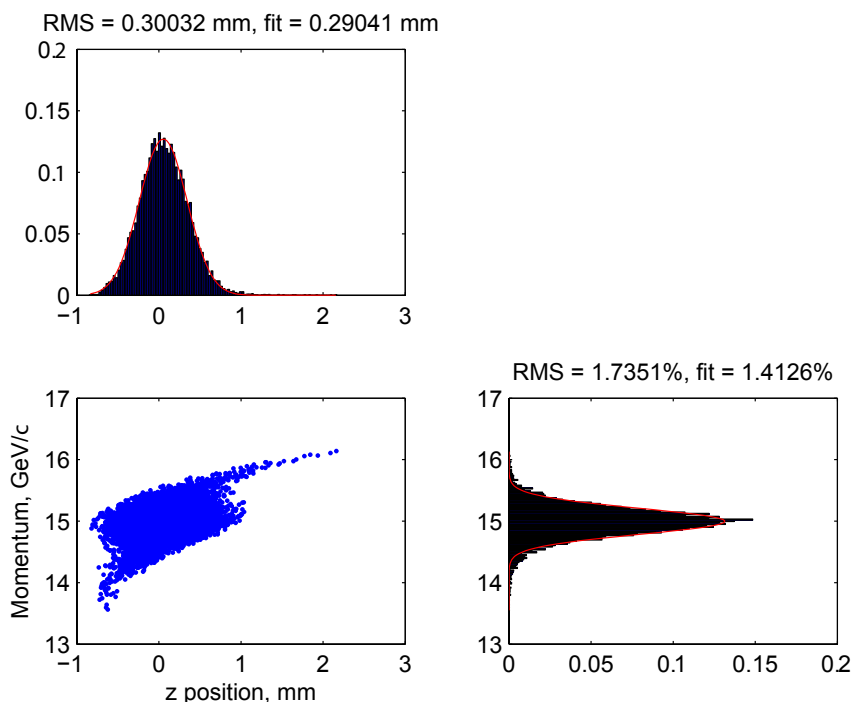
FIGURE 2.5-3. Longitudinal phase space of the compressed bunch.

Global Dispersion Correction: The Arc, the BC1 wiggler, and the BC2 wiggler contain normal and skew quads in regions of horizontal dispersion which are used to tune any residual dispersion due to misalignments and errors. The quads are arranged in pairs, with an optical $-I$ transform between the two quads in a pair; this permits the tuning of the dispersion without introducing any betatron coupling or beta beats. The dispersions in the Turnaround are adjusted by tuning normal quads in the horizontal and vertical doglegs at the upstream end of the Turnaround; similarly, tuning the normal quads in the Escalator allows its vertical dispersion to be tuned.

Global Coupling Correction: There are two decoupling regions: the first is immediately downstream of the Arc, and the second is immediately downstream of the Spin Rotator. Each decoupling region contains 4 orthonormal skew quads in regions of zero dispersion, which allow complete and independent control of the 4 betatron coupling terms. The first station is conceptually intended to correct the coupling introduced by the damping ring extraction system, while the second corrects coupling generated by errors in the spin rotation system, as well as the remaining betatron coupling from small rotation errors on the RTML quads.

Emittance Measurement: There are three emittance measurement stations: the first is between the first decoupling section and the first collimation section, the second is between the second decoupling station and the bunch compressor, and the third is between the bunch compressor and the linac. Each of these stations contains 4 laser wire scanners embedded in a FODO lattice with 45° betatron phase; each station can therefore measure the projected x and y emittances of the beam. The first station can be used to tune the Arc dispersion and the skew quads in the first decoupler; the second station can be used to tune the Turnaround dispersion and the skew quads in the second decoupler; the third station can be used to tune the dispersion correction in the Bunch Compressor wigglers. Although none of the systems have the capability to directly measure normal-mode emittances and coupling parameters,

the optics of the first two stations are compatible with a later upgrade if needed.

Beam Position Monitors: There are cavity-type beam position monitors (BPMs) with horizontal and vertical readout at each quadrupole, with additional units close to the laser wires, at high-dispersion regions in the Bunch Compressor wigglers, and at other critical locations. The BPMs in the room-temperature sections of the RTML almost all operate in the 6 GHz frequency band ("C-band"), while the BPMs in the cryomodules and at a handful of other locations use the 1 GHz frequency band ("L-band"). At the nominal bunch charge of 3.2 nC, these BPMs can achieve sub-micron single-bunch resolution. The standard RTML BPM requires high precision and stability of the BPM's offset with respect to the device's mechanical center; a few of the BPMs have other requirements, such as high bandwidth or low latency.

Longitudinal Diagnostics: Each stage of the Bunch Compressor contains arrival-time (phase) monitors, beam position monitors at dispersive locations, X-ray synchrotron light monitors, and two types of bunch length monitors (a passive device based on measuring the RF spectrum of the bunch, and an active device based on transverse deflecting cavities [40]). The active bunch length monitor can also measure the correlation between energy and longitudinal position within a bunch.

Feedback and Feed-Forward: The RTML is not expected to require any intra-train trajectory feedback systems, although there will be a number of train-to-train (5 Hz) trajectory feedbacks. In addition, the beam energy at BC1 and BC2 will be controlled by a 5 Hz feedback, as will the electron-positron path length difference through their respective bunch compressors (see 2.5.4). There is also a trajectory feed-forward that uses BPMs at the end of the Return line to make bunch-by-bunch orbit measurements, which are fed forward to a set of fast correctors downstream of the Turnaround. The speed-of-light travel time between these two points is about 600 nanoseconds, and the actual distance between them is on the order of a few tens of meters; the resulting delay of the beam relative to the propagated signal is more than adequate for a digital low-latency orbit correction system [41].

Intermediate Extraction Points: There are 3 locations where the beam in the RTML may be directed to a beam dump: downstream of the first collimation section, downstream of BC1, and downstream of BC2. At each of these locations, there are both pulsed kickers and pulsed bends for beam extraction. The kickers are used when an intra-train extraction is required, for example during a machine protection fault, while the bends are used to send entire trains to their beam dumps. The pulsed bends can also be energized by DC power supplies if a long period of continual dump running is foreseen. All 3 dumps are capable of absorbing 220 kW of beam power. This implies that the first 2 dumps, which are at 5 GeV, can absorb the full beam power, while the third dump, at 15 GeV, can absorb only about 1/3 of the nominal beam power. Full trains can be run to this dump at reduced repetition rate, or short trains at full rate.

Access Segmentation: During personnel access to the main linac or downstream RTML beam tunnels, the beam can be sent to the first RTML dump. For additional safety, the bend magnets in the Escalator are switched off and additional personnel protection stoppers are inserted into the beamline. This allows the damping ring complex, the Arc dispersion tuning, the first decoupler, and the first emittance measurement station to be used at full beam power during linac access.

2.5.4 Accelerator Physics Considerations

A number of beam dynamics issues were considered in the design and specifications of the RTML.

Incoherent (ISR) and Coherent (CSR) Synchrotron Radiation: Current estimates indicate that the horizontal emittance growth from ISR will be around 90 nm (1.1%) in the Arc, 380 nm (4.8%) in the Turnaround, and 430 nm (5.4%) in the Bunch Compressor in its nominal configuration. Vertical emittance growth from ISR in the Escalator is negligible.

Studies of the ILC Bunch Compressor indicate that there are no important effects of coherent synchrotron radiation, primarily because the longitudinal emittance of the beam extracted from the damping ring is so large [42].

Stray Fields: Studies have found that fields at the level of 2.0 nTesla will lead to beam jitter at the level of 0.2 σ_y [43]. This is considered acceptable since the orbit feed-forward will correct most of this beam motion. Measurements at existing laboratories [44] indicate that 2 nTesla is a reasonable estimate for the stray field magnitude in the ILC. Emittance growth considerations also place limits on the acceptable stray fields, but these are significantly higher.

Beam-Ion Instabilities: Because of its length and its weak focusing, the electron Return line will have potential issues with ion instabilities. To limit these to acceptable levels, the base pressure in the Return line must be limited to 20 nTorr [45].

Static Misalignments: The main issues for emittance growth are: betatron coupling introduced by the Spin Rotator or by rotated quads; dispersion introduced by rotated bends, rotated quads in dispersive regions, or misaligned components; wakefields from misaligned RF cavities; and time-varying transverse kicks from pitched RF cavities.

Studies of emittance growth and control in the region from the start of the Turnaround to the end of the second emittance region have shown that a combination of beam steering, global dispersion correction, and global decoupling can reduce emittance growth from magnetostatic sources to negligible levels, subject to the resolution limits of the measurements performed by the laser wires [46, 47]. Although the upstream RTML is much longer than the downstream RTML, its focusing is relatively weak and as a result its alignment tolerances are actually looser. Studies have shown that the same tuning techniques can be used in the upstream RTML with the desired effectiveness [48]. The tolerances for RF cavity misalignment in the RTML are large (0.5 mm RMS would be acceptable) because the number of cavities is small and the wakefields are relatively weak [49]. Although in principle the RF pitch effect is difficult to manage, in practice it leads to a position-energy correlation which can be addressed by the Bunch Compressor global dispersion correction [50]. A full and complete set of tuning simulations have not yet been performed, but it is expected that the baseline design for the RTML can satisfy the emittance preservation requirements.

Phase Jitter: Phase and amplitude errors in the bunch compressor RF will lead to energy and timing jitter at the IP, the latter directly resulting in a loss of luminosity. Table 2.5-3 shows the RMS tolerances required to limit the integrated luminosity loss to 2%, and to limit growth in IP energy spread to 10% of the nominal energy spread [51]. The tightest tolerance which influences the arrival time is the relative phase of the RF systems on the two sides: in the nominal configuration, a phase jitter of the electron and positron RF systems of 0.24° RMS, relative to a common master oscillator, results in 2% luminosity loss. The tight tolerances will be met through a three-level system:

- Over short time scales, such as 1 second, the low-level RF system will be required to

TABLE 2.5-3
Key tolerances for the two-stage bunch compressor.

Parameter	Arrival Time Tolerance	Energy Spread Tolerance
Correlated BC phase errors	0.24°	0.35°
Uncorrelated BC phase errors	0.48°	0.59°
Correlated BC amplitude errors	0.5%	1.8%
Uncorrelated BC amplitude errors	1.6%	2.8%

keep the two RF systems phase-locked to the level of 0.24 degrees of 1.3 GHz. See Section 3.9 for a fuller description of the low-level RF system.

- Over longer time periods, the arrival times of the two beams will be directly measured at the IP and a feedback loop will adjust the low-level RF system to synchronize the beams. This system is required to compensate for drifts in the low-level RF phase-locking system which occur over time scales long compared to a second.

- Over a period of many minutes to a few hours, the arrival time of one beam will be "dithered" with respect to the arrival time of the other beam, and the relative offset which maximizes the luminosity will be determined. This offset will be used as a new set-point for the IP arrival-time feedback loop, and serve to eliminate drifts which arise over time scales long compared to a minute.

Halo Formation from Scattering: Halo formation is dominated by Coulomb scattering from the nuclei of residual gas atoms, and it is estimated that 100 nTorr base pressure in the downstream RTML will cause approximately 9×10^{-7} of the beam population to enter the halo [52]. A similar calculation was performed for the upstream RTML, which indicates that 20 nTorr base pressure will cause approximately 2×10^{-6} of the beam population to enter the halo. This is well below the budget of 10^{-5} which has been set for all beamlines between the damping ring and the BDS collimators (see 2.7.3.2.2).

Space Charge: In the long, low-energy, low-emittance transfer line from the damping ring to the bunch compressor, the incoherent space-charge tune shift will be on the order of 0.15 in the vertical. The implications of such large values in a single-pass beamline have not been studied.

Collimator Wakefields: Assuming collimation of the beam extracted from the damping ring at $10\sigma_x$, $60\sigma_y$, and $\pm1.5\%$ ($10\sigma_\delta$) in momentum, the worst-case jitter amplification for untapered, "razor-blade" spoilers is expected to be around 10% in x, around 75% in y, and the contribution to x jitter from energy jitter is expected to be negligible [53, 54]. The vertical jitter amplification figure is marginal, but can be substantially improved through use of spoilers with modest longitudinal tapers. The other collimator wakefield "figures of merit" are acceptable even assuming untapered spoilers.

2.5.5 Accelerator Components

Table 2.5-4 shows the total number of components of each type in each RTML. The number of quadrupoles, dipole correctors, and BPMs is larger in the electron RTML than in the positron RTML due to the longer electron Return line; for these 3 component classes, the different totals for each side are shown in Table 2.5-4. Each quadrupole and dipole has its own power supply, while other magnets are generally powered in series with one power supply supporting many magnets. The cost estimate for the S-band dipole-mode structures

was developed by the RTML Area Systems group based on recent experience with accelerator structure construction at IHEP; all other component cost estimates were developed by the ILC Technical and Global Systems groups.

TABLE 2.5-4
Total number of components in each RTML. Where 2 totals are shown, the larger number refers to the longer electron-side RTML, the smaller number refers to the shorter positron-side RTML.

Magnets		Instrumentation		RF	
Bends	362	BPMs	772/740	1.3 GHz cavities	414
Quads	789/752	Wires	12	1.3 GHz cryomodules	48
Dipoles	1185/1137	BLMs	2	1.3 GHz sources	$16 + 1$
Kickers	17	OTRs	5	S-band structures	2
Septa	7	Phase monitors	3	S-band sources	2
Rasters	6	Xray SLMs	2		
Solenoids	4				

Table 2.5-5 shows the system lengths for the RTML beamlines.

TABLE 2.5-5
System lengths for each RTML beamline. Where 2 values are shown, the larger number refers to the longer electron-side RTML, the smaller number refers to the shorter positron-side RTML.

Upstream RTML	Turn	Spin	Emit	BC	Dumplines
15,447 m / 14,247 m	275 m	82 m	47 m	1,105 m	180 m
Total				17,136 m / 15,936 m	
Total, excluding extraction lines				16,956 m / 15,756 m	
Footprint length				1,301 m	

2.5.5.1 Vacuum Systems

The base pressure requirement for the downstream RTML is set by limiting the generation of beam halo to tolerable levels, while in the upstream RTML it is set by the necessity of avoiding beam-ion instabilities. As described in 2.5.4, the base pressure requirement for the downstream RTML is 100 nTorr, while in the upstream RTML it is 20 nTorr. Both upstream and downstream RTML vacuum systems will be stainless steel with 2 cm OD; the upstream RTML vacuum system will be installed with heaters to allow *in situ* baking, while the downstream RTML vacuum system will not. The bending sections of the turnaround and bunch compressors are not expected to need photon stops or other sophisticated vacuum systems, as the average beam current is low, and the fractional power loss of the beam in the bending regions is already small to limit emittance growth from ISR.

2.5.5.2 Service Tunnel

There is a service tunnel that runs parallel to the beam tunnel for the full length of the RTML and is shared with other systems. All of the power supplies, RF sources, and rack-

mounted instrumentation and controls equipment and computers are installed in the service tunnel This configuration allows repairs and maintenance to be performed while minimizing disruption to the accelerator itself.

2.6 MAIN LINACS

2.6.1 Overview

The two main linacs accelerate the electron and positron beams from their injected energy of 15 GeV to the final beam energy of 250 GeV over a combined length of 23 km. This must be accomplished while preserving the small bunch emittances, which requires precise orbit control based on data from high resolution beam position monitors. The linacs utilize L-band (1.3 GHz) superconducting technology, with nine-cell standing-wave niobium cavities operating at an average gradient of 31.5 MV/m in a 2K superfluid helium bath. The choice of operating frequency is a balance between the high cavity cost due to size at lower frequency and the lower sustainable gradient due to increased surface resistivity at higher frequency. The accelerator gradient is somewhat higher than that typically achievable today and assumes that further progress will be made during the next few years in the aggressive program that is being pursued to improve cavity performance.

2.6.2 Beam Parameters

Table 2.6-1 lists the key beam parameters in the main linac. A description of the tradeoffs which led to the selection of the parameters can be found in Section 2.1.

TABLE 2.6-1
Nominal beam parameters in the ILC Main Linacs.

Parameter	Value	Units	Parameter	Value	Units
Initial beam energy	15	GeV	Initial $\gamma\epsilon_x$	8.4	μm
Final beam energy	250	GeV	Final $\gamma\epsilon_x$	9.4	μm
Particles per Bunch	2×10^{10}		Initial $\gamma\epsilon_y$	24	nm
Beam current	9.0	mA	Final $\gamma\epsilon_y$	34	nm
Bunch spacing	369	ns	σ_z	0.3	mm
Bunch train length	969	μs	Initial σ_E/E	1.5	%
Number of bunches		2625	Final σ_E/E	0.10	%
Pulse repetition rate	5	Hz	Beam phase wrt RF crest	5	°

The rms bunch length remains constant along the linacs, while the bunch fractional energy spread decreases roughly as E_0/E, where E is the beam energy and E_0 is the initial main linac beam energy. The bunches are phased 5° off-crest to minimize their energy spread. No BNS energy spread is included to suppress resonant head-to-tail bunch trajectory growth as the short-range wakefield is fairly weak. For this same reason, the focusing strength of the quadrupole lattice in the linacs is kept fairly weak to reduce emittance growth from quadrupole misalignments.

2.6.3 System Description

2.6.3.1 RF Unit

The main linacs are composed of RF units whose layout is illustrated in Figure 2.6-1 and whose parameters are listed in Table 2.6-2. Each unit has a stand-alone RF source that powers three contiguous cryomodules containing a total of 26 cavities (with 9, 8 and 9 cavities in each cryomodule, respectively). The RF source includes a high-voltage modulator, a 10 MW klystron and a waveguide system that distributes the RF power to the cavities. It also includes the low-level RF (LLRF) system to regulate the cavity field levels, interlock systems to protect the source components, and the power supplies and support electronics associated with the operation of the source. To facilitate maintenance and limit radiation exposure, the RF source is housed mainly in a separate service tunnel that runs parallel to the beam tunnel.
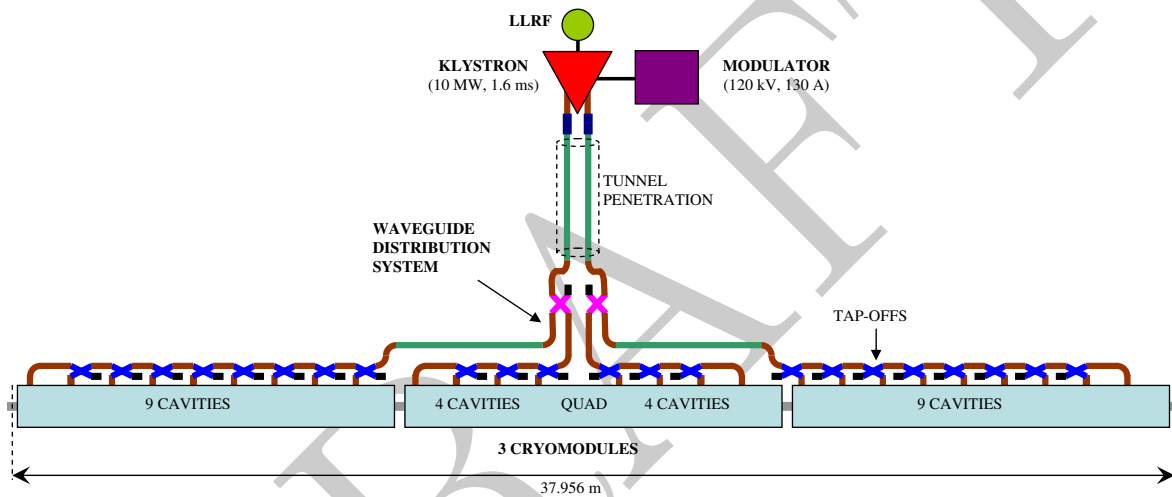
FIGURE 2.6-1. RF unit layout.

The modulator is a conventional pulse-transformer type with a bouncer circuit to compensate the voltage droop that occurs in the main storage capacitor during the pulse. The modulator produces 120 kV, 130 A, 1.6 ms, 5 Hz pulses with an efficiency of 83%, including the charging supply and rise time losses. These high voltage pulses power a multi-beam klystron (MBK) that amplifies $\sim$ 100 W, 1.6 ms RF pulses from the LLRF system up to 10 MW. This klystron has higher power and improved efficiency (65% goal) relative to commercial 5 MW tubes (40-45%). Two waveguides transport the power from the dual MBK outputs through a penetration to the beam tunnel where the power in each waveguide is then split to feed half of the middle cryomodule and one end cryomodule (see Figure 2.6-1).

The distribution system is composed primarily of aluminum WR650 (6.50" x 3.25") waveguide components. For long runs, WR770 is substituted to minimize distribution losses, estimated to be 7%, including 2% in the circulators. Along each cryomodule, RF power is equally distributed among the cavities through a series of hybrid-style 4-port tap-offs, each with appropriate fractional coupling (e.g. 1/9, 1/8, ...1/2). Between each tap-off output and its associated cavity power coupler, there are a bend, a semi-flexible section, a circulator, a three-stub tuner, and a diagnostic directional coupler. The three-stub tuner allows fine

TABLE 2.6-2
RF unit parameters.

Parameter	Value	Units
Modulator overall efficiency	82.8	%
Maximum klyston output power	10	MW
Klystron efficiency	65	%
RF distribution system power loss	7	%
Number of cavities	26	
Effective cavity length	1.038	m
Nominal gradient with 22% tuning overhead	31.5	MV/m
Power limited gradient with 16% tuning overhead	33.0	MV/m
RF pulse power per cavity	293.7	kW
RF pulse length	1.565	ms
Average RF power to 26 cavities	59.8	kW
Average power transferred to beam	36.9	kW

adjustment of cavity phase and can be used to adjust the cavity Q_{ext}, although this is mainly adjusted via motor control of the position of the inner conductor in the cavity power coupler. The circulator, with a load on its third port, absorbs the RF power reflected from the cavities during filling and discharge, and so provides protection to the klystron and isolation between cavities.

The cryomodule design is a modification of the Type-3 version developed and used at DESY (see Figure 2.6-2). Within the cryomodules, a 300 mm diameter He gas return pipe serves as a strongback to support the cavities and other beam line components. Invar rods are used to maintain the spacing between the components when the cryomodule cools down, which requires roller-type support fixtures. The gas return pipe itself is supported at three locations off of the top of the outer vacuum vessel, with only the center support fixed. The middle cryomodule in each RF unit contains eight cavities, rather than nine, to accommodate a quad package that includes a superconducting quadrupole magnet at the center, a cavity BPM, and superconducting horizontal and vertical corrector magnets. All cryomodules, whether with or without the quad package, are 12.652 m long so the active length to actual length ratio in a 9-cavity cryomodule is 73.8%. Each also contains a 300 mm long HOM beam absorber assembly that removes energy through the 40-80K cooling system from beam-induced higher order modes above the cavity cutoff frequency.

The cavities illustrated in Figure 2.6-2 are "dressed" in that the cells are enclosed in a titanium vessel containing the liquid helium, a tuner system is mounted around the center to control the cavity length, and a coaxial power coupler (not shown) connects the cavity to the external waveguide feed. The cavity spacing within the cryomodules is 5 3/4 λ_0 = 1.326 m, which facilitates powering the cavities in pairs via 3 db hybrids as an alternate distribution scheme that eliminates or reduces the number of circulators. However, the spacing would not be significantly reduced otherwise due to the required length of bellows between cavities and space for flange accessibility.

To operate the cavities at 2K, they are immersed in a saturated He II bath, and helium gas-cooled shields intercept thermal radiation and thermal conduction at 5–8 K and at 40–80 K.
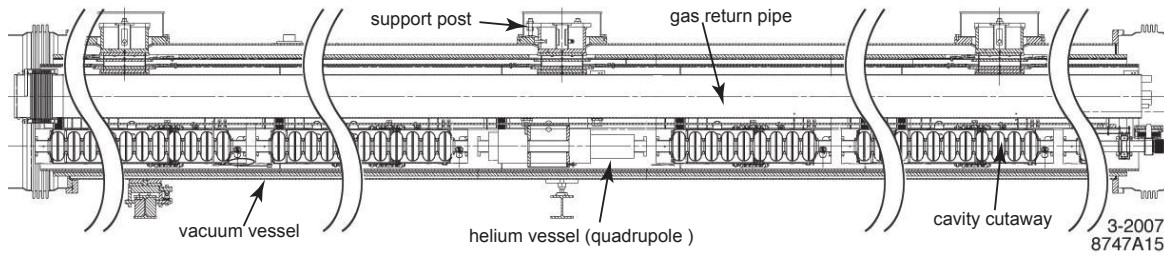
FIGURE 2.6-2. Side view of a cryomodule with a quadrupole magnet in the center. The figure has been compressed as indicated by the two white gaps, so not all eight cavities are shown.

The estimated cryogenic heat loads per RF unit are listed in Table 2.6-3, and were obtained by scaling the TESLA TDR estimates. Also, for each of the three cooling systems, the associated cryoplant power is listed for both the static and dynamic contributions from an RF unit and associated transfer line and distribution components, including a 50% overcapacity factor. The dynamic 2 K heat loss, attributable mainly to the RF and beam HOM losses in the cavities, constitutes about half the total installed power.

TABLE 2.6-3
RF cryogenic heat loads and installed AC cryogenic plant power to remove the heat.

	40–80 K		5–8 K		2 K		Total
	Static	Dynamic	Static	Dynamic	Static	Dynamic	
Heat load (W)	177.6	270.3	31.7	12.5	5.1	29.0	
Installed power	4.4	6.2	9.6	3.5	8.1	28.5	60.4

2.6.3.2 Linac Layout

The Main Linac components are housed in two tunnels, each of which has an interior diameter of 4.5 meters. The tunnels are separated from one another by 5.0 m to 7.5 m depending on the geology at the ILC site. As illustrated in Figure 2.6-3, the cryomodules occupy the beam tunnel while most of the RF system, including modulators, klystrons, power supplies, and instrumentation racks, are located in the service tunnel. This arrangement permits access to the equipment in the service tunnel for maintenance, repair, or replacement during beam operation and limits radiation exposure to most of the electronics (except motors in or near the cryomodules). The two tunnels are connected by three penetrations along each RF unit: one for the waveguide, one for signal cables, and one for power and high voltage cables. Personnel access points between the two tunnels are located at roughly 500 meter intervals. Rather than being "laser straight", the tunnels are curved in the vertical plane, with a radius of curvature slightly smaller than that of the Earth. This allows the beam delivery system to lie in a plane at the center of the site, while the cryomodules nearly follow a gravitational equipotential to simplify distribution of cryogenic fluids.

The positron linac contains 278 RF units, and the electron linac has 282 RF units; the four additional RF units are needed to compensate for the beam energy lost in the undulator that is used to generate gamma rays for positron production. The positron system section within the electron linac is 1,257 m long and is located near the 150 GeV point (see Section 2.3). Coasting sections, about 400 m long, are included at the end of the linacs so that
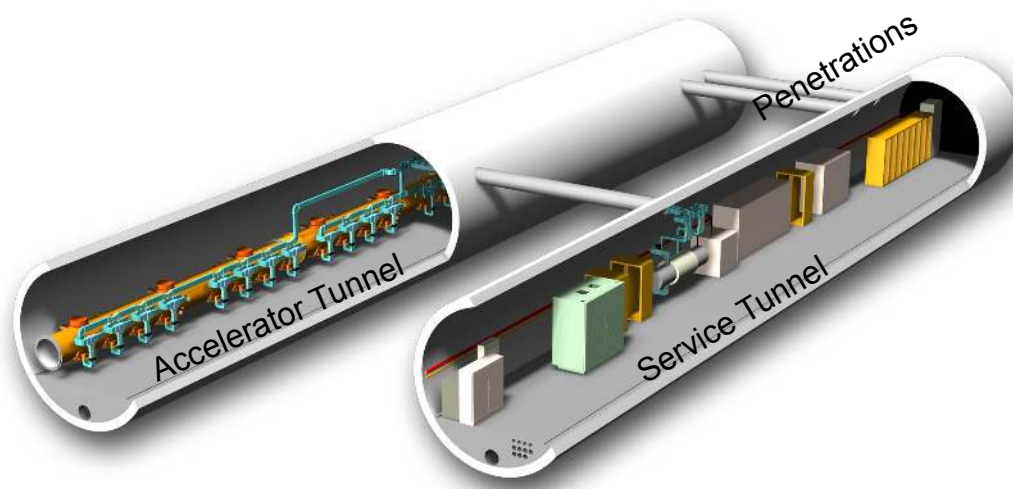
FIGURE 2.6-3. Cutaway view of the linac dual-tunnel configuration.

additional RF units can be installed as an upgrade to provide up to 3.5% energy overhead during 500 GeV CM operation. No additional tunnel is included for a future upgrade to higher energies, although the site is sized to allow expansion for 1 TeV CM operation.

The tunnels in the present sample sites are 100-150 meters underground and are connected to the surface through vertical shafts. Each of the main linacs includes three shafts, roughly 5 km apart as dictated by the cryogenic system. The upstream shafts in each linac have diameters of 14 m to accommodate lowering cryomodules horizontally, and the downstream shaft in each linac is 9 m in diameter, which is the minimum size required to accommodate tunnel boring machines. At the base of each shaft is a 14,100 cubic meter cavern for staging installation and housing utilities and parts of the cryoplant, most of which are located on the surface.

The layout of the RF units in the main linac is not uniform, but includes an additional 2.5 m long "end box" after every 4 RF units that terminates the 2K He distribution to the upstream cavities and restarts it from the main 2K feed line for the downstream cavities. The linac section from one such end box to the next is called a "cryo string." In a few locations, cryo-strings of three RF units are used instead of four RF units. Cryo-strings are arranged in groups of 10 to 16 to form a cryogenic unit which is supported by a single cryoplant. Each cryogenic unit also includes 2.5 m long "service boxes" on each end (one service box replaces a cryo-string end box), and is separated from the next cryogenic unit by a 7.7 m warm section that includes vacuum system components and a laser wire to measure beam size. Accounting for these additional sections and the quad package length, the active to actual length ratio in the linacs is 69.7% (excluding the undulator section and the coasting section at the end of each linac). Table 2.6-4 summarizes the linac component lengths and numbers.

There are five, 4 MW-size cryoplants in each linac that also provide cooling for the RTML and undulator region. The total cryogenic capacity of the ILC linacs is comparable to that of the LHC. The plants are paired at each linac shaft, one feeding downstream cryomodules and the other upstream cryomodules, except for the downstream most shaft, where there is only one plant that feeds upstream cryomodules. The plants are sized with a 40% overcapacity to account for degradation of plant performance, variation in cooling water temperature, and operational overhead.

Conventional water cooling towers are also located on the site surface near each linac

TABLE 2.6-4

Subdivision lengths and numbers in the two main linacs. Total linac lengths exclude the length of the positron production insertion and the coasting length at the end of each linac.

Subdivision	Length (m)	Number
Cavities (9 cells + ends)	1.326	14,560
Cryomodule (9 cavities or 8 cavities + quad)	12.652	1,680
RF unit (3 cryomodules)	37.956	560
Cryo-string of 4 RF units (3 RF units)	154.3 (116.4)	71 (6)
Cryogenic unit with 10 to 16 strings	1,546 to 2,472	10
Electron (positron) linac	10,917 (10,770)	1 (1)

shaft. Through various distribution loops, they provide 35°C process water that removes most of the heat generated by the RF system, and 8°C chilled water for heat exchangers that maintain the tunnel air temperature at 29°C and cool electronics racks via closed, circulated-air systems. In each RF unit, roughly 10 kW of heat are dissipated in the racks, and another 10 kW are dissipated into the air from convection off of the RF source components.

The electrical requirements of the main linac are supplied by two high-voltage cable systems. One of the systems supports the conventional services, while the other supports the RF system. Table 2.6-5 summarizes the combined power consumption of the two main linacs. Of this power, 20.5 MW is transferred to the beams, for a net efficiency of 13.7%.

TABLE 2.6-5

AC power consumption of the two main linacs.

System	AC Power (MW)
Modulators	81.4
Other RF system and controls	8.4
Conventional facilities	25.7
Cryogenic	33.8
Total	149.3

2.6.4   Accelerator Physics

2.6.4.1   Optics

The main linac lattice uses a weak focusing FODO optics, with a quad spacing of 37.956 m, corresponding to one quad per RF unit. Each quadrupole magnet is accompanied by horizontal and vertical dipole correctors and a cavity BPM which operates at 1.3 GHz. Because of the aperiodicity conditions imposed by the cryogenic system, the lattice functions are not perfectly regular. The mean phase advance per cell is 75° in the horizontal plane and 60° in the vertical plane. The vertical curvature is provided by the vertical correctors at the quadrupole locations, rather than by dedicated bend magnets. Dispersion matching and suppression at the beginning and end of the linac and around the undulator insertion are achieved by supplying additional excitation to small numbers of correctors in "dispersion-bump" configurations. Figure 2.6-4 shows the optical functions of the electron linac, including the undulator

insertion. The functions for the positron main linac are basically the same except that the undulator insertion is not present.
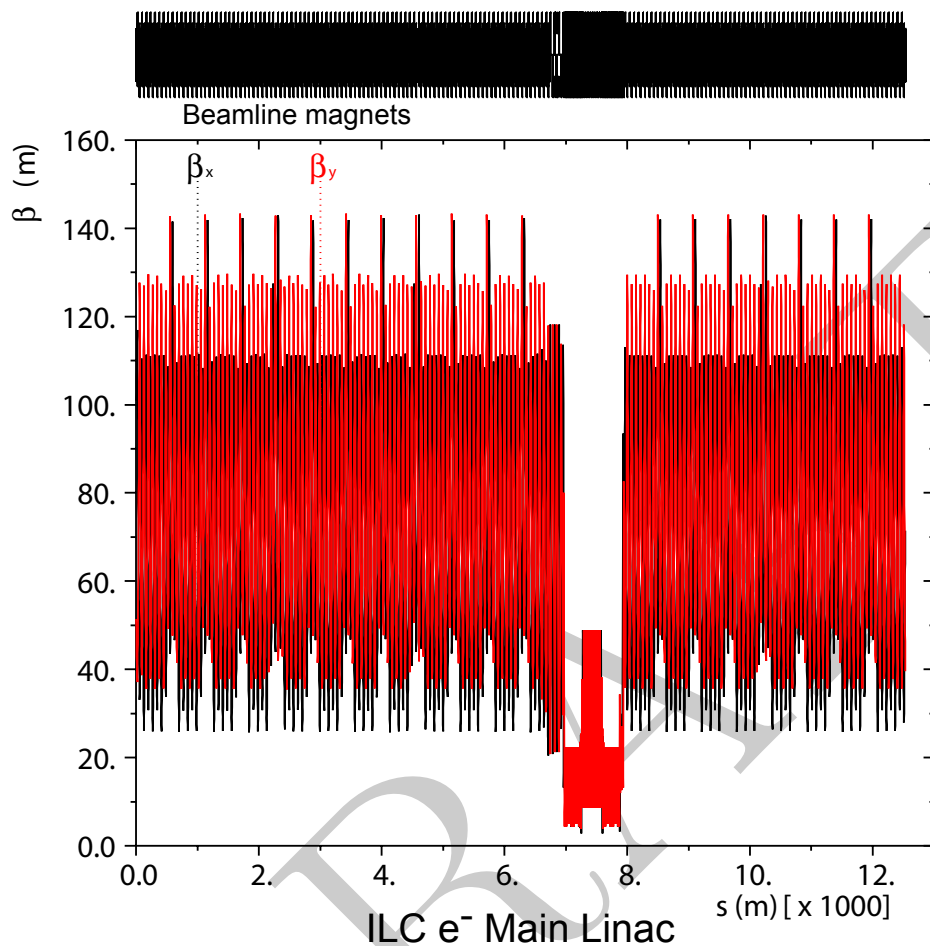
FIGURE 2.6-4. Beam optics functions for the electron main linac. The discontinuity of the pattern around s∼ 8 km represents the undulator section for positron production.

2.6.4.2 Beam Dynamics

A key requirement of the main linacs is that they preserves the small emittances which are produced in the damping rings and transported through the RTMLs. This is particularly true for the vertical emittance, which is smaller than the horizontal emittance by a factor of 400. The main obstacles to emittance preservation in the linacs are transverse wakefields, betatron coupling, and dispersion.

The short-range transverse wakefields in the ILC cavities are quite weak compared to the wakefields typically associated with higher-frequency RF cavities. Alignment tolerances for cavities and cryomodules in the range of 200-300 μm RMS are expected to yield emittance growth on the order of 2 nm (10%) in the vertical plane. It is possible that even this small amount of emittance dilution can be corrected by the use of "wake bumps" (local orbit distortions which excite wakefields but not other aberrations).

The long-range wakefields in the ILC cavities are potentially more harmful given the high Q values typical in superconducting cavities. These wakefields are mitigated through HOM

damping ports on the cavities, additional HOM absorbers in each RF unit at the location of the quadrupole magnet package, and detuning of the HOM's at the level of 10^{-3}. The combination of damping and detuning reduces the multi-bunch emittance growth to 0.3 nm (1.5%).

Azimuthal deformations to the cavities from construction errors or from the placement of the HOM and fundamental mode ports can cause the HOM's to develop diagonal polarizations instead of horizontal and vertical polarizations. Diagonally-polarized (or "mode-rotation") HOM's can couple beam jitter from the horizontal to the vertical, resulting in unacceptable vertical emittance dilution. This is mitigated in the main linacs by making the horizontal and vertical betatron tunes highly unequal. Setting the horizontal phase advance per cell to 75° and the vertical to 60° limits emittance growth from this effect to 0.4 nm (2%).

Betatron coupling between the relatively large horizontal mode and the relatively small vertical mode is driven by unwanted rotations of the main linac quadrupole magnets. By limiting the rms rotations of the quads to 0.3 mrad, the resulting emittance growth can be limited to 2 nm (10%). Most of this emittance growth can be globally corrected by the decoupler at the start of the beam delivery section (see Section 2.7.3.1.2), subject to the resolution limits of the laser wire profile monitors in the BDS.

Dispersion in the main linac is created by misaligned quadrupole magnets and pitched RF cavities. Emittance growth from this effect is mainly corrected through local or quasi-local steering algorithms such as Ballistic Alignment (BA), Kick Minimization (KM), or Dispersion Free Steering (DFS), with additional correction achieved through local orbit distortions which produce measured amounts of dispersion in a given phase ("dispersion bumps"). Simulations indicate that emittance growth from dispersion can be limited to about 5 nm (25%) through combinations of these techniques.

The principal main linac beam diagnostic is the suite of beam position monitors: a BPM with horizontal and vertical readout and sub-micron single-bunch resolution is located adjacent to each quadrupole magnet. For beam size monitoring, a single laser wire is located in each of the warm sections between main linac cryogenics units (about every 2.5 km). Upstream quadrupole magnets are varied to make local measurements of the beam emittances.

The main linacs do not contain any equipment for intra-train trajectory control. Such trajectory control is implemented only in the warm regions upstream and downstream of the main linacs and in the undulator section. There are no diagnostics for measuring energy or energy spread in the main linacs. These measurements are made upstream and downstream of the main linacs and in the undulator section. There are no beam abort systems in the main linacs. Machine protection in the linac is ensured by verifying the state of the main linac hardware (both RF and magnets) prior to beam extraction from the RTML, and by verifying that the orbit in each damping ring is correct. The limiting aperture along the main linacs is the 70 mm diameter cavity iris.

2.6.4.3 Operation

Within each RF unit, a low level RF (LLRF) system monitors the vector sum of the fields in the 26 cavities. It makes adjustments to flatten the energy gain along the bunch train and keeps the beam-to-rf phase constant. It compensates for perturbations including cavity frequency variations (e.g. due to microphonics and residual Lorentz force detuning after feed-forward piezo-electric controller compensation), inter-pulse beam current variations, and non-flatness of the klystron pulse. In addition to the phase and amplitude of the klystron,

this system has remote control over individual cavity phases (through the RF distribution system), external quality factors Q_{ext} (through the moveable coupler center conductor), and resonant frequencies (through slow and faster tuners).

The cavities are qualified at 35 MV/m or greater during initial testing (i.e. so-called "vertical" tests) prior to installation in cryomodules. This should allow them to run at 31.5 MV/m on average, installed, although the variation of sustainable gradients may be significant according to current data. Some cryomodule gradient variation within an rf unit can be accommodated by one-time adjustments in the main feed line power splitters and the in-line attenuators in each of the two feed lines.

For 500 GeV operation, there is no energy overhead if the average sustainable cavity gradient is the design value of 31.5 MV/m. With failed RF units, the ILC can only reach 500 GeV if the cavities achieve a higher average gradient (power limited to 33 MeV/m) or if additional RF units are eventually installed in the reserved drift region at the end of the linacs. The beam energy is coarsely adjusted by turning on or off RF units, each of which contributes about 0.3% of the beam energy, and finely adjusted by cross-phasing RF units near the end of the linacs.

2.6.5 Accelerator Components

2.6.5.1 Cavities and Cryomodules

The 1.3 GHz superconducting accelerating cavity is the fundamental building block of the ILC main linacs. Its parameters are listed in Table 3.6-1. A partially "dressed" cavity for installation in a cryomodule is shown Figure 2.6-5, together with the power coupler schematic. Each cavity is qualified for installation in the main linac in a vertical test stand; cavities which can sustain a gradient in excess of 35 MV/m with a Q value in excess of 0.8×10^{10} are then installed in cryomodules for use in the main linac. More information on the construction and testing of cavities can be found in Section 3.6.
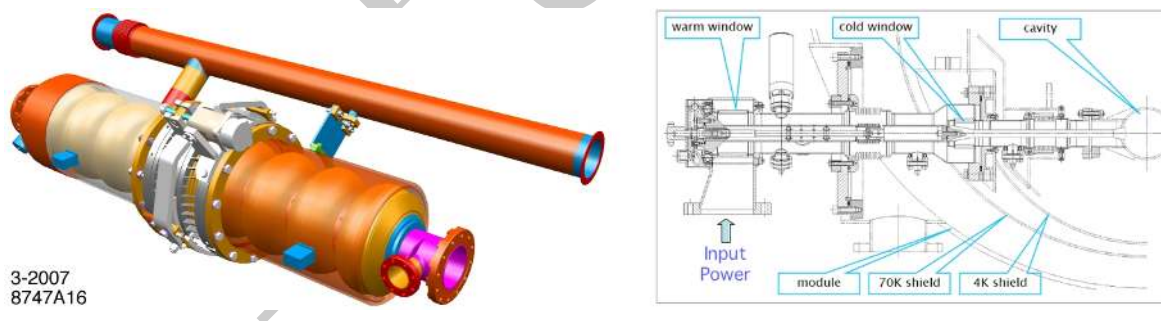
FIGURE 2.6-5. Left: A partially dressed cavity including the helium vessel, 2K He feed line and frequency tuners. Two HOM couplers and an RF pickup (not visible) are located near the ends of the cavity. Right: Schematic of the coaxial power coupler that attaches to the off-axis port shown in the left figure.

2.6.5.2 Quad Package

In addition to cavities, the center cryomodule in each RF unit contains a 1.2 m long quad package that includes a quadrupole magnet, combined horizontal and vertical corrector magnets, and a cavity beam position monitor. At the low-energy end of the linac the quadrupoles

TABLE 2.6-6
Cavity Parameters.

Parameter	Value	Units
Type	9 cell, π-mode	
R/Q of fundamental mode	1036	Ω
Iris diameter	70	mm
Cell-to-cell coupling	1.9	%
Average Q_0	1.0×10^{10}	
Average Q_{ext}	3.5×10^6	
Fill time	596	μs
Cavity resonance width	370	Hz

and correctors are superferric types, while $\cos(2\theta)$ and $\cos(\theta)$ superconducting magnets are used at the high-energy end of the linac. The maximum gradient required in the quadrupoles at the high energy end of each linac is 60 T/m, while the maximum dipole integrated strength required is about 0.05 T-m. The beam position monitor is an L-band design capable of measuring horizontal and vertical positions with 1 micrometer resolution for a single bunch at full charge. All of the elements in the quad package have an aperture which is larger than the 70 mm aperture of the superconducting cavities.

2.6.5.3   Vacuum System

There are three independent vacuum systems along the accelerator: the beamline system that includes the volume in the cavities and other beamline components, the coupler system that includes the volume between the two windows in each coupler, and the insulation system that includes the volume within the cryomodule vacuum vessel. The beamline system runs the length of the linacs and includes slow valves with second-scale response times in each 154 m cryo-string plus fast valves with ms-scale responses in the warm sections between cryogenic units. In the event of a major vent, these systems will limit the length of linac which is exposed to air to one or two cryo strings. Finally, the coupler vacuum system is segmented by cryomodule, and all couplers therein are pumped in common. With this system, a leak in one of the cold windows is fairly benign.

2.6.5.4   Beamline Components

Table 2.6-7 lists the basic beamline components and the total number of each contained in the two main linacs, excluding those in the positron production undulator region.

TABLE 2.6-7
Main Linac Beamline Components.

Component	Number (total)
Cavities	14,560
SC quadrupole magnets	560
X-correctors	560
Y-correctors	560
SRF BPMs	560
Laser wire scanners	7

2.7   BEAM DELIVERY SYSTEMS

2.7.1   Overview

The ILC Beam Delivery System (BDS) is responsible for transporting the e^+/e^- beams from the exit of the high energy linacs, focusing them to the sizes required to meet the ILC luminosity goals ($\sigma_x^* = 639$ nm, $\sigma_y^* = 5.7$ nm in the nominal parameters), bringing them into collision, and then transporting the spent beams to the main beam dumps. In addition, the BDS must perform several critical functions:

- measure the linac beam and match it into the final focus;
- protect the beamline and detector against mis-steered beams from the main linacs;
- remove any large amplitude particles (beam-halo) from the linac to minimize background in the detectors;
- measure and monitor the key physics parameters such as energy and polarization before and after the collisions;

The BDS must provide sufficient instrumentation, diagnostics and feedback systems to achieve these goals.

2.7.2   Beam Parameters

Table 2.7-1 shows the key BDS parameters. The IP beam parameters are shown for the nominal parameter set at 500 GeV CM.

2.7.3   System Description

The main subsystems of the beam delivery starting from the exit of the main linacs are the diagnostics region, the fast extraction and tuneup beamline, the betatron and energy collimation, the final focus, the interaction region and the extraction line. The layout of the beam delivery system is shown in Figures 2.7-1 and 2.7-2. The BDS is designed for 500 GeV center of mass but can be upgraded to 1 TeV with additional magnets.

There is a single collision point with a 14 mrad crossing angle. To support future energy upgrades, the beam delivery systems are in line with the linacs and the linacs are also oriented at a 14 mrad angle. The 14 mrad geometry provides space for separate extraction lines and requires crab cavities to rotate the bunches horizontally for head-on collisions. There are two detectors in a common IR hall which alternately occupy the single collision point, in a so-called "push-pull" configuration. The detectors are pre-assembled on the surface and then lowered into the IR hall in large subsections once the hall is ready for occupancy.

2.7.3.1   Diagnostics, Tune-up dump, Machine Protection

The initial part of the BDS, from the end of the main linac to the start of the collimation system (known for historical reasons as the Beam Switch Yard or "BSY"), is responsible for measuring and correcting the properties of the beam before it enters the Collimation and Final Focus systems. In addition, errant beams must be detected here and safely extracted in order to protect the downstream systems. Starting at the exit of the main linac, the system includes the MPS collimation system, skew correction section, emittance diagnostic section, polarimeter with energy diagnostics, fast extraction/tuning system and beta matching section.

TABLE 2.7-1
Key parameters of the BDS. The range of L*, the distance from the final quadrupole to the IP, corresponds to values considered for the existing detector concepts.

Parameter	Units	Value
Length (linac exit to IP distance)/side	m	2226
Length of main (tune-up) extraction line	m	300 (467)
Max Energy/beam (with more magnets)	GeV	250 (500)
Distance from IP to first quad, L*	m	3.5-(4.5)
Crossing angle at the IP	mrad	14
Nominal beam size at IP, σ^*, x/y	nm	639/5.7
Nominal beam divergence at IP, θ^*, x/y	μrad	32/14
Nominal beta-function at IP, β^*, x/y	mm	20/0.4
Nominal bunch length, σ_z	μm	300
Nominal disruption parameters, x/y		0.17/19.4
Nominal bunch population, N		2×10^{10}
Beam power in each beam	MW	10.8
Preferred entrance train to train jitter	σ_y	< 0.5
Preferred entrance bunch to bunch jitter	σ_y	< 0.1
Typical nominal collimation aperture, x/y		8–10/60
Vacuum pressure level, near/far from IP	nTorr	1/50

2.7.3.1.1 MPS collimation   At the exit of the main linac is a short 90° FODO lattice, composed of large bore quadrupoles, which contains a set of sacrificial collimators of decreasing aperture. The purpose of this system is to protect the 12 mm aperture BDS from any beam which develops an extremely large trajectory in the 7 cm aperture main linac (the effective aperture is $R/\beta^{1/2}$, which is 3–4 times smaller in the BDS than in the linac). This section also contains kickers and cavity BPMs for inter- and intra-train trajectory feedback.

2.7.3.1.2 Skew Correction   The skew correction section contains 4 orthonormal skew quadrupoles which provide complete and independent control of the 4 betatron coupling parameters. This scheme allows correction of any arbitrary linearized coupled beam.

2.7.3.1.3 Emittance Diagnostics   The emittance diagnostic section contains 4 laser wires which are capable of measuring horizontal and vertical RMS beam sizes down to 1 μm. The wire scanners are separated by 45° in betatron phase to allow a complete measurement of 2D transverse phase space and determination of the projected horizontal and vertical emittances.

2.7.3.1.4 Polarimeter and Energy Diagnostics   Following the emittance diagnostic section is a magnetic chicane which is used for both Compton polarimetry and beam energy diagnostics. At the center of the chicane is the Compton IP, a BPM for measuring relative beam energy changes, and a sacrificial machine protection system (MPS) energy collimator which defines the energy acceptance of the tune-up extraction line. The length of the chicane
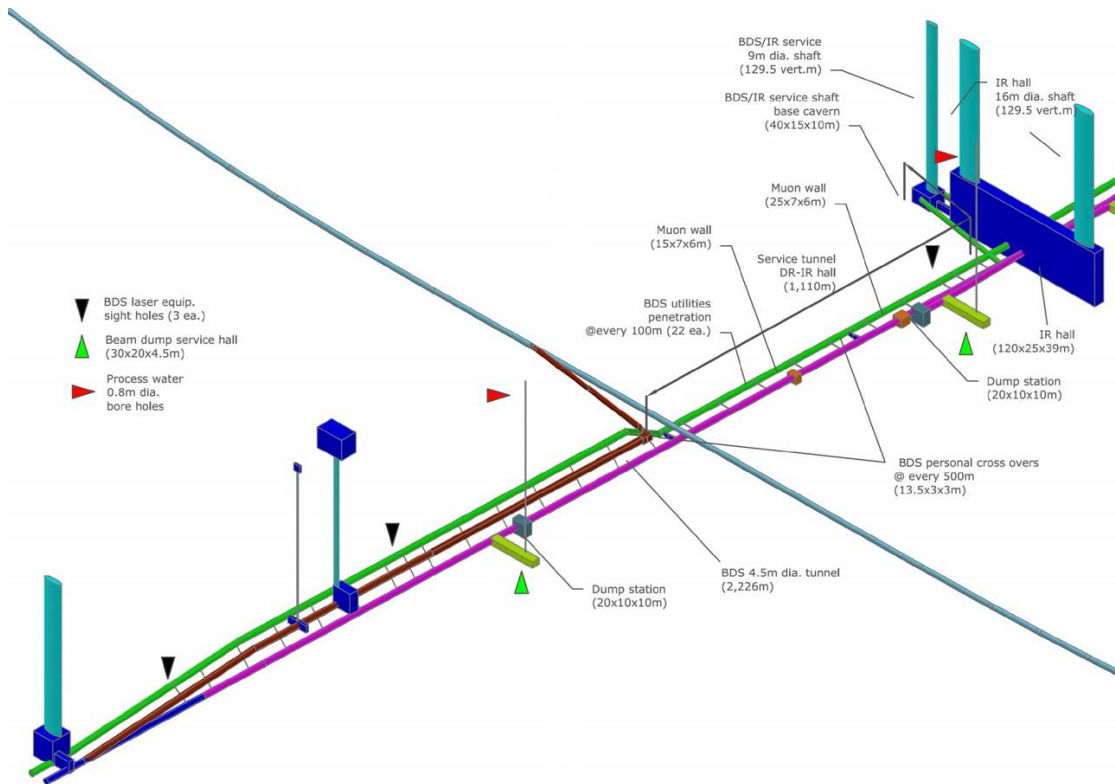
FIGURE 2.7-1. BDS layout, beam and service tunnels (shown in magenta and green), shafts, experimental hall.

is set to limit horizontal emittance growth due to synchrotron radiation to less than 1% with a 500 GeV/beam. A detector for the Compton-scattered photons from the laser wires is included in the chicane.

2.7.3.1.5 Tune-up and Emergency Extraction System   The BSY pulsed extraction system is used to extract beams in the event of an intra-train MPS fault. It is also used any time when beams are not desired in the collimation, final focus, or IR areas, for example during commissioning of the main linacs. The extraction system includes both fast kickers which can rise to full strength in the 300 ns between bunches, and pulsed bends which can rise to full strength in the 200 ms between trains. These are followed by a transfer line with $\pm 10\%$ momentum acceptance which transports the beam to a full-beam-power water-filled dump. There is a 125 m drift which allows the beam size to grow to an area of 2π mm^2 at the dump. A set of rastering kickers sweep the beam in a 3 cm radius circle on the dump window. By using the nearby and upstream BPMs in the polarimeter chicane and emittance sections, it is possible to limit the number of errant bunches which pass into the collimation system to 1–2.

2.7.3.2   Collimation System

Particles in the beam halo produce backgrounds in the detector and must be removed in the BDS collimation system. One of the design requirements for the ILC BDS is that no particles are lost in the last several hundred meters of beamline before the IP. Another requirement is that all synchrotron radiation passes cleanly through the IP to the extraction line. The
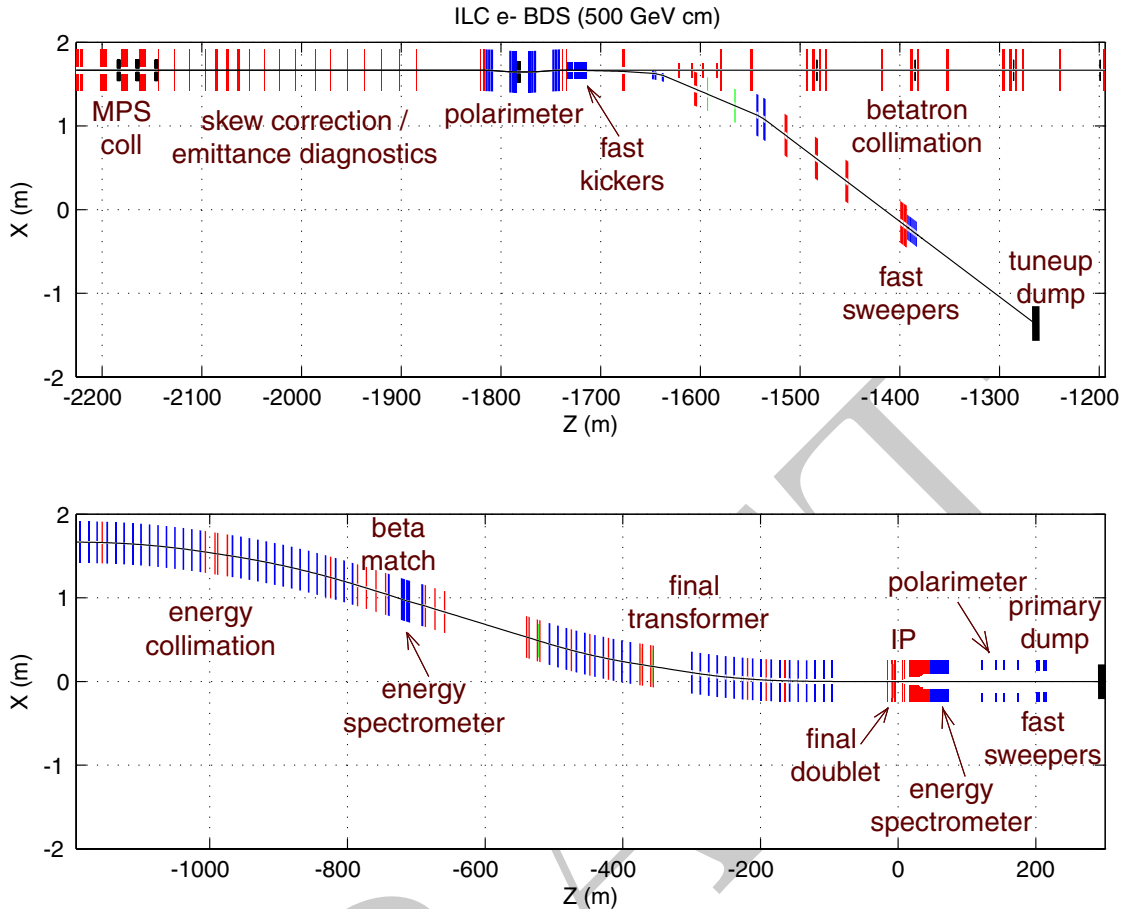
FIGURE 2.7-2.   BDS layout showing functional subsystems, starting from the linac exit; X – horizontal position of elements, Z – distance measured from the IP.

BDS collimation must remove any particles in the beam halo which do not satisfy these criteria. These requirements define a system where the collimators have very narrow gaps and the system is designed to address the resulting machine protection, survivability and beam emittance dilution issues.

The collimation system has a betatron collimation section followed by energy collimators. The downstream energy collimators help to remove the degraded energy particles originating from the betatron collimation section but not absorbed there. The betatron collimation system has two spoiler/absorber x/y pairs located at high beta points, providing single-stage collimation at each of the final doublet (FD) and IP betatron phases. The energy collimation section has a single spoiler located at the central high dispersion point (1530 μm/%). All spoilers and absorbers have adjustable gaps. Protection collimators (PC) are located throughout to provide local protection of components and additional absorption of scattered halo particles.

The spoilers are 0.5 to 1 X_0 (radiation length) thick, the absorbers are 30 X_0, and the protection collimators are 45 X_0. The betatron spoilers as well as the energy spoiler are "survivable" – they can withstand a hit of two errant bunches of 250 GeV/beam, matching the emergency extraction design goal. With 500 GeV beam, they would survive only one bunch, and would therefore require more effective MPS or the use of a pre-radiator scheme.

The collimation apertures required are approximately $\sim 8 - 10\sigma_x$ in the x plane and

$\sim 60 - 80\sigma_y$ in the y plane. These correspond to typical half-gaps of betatron spoiler of ~ 1 mm in the x plane and ~ 0.5 mm in the y plane.

Wakefield calculations for the BDS spoilers and absorbers give IP jitter amplification factors [56] of $\mathcal{A}_x = 0.14$ and $\mathcal{A}_y = 1.05$. Estimated as $\delta\varepsilon/\varepsilon = (0.4 n_{\text{jitter}}\mathcal{A})^2$ this gives emittance dilutions of 0.08% and 4.4% in the x and y planes respectively, for 0.5 σ incoming beam jitter. Energy jitter at the collimators also amplifies the horizontal jitter at the IP. An energy jitter of 1% produces a horizontal emittance growth of 2.2%.

2.7.3.2.1 Muon suppression   Electromagnetic showers created by primary beam particles in the collimators produce penetrating muons which can easily reach the collider hall. The muon flux through the detector is reduced by a 5 m long magnetized iron shield 330 m upstream of the collision point which fills the cross-sectional area of the tunnel and extends 0.6 m beyond the ID of the tunnel, as shown in Figure 2.7-3. The shield has a magnetic field of 1.5 T, with opposite polarities in the left and right halves of the shield such that the field at the beamline is zero. The shield also provides radiation protection for the collider hall during access periods when beam is present in the linac and beam switch yard.
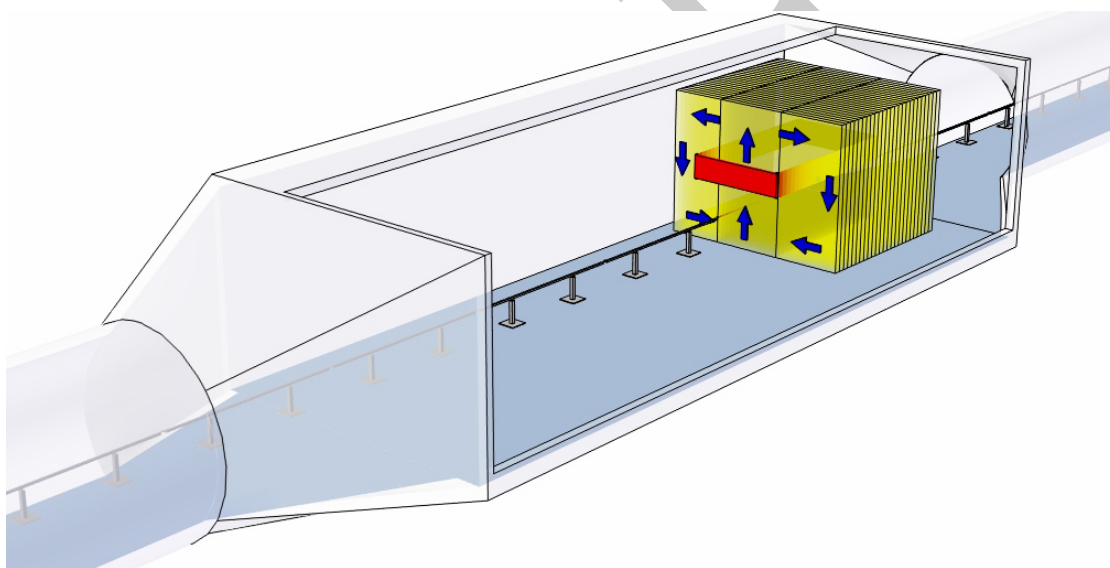
FIGURE 2.7-3.   Schematics of the 5-meter magnetized muon shield installed in a tunnel vault which is configured to accommodate possible upgrade to 19-meter shield. The coil is shown in red, and blue arrows indicate direction of the magnetic field in the iron.

2.7.3.2.2 Halo power handling   The power handling capacity of the collimation system is set by two factors: the ability of the collimators to absorb the incident beam power, and the ability of the muon suppression system to reduce the muon flux through the detector. In the baseline design, the muon suppression system presents the more restrictive limitation, setting a tolerance of $1-2\times 10^{-5}$ on the fraction of the beam which is collimated in the BDS. With these losses and the 5 m wall, the number of muons reaching the collider hall would be a few muons per 150 bunches (a reduction of more than 10^{-2}). Since the actual beam halo conditions are somewhat uncertain, the BDS includes caverns large enough to increase the muon shield from 5 m to 18 m and to add an additional 9 m shield downstream. Filling all of

these caverns with magnetized muon shields would increase the muon suppression capacity of the system to 1×10^{-3} of the beam. The primary beam spoilers and absorbers are water cooled and capable of absorbing 1×10^{-3} of the beam continuously.

2.7.3.2.3   Tail-folding octupoles   The final focus includes two superconducting octupole doublets. These doublets use nonlinear focusing to reduce the amplitude of beam halo particles while leaving the beam core untouched [57]. This "tail-folding" would permit larger collimation amplitudes, which in turn would dramatically reduce the amount of beam power intercepted and the wakefields. In the interest of conservatism the collimation system design described above does not take this tail folding into account in the selection of apertures and other parameters.

2.7.3.3   Final focus

The role of the final focus (FF) system is to demagnify the beam to the required size ($\sim$639 nm (horz) and $\sim$5.7 nm (vert)) at the IP. The FF optics creates a large and almost parallel beam at the entrance to the final doublet (FD) of strong quadrupoles. Since particles of different energies have different focal points, even a relatively small energy spread of $\sim$0.1% significantly dilutes the beam size, unless adequate corrections are applied. The design of the FF is thus mainly driven by the need to cancel the chromaticity of the FD. The ILC FF has local chromaticity correction [55] using sextupoles next to the final doublets. A bend upstream generates dispersion across the FD, which is required for the sextupoles to cancel the chromaticity. The dispersion at the IP is zero and the angular dispersion is about $\eta'_x \sim$0.009, i.e. small enough that it does not significantly increase the beam divergence. Half of the total horizontal chromaticity of the whole final focus is generated upstream of the bend in order for the sextupoles to simultaneously cancel the chromaticity and the second-order dispersion.
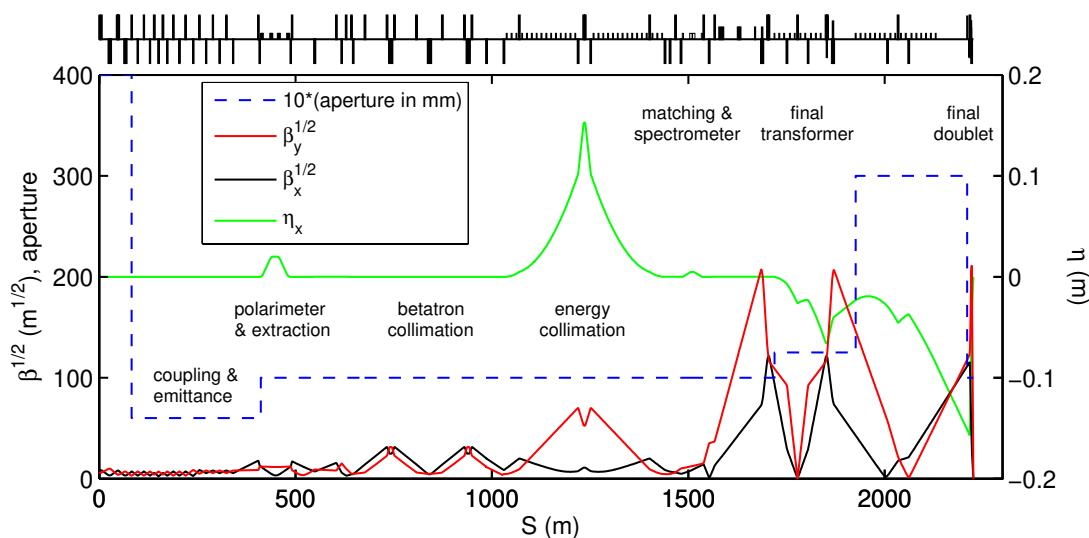
FIGURE 2.7-4. BDS optics, subsystems and vacuum chamber aperture; S is distance measured from the entrance.

The horizontal and the vertical sextupoles are interleaved in this design, so they generate third-order geometric aberrations. Additional sextupoles upstream and in proper phases with the FD sextupoles partially cancel the third order aberrations. The residual higher-order aberrations are minimized further with octupoles and decapoles. The final focus optics is shown in Figure 2.7-4.

Synchrotron radiation from the bending magnets causes emittance dilution, so it is important to maximize the bending radius, especially at higher energies. The FF includes sufficient bend magnets for 500 GeV CM and space for additional bend magnets which are necessary at energies above 500 GeV CM. With the reserved space filled with bends, the emittance dilution due to bends at 1 TeV CM is about a percent, and at 500 GeV CM, with only every fifth bend installed, about half of that.

In addition to the final doublet and chromaticity correction optics, the final focus includes: an energy spectrometer (see Section 2.7.4.3.1); additional absorbers for the small number of halo particles which escape the collimation section; tail folding octupoles (see Section 2.7.3.2); the crab cavities (see Section 2.7.4.1); and additional collimators for machine protection or synchrotron radiation masking of the detector.

2.7.3.4   IR design and integration to detector

The ILC final focus uses independently adjustable compact superconducting magnets for the incoming and extraction beam lines. The adjustability is needed to accommodate beam energy changes and the separate beamline allows optics suitable for post IP beam diagnostics. The BNL direct wind technology is used to produce closely spaced coil layers of superconducting multi-strand cable. The design is extremely compact and the coils are almost touching in shared cold mass volumes. Cooling is provided by superfluid helium at 2 K. The technology has been demonstrated by a series of short prototype multi-pole coils. The schematic layout of magnets in the IR is shown in Figure 2.7-5 and Figure 2.7-11. The quadrupoles closest to the IP are actually inside the detector solenoidal field and therefore cannot have magnetic flux return yokes; at the closest coil spacing the magnetic cross talk between the two beam apertures is controlled by using actively shielded coil configurations and by use of local correction coils, dipole, skew-dipole and skew-quadrupole or skew-sextupole, as appropriate. Figure 2.7-6 shows the prototype of QD0 quadrupole and illustrates the principle of active shielding.

To facilitate a rapid, "push-pull" style exchange of detectors at a shared IP, the superconducting final focus magnets are arranged into two groups so that they can be housed in two separate cryostats as shown in Figure 2.7-5, with only warm components and vacuum valves placed in between. The cryostat on the left in Figure 2.7-5 moves with the detector during switchover, while the cryostat on the right remains fixed on the beamline.

Additional optical elements are required in the IR to compensate the effects of the detector solenoid field interacting with the accelerator IR magnets. The first is a large aperture anti-solenoid in the endcap region to avoid luminosity loss due to beam optics effects [60]. The second is a large aperture Detector Integrated Dipole (DID) [61] that is used to reduce detector background at high beam energies or to minimize orbit deflections at low beam energies.

The vertical position of the incoming beam line quadrupole field center must be stable to order of a few tens of nanometers, in order to stay within the capture range of the intra-train collision feedback (see 2.7.4.2). This requirement is well beyond experience at existing
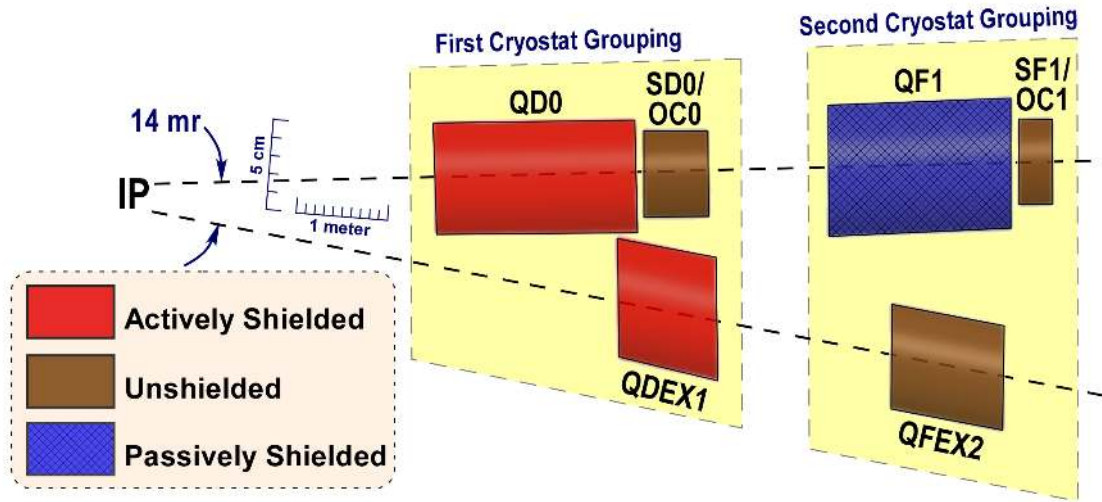
FIGURE 2.7-5. Schematic layout of magnets in the IR.

FIGURE 2.7-6. Prototype of QD0 quadrupole and its active shield (left); calculated field pattern with and without activation of the shielding coils (right).

accelerators and is being addressed in ongoing R&D.

2.7.3.5 Extraction line

The ILC extraction line [58, 59] has to transport the beams from the IP to the dump with acceptable beam losses, while providing dedicated optics for beam diagnostics. After collision, the beam has a large angular divergence and a huge energy spread with very low energy tails. It is also accompanied by a high power beamstrahlung photon beam and other secondary particles. The extraction line must therefore have a very large geometric and energy acceptance to minimize beam loss.

The optics of the ILC extraction line is shown in Figure 2.7-7. The extraction line can transport particles with momentum offsets of up to 60% to the dump. There is no net bending in the extraction line, which allows the charged particle dump to also act as a dump for beamstrahlung photons with angles of up to 0.75 mrad.

The first quadrupole is a superconducting magnet 5.5 m from the IP, as shown in Figure 2.7-5. The second quadrupole is also superconducting, with a warm section between the cryostats for these two quadrupoles. The downstream magnets are normal conducting, with a drift space to accommodate the crab cavity in the adjacent beamline. The quadrupoles
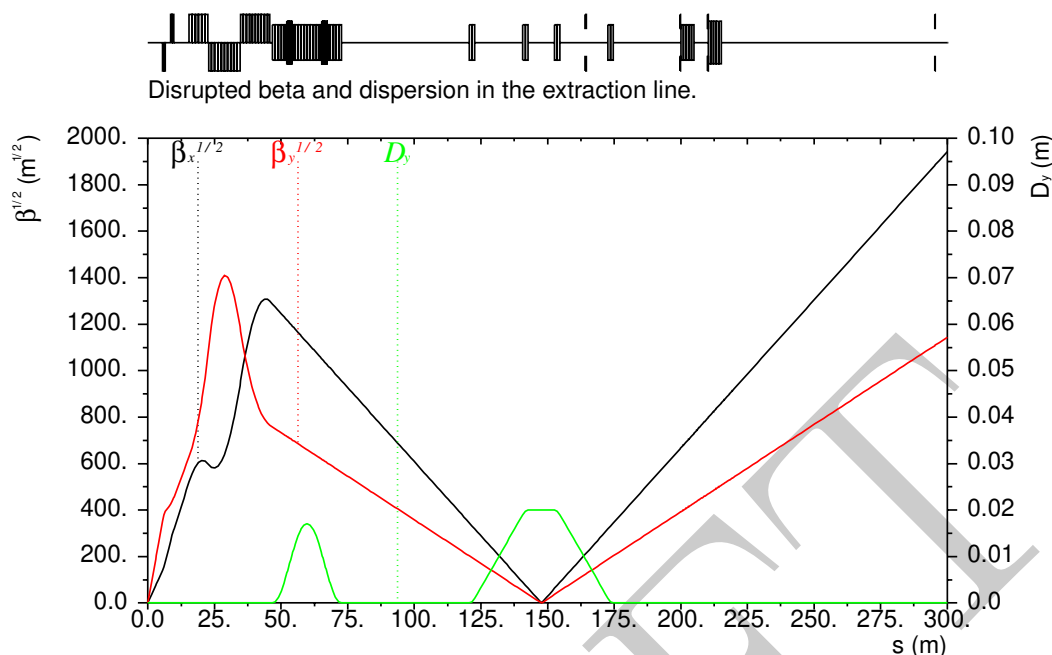
FIGURE 2.7-7. Disrupted β-functions and dispersion in the extraction line for the nominal 250 GeV beam.

are followed by two diagnostic vertical chicanes for the energy spectrometer and Compton polarimeter, with a secondary focal point in the center of the latter. The horizontal angular amplification (R_{22}) from the IP to the Compton IP is set to -0.5 so that the measured Compton polarization is close to the luminosity weighted polarization at the IP. The lowest energy particles are removed by a vertical collimator in the middle of the energy chicane. A large chromatic acceptance is achieved through the soft D-F-D-F quadruplet system and careful optimization of the quadrupole strengths and apertures. The two SC quadrupoles are compatible with up to 250 GeV beam energy, and the warm quadrupoles and the chicane bends with up to 500 GeV beam.

The diagnostic section is followed by a 100 m long drift to allow adequate transverse separation (>3.5 m) between the dump and the incoming line. It also allows the beam size to expand enough to protect the dump window from the small undisrupted beam. A set of rastering kickers sweep the beam in a 3 cm circle on the window to avoid boiling the water in the dump vessel. Three protection collimators in the 100 m drift remove particles that would hit outside of the 15 cm radius dump window and protect the rastering kicker magnets.

Extraction beam loss has been simulated for realistic 250 GeV GUINEA-PIG beam distributions [62], with and without beam offset at the IP. No primary particles are lost in the SC quadrupoles, and all particles above 40% of the nominal beam energy are transmitted cleanly through the extraction magnets. The total primary loss on the warm quadrupoles and bends is a few watts, and the loss on the protection collimators is a few kW for the nominal beam parameters. Figure 2.7-8 shows that even for an extreme set of parameters, with very high beamstrahllung energy loss, the radiation deposition in the magnet region is manageable.

2.7.4 Accelerator Components

The BDS accelerator components are described in the following sections and the total counts are shown in Table 2.7-2.
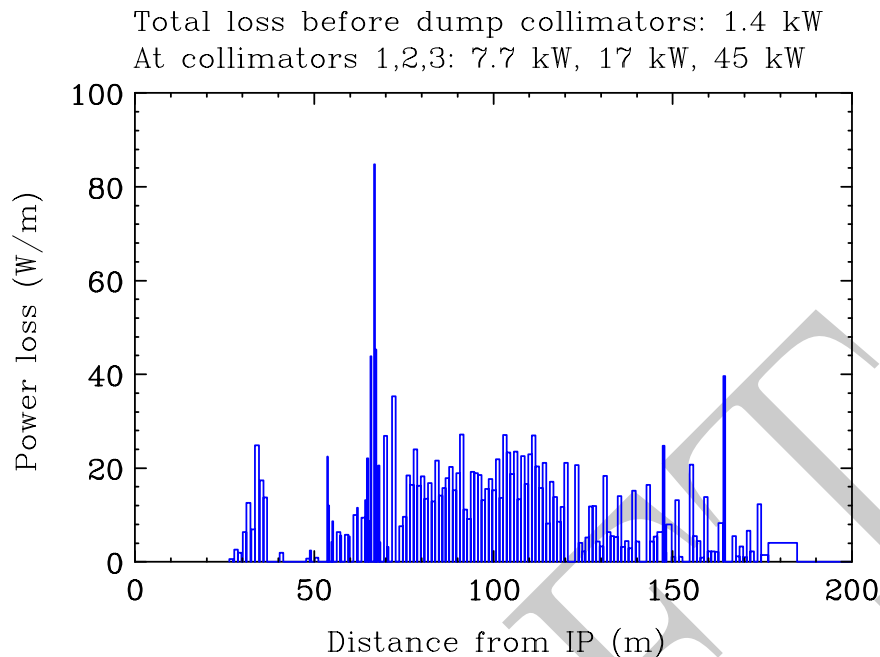
FIGURE 2.7-8. Power loss density in the magnet region for disrupted beam at 250 GeV, with an extreme choice of parameters.

2.7.4.1 Crab cavity system

With a 14 mrad crossing angle, crab cavities are required to rotate the bunches so they collide head on. Two 3.9 GHz SC 9-cell cavities in a 2–3 m long cryomodule are located 13.4 m from the IP. The cavities are based on the Fermilab design for a 3.9 GHz TM_{110} π mode 13-cell cavity [63]. The three cell prototype of this cavity is shown in Figure 2.7-9. The ILC has two 9-cell versions of this design operated at 5 MV/m peak deflection. This provides enough rotation for a 500 GeV beam and 100% redundancy for a 250 GeV beam.

FIGURE 2.7-9. Photo of a 3.9GHz 3 cells deflecting cavity built at Fermilab, which achieved 7.5MV/m.

The most challenging specification of the crab cavity system is on the uncorrelated phase jitter between the incoming positron and electron cavities which must be controlled to 61 fsec to maintain optimized collisions [64]. A proof-of-principle test of a 7 cell 1.5 GHz cavity at the

JLab ERL facility [65] has achieved a 37 fsec level of control, demonstrating feasibility. The higher- and lower-order modes of the cavity must be damped effectively to limit unwanted vertical deflections at the IP, as must the vertical polarization of the main deflecting mode.

Couplers with lower Q_{ext} and greater power handling capability are required to handle beam loading and LLRF feedback for off-axis beam. The crab cavity needs ∼3 kW per cavity for about 10 msec, with a Q_{ext} of ∼ 10^6 [66, 67]. The crab cavity is placed in a cryostat with tuner, x-y and roll adjustment which provides proper mechanical stability and microphonic rejection. The cryostat also accommodates the beampipe of the extraction line which passes about 19 cm from the center of the cavity axis.

2.7.4.2   Feedback systems and Stability

Maintaining the stability of the BDS is an essential prerequisite to producing luminosity. Since the beams have RMS vertical sizes of 5.7 nm at the IP, vertical offsets of about 1 nm will noticeably reduce the luminosity. In addition, especially for parameter sets with higher disruption, the beam-beam interaction is so strong that the luminosity is extremely sensitive to small variations in the longitudinal shape of the bunch caused by short-range wakefields. Finally, the size of the beam at the IP is sensitive to the orbit of the beam through the final doublet quads, the sextupoles, and other strong optical elements of the BDS. Care must be taken to minimize thermal and mechanical disturbances, by stabilizing the air temperature to $0.5°$C and the cooling water to $0.1°$C, and by limiting high frequency vibrations due to local equipment to the order of 10 nm.

Beam-based orbit feedback loops are used to maintain the size and position of the beam at the IP. All of the feedback loops use beam position monitors with micrometer-level resolution to detect the beam position, and dipole magnets or stripline kickers to deflect the beam. There are two basic forms of feedback in the BDS: train-by-train feedbacks, which operate at the 5 Hz repetition rate of the ILC, and intra-train feedbacks, which can apply a correction to the beam between bunches of a single train.

2.7.4.2.1 Train-by-train feedback   A train-by-train feedback with 5 correctors controls the orbit through the sextupoles in the horizontal and vertical planes, where the optical tolerances are tightest. Additional correctors throughout the BDS help reduce long-term beam size growth. The orbit control feedback can maintain the required beam sizes at the IP over periods from a few hours to several days depending on details of the environment. On longer timescales, IP dispersion and coupling knobs need to be applied.

2.7.4.2.2 Intra-Train IP position and angle feedbacks   The intra-train feedbacks use the signals detected on early bunches in the train to correct the IP position and angle of subsequent bunches. The offset of the beams at the IP is determined by measuring the deflections from the beam-beam interaction; this interaction is so strong that nm-level offsets generate deflections of tens of microradians, and thus BPMs with micron-level resolution can be used to detect offsets at the level of a fraction of a nanometer. Corrections are applied with a stripline kicker located in the incoming beamline between SD0 and QF1. The angle of the beams at the IP is determined by measuring the beam positions at locations $90°$ out of phase with the IP; at these locations the beam is relatively large so micron resolution is sufficient to directly measure the beam position (and hence the IP angle) to a small fraction

of its RMS size. A stripline kicker is located at the entrance to the FF causing a latency of about 4 bunch spacings.

The position feedback BPM is located near the IP in a region where electromagnetic backgrounds or particle debris from the collisions are a concern. Preliminary results from simulations and from a test-beam experiment indicate that backgrounds are an order of magnitude too small to cause a problem [68].

2.7.4.2.3 Luminosity feedback Because the luminosity may be extremely sensitive to bunch shape, the maximum luminosity may be achieved when the beams are slightly offset from one another vertically, or with a slight nonzero beam-beam deflection. After the IP position and angle feedbacks have converged, the luminosity feedback varies the position and angle of one beam with respect to the other in small steps to maximize the measured luminosity.

2.7.4.2.4 BDS Entrance Feedback ('train-straightener') A bunch-to-bunch correction at the end of the Linac removes systematic transverse position offsets within the train due to long-range wakefield kicks in the accelerating cavities. This system consists of two kicker-BPM systems similar to those described above. Each pair operates at a different phase to null the orbit in both vertical degrees of freedom.

For stripline kickers the maximum correction would be about 8–10 μm, and the BPM resolution requirements are about 200 nm. This requires cavity BPMs that are read out in bunch-bunch mode and processed with low-latency electronics. The kicker-BPM separations imply latencies of about 400 ns, allowing feedback on every-other bunch.

2.7.4.2.5 Hardware Implementation for intra-train feedbacks High bandwidth, low-latency ($\sim$5 ns) signal processors for stripline and button BPMs have been tested at the NLCTA and ATF [69]. The feedback processor has been prototyped using fast state of the art FPGAs; a system prototype has been demonstrated with a FB board latency of $\sim$70 ns [70]. Commercial boards that meet the latency requirement are not available without custom firmware modification; one such board has been tested by the FONT group and would meet the ILC latency specification for bunch-bunch operation.

2.7.4.3 Energy, Luminosity and polarization measurements

2.7.4.3.1 Energy measurements Absolute beam energy measurements are required by the ILC physics program to set the energy scale for particle masses. An absolute accuracy better than 200 ppm is required for the center-of-mass energy, which implies a requirement of 100 ppm on determination of the absolute beam energy. The intra-train relative variation in bunch energies must be measured with a comparable resolution. Measurements of the disrupted energy spectrum downstream of the IP are also useful to provide direct information about the collision process.

To achieve these requirements, there are two independent and complementary detectors for each beam. Upstream from the IP, a spectrometer based on the LEP-II energy spectrometer is capable of making high-precision bunch-to-bunch relative measurements in addition to measuring the absolute beam energy scale. A four-magnet chicane in the instrumentation region provides a point of dispersion which can be measured using triplets of high-precision

RF BPMs. The maximum displacement of the beam is a few millimeters and must be measured to a precision below 100 nanometers. Precision movers keep the beam nearly centered in the BPMs in order to achieve this accuracy.

Downstream from the IP, there is a synchrotron radiation spectrometer. A three-magnet chicane in the extraction line provides the necessary beam deflection, while the trajectory of the beam in the chicane is measured using synchrotron radiation produced in wiggler magnets imaged ∼70 meters downstream at a secondary focus near the polarimeter chicane.

2.7.4.3.2   Luminosity measurements   The ILC luminosity can be measured with a precision of 10^{-3} or better by measuring the Bhabha rate in the polar-angle region from 30-90 mrad. Two detectors are located just in front of the final doublets as shown in Figure 2.7-11. The *LumiCal* covers the range from 30-90 mrad and the *BeamCal* covers the range from 5-30 mrad. At 500 GeV center-of-mass energy, the expected rate in the *LumiCal* region is ∼10 Bhabhas per bunch train, which is too low to permit its use as an intra-train diagnostic for tuning and feedback. At smaller polar angles of 5-30 mrad the rate or energy deposition of beamstrahlung e+e- pairs can be measured for a fast luminosity diagnostic. The expected rate in this region is 15,000 pairs (and 50 TeV energy deposition) per bunch crossing. Furthermore, the spatial distributions of pairs in this region can be used to determine beam collision parameters such as transverse sizes and bunch lengths.

2.7.4.3.3   Polarization measurements   Precise polarimetry with 0.25% accuracy is needed to achieve the ILC physics goals Compton polarimeters citeMoffeit-SLACPUB11322,Meyners-LCWS05 are located both ∼1800 m upstream of the IP, as shown in Figure 2.7-2, and downstream of the IP, as shown in Figure 2.7-10, to achieve the best accuracy for polarimetry and to aid in the alignment of the spin vector.
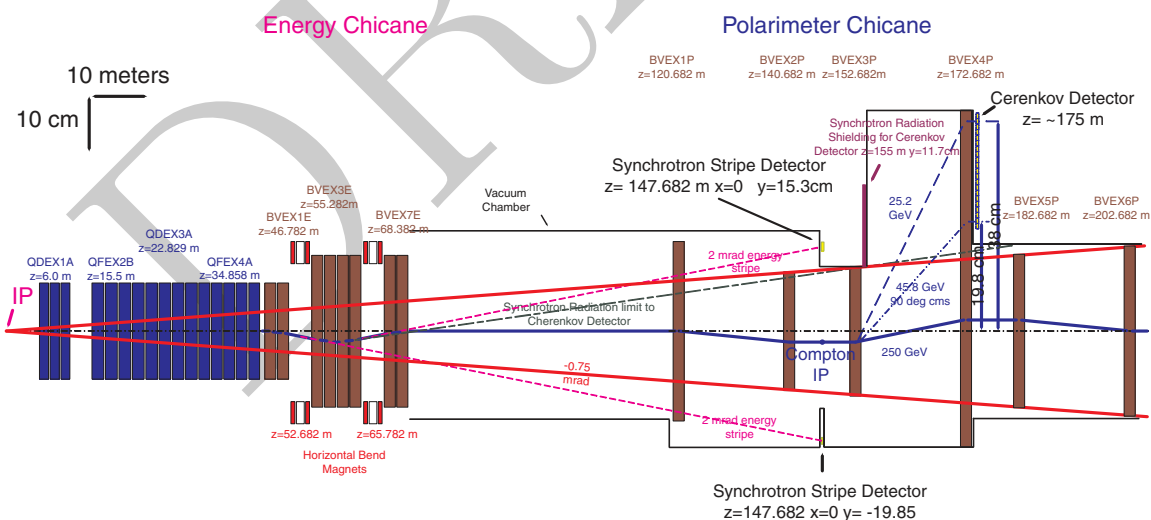
FIGURE 2.7-10. Schematics of energy and polarimeter chicanes in the 14 mrad extraction line, shown in a configuration with two additional bends at the end. Longitudinal distances are given from the IP. Also shown is the 0.75 mrad beam stay-clear from the IP.

The upstream polarimeter measures the undisturbed beam before collisions. The rela-

tively clean environment allows a laser system that measures every single bunch in the train and a large lever arm in analyzing power for a multi-channel polarimeter, which facilitates internal systematic checks. The good field region of the individual dipoles is wide enough to accommodate the lowest expected beam energy of 45.6 GeV. The downstream polarimeter measures the polarization of the outgoing beam after collision. The estimated average depolarization for colliding beams is 0.3%, and for the outgoing beam 1%. A schematic drawing of the extraction line is shown in Figure 2.7-10.

Each polarimeter has a dedicated 4-bend chicane to facilitate injection of the laser light and extraction of the Compton signal. The upstream polarimeter uses a horizontal chicane to minimize emittance growth from synchrotron radiation, while the downstream polarimeter uses a vertical chicane to maximize analyzing power. The systems are designed to meet the physics requirements at all energies from the Z pole to the full energy of the ILC.

2.7.4.4 Beam dumps and Collimators

The beam delivery system contains two tune-up dumps and two main beam dumps. These four dumps are all designed for a peak beam power at nominal parameters of 17 MW at 500 GeV per beam. These dumps consist of 1.5 m diameter cylindrical stainless steel high pressure (10 bar) water vessels with a 30 cm diameter 1 mm thick Ti window; and also include their shielding and associated water systems.

The dumps absorb the energy of the electromagnetic shower cascade in 6.5 m (18 X_0) of water followed by 1 m of water cooled Cu plates (22 X_0). Each dump incorporates a beam sweeping magnet system to move the charged beam spot in a circular arc of 3 cm radius during the passage of the 1 ms long bunch train. Each dump operates at 10 bar pressure and also incorporates a vortex-flow system to keep the water moving across the beam at 1.0-1.5 m/s. In normal operation with 250 GeV beam energy, the combination of the water velocity and the beam sweepers limits the water temperature rise during a bunch train to 40°C. The pressurization raises the boiling temperature of the dump water; in the event of a failure of the sweeper, the dump can absorb up to 250 bunches without boiling the dump water.

The integrity of the dump window, the processing of the radiolytically evolved hydrogen and oxygen, and containment of the activated water are important issues for the full power dumps. The dump service caverns include three loop pump driven 2300 gallon per minute heat exchanger systems, devices to remotely exchange dump windows as periodic maintenance, catalytic H_2-O_2 recombiners, mixed bed ion exchange columns for filtering of ^{7}Be, and sufficient storage to house the volume of tritiated water during maintenance operations.

In addition to the main dumps, the BDS contains 16 stoppers, of which 14 are equipped with burn-through monitors, and the extraction lines have 6 fixed aperture high power devices composed of 10 mm aluminum balls immersed in water. The beam delivery system contains 32 variable aperture collimators and 32 fixed aperture collimators. The devices with the smallest apertures are the 12 adjustable spoilers in the collimation system. To limit their impedance to acceptable levels, these 0.6-1.0 X_0 Ti spoilers have longitudinal Be tapers.

2.7.4.5 BDS Magnets

The BDS has a wide variety of different magnet requirements, and the most distinct magnet styles (67) of any ILC area, even though there are only 636 magnets in total. Of these, 86 are superconducting magnets clustered into 4 cryostats close to the IP, as described in

TABLE 2.7-2
BDS components, total counts.

Magnets		Instrumentation		Dumps & Collimators	
Warm dipoles	190	BPMs C-band	262	Full power dumps	4
Warm quads	204	BPMs L-band	42	Insertable dumps	2
Warm sextupoles	10	BPMs S-band	14	Adjustable collim.	32
Warm octupoles	4	BPMs stripline/button	120	Fixed apert. collim.	32
SC quads	32	Laser wire	8	Stoppers	14
SC sextupoles	12	SR transv. profile imager	10		
SC octupoles	14	OTR screens	2	Vacuum	
Muon spoilers	2	Crab & deflection cavities	4	Pumps	3150
Anti-solenoid	4	Loss monit. (ion chamb., PMT)	110	Gauges	28
Warm correctors	64	Current monitors	10	Gate valves	30
SC correctors	36	Pick-up phase monitors	2	T-connections	10
Kickers/septa	64	Polarimeter lasers	3	Switches	30

section 2.7.3.4, and the tail-folding octupoles described below. There are 64 pulsed magnets: 5 styles of abort kickers, sweepers and septa. These are used to extract the beams to a fast extraction/tuning dump and to sweep the extracted beam in a 3 cm circle on a dump window.

The remaining 474 magnets are conventional room temperature magnets, mostly with water-cooled hollow copper conductor coils and low carbon steel cores. The bend magnets in the final focus have fields of less than 0.5 kG to minimize synchrotron radiation that would cause beam dilution; they use solid wire coils. The quadrupoles and sextupoles have straightforward designs adequate for up to 500 GeV beam. The extraction line magnets have large apertures, e.g. over 90 mm and up to 272 mm, to accommodate the disrupted beam and the photons emerging from the IP. These magnets must fit in alongside the incoming beamline.

The main technical issue with the BDS magnets is their positional stability. All the incoming beamline quadrupoles and sextupoles sit on 5 degree of freedom magnet movers with a 50 nm smallest step size. BPMs inserted in the magnet bores provide data on the relative position of each magnet with respect to the beam so that it can be moved if necessary. The absolute field strength of the BDS magnets has a tight tolerance, requiring power supplies with stability of a few tens of ppm. Magnet temperature changes lead to strength and position variations so the ambient temperature in the tunnel must be controlled to within about 0.5°C and the cooling water to within 0.1°C.

2.7.4.5.1 BDS Magnets: Tail Folding Octupoles The tail folding octupoles are the only superconducting magnets in the BDS (other than the FD and extraction quadrupoles) and have the smallest, 14 mm ID, clear working aperture in order to reach the highest practical operating gradient. The magnets are energized via NbTi conductor cooled to 4.5 K. With such a small aperture, the beam pipe must have high conductivity to minimize the impact of wakefields. This can be achieved with a cold aluminum beam pipe at 4.5 K or a cold stainless steel beam pipe with a high conductivity coating. Because these magnets are

isolated in the BDS, being far from either the IP or the end of the linac, cryocoolers are used to provide standalone cooling.

2.7.4.6   Vacuum system

While the aperture of the BDS vacuum chamber is defined by the sizes of the beam, its halo and other constraints, the design of the chambers and vacuum level are governed mainly by two effects: resistive and geometric wakes and the need to preserve the beam emittance; beam-gas scattering and minimization of detector background.

2.7.4.6.1   Wakes in vacuum system   The resistive wall (RW) wakefield of the BDS vacuum system and the geometric wakefield of the transitions in the beam pipe may cause emittance growth due to incoming (transverse) jitter or drift, or due to beam pipe misalignment. In order to limit these effects to tolerable levels, the BDS vacuum chamber must be coated with copper, the vacuum chambers must be aligned with an RMS accuracy of $\sim 100\ \mu$m [73], and incoming beam jitter must be limited to 0.5 σ_y train-to-train and 0.25 σ_y within a train, to limit the emittance growth to 1-2%.

2.7.4.6.2   Beam-gas scattering   The specification for the pressure in the BDS beam pipe is driven by detector background tolerance to beam-gas scattering. Studies have shown that electrons which are scattered within 200 m of the IP can strike the beam pipe within the detector and produce intolerable backgrounds, while electrons which scatter in the region from 200 to 800 m from the IP are much more likely to hit the protection collimator upstream of the final doublet and produce far less severe detector backgrounds [74]. Based on these studies, the vacuum in the BDS is specified to be 1 nTorr within 200 m of the IP, 10 nTorr from 200 m to 800 m from the IP, and 50 nTorr more than 800 m from the IP.

In the extraction lines the pressure is determined by beam-gas scattering backgrounds in the Compton Polarimeter [**?**] located about 200 m from the IP. Here the signal rates are large enough that 50 nTorr would contribute a negligible background in the detectors.

2.7.4.6.3   Vacuum system design   The BDS vacuum is a standard UHV system. The main beampipes are stainless steel, copper coated to reduce the impedance, with the *option* of an aluminum alloy chamber. In locations where there is high synchrotron radiation (SR) power ($\geq$10 kW/m) (e.g. in the chicanes or septa regions), the beampipe is copper with a water-cooled mask to intercept the photons. The beampipes are cleaned and baked before installation. There is no *in situ* baking required except possibly for the long drift before the IP.

The required maximum pressure of 50 nTorr (N_2/CO equivalent) can be achieved by standard ion pumps located at appropriate intervals. The beampipe near the IP must have pressure below 1 nTorr for background suppression, and may be baked *in situ* or NEG-coated.

2.7.4.7   IR arrangements for two detectors

There are two detectors in a common IR hall which alternately occupy the single IR, in a so-called "push-pull" configuration. The detector hall is 120 m (long) $\times$ 25 m (wide) $\times$ 38 m (high). The layout of the hall is compatible with surface assembly of the detectors. The
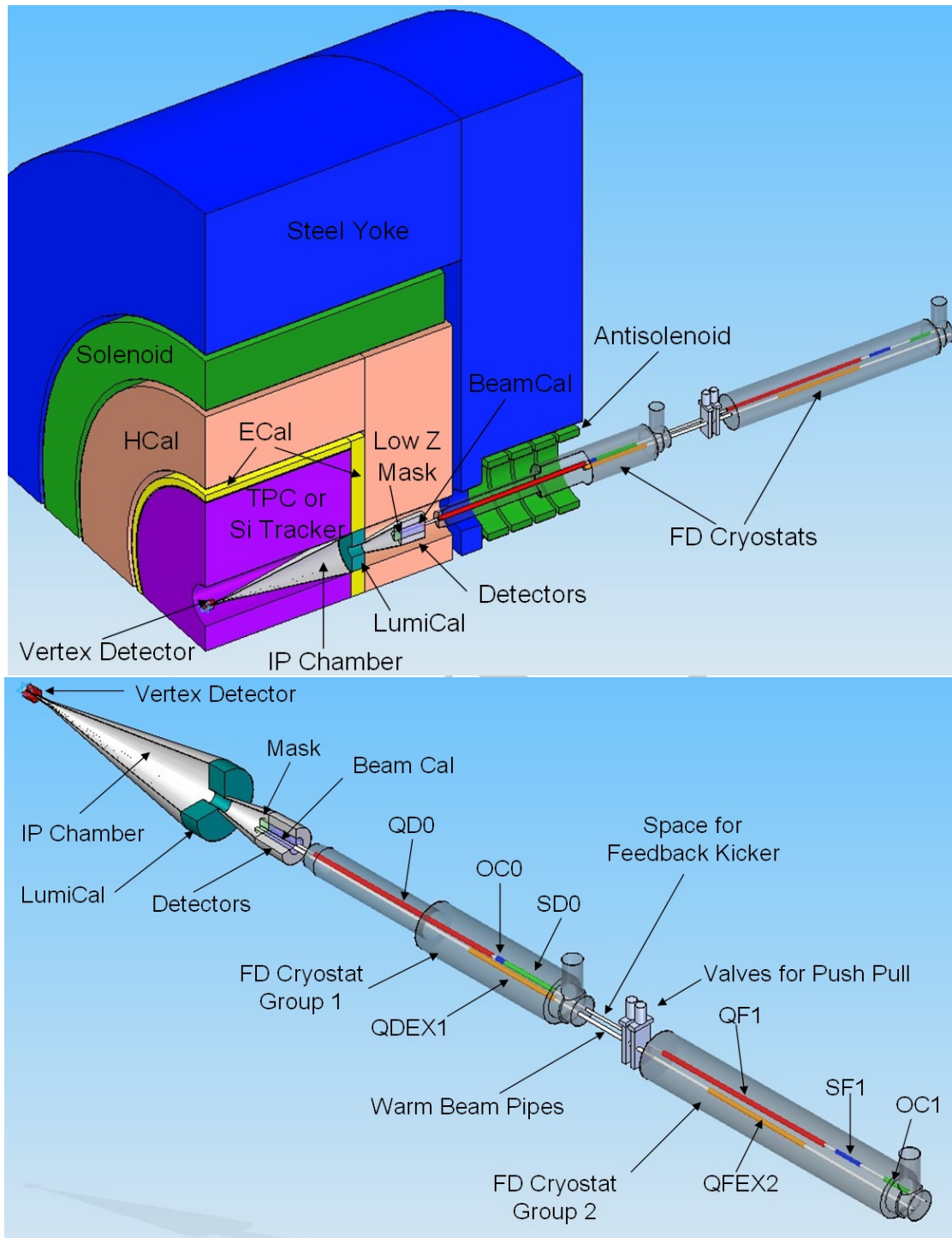
FIGURE 2.7-11. Generic detector and IR arrangements, showing the location of beamline elements near the IR and their integration with the detector.

previous layout with two 14 mrad IRs is kept as an *alternative configuration*, and is about 50% more expensive than the single IR.

To facilitate the exchange of detectors, there is a breakpoint in the beam line near the edge of the detector, between the two final doublet cryostat halves as shown in Figure 2.7-5 and Figure 2.7-11. A necessary condition for efficient push-pull operation is to avoid disconnecting

any of the systems for the detectors during the exchange. One possible solution is to equip each detector with an adjacent services platform which moves together with the detector. The platforms would house the cryogenic systems, high current power supplies for solenoids and FD, and detector electronics. All the connections between the platform and detector would be fixed and not disconnected during the exchange. The movable detector service platform would have flexible connections to fixed services (including high voltage AC, room temperature high pressure He supply and return, data I/O, etc.), that do not need to be disconnected during the exchange.

The FD alignment and support system is designed to be compatible with rapid exchange, in particular, an interferometer network between the two parts of the FD and the walls may be needed. The push-pull arrangement of two detectors implies specific requirements for the radiation safety design of the detector and of the collider hall shielding. Since the off-beam axis detector needs to be accessible during beam operation, the detectors either need to be self shielded or there must be a shielding wall between them.

Several technical solutions for moving the detectors are under consideration, including rails, Hilman Rollers or air pads. A guiding mechanism is needed to determine the path for the detector motion and its accurate positioning. The motion of a heavy detector (up to 14 kton) in the collider hall produces deformations, which are estimated to be less than a millimeter [75]. The detector support system must ensure that those deformations, as well as possible deformations during lifting, do not affect its internal alignment. To minimize deformations, the detector may require a support platform. The 5 cm thick steel plates covering most of the experimental hall area also facilitate stability and allow the use of air-pads.

2.7.4.8 Diagnostic and Correction devices

Each quadrupole, sextupole, and octupole magnet in the incoming BDS beamlines is placed on an x/y/roll/pitch/yaw mover, and has an associated BPM. There are also several tens of correctors in the incoming beamlines for 5 Hz feedback, and in the extraction lines, where there are no movers. The BPMs in the incoming beamline are RF-cavities, either S, C or L-band, depending on the beamline aperture. Long chains of bends or kickers have sparsely placed BPMs. BPMs in the extraction lines are button or strip-line design.

Additional instrumentation in the BDS includes a deflecting cavity to measure Y-T correlation, ion chamber and PMT loss monitors, X-synchrotron light transverse profile monitors, OTR monitors, current monitors, pickup phase monitors, etc.

2.8 EMITTANCE PRESERVATION AND LUMINOSITY STABI-LIZATION

2.8.1 Overview

The luminosity performance of the ILC will be affected by many issues ranging from space charge effects at the electron gun to instabilities in the damping rings to timing errors at the IP. This section addresses issues associated with the emittance preservation from the damping ring extraction to the IP which is referred to as the Low Emittance Transport (LET). Other accelerator physics issues are addressed in the respective subsystem descriptions.

Static and dynamic imperfections in the LET impact the luminosity performance; examples are the survey errors of beamline components and ground motion. Preserving the ultra-small emittances requires component alignment tolerances far beyond that which can be achieved by traditional mechanical and optical alignment techniques, hence the use of beam-based alignment and tuning techniques are essential in obtaining the design luminosity. The corresponding sensitivity to ground motion and vibration mandates the use of continuous trajectory correction feedback systems in maintaining that luminosity. The accelerator physics group must develop the necessary procedures, specify the required hardware and assess the potential luminosity degradations.

Estimation of the luminosity performance relies on complex simulations. Experimental verification of the predictions of the codes is difficult, since the very small emittances are not readily available in test facilities. Nonetheless, several of the fundamental aspects of the algorithms have been successfully tested. Many of the emittance transport concepts were demonstrated and benchmarked in the Stanford Linear Collider (SLC) which operated from 1987 to 1998. Beam-based alignment has been demonstrated in SLC [?], LEP [76], and the final focus test beam [?] — a first test of the final focus which demonstrated the demagnification required for the ILC, and achieved a final spot size of 50 nm. The SLC operated with tolerances that are very similar to those required for the ILC. The Accelerator Test Facility (ATF) Damping Ring at KEK is a low-emittance test facility that addresses some of the emittance issues, and is being extended into a Beam Delivery System test facility (ATF2). While not a full-scale test of the ILC damping ring and beam delivery system, they can test a number of aspects of low-emittance generation and preservation.

The simulation tools in use have been developed and refined over many years. Extensive studies for a superconducting linear collider were performed for the TESLA TDR [2] and the ILC Technical Review Committee [?], many of which are quite applicable to the present ILC and provide confidence in the design concepts. In addition, extensive studies have been made for linear collider designs based on normal conducting acceleration at X-band (JLC/NLC) and K-band (CLIC), which were designed to operate under more stringent beam dynamics regimes.

For the aspects of the machine performance that cannot be tested experimentally before construction, simulations provide the only tool. Fully integrated and realistic simulations are needed to study both the static (peak luminosity) and dynamic (integrated luminosity) behavior of the machine.

The performance of the ILC has been simulated for a variety of errors and procedures. Design performance was achieved in essentially all of these studies. Although the studies are not yet complete, they are not expected to uncover major obstacles that would prevent the ILC from reaching design performance.

2.8.2   Sources of Luminosity Degradation

The performance of the real machine is rapidly degraded by errors in both component alignment and field quality. For example, misaligned magnets result in beam trajectory errors which cause emittance growth via chromatic effects (dispersion) or impedance effects (wakefields). The primary sources of emittance degradation considered are:

- Dispersion: The anomalous kicks from misaligned quadrupoles, coupled with the non-zero energy spread of the beam, cause dispersive emittance growth.
- X-Y Coupling: Rotated quadrupoles and vertically misaligned sextupoles (for example) couple some fraction of the large horizontal emittance into the small vertical emittance.

- Single-bunch wakefields: An off-axis bunch in a cavity or beampipe generates a dipole wakefield, causing a transverse deflection of the tail of the bunch with respect to the head. The wakefields are relatively weak for the SCRF accelerating cavities, and the cavity alignment tolerances correspondingly loose.
- Multi-bunch wakefields (Higher-Order modes): Leading bunches kick trailing bunches, which can lead to individual bunches in a train being on different trajectories.
- Cavity tilts: The transverse component of the accelerating field causes a transverse kick on the beam.

2.8.3   Impact of Static Imperfections

2.8.3.1   Beam-Based Alignment and Tuning

The beam emittance at damping ring extraction is $\gamma\epsilon_x = 8$ μm and $\gamma\epsilon_y = 20$ nm. In a perfect machine, the emittance would be essentially the same at the interaction point. To allow for imperfections, the ILC parameters specify a target emittance at the IP of $\gamma\epsilon_x = 10$ μm and $\gamma\epsilon_y = 40$ nm. An emittance growth budget for the various regions has been set at $\Delta\epsilon_y \leq 4$ nm for the RTML, $\Delta\epsilon_y \leq 10$ nm for the main linac, including the positron source, and $\Delta\epsilon_y \leq 6$ nm for the BDS. These allocations may be redistributed as the RTML budget currently appears too optimistic while the main linac budget appears generous. Depending on the actual misalignments, the machine performance can differ significantly. The goal for the alignment and tuning procedures is to ensure that the emittance growth is within the budget with a likelyhood of at least 90%.

Similar beam-based alignment and tuning procedures are applied in the different subsystems of the LET. First, the elements are aligned in the tunnel with high precision. When the beam is established, the corrector dipoles are used to zero the readings in the Beam Position Monitors (BPMs) (so-called one-to-one steering). Even with a very good installation accuracy, the final emittance will be significantly above the target; table 2.8-1 lists the expected main linac alignment errors together with the emittance growth resulting from each error after simple steering. The most important error source is the total BPM offset (with respect to the design ideal reference; note that an offset of a cryomodule also results in a BPM offset). Achieving the emittance goal requires beam-based alignment (BBA) to minimize the dispersive emittance growth (the dominant source of aberration).

All BBA algorithms attempt to steer the beam in a dispersion-free path through the centers of the quadrupoles, either by physically moving the magnets (remote magnet movers) or by using corrector dipoles close to the quadrupoles. The exact details of the algorithms and their relative merits differ. The three most studied methods are:

TABLE 2.8-1
Assumed installation errors in the main linac, and the emittance growth for each error assuming simple one-to-one steering. The required emittance preservation can only be achieved using beam-based alignment of the magnets/BPMs.

Error	with respect to	value	$\Delta\gamma\epsilon_y$ [nm]
Cavity offset	module	300 μm	0.2
Cavity tilt	module	300 $\mu radian$	< 0.1
BPM offset	module	300 μm	400
Quadrupole offset	module	300 μm	0
Quadrupole roll	module	300 $\mu radian$	2.5
Module offset	perfect line	200 μm	148
Module tilt	perfect line	20 $\mu radian$	0.7

- Dispersion Free Steering (DFS): Beam trajectories are measured for different beam energies, and the final trajectory minimizes the difference, thus minimizing the dispersion.

- Kick Minimisation (KM): The BPM offsets with respect to the associated quadrupole magnetic centers are determined by varying the quadrupole strength and monitoring the resulting downstream beam motion. This information is used in a second step to find a solution for the beam trajectory where the total kick from quadrupoles and correctors on the beam is minimized.

- Ballistic Alignment (BA): A contiguous section of quadrupoles (and in the linac the RF) is switched off and the ballistic beam is used to determine the BPM offsets with respect to a straight line. The quadrupoles/RF are then restored, and the beam is steered to match the established straight line.

All BBA techniques rely on precise measurements of the BPMs to determine a near dispersive-free trajectory. The final performance of the algorithms is determined by the resolution of the monitors.

Once BBA is complete, a final beam-based tuning either minimizes the beam emittance by direct measurement of the beam size (emittance) or maximizes the luminosity. Closed-trajectory bumps or specially located and powered tuning magnets are used as orthogonal knobs to generate specific aberrations, such as dispersion or X-Y coupling. The knobs are tuned to minimize the emittance (or maximize the luminosity) by canceling the remaining aberrations in the beam.

2.8.3.2 RTML before the Bunch Compressor

The issue of static emittance growth from misalignments and errors has been studied in some detail for the section of the RTML from the turnaround to the launch into the bunch compressor. The strong focusing, strong bending, strong solenoids, and large number of betatron wavelengths in this area can potentially lead to very serious growth in the vertical emittance, despite the relatively low energy spread of the beam extracted from the damping rings.

The tolerances used in the study were similar to those found at the Final Focus Test Beam for warm, solid-core iron-dominated magnets and are listed in table 2.8-2.

ACCELERATOR DESCRIPTION

TABLE 2.8-2
Alignment tolerance for RTML section up to the bunch compressors.

Misalignment	RMS Value	wrt
Quadrupole Misalignment (x,y)	150 μ m	Survey Line
BPM Misalignment (x,y)	7 μ m	Quad Center
Quadrupole Strength Error	0.25%	Design Value
Bend Strength Error	0.5%	Design Value
Quadrupole Rotation	300 μ rad	Survey Line
Bend Rotation	300 μ rad	Survey Line

Dispersion Correction: The preferred dispersion correction method was found to be a combination of Kick Minimization (KM) and dispersion knobs, the latter consisting of pairs of dedicated skew quadrupoles located in the turnaround, where there is non-zero horizontal dispersion. The two skew quads in a pair are separated by a $-I$ transform such that exciting the quads with equal-and-opposite strengths causes the resulting betatron coupling to cancel and the dispersion coupling to add. There are two such dispersion knobs in the turnaround, which allows correction of dispersion at each betatron phase. Simulations indicate that in the absence of measurement errors, the combination of KM and dispersion knobs (DK) can completely eliminate dispersion as a source of emittance growth in this part of the RTML. The principal remaining source of emittance dilution is betatron coupling, which typically contributes about 7.2 nm of emittance growth.

Coupling Correction: The coupling correction section consists of four skew quads phased appropriately to control all four betatron coupling parameters of the beam. The skew quads are used to minimize the vertical beam sizes as measured in the downstream emittance measurement station. The correction system is can completely eliminate the betatron coupling introduced by misalignments and errors in this section of the RTML.

In addition to the studies described above, the emittance preservation issues in the long transfer line from the damping ring to the turnaround have been examined. Because of the weaker focusing, the alignment tolerances are much looser than in the turnaround area, and emittance preservation is relatively straightforward [78]. One possible remaining error source in the long transfer line is the impact of time-varying stray fields, which can drive orbit oscillations. This can be cancelled by the feed-forward system located across the turnaround. Measurements at existing laboratories [79] indicate a reasonable estimate for the magnitude of time-dependent stray field is $\tilde{2}$ nTesla, which will not cause a problem.

2.8.3.3 Bunch Compressors

The RF in the bunch compressor introduces an energy correlation along the bunch. The long bunch from the Damping Ring (9 mm) makes the beam particularly sensitive to cavity tilts in the bunch compressor RF. The near-zero phase crossing of the bunch induces a strong transverse kick which is also correlated to the longitudinal location in the bunch (i.e. the bunch is crabbed), and therefore also strongly correlated to the induced energy spread. The resulting kick-energy correlation can effectively be compensated using downstream dispersion knobs. Wakefield-driven head-tail correlations can also be compensated the same way. As with other sections of the LET, the other primary source of emittance dilution is dispersion due to misaligned quadrupoles.

Simulation studies with RMS random quadrupole offsets of 0.3 mm, cavity offsets of 0.3 mm and cavity pitch of 0.3 mrad, indicate that combined DFS and DK will reduce the mean emittance dilution to less than 2 nm [81]. Simulations of combined KM and DK result in several nm of residual emittance dilution. The expected 0.3 mrad RMS quadrupole roll errors cause a modest average increase of the vertical emittance of less than 1 nm without any corrections. Although very promising, these results are preliminary and further study is required with more realistic errors [80].

2.8.3.4   Main Linac
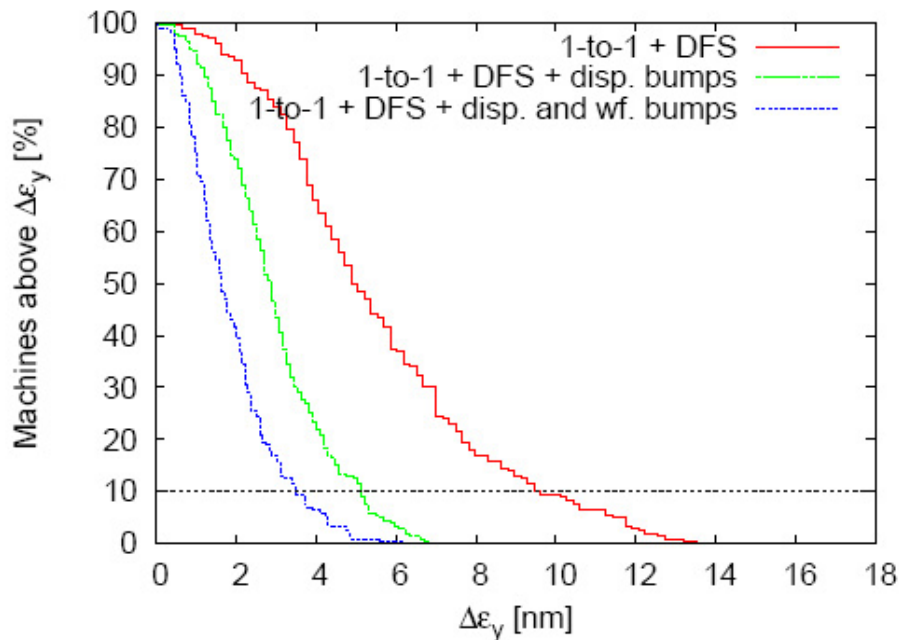
FIGURE 2.8-1. The fraction of simulated cases staying below the emittance growth target for the main linac after Dispersion Free Steering (red), followed by application of dispersion knobs (blue), followed by wakefield knobs (green).

Single-bunch emittance dilution in the main linac is dominated by chromatic (dispersive) effects and wakefield kicks arising from misaligned quadrupoles and cavities respectively. X-Y coupling arising from quadrupole rotation errors also adds a small contribution to the vertical emittance growth. The assumed installation errors are listed in table 2.8-1. The tolerances for cavity offsets and quadrupole rolls can be achieved mechanically, but beam-based tuning is required for the quadrupole and BPM offsets.

The main linac follows the gravitational equipotential of the earth, and is therefore not laser-straight. This gentle bending in the vertical plane results in a small but non-negligible design dispersion which must be matched, and taken into consideration during beam-based alignment. A variant of dispersion free steering, dispersion matched steering (DMS), is used to attain the matched dispersion function along the lattice. This modified form of DFS requires well calibrated BPMs [83] to the level of 5-10% with very stable readout. The

method achieves the required performance in simulations[82, 83, 84, 85]. Additional tuning knobs to modify the dispersion at the beginning and end of the linac reduce the emittance growth still further to well below the budget[89], see Fig. 2.8-1. Further improvement is possible with wakefield tuning knobs.

Studies of kick minimisation have shown similar performance as DMS[90]. The ballistic alignment method has not been applied to the latest ILC lattice, however studies for TESLA showed that ballistic alignment and dispersion free steering yielded comparable results (for a laser-straight machine).

The suppression of multi-bunch wakefields (high-order modes, HOMs) have been a major part of the SCRF R&D effort over the last decade. If left unsuppressed, the HOMs, which can have very high Q-values, would lead to unacceptable multi-bunch emittance growth. Suppression is achieved by random cavity detuning (0.1effect is mitigated by using a split-tune lattice in which the vertical and horizontal beam oscillation wavelengths are different, thus avoiding resonant coupling.

Different codes have been compared in detail for the main linac[86] finding excellent agreement for both tracking and performance predictions for a specific beam-based alignment method. This cross-benchmarking increases confidence in the results of each individual code.

2.8.3.5 Undulator Section for Positron Production

At the nominal 150 GeV point in the electron main linac, the beam passes through an undulator and emits hard photons for positron production. This insert has several potential consequences for emittance preservation which still require detailed study:

- Stronger focusing in the 1.2 km insert leads to additional dispersive emittance growth. This should be correctible using BBA methods.

- The undulator increases the energy spread of the beam, which increases the dispersive emittance growth in the downstream linac. This effect is expected to be small.

- The narrow bore vacuum vessel in the undulator is a potential source of transverse wakefields. Initial studies indicate these effects to be small.

- The restricted bandwidth of the undulator chicane may hinder the use of DFS algorithms in the downstream linac. This problem can be alleviated by a straight-ahead bypass for tuning purposes.

Preliminary studies indicate the total emittance growth in this insertion to be small compared to the overall main linac budget. Further studies are required, however, including integration into the complete electron LET simulations.

2.8.3.6 Beam Delivery System (BDS)

Beam-based procedures has been developed to align and tune the BDS. First, all multipoles are switched off and the quadrupoles and BPMs are aligned. Second the multipoles are switched on and aligned. Finally, tuning knobs are used to correct the different beam aberrations at the interaction point. Detailed simulations have been made assuming the realistic installation alignment errors and magnet field errors given in Table 2.8-3.

TABLE 2.8-3
Assumed imperfections in the BDS. The assumed magnet strength errors are very tight, it is expected that more realistic larger errors mainly lead to slower convergence of the procedures.

Error	with respect to	size
Quad, Sext, Oct x/y transverse alignment	perfect machine	200 um
Quad, Sext, Oct x/y roll alignment	element axis	300 urad
Initial BPM alignment	magnet center	30 um
Strength Quads, Sexts, Octs	nominal	1e-4
Mover resolution (x/y)		50 nm
BPM resolutions (Quads)		1 um
BPM resolutions (Sexts, Octs)		100 nm
Power supply resolution		14bit
Luminosity measurement		0.1%

The current studies have been performed using the beam-beam interaction code GUINEA-PIG to give a realistic estimate of the luminosity, but assuming that the luminosity is measured accurately. Further studies are planned including a realistic simulation of luminosity measurement. The studies will also be crosschecked with other simulation codes. Results to date indicate that the design goals can be achieved with some overhead.

2.8.4   Dynamic Effects

The ILC relies on several different feedback systems to mitigate the impact of dynamic imperfections on the luminosity. These feedback systems act on different timescales. The long $\tilde{1}$ ms pulse length and relatively large bunch spacing ($\tilde{3}00$ ns) makes it possible to use bunch-to-bunch (or intra-train) feedbacks located at critical points, the most important one being the beam-beam feedback at the interaction point which maintains the two beams in collision. Other feedback systems act from train to train (inter-train) at the 5 Hz pulse repetition rate of the machine. Over longer timescales (typically days or more) the beam may have to be invasively re-tuned.

The performance of the feedback systems is governed by the effective loop gain. A large gain (large bandwidth) is desirable to decrease the response time of the feedback; this is particularly true for the intra-train feedback, which reacts to each new pulse. A fast response time minimizes the number of initial bunches over which the feedback converges (normally a few percent effect). A low gain is desirable to reduce the amplification of high-frequency noise in the beam, and to effectively integrate away (average over) monitor resolution. The exact choice of gain is an optimization based on the noise spectrum being corrected (both in the beam and the monitors).

The number, type and location of feedback systems along the machine is also an optimization which is currently under study.

Very important sources of dynamic imperfections are ground motion and component vibration. The ground motion depends strongly on the site location. For the ILC-TRC study three ground motion models were developed, all based on measurements at existing sites: Model A represents a very quiet site (deep tunnel at CERN); Model B a medium site (linac tunnel at SLAC); Model C a noisy site (shallow tunnel at DESY). A fourth model (K) was

later developed based on measurements at KEK and is roughly equivalent to C. These models have been used in all subsequent simulations of the dynamic behavior of the ILC.

2.8.4.1 Bunch-to-Bunch (Intra-Train) Feedback and Feedforward Systems

The damping ring extraction kicker extracts each bunch individually. If this kicker does not fully achieve the required reproducibility, the beam will have bunch-to-bunch variations that cannot be removed by an intra-pulse feedback system (effective white-noise). The feedforward system in the RTML is designed to mitigate this effect. The position jitter of each bunch is measured before the turn-around and then corrected on that very bunch after the turn-around.

Quadrupole vibration in the downstream bunch compressor and (predominantly) in the main linac will induce transverse beam jitter (coherent betatron oscillations). The tolerance on the amplitude of this jitter (and hence on the quadrupole vibration) from the main linac itself is relatively relaxed. Quadrupole vibration amplitudes of the order of 100 nm RMS lead to negligible pulse-to-pulse emittance growth. However the resulting oscillation (one- to two-sigma in the vertical plane) in the BDS could lead to significant emittance degradation from sources such as collimator wakefields. An intra-train feedback at the exit of the linac solves this problem. In addition, this feedback could correct any residual static HOM disturbance in the bunch train. If the main linac quadrupole vibrations are significantly less than 100 nm (e.g. 30 nm RMS, as expected for a typical quiet site), then a intra-train feedback at the exit of the linac may not be required.

Small relative offsets of the two colliding beams, in the range of nanometers, lead to significant luminosity loss. The offsets are particularly sensitive to transverse jitter of the quadrupoles of the final doublet. Fortunately, the strong beam-beam kick causes a large mutual deflection of the offset beams, which can be measured using BPMs just downstream of the final quadrupoles. The intra-train feedback system zeros the beam-beam kick by steering one (or both) beams using upstream fast kickers. The system typically brings the bunch trains into collision within several leading bunches (depending on the gain). The IP fast feedback and the long bunch train also affords the possibility to optimize the luminosity within a single train, using the fast pair monitor as a luminosity signal [?].

Studies performed as part of the TRC indicated that in a quiet site (B or better) the fast beam-beam feedback and a slow orbit correction in the beam delivery system keeps the luminosity loss due to dynamic effects negligible [?, ?]. In a noisy site (e.g. C) some luminosity loss occurs.

2.8.4.2 Train-to-Train (5Hz) Feedback

The exact layout of the train-to-train feedback has not yet been finalized and different options are being studied. A simple but workable option is to use a number of local feedbacks. At certain locations in the machine a few correctors are used to steer the beam back through a few selected BPMs thus keeping the trajectory locally fixed. These feedback systems can be used in a cascaded mode where each of the feedback anticipates the trajectory change due to the upstream feedback systems. Such a system was successfully implemented at SLC.

Since the system corrects only locally, a residual of the dynamic imperfections will remain, due to deterioration of the trajectory between the feedback locations. After longer times this will require a complete re-steering of the machine back the exact trajectory determined from the initial beam-based alignment (gold-orbit).

Other envisaged options are to perform permanent re-steering with a very low gain; this method avoids the additional layer of steering but may be slower than local feedback. A further option is the use of a MICADO-type correction. In this procedure all BPMs are used to determine the beam orbit. A small number of most effective correctors is identified after each measurement and these are used to correct the trajectory.

2.8.4.3   Feedback Performance (Luminosity Stabilization)

A complete and realistic simulation of the dynamic performance of the collider requires complex software models which can accurately model both the beam physics and the errors (e.g. ground motion and vibration). The problem is further complicated by the various time scales which must be considered, which span many orders of magnitude: performance of the fast intra-train feedbacks requires modelling of the detailed 10 MHz bunch train; fast mechanical vibrations at the $\tilde{\mathrm{H}}$z level need to be accurately modelled to test the performance of the pulse-to-pulse feedback systems; long-term slow drifts of accelerator components over many days must be studied to determine long-term stability and the mean time between invasive (re-)application of BBA. Ideally all these elements need to be integrated into a single simulation of the complete machine.

Progress towards such complete simulations is on-going. However, many simulations have already been made, which have focused on individual aspects of the problem (time-scales), with varying degrees of sophistication of the feedback models. The results thus far give every indication that the ILC can achieve and maintain the desired performance. For example:

- Extensive simulations have been made of the performance of the fast beam-beam (and other) intra-train feedback using a model of the main linac and BDS to generate realistic bunch trains [95, 97]. For realistic component vibration amplitudes, the results indicate that feedback can maintain the luminosity within a few percent of peak on a pulse-to-pulse timescale (5 Hz). See for example Figure 2.8-2. These results are in agreement with earlier studies [?, ?].

- Drifts of components on the timescale of seconds to minutes have been studied [?, ?]. Simulations of 5 Hz operation with all ground motion models, and assuming the beams are maintained in collision by the fast IP feedback, indicate a slow degradation in luminosity. This can be mitigated by pulse-to-pulse feedback, especially in the BDS, where the tolerances are tightest. Noisy sites (model C) showed the most pronounced effect, and would place most demand on the slower feedback systems.

- Longer term stability has been studied, assuming a variety of configurations for the slower pulse-to-pulse feedbacks. Studies of the main linac [?] using local distributed feedback systems indicate that the time between re-steering ranges from a few hours to a few days for ground motion models C and B respectively. After 10/200 days (models C/B) simple re-steering does not recover the emittance, at which point a complete re-tuning would be necessary.

- Recent dynamic studies integrating the main linac and BDS, again based on distributed local pulse-to-pulse feedback systems (including one in the BDS) and incorporating many error sources and comparing all ground motion models have been made [98]. The noisy sites (models C and K) show a luminosity reduction of up to $\tilde{3}0\%$, coming almost entirely from the BDS. Based on results from earlier simulation of other collider designs
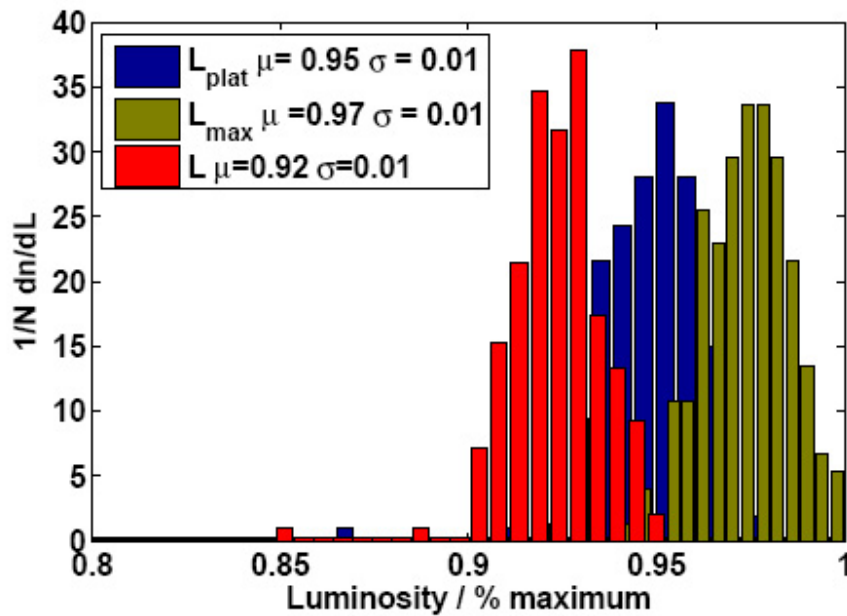
FIGURE 2.8-2. Example of integrated dynamic simulations, showing the performance of the beam-beam intra-train feedback system with realistic beams and beam jitter (simulated from the Main Linac and BDS). The histograms show performance over 100 seeds of random vibration motion: brown - achieved luminosity for an infinitely fast beam-beam feedback and no bunch-to-bunch variations (3% reduction from ideal); blue performance including bunch-to-bunch variations (driven by long-range wakefields in the Main Linac); red as blue but including a finite response time for the feedback (8% reduction from ideal). Taken from [95, 97].

(notably TESLA), it is expected that optimization of the BDS feedback configuration, together with possible additional stabilization of critical magnets, can recover a significant fraction of the loss. By contrast, quiet sites (models A and B) show only a few percent loss for the configuration studied.

Figure 2.8-2 shows the results of running 200 such simulations with differing random seeds. The brown histogram shows the achieved luminosity for an infinitely fast feedback and no bunch-to-bunch variations, it is 3% below the case without dynamic effects. The blue histogram includes the bunch-to-bunch variations while the red one also includes the time to convergence, leading to an average luminosity 8% below nominal. By optimizing the feedback gain and the intra-pulse luminosity tuning strategy, one can hope to recover part of the 5% additional loss.

2.8.5 Remaining Issues

Simulation tools must be developed further to fully specify the tuning algorithms, and in particular instrumentation, required to achieve and maintain the design luminosity. The cost impact should be minor, but the impact on the performance, in particular during commissioning of the machine, will be important.

The beam-based alignment and tuning procedures need to be fully specified for all subsystems. In particular, both the RTML and the positron source insertion in the electron linac need further detailed study. Detailed, fully-integrated and realistic studies of all the feedback systems also remains to be done. Of particular importance is to quantify the impact of dynamic errors and equipment failure on the initial static error tuning (beam-based alignment and knob-based tuning). Preliminary studies have shown no indication of a severe problem but more study is required.

More thorough studies of the effect of the phase stability of the crab-cavities in the Interaction Region are required, and particularly their interaction with the beam-beam feedbacks. In addition the crab-cavity wakefields can potentially amplify beam jitter and lead to emittance dilution [99]. This can be avoided by ensuring that the transverse modes are not resonant with the bunch frequency. Further study of collimator wakefields (and other general impedance issues in the BDS) is also required. Depolarization during the beam transport from the damping ring to the IP has been found not to be a problem[100, 87].

2.9   AVAILABILITY, COMMISSIONING AND OPERATIONS

2.9.1   Overview

The ILC is a complex machine with hundreds of thousands of components most of which must be tuned with exquisite precision to achieve design luminosity. This high luminosity must be maintained routinely in order to deliver the required integrated luminosity. Great care must be taken at all stages of the design to ensure that the ILC can be commissioned rapidly and operate efficiently with minimal downtime. Some of the critical design issues are:

- high availability components and redundancy to minimize downtime;
- ease of commissioning;
- separation of regions to allow beam in one region while another is in access;
- Machine Protection System (MPS) to prevent the beam from damaging the accelerator while ensuring automated rapid recovery;
- feedback systems and control procedures to maintain optimum performance.

Many of these issues are mentioned elsewhere but are presented here as an integrated package to emphasize their importance to the ILC.

2.9.2   Availability

2.9.2.1   Importance of Availability

The important figure of merit for the ILC is not the peak luminosity but the *integrated* luminosity. The integrated luminosity is the average luminosity multiplied by the uptime. Having surveyed the uptime fraction (availability) of previous accelerators, a goal of 75% availability has been chosen for the ILC. This is comparable to HEP accelerators whose average complexity is much less than that of the ILC. As such it should be a challenging, but achievable goal. This goal is made even more challenging by the fact that all ILC subsystems must be performing well to generate luminosity. In contrast, a storage ring has an injector complex that can be offline between fills without impacting performance.

Because it has more components and all systems must be working all the time, attaining the target availability for the ILC requires higher availability components and more redundancy than previous accelerator designs. High availability must be an essential part of the design from the very beginning. A methodology is in place to apportion the allowed downtime among various components and arrive at availability requirements for the components.

2.9.2.2   Methodology

A simulation has been developed that calculates accelerator availability based on a list of parts (e.g. magnet, klystron, power supply, water pump). Input includes the numbers of each component, an estimate of its mean time between failure (MTBF) and mean time to repair (MTTR), and a characterization of the effect of its failure (e.g. loss of energy headroom, minor loss of luminosity, or ILC down). The simulation includes extra repair time for components in the accelerator tunnel (for radiation cool-down and to turn devices off and on), repair of accessible devices while the accelerator is running, repair of devices in parallel to overlap their downtimes, and extra time to recover the beam after repairs are completed.

It also allows repairs to be made in one region of the ILC while beam is used for accelerator physics studies in an upstream region.

The inputs to the simulation were varied to test different machine configurations and different MTBFs/MTTRs to develop a machine design that had a calculated downtime of 15%. The ILC design goal is >75% uptime, but 10% downtime was reserved as contingency for things that are missing from the simulation or for design errors. The major design issues are described in the next section.

2.9.2.3   High Availability Design Features

There are some design features of the ILC that are particularly important to achieving a high availability. These features were assumed in the simulation and if for some reason the ILC design is changed so these assumptions are no longer valid, then other improvements need to be made to maintain an adequate availability.

RF Power Sources: High power rf sources typically have a short MTBF either due to faults or to component lifetime. Large linacs ensure smooth operation by having spare units that can be switched in quickly to replace the energy lost by the failed unit. The ILC was assumed to have a 3% energy overhead in each main linac. In the low energy linac regions (5 GeV booster, bunch compressor, crab cavities...), the fractional energy change due to a klystron failure is very high making it impractical to replace the energy lost with a unit in a different location. In these regions, there are hot spare klystron/modulator units with waveguide switches that can immediately replace the power to the same section of accelerator. One hot spare for each low energy linac is sufficient. Klystrons and modulators are accessible with the beam on and can be replaced with only a few minute interruption to the beam to disconnect the waveguide.

Power supplies and electronics: Power supplies are designed to have a modular architecture with an extra module for redundancy. Most electronics modules not in the accelerator tunnel are designed to be replaceable without interrupting power to their crate. This allows broken modules to be replaced without further impact on the beam.

Separation of regions: There are tune up dumps and shielding between each region of the accelerator so that one region can be run while people are in another region. The ILC regions are injectors, DR, main linac and BDS.

Site power: Problems with the overall site power are allocated only 0.5% downtime. Present experience is that a quarter second power dip can bring an accelerator down for 8 to 24 hours. For the ILC, one 24 hour outage would consume much of the downtime budget. This places very stringent requirements on the reliability of the incoming power and on-site power distribution system. The present design of the power distribution system has some redundancy but the projected performance needs to be reviewed and possibly a larger downtime budget allocated.

Cryo: The downtime budget allocated to the entire cryogenic systems is set at 1%. This includes all the time for which there cannot be full power beam due to the outage, including even possible cool downs after a warm up. With 10 large cryo plants for the main linac and 3 smaller plants for other systems, the required availability of each plant is 99.9% including outages due to incoming utilities (electricity, house-air, cooling water, ventilation). This is 10-20 times better than the existing Fermilab or LEP cryo plants, where around half of the cryo system downtime is due to the incoming utilities. Achieving this goal requires both more reliable utilities and more reliable cryo plants.

Positron source: The positron target and capture section will become too radioactive for hands-on maintenance. As the present design does not have a spare target and capture section on the beam line, it is vitally important that the components be designed so they can be replaced with the use of remote handling equipment in less than a day. There is a positron keep-alive source (KAS) that can provide low intensity positrons to the e+ DR when the electron system in inoperable for some reason. The intensity is high enough for BPMs to work at their full specifications, about 10% of the design intensity. The KAS is expected to improve the availability by as much as 7%.

2.9.2.4 Required MTBF and MTTR Improvements

In addition to all the specific design features described in the previous section, many of the individual components must be designed to have better MTBF and/or MTTR than measured in present accelerators. Note that for all practical purposes, decreasing the MTTR is equivalent to increasing the MTBF, so components can be improved in whichever manner is most practical.

Table 2.9.2.4 shows the MTBFs and MTTRs needed to attain the desired downtime goals. As engineering continues, these goals will be refined to minimize the cost of the project while maintaining the desired availability.

Note that an MTBF of 1 million hours does not mean that a device must run for 114 years without attention and without failing. Preventive maintenance and even periodic replacement of components is allowed. It is only failures that occur while the accelerator is running that count towards the MTBF.

The pie chart in Figure 2.9-1 summarizes how much of the downtime is caused by the various regions of the ILC. The chart in Figure 2.9-2 shows which systems are causing the downtime. These charts give starting values for how the unavailability budget is divided among the regions and systems.

2.9.2.5 High Availability R&D

Table 2.9.2.4 gives the MTBFs and MTTRs that were used to obtain a 15% downtime. The desired MTBF is the product of the nominal MTBF in column four and an improvement factor in column two. The nominal MTBFs give a rough idea of what has been achieved at present accelerators. The third column shows the percentage downtime caused by the devices after the MTBF improvements listed. These can be used to *estimate* the effect of not meeting one of the MTBF goals. Fairly large improvements are needed for several types of hardware components. Some of these are being addressed by ILC R&D projects summarized here.

The factor of 20 improvement in magnet power supply MTBFs is mainly to be accomplished with redundancy. SLAC has purchased a commercial supply with five 1 kW regulators to feed a 4 kW load. Tests show a very short dip in the current when one of the regulators dies. Another 20 supplies of an improved version are to be installed in ATF2 to provide an extended test. Other improvements such as redundant controllers and embedded diagnostic boards are planned.

Magnets need an MTBF of 18 million hours. While the average MTBF at SLAC and FNAL was about 3 million hours, measured MTBFs range from 0.5 to 12 million hours depending on the sets of magnets used and the time period. The magnet designers from different facilities are working together to develop a set of best practices that should result in magnets with MTBFs near the ILC requirements. Serious consideration should be given

TABLE 2.9-1
This table shows the MTBFs that were used to obtain the desired 15% downtime. Note that the desired MTBF is the product of the nominal MTBF and the improvement factor. The nominal MTBFs give a rough idea of what has been achieved at present accelerators. The third column shows the percentage downtime caused by the devices with the MTBF improvements given in the second column. These can be used to estimate the effect of not meeting one of the MTBF goals.

Device	Needed improvement factor	Downtime to these devices (%)	Nominal MTBF (hours)	Nominal MTTR (hours)
Power supplies	20	0.2	50,000	2
Power supply controllers	10	0.6	100,000	1
Flow switches	10	0.5	250,000	1
Water instrumentation near pump	10	0.2	30,000	2
Magnets - water cooled	6	0.4	3,000,000	8
Kicker pulser	5	0.3	100,000	2
Coupler interlock sensors	5	0.2	1000,000	1
Collimators and beam stoppers	5	0.3	100,000	8
All electronics modules	3	1.0	100,000	1
AC breakers < 500 kW		0.8	360,000	2
Vacuum valve controllers		1.1	190,000	2
Regional MPS system		1.1	5,000	1
Power supply - corrector		0.9	400,000	1
Vacuum valves		0.8	1,000,000	4
Water pumps		0.4	120,000	4
Modulator		0.4	50,000	4
Klystron - linac		0.8	40,000	8
Coupler interlock electronics		0.4	1,000,000	1
Vacuum pumps		0.9	10,000,000	4
Controls backbone		0.8	300,000	1

to having an analog readout for each thermal and flow interlock so that impending problems can be fixed before affecting operations.

There is no active work on flow switches and water instrumentation. The approach is likely to be to reduce the number of flow switches and/or give them analog readout and add redundancy to the other water instrumentation.

Kicker pulsers with built-in redundancy to provide high availability have been developed. Most kicker installations also use multiple kickers each with its own pulser, with one or more spare units to replace a failed unit.

Electronic modules were assumed to have a factor of 3 improvement in MTBF. The plan is to achieve this through the use of the advanced telecommunications architecture, ATCA. This provides crates with redundant power supplies and fans, and modules that are hot swappable. ATCA prototype systems are being tested to learn how this technology can best
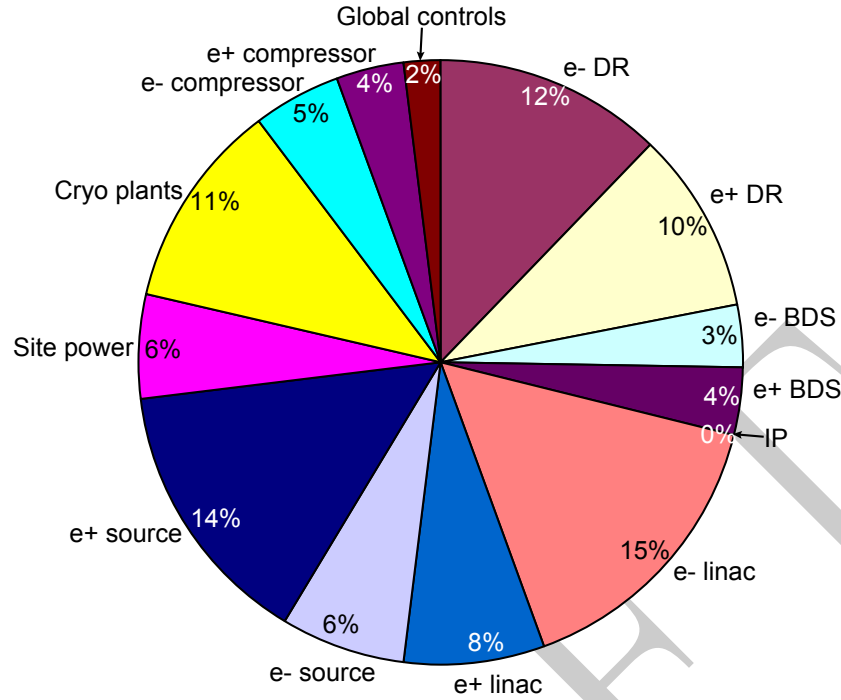
FIGURE 2.9-1. This shows how the total downtime of 17% is distributed among the various regions of the ILC.
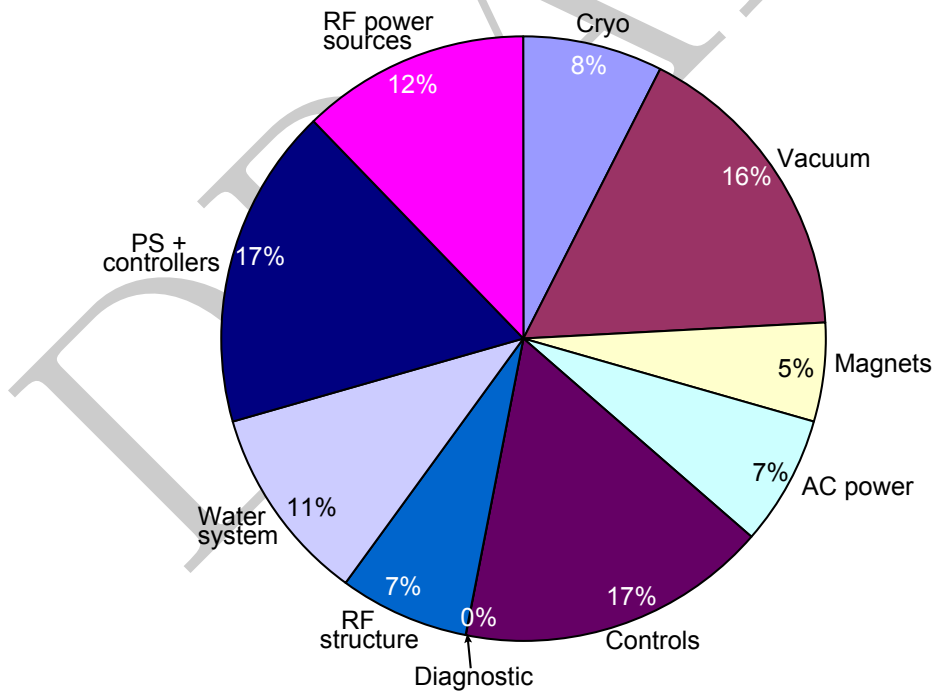
FIGURE 2.9-2. This shows how the total downtime is distributed among the various systems of the ILC. Note that the global system (site power, cryo plants, site-wide controls) are not shown in this chart.

be used for the ILC. Commercial ATCA modules provide redundant CPUs and networking with automatic fail-over, but the ILC also needs to develop I/O boards that are sufficiently reliable. The ability to replace a module with the crate powered eases requirements on

modules such as BPMs which degrade performance without causing actual downtime.

2.9.3   Commissioning

This section describes initial ideas on commissioning. The actual implementation will evolve with the schedule for construction of the conventional facilities and the availability of early access to regions of the accelerator. The plan needs further development during the EDR phase.

2.9.3.1   Phased Commissioning

To minimize the time from completion of construction of the ILC to operation for high luminosity, it is desirable to complete upstream regions of the accelerator early. Commissioning can then start on these regions while construction continues downstream. This is called *phased commissioning*. In particular, it would be beneficial to complete the electron injector and damping rings in time to allow one or two years of commissioning while construction of the linacs and BDS continues.

If a sufficient number of tunnel boring machines are available to start all civil engineering projects simultaneously (i.e. the main linacs, the beam delivery system and the damping rings), there is about a year period available for phased commissioning. This is because the damping ring tunnel, being shorter than the main linacs, can be completed earlier. If the number of boring machines is limited, the preferred order of completion is injector, damping rings, electron linac, positron linac and then beam delivery system.

A large amount of hardware validation and alignment and beam commissioning studies are necessary to produce low emittance beams with good stability and availability. Consequently, it is important to allocate a sufficient amount of commissioning time at an early stage. A major function of the DR commissioning period is to achieve the alignment of optical components and to establish a small beam emittance. In addition, there are beam intensity related issues that need to be checked and high intensity beams are needed for vacuum chamber scrubbing. The use of the damping rings obviously necessitates functional beam source systems. Since both DRs are in the same tunnel, a schedule optimization has to be done to determine if it is best to install both DRs at the same time or if the e- ring should be installed and commissioned followed by the e+ ring. The trial construction schedule shown in Figure 2.9-3 assumes that both rings are installed together.

Commissioning of the positron damping ring can begin with electrons and then positrons from the positron-keep-alive source. However, high-current commissioning must await partial commissioning of the electron main linac up to the undulator at the 150GeV point and the e+ transport line to the DR. The electrons that are used for producing the positrons are dumped at the end of the main linac. Care has to be taken to avoid interference with installation work on the beam delivery system which may still be ongoing at that time.

The actual commissioning scenario depends on the construction duration which is largely influenced by financial resources. Nonetheless the general features are seen in Figure 2.9-3.

The construction of the experiment is likely to consume the largest contiguous amount of time. It is recognized that construction of the underground detector hall is a major undertaking which cannot be completed several years after groundbreaking of ILC. To mitigate the schedule impact, most of the sub-assemblies of ILC detector facilities are built on surface and lowered later into the hall in large pieces [108].
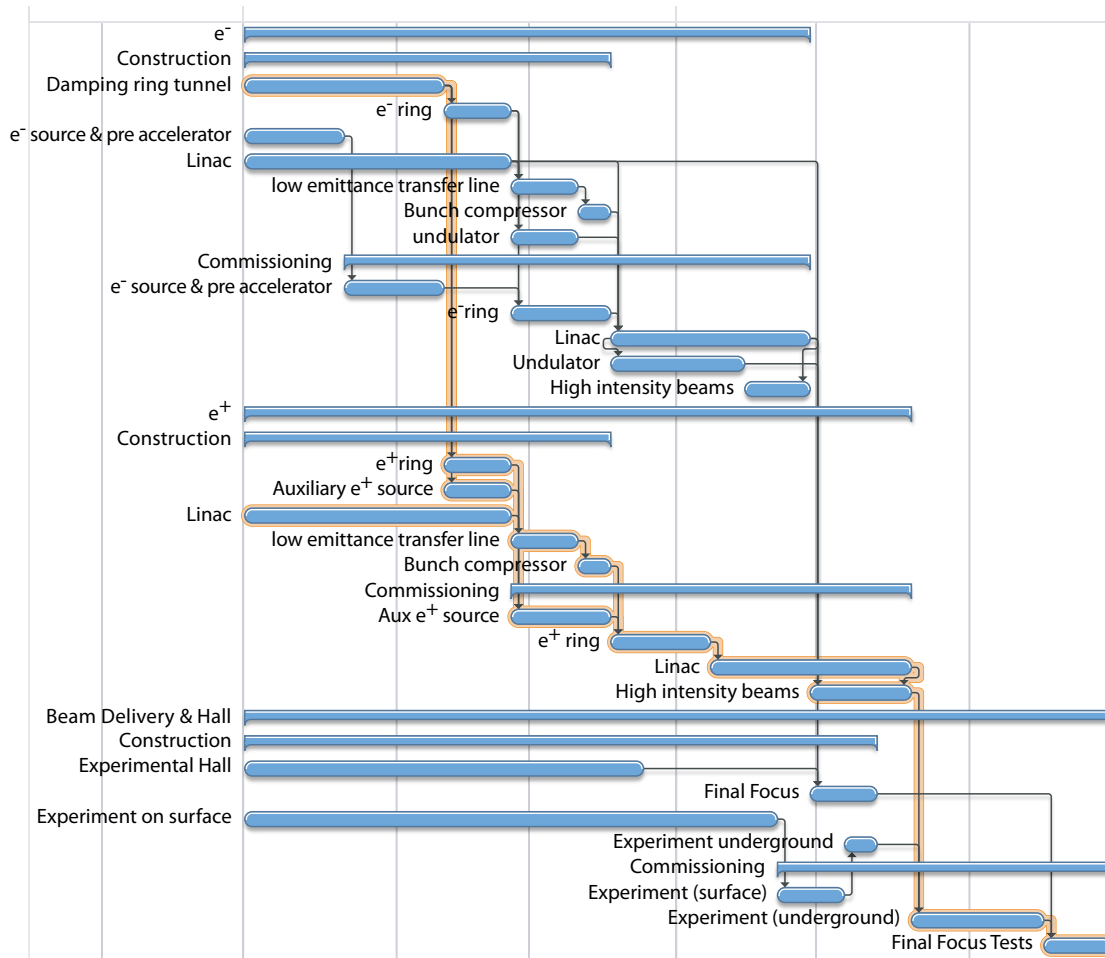
FIGURE 2.9-3. A sketch of the dependencies of the various construction tasks and the implications on commissioning. Construction of e^-, e^+ and Beam Delivery are shown and separated from the respective commissioning steps. Length of time lines are not to scale and the critical path indicated varies accordingly.

2.9.3.2 Electron Source and Reversible Positron Damping Ring for Commissioning

The positron sources have a large emittance which by design nearly fills the aperture of the positron damping ring. This makes initial commissioning of the e^+ ring with positrons challenging, since initial construction and alignment errors cause substantial beam losses which tend to produce false data from beam instrumentation. Hence it is desirable to conduct some aspects of very early commissioning of the positron damping ring with low emittance electrons. The electron injector of the keep-alive-source is designed so it can provide these electrons. For this commissioning with electrons, The positron ring needs to have its magnet polarities reversed. Reversal of the DR polarity may be allowed to take several days as it is not done frequently.

2.9.4 Radiation Shielding and PPS Zones

To enable efficient operation and commissioning, the personnel protection system (PPS) is designed to allow personnel access in one region while beam is in another region. As an

example, the main linac beam tunnel can be in access while there is beam in the damping ring. It is assumed that all accelerator housings could have radiation levels that exceed the requirements for non-radiation workers. Therefore, the radiation shielding and PPS zones described here are designed for radiation workers.

2.9.4.1 Summary of Regions' Radiation Requirements

Maximum allowable radiation levels for radiation workers for each region are summarized in Table 2.9.4.1. Radiation shielding and PPS devices must be designed to satisfy these criteria under the ILC beam-loss scenarios.

TABLE 2.9-2
Maximum allowable radiation levels and doses. The one in bold is the lowest and have been used in our design.
(a) Radiation Protection Instructions, DESY, June 2004.
(b) Radiation Safety Instructions, KEK, in Japanese, June 2004.
(c) Radiation Safety System, SLAC, April, 2006.
(d) Fermilab Radiological Control Manual, FNAL, July, 2004.

	DESY (a)	TESLA	KEK (b)	SLAC (c)	FNAL (d)
Standard	20 mSv/yr	1.5 mSv/yr	20 mSv/yr		50 mSv/yr
Fertile women	2 mSv/month	1.5 mSv/yr	6 mSv/yr 2 mSv/3months		
Pregnant women	1 mSv /pregnancy	1.5 mSv/yr	1 mSv /pregnancy		5 mSv /pregnancy
Operating conditions					
Normal			20 μSv/hr (1mSv/week)	5 μSv/hr (10 mSv/year)	
Mis-steering			20 mSv/event (20 mSv/year)	4 mSv/hr	
System failure			20 mSv/event (20 mSv/year)	250 mSv/hr for max. credible beam (30 mSv/event)	

The TESLA TDR cited beam-loss scenarios for the main linac as 0.1 W/m loss for normal operation and 100 W/m loss for 100 hours per year for mis-steering condition.

The SLAC maximum credible beam loss condition is the full beam power of 18 MW. Using these scenarios and the maximum allowable radiation levels, the most stringent criteria comes from the SLAC maximum credible beam condition. This gives a limit of 0.014 mSv/hr/kW loss for the main linac.

The interaction region will be occupied by many experimentalists. Hence tighter radiation design critera have been used so that occupants do not need to have radiation worker training. For normal operation, the IR hall radiation design limit is 0.5 microSv/h. For the maximum credible incident the limits are 250 mSv/h and 1mSv/event.
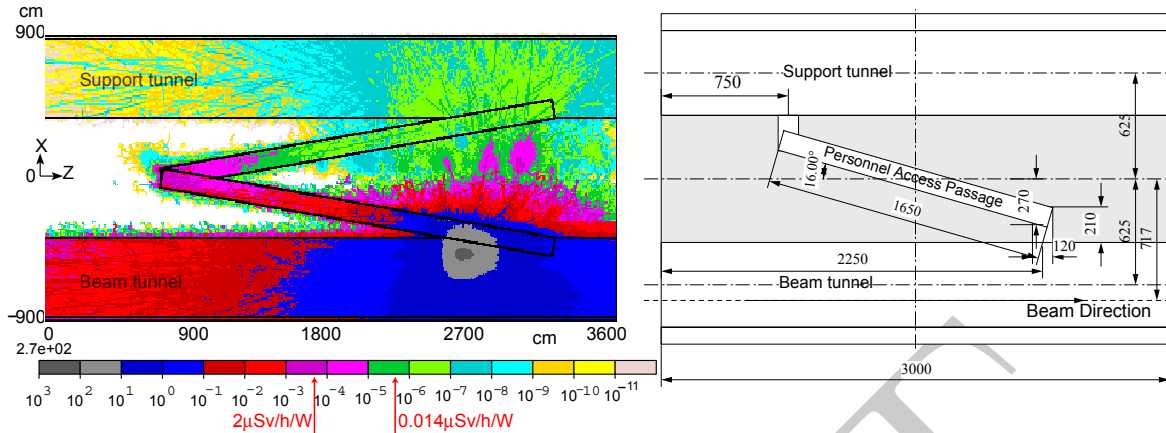
FIGURE 2.9-4. Two designs for passageways between the tunnels that give adequate radiation shielding.

2.9.4.2 Shielding Calculation between Two Tunnels

The linac design has a beamline and a service tunnel separated by 7.5 m. Radiation levels must be low enough in the service tunnel to allow occupancy for repairs when beam is in the beam tunnel. Radiation dose rates were evaluated using the Monte Carlo codes, MARS and FLUKA, and the two tunnel configuration satisfies the radiation dose limit of 0.014 mSv/hr/kW. Here are a few selected results.

- For sections with no penetrations between two tunnels, 4 m of earth provides adequate shielding. This was evaluated by the MARS code and the Jenkins formula with a soil density 1.9 g/cm^3 and a 250 GeV electron beam incident on the worst case target: a thick copper cylinder 20 X_0 long and a radius of 1 X_0.

- In sections which have a penetration for waveguides or cables, the radiation near the penetration is above the allowed limit. However, the radiation level falls off rapidly with distance so it is sufficient to fence off the area immediately next to the penetration. The penetrations are located near the top of the tunnel, well above the personnel passage, so the fencing does not significantly restrict access in the service tunnel. In the calculations, the penetration was assumed to be a 7.5 m long circular hole with a diameter of 48 cm, and no shielding in the penetration. Suitable shielding could potentially lower the radiation levels further.

- Personnel access passages between the two tunnels are located every 500 m along the main linac for emergency egress. Heavy movable shielding doors cannot be used because of the need for a fast escape route. These passages cannot have a direct line-of-sight or the radiation dose in the service tunnel would be unacceptable, but two designs adequately reduced the radiation in the service tunnel below the limit. These are shown in Figure 2.9-4 and described below.

  1. A rotated "V" shape passageway gave the lowest dose rate, about 20% of the limit. In this simulation, the access passageway had a width of 1.2 m, a height of 2 m and the arms of the "V" were angled 10 degrees away from the accelerator tunnels. The total length of the passage was about 50 m.
  2. Another design is a modified crank with an inclined center passageway. The dose rate calculated by the simulation was about 80% of the limit.

2.9.4.3   PPS Zones

The personnel protection system (PPS) prevents people from being in the accelerator tunnel when beam is on. A system of gates and interlocks turn off the beam before allowing access to the accelerator housing. Access to the service tunnel is not part of the PPS system. The ILC is divided into different regions (PPS zones) with tune up dumps and shielding to allow beam in one region while there is access in another region. The PPS zones are the injectors, DR, main linac and BDS. Entrance gates for PPS zones are monitored and stop the beam when opened.

The ILC PPS zones are long and it would be burdensome to search the full region after each permitted access. To ameliorate this problem, they are divided into multiple search zones separated by fences with gates that are also monitored. The search zones are up to several hundred meters long. For example, in the linac a search zone is 500 m long and is separated by gates midway between each cross tunnel passageway.

Personnel access from a service area (service tunnel, shaft, detector hall etc.) to an accelerator area is controlled by PPS gates, as is the access from one accelerator region (PPS zone) to another accelerator region. Fences, doors, or moving shields are used for these gates and they have redundant gate-closed status switches for PPS monitoring. They are locked to prevent careless access but have an unlocking mechanism for emergencies. Information and communication systems are provided at the gates to show the operational status and allow communication between a person at the gate and an operator granting permission to go through the gate.

There are personnel access passages between accelerator area and service area at the main linac, shafts, alcoves and the detector hall with PPS gates near each end. Since the passageways are used as emergency exits, heavy moving doors are avoided if possible. PPS gates between the accelerator areas and the service areas (including the access passageway) need to restrict the flow of activated air from the accelerator tunnel to the service area.

2.9.4.4   Shielding between PPS Zones

Shielding between PPS zones is designed to allow beam in the upstream zone while people are in the downstream zone. The upstream beam is deflected into a tune-up dump and there are triply redundant beam stoppers between the beam and the accessed region to ensure the beam does not enter the accessed region.

2.9.5   Machine Protection System

The task of the machine protection system, MPS, is to protect the machine components from being damaged by the beam when equipment failure or human error causes the beam to strike the vacuum envelope. The MPS design must take into account the types of failures that may occur and the damage they could produce.

2.9.5.1   Overview

The ILC Machine Protection System (MPS) is a collection of devices intended to keep the beam from damaging machine components. The nominal average beam power is 20 MW, consisting of 14,000 bunches of 2×10^{10} particles per second, and typical beam sizes near 10×1 μm. Both the damage caused by a single bunch and the residual radiation or heating

caused by small (fractional) losses of many bunches are important for MPS. The MPS consists of 1) a single bunch damage mitigation system, 2) an average beam loss limiting system, 3) a series of abort kickers and dumps, 4) a restart ramp sequence, 5) a fault analysis recorder system, 6) a strategy for limiting the rate with which magnetic fields (and insertable device positions) can change, 7) a sequencing system that provides for the appropriate level of protection depending on machine mode or state, and 8) a protection collimator system. The systems listed must be tightly integrated in order to minimize time lost to aberrant beams and associated faults.

2.9.5.2 Single Pulse Damage

Single pulse damage is mitigated by systems that check the preparedness of the machine before the high power beam passes. Single pulse damage control is only necessary in the 'damped-beam' section of the ILC. Three basic subsystems are involved: 1) a beam permit system that surveys all appropriate devices before damping ring beam extraction begins and provides a permit if each device is in the proper state 2) an abort system that stops the remaining bunches of a train if a bunch does not arrive at its intended destination 3) spoilers upstream of devices (typically collimators) to expand the beam size enough that several incident bunches do not cause damage. In addition, some exceptional devices (damping ring RF and extraction kickers for example) have fast monitoring systems and redundancy.

Spoilers or sacrificial collimators are placed before the bunch compressors, in the undulator chicane, at the beginning of the BDS system and in the collimator section of the BDS. Locations with dispersion downstream of an accelerator section have spoilers to intercept off-energy beam caused by klystron faults or phase errors before the beam can hit a downstream collimator or beam pipe. The spoilers are designed to survive the number of incident bunches that hit before the abort system can stop the beam. If this design becomes problematic, the use of a *pilot bunch* is being kept as an option. A pilot bunch is one percent of nominal current and is spaced 10 μs ahead of the start of the nominal train. If it does not arrive at its intended destination, the beam abort system is triggered to prevent full intensity bunches from hitting the spoiler.

Studies [102] have shown that for many failure scenarios such as quadrupole errors or klystron phase errors, the beam is so defocused by the time it hits the linac aperture that it does not cause damage. For this reason, no spoilers or extra beam abort kickers are included in the linac.

The beam abort system uses BPMs and current detectors to monitor the beam trajectory and detect losses. On a bunch by bunch basis, the system checks for major steering errors or loss of beam. When a problem is detected it inhibits extraction from the damping ring and fires all abort kickers upstream of the problem. The abort kickers cleanly extract the beam into dumps, protecting downstream beamlines.

In the few milliseconds before the start of the pulse train, the beam permit system checks the readiness of the modulators and kicker pulsers, and the settings of many magnets before allowing extraction of beam from the damping rings.

2.9.5.3 Average Beam Loss Limiting System

Average beam loss is limited, throughout the ILC, by using a combination of radiation, thermal, beam intensity and other special sensors. This system functions in a manner similar to other machines, such as SLC, LHC, SNS and Tevatron. If exposure limits are exceeded

at some point during the passage of the train, damping ring extraction or source production (e^+/e^-) are stopped. For stability, it is important to keep as much of the machine as possible operating at a nominal power level. This is done by segmenting it into operational MPS regions. There are 11 of these regions, as noted in Table 2.9-3. Beam rate or train length can be limited in a downstream region while higher rate and train lengths are maintained in upstream regions.

TABLE 2.9-3
Beam shut off points. Each of these segmentation points is capable of handling the full beam power, i.e. both a kicker and dump are required. These systems also serve as fast abort locations for single bunch damage mitigation.

	Region name	Begin	End
1	e^- injector	Source (gun)	e^- Damping ring injection (before)
2	e^- damping ring	Ring injection	e^- Ring extraction (after)
3	e^- RTML	Ring extraction	e^- Linac injection (before)
4	e^- linac	Linac injection	Undulator (before)
5	Undulator	Undulator	BD; e^+ target
6	e^- BDS	BD start	e^- Main dump
7	e^+ target	e^+ target	e^+ damping ring injection
8	e^+ damping ring	Ring injection	e^+ ring extraction
9	e^+ RTML	Ring extraction	e^+ linac injection
10	e^+ linac	Linac injection	e^+ BDS
11	e^+ BDS	e^+ BDS	e^+ main dump

2.9.5.4 Abort Kickers and Dumps

Abort systems are needed to protect machine components from single bunch damage. It is expected that a single bunch impact on a vacuum chamber will leave a small hole, roughly the diameter of the beam. Each abort system uses a fast kicker to divert the beam onto a dump. The kicker rise time must be fast enough to produce a guaranteed displacement of more than the beampipe radius in an inter-bunch interval.

There are three abort systems in each RTML, one at the undulator entrance, and one at the entrance to each BDS.

There will be many meters of fast kickers needed at each dump and megawatts of peak power from pulsers. R&D is need to optimize the system and and ensure its reliability.

2.9.5.5 Restart Ramp Sequence

Actual running experience is needed to exactly define the restart ramp sequence. For that reason the sequencer must be flexible and programmable. Depending on the beam dynamics of the long trains, it may be advisable to program short trains into a restart sequence. There may also be single bunch, intensity dependent effects that require an intensity ramp. In order to avoid relaxation oscillator performance of the average beam loss MPS, the system must be able to determine in advance if the beam loss expected at the next stage in the ramp

sequence is acceptable. Given the number of stages and regions, the sequence controller must distribute its intentions so that all subsidiary controls can respond appropriately and data acquisition systems are properly aligned.

The sequence may need to generate a 'benign' bunch sequence with the nominal intensity but large emittance. The initial stages of the sequence can be used to produce 'diagnostic' pulses to be used during commissioning, setup and testing.

2.9.5.6 Fault Analysis Recorder System

A post mortem analysis capability is required that captures the state of the system at each trip. This must have enough information to allow the circumstances that led to the fault to be uncovered. Data to be recorded on each fault include: bunch by bunch trajectories, loss monitor data, machine component states (magnets, temperature, RF, insertable device states), control system states (timing system, network status) and global system status (sequencer states, PPS, electrical, water and related sensors). The fault analysis system must automatically sort this information to find what is relevant.

2.9.5.7 Rapidly Changing Fields

In addition to the above, there are critical devices whose fields (or positions) can change quickly, perhaps during the pulse, or (more likely) between pulses. These devices need 1) special controls protocols, 2) redundancy or 3) external stabilization and verification systems.

1. Depending on the state of the machine, there are programmed (perhaps at a very low level) ramp rate limits that keep critical components from changing too quickly. For example, a dipole magnet is not allowed to change its kick by more than a small fraction of the aperture (few percent) between beam pulses during full power operation. This may have an impact on the speed of beam based feedbacks. Some devices, such as collimators are effectively frozen in position at the highest beam power level. There may be several different modes, basically defined by beam power, that indicate different ramp rate limits.

2. There are a few critical, high power, high speed devices (damping ring kicker and RF, linac front end RF, bunch compressor RF and dump magnets) which need some level of redundancy or extra monitoring in order to reduce the consequence of failure. In the case of the extraction kicker, this is done by having a sequence of independent power supplies and stripline magnets that have minimal common mode failure mechanisms.

3. There are several serious common mode failures in the timing and phase distribution system that need specially engineered controls. This is necessary so that, for example, the bunch compressor or linac common phase cannot change drastically compared to some previously defined reference, even if commanded to do so by the controls, unless the system is in the benign beam-tune-up mode.

2.9.5.8 Sequencing System Depending on Machine State

The ILC is divided into segments delineated by beam stoppers and dump lines. There may be several of these in the injector system, two beam dumps in each RTML, and 2 (or 3) in the beam delivery and undulator system. In addition, the ring extraction system effectively operates as a beam stopper assuming the beam can remain stored in the ring for an indefinite

period. This part of the MPS assumes that the beam power in each of these segments can be different and reconfigures the protection systems noted above accordingly.

2.9.5.9 Protection Collimators

The entire ILC requires protection collimators and spoilers that effectively shadow critical components. These devices must be engineered to withstand innumerable single pulse impacts. The number and locations of these protection collimators are documented in the descriptions of each accelerator region.

2.9.6 Operability

To ensure high average luminosity it is important that the ILC have many features built in to make its operation mostly automatic and efficient. These features include:

- Accurate, reliable, robust diagnostics
- Monitoring, recording, and flagging of out-of-tolerance readings of all parameters that can affect the beam. Some of these must be checked milliseconds before each pulse train so beam can be aborted if there is a problem.
- Beam-based feedback loops to keep the beam stable through disturbances like temperature changes and ground motion
- Automated procedures to perform beam based alignment, steering, dispersion correction, etc.
- Automatic recovery from MPS trips starting with a low intensity high emittance beam and gradually increasing to nominal beam parameters

2.9.6.1 Feedback systems

The transport of the beam through the ILC requires a large number of feedback systems to be active to steer the beam to the interaction point. These feedback systems include measurements from various beam position monitors, from laserwires scanning the beam profile and other diagnostics. The feedback loops must be carefully designed to be orthogonal and to maintain corrections that are within the device ranges. The feedback systems must avoid trying to compensate for large deviations of the beam due to component failure. It is hence necessary to use flexible setups for the control loops such as provided by MATLAB tools and analysis techniques.

CHAPTER 3

Technical Systems

3.1 MAGNET SYSTEMS

3.1.1 Overview

The ILC has ∼80 km of beamlines which require magnets for focusing and steering the beams. There are over 13,000 individual magnets, of which approximately 18% are superconducting and the rest "conventional" warm iron-dominated magnets with copper coils. About 40% are low-current corrector magnets. Superconducting technology is primarily used for the magnets located in the RF cryomodules, but it is also required for the spin rotation solenoids, damping ring wigglers, positron source undulator and beam delivery octupoles, sextupoles and final doublet quadrupoles.

3.1.2 Technical Description

The scope of the Magnet Technical System includes the magnets and their power systems, as well as the magnet support stands and positioning devices needed for precise magnet alignment in the beamlines. Power systems include the power supplies, cabling to the magnets, sensors and systems for local control, monitoring, and magnet protection. Pulsed kicker and septum magnets used for beam injection, extraction, and/or protection are particularly challenging. Almost all of the room temperature magnets have easily achievable requirements. The major technical issues, challenges and special purpose magnet systems are presented below. Challenging technical issues unique to particular Areas (especially BDS and DR) are discussed in those sections.

The magnet design process starts with the Area System leaders who specify a standard set of requirements based upon the lattice designs, machine layout, and envisioned operating scenarios. Conceptual magnet designs follow primarily from the specified integrated strength, field quality, clear bore aperture, and slot length constraints. Given the conceptual magnet design, a power supply (PS) design is developed based on the magnet-specific current, voltage and stability requirements, and the need to power magnets individually or in series.

3.1.3 Technical Issues and Challenges

3.1.3.1 High Availability and Low Cost

A major criterion for ILC magnet design is to achieve very high availability in spite of the very large number of magnets. The "availability" goal of the ILC is 75% (or better) and the magnets have been budgeted to incur no more than 0.75% down time. The availability "A" of a component is given as A = MTBF/(MTBF+MTTR), where MTBF is Mean Time Between Failures, and MTTR is Mean Time To Repair a magnet, turn it back on and restore the beam. Detailed studies of magnet failures at three high energy physics labs indicate that most failures are with conventional water-cooled magnets, which had an MTBF ranging from about 0.5 million to 12 million hours based on tens of millions of integrated magnet-hours. The ILC has 6873 such magnets. With an MTTR of 16 hours, the MTBF of each one must be longer than 18 million hours in order to achieve the desired availability.

This reliability level should be achievable, without incurring a significant increase in cost, by applying the assembled magnet design, production and operation experience at existing HEP accelerators. The approach is to apply best modern magnet engineering practices, ensure adequate quality control of materials and procedures during fabrication, and use established guidelines for operating within reasonable environmental limits (such as ambient temperature and allowed temperature rise, maintaining proper water flow conditions, and keeping electronic components out of radiation areas where possible). Power system electronic components typically have much lower MTBF values of around 100,000 hours. Here, the solution is to build in redundancy for crucial elements, and use "smart" electronics that can detect failure and rapidly switch to redundant units. Replacement of failed units can then be scheduled to occur during beam downtimes. Comprehensive failure mode and effects analyses (FMEA) are thus viewed as an essential part of the magnet system engineering effort.

3.1.3.2 Field Quality and Alignment

The field quality requirements in most normal-conducting ILC magnets are similar to those at other accelerators currently in operation, and not particularly challenging. Higher order harmonics must be on the order of a "few units" (1 unit = 10^{-4}) of the main field strength, and are most stringent in the Damping Rings where beam circulates for many turns. For corrector magnets, a few tens of units is characteristic. In warm iron-dominated electromagnets, these levels are achieved through careful control of pole shapes and their positioning. Similarly, control of coil position is important for superconducting magnet field quality, and is achievable with proper mechanical design and tooling. Large room temperature magnets have a split yoke design to reduce repair time in the tunnel; experience shows that field quality can be maintained with proper design and care in re-assembly.

Alignment and mechanical stability requirements in many areas are very challenging. In the BDS, beam positions must be maintained at sub-micron levels to collide the beams, so precision 5-axis magnet positioning mounts, or "movers," are needed for continuous adjustment of all the quads and sextupoles in the final focus region. For the regions where movers are not required, room temperature and cryogenic magnet stands use a robust and precisely adjustable design. In some areas, pedestals are required to offset the precision stands from the tunnel floor. Alignment tolerances on the relative positions of Beam Position Monitors (BPMs) to quadrupoles differ by area ($\sim$10 μm in BDS, $\sim$100 μm in ML). In the BDS this

results in stringent temperature control requirements locally, where geometry-sensitive cavity style BPMs are affixed to the thermally active magnets.

3.1.3.3 Superconducting Magnets

There are 2318 superconducting (SC) magnets in a variety of applications throughout the ILC, but fewer than 10% of them require high integrated field strength in limited space and about 60% are correcting coils wound in the same physical space as the main coils. Most of the SC magnets are not very strong and are located in the RF cryomodules. A package containing a focusing quadrupole (quad), steering dipole correctors and a Beam Position Monitor is located at the center of every third main linac cryomodule. This location makes it challenging to maintain the quad positions during thermal cycles and to measure and relate the quad positions to external survey fiducials and to the BPMs used to keep the beam centered in the quads (at the 100 micron level, over a distance of $\sim$6 meters). The resulting magnetic center in nested dipole and quad designs may also be affected by persistent current effects. Alternative designs and further research are needed to understand these issues and develop the magnet support and measurement techniques; there could be significant advantages to moving the magnets and BPMs from the RF cryomodule out to a separate cryostat.

The superconducting wigglers in the damping rings and the superconducting undulators in the positron source also require great mechanical precision; their particular challenges are described in their respective chapters. The most challenging superconducting magnets, those just before the interaction point, are described in the BDS chapter. They have strong gradient fields with many layers of correcting coils, and must fit into as small a radius possible to not interfere with the detector. In the ILC sources, there are superconducting solenoids for spin rotation and a few large aperture magnets that may be either conventional or superconducting, depending on detailed optimization of operating versus capital cost.

3.1.3.4 Power Systems Design

The non-pulsed ILC magnets operate with DC currents, with set points that may be adjusted periodically but only slowly ($\sim$5 A/s or less). Most magnets are individually powered to allow independent control. Power supply stability requirements are assumed to be comparable to performance of existing commercial units. The design of a power system, whether for an individual or a string of magnets, requires a conceptual magnet design which determines the required operating current, defines the coil resistance and inductance and cooling requirements (air or water). The magnet position, with respect to power supplies located in alcoves, defines the cable length; cables are sized for the maximum operating current using two sizes above the NEC rated minimum, to reduce voltage drop and heat generation. The required maximum power supply voltage is then determined by the cable and coil resistive drop at maximum current, plus the inductive drop at the maximum ramp rate. The supply is sized with a 10% margin on the power rating, to accommodate uncertainties in magnet strength, inductance, cable lengths, etc. The summed power ratings set requirements for AC power, air and water conditioning in each area.

Power systems are classified by their size and type, and standard models were developed for each of the various system categories: they are distinguished by "normal" versus "superconducting", "individually powered" versus "series connected", "rack mounted" versus "free standing". These styles have certain elements in common, but may differ in detail (water

versus air cooling, for example); Figure 3.1-1 shows one example which contains all of the power system elements, and illustrates interconnections between components and systems. Each power system provides local control and magnet protection (via PLCs and FPGAs), and has the capability of diagnostic data capture. The design incorporates redundant current transductors, controllers, and Ethernet IOCs, which are utilized for communication with machine control, protection, and other technical systems (e.g., to obtain cryogenic or LCW process variables for operating permissive). Smaller rack-mount supplies can accommodate a redundant supply within the rack, for automatic switch-over in case of a failure. The conceptual design for the superconducting magnets is based on the generic model shown, although the protection elements may be simplified after detailed magnet design.
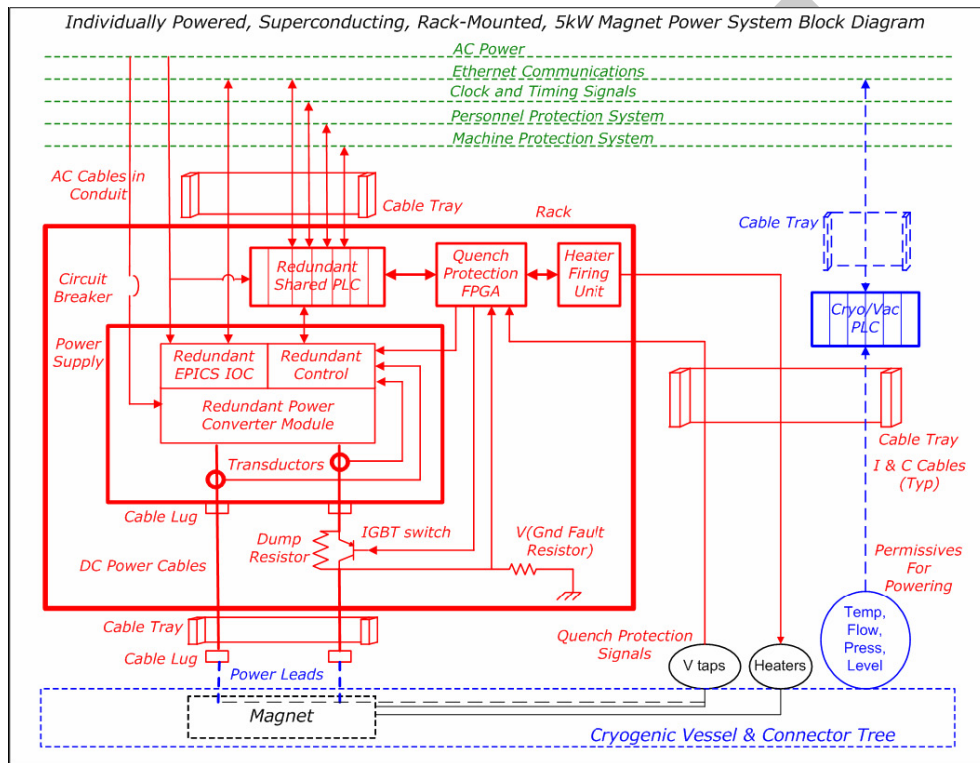
FIGURE 3.1-1. An example DC power system style: items in red are specific to the power system, magnet elements are in black; relevant interfaces are shown, where blue and green lines are responsibility of other groups (global controls, cryogenics, vacuum, facilities, etc.)

3.1.3.5 Kicker, Septum, and Pulsed Magnets

A kicker is a device that makes fast time-dependent changes in the beam path. A septum magnet has regions with very different magnetic field with a material septum between them. A kicker diverts the beam from one side of the septum to the other, and the much higher field of the septum diverts the beam by a much larger angle, typically around some downstream obstacle like a quadrupole magnet. A pulsed magnet changes its field as part of normal operation, but less rapidly than a kicker. The high power beam dumps have pulsed magnets upstream to sweep the beam across the dump to avoid localized damage. Fast actuators in the beam feedback systems in the damping rings and at the IP, which are also sometimes called "kickers," are described in the area chapters.

There are several classes of kickers in the ILC. The damping ring injection and extraction kickers are pulsed every few hundred ns for single bunches during each millisecond linac pulse, and need rise and fall times of a few ns. A damping ring abort kicker is only fired when an abnormal beam condition is detected, to divert the stored beam to a dump, and avoid damage to machine components. The rise time must be less than the ion-clearing or abort gap in the ring filling pattern, with a pulse width of a full ring turn ($\approx$22 μs).

There are other abort kickers at several locations outside the damping rings, with rise times of less than the time between bunches ($\approx$100 ns). When used as abort kickers, the pulse rate is nearly zero, and the pulse width need only be long enough for the bunches that cannot be stopped upstream. An abort kicker can also be used to limit the beam power downstream, by firing it after a fraction of the beam bunches in the train have passed. In this application, the kicker may be fired on every linac pulse, for the full linac pulse duration.

The ILC kickers are all stripline structures inside the vacuum chamber, driven by pulsed power supplies. The injection and extraction kickers have short strips and extremely fast pulsers to achieve fast rise and fall times. The required total kicker strength (kilovolt-meters) is set essentially by the beam size and energy, with the result that a large number of stripline and pulser units are needed for each installation. The damping ring abort kickers use more conventional thyratron or FET pulsers and longer strips since the rise time can be longer, the pulse length is moderate, and the rate is low. The other abort kickers have relaxed rise time requirements, but the pulse may need to be a millisecond long at full linac rate, and higher beam energies require more kicker field energy. The pulser power required scales inversely with the cube of the available length, and can be quite high. The beam delivery system abort kicker installations each require several pulsers of the scale of main linac modulators.

The baseline design has a thin and a thick pulsed eddy-current septum magnet for each damping ring kicker. This design is inspired by the Argonne APS septa, but R&D is required to make a millisecond flat top to the required tolerance. An alternative optics design is under consideration for injection and extraction that allows a DC current-sheet septum of moderate current density to be used. An abort septum must be DC, and could be a current sheet septum, or an iron magnet with a beam-hole in its pole region (Lambertson septum). The damping ring abort region optics, and thus the type and parameters of its septum, are discussed in the Damping Ring chapter. The RTML and beam delivery abort septa are DC current sheets. The undulator protection abort septa are dogleg bend magnets modified to be Lambertson septa. All of the abort dumps downstream of the damping ring require sweeper magnets.

3.1.3.6 Fabrication, Test, and Storage

The program of fabrication and testing of ILC magnets follows a 7 year schedule, with one year of preparation, five years of production and testing, and (overlapping) four years of installation. Magnet fabrication utilizes industrial suppliers world-wide; tooling developed for ILC magnet fabrication belongs to ILC for future use. A large fraction of solid-wire corrector magnets are tested by manufacturers, and all non-corrector magnets are tested and magnetically measured at the ILC test facility. Superconducting test stands share cryogenic resources with nearby SRF test facilities and have both production and special measurement areas and test systems. The conventional magnet measurement area is large, with multiple stands for efficient and high throughput, with space for temporary magnet storage. Alignment and survey capabilities are needed for all magnet styles. In the long term, some space could be

converted for storage of tooling and spare magnets (or coils and parts), and part of the facility could be devoted to repair and new magnet fabrication. Also an area remains dedicated to making tests and measurements, and conducting R&D for later machine improvements. Such a facility is necessary to ensure the initial high quality of ILC magnets.

3.1.4   Cost Estimation

The cost estimate is based on the conceptual designs for magnets, power systems, stands and movers described above, with additional assumptions about estimated costs of material and labor. Given time and resource limitations, detailed conceptual designs were developed for only a small number of the magnet styles. The majority of estimates are "engineering estimates" based on existing designs with similar requirements. Standardized labor rates were determined from laboratory and industrial sources[1]. In order to determine the material costs, the weights of magnet and cable materials, primarily copper and iron, have been estimated and summed, and current world commodity prices obtained. Similarly, prices have been obtained for commercially available electronic components such as power supplies, FPGAs and PLCs, controllers and Ethernet interfaces.

In one instance, a design and a complete set of drawings was developed for a e^+ Source transfer line quadrupole (a large quantity item) and a request for quote sent to a number of magnet vendors. The cost estimates obtained were in reasonable agreement with an internal estimate: the average agreed within a few percent of the internal estimate, with a spread of ~25%. For a few magnet systems, more detailed cost estimates were provided based on either existing designs (Cornell wigglers) or R&D prototypes already in progress (Daresbury/Rutherford undulators); in a similar fashion, Brookhaven provided detailed cost estimates for the superconducting insertion magnets at the IR based on experience with similar magnet designs.

Estimates of EDIA labor costs were based upon reviews of recent large accelerator magnet and power supply projects at SLAC and Fermilab, where the materials, fabrication and EDIA labor fractions are well known. The fractional distribution of EDIA among several types of laborers, which were costed at the standardized labor rates, was assigned on the basis of project management experience.

3.1.5   Component Counts

The number of conventional and superconducting magnets and magnet styles in each of the ILC Areas is shown in Table 3.1-1. There are compelling reasons to reduce the number of magnet styles - to reduce cost and increase maintainability and reliability - and this process is an iterative one, that has not yet been fully optimized.

---

[1]It should be noted that rates for different world regions have not been incorporated at this time. It should also be recognized that labor rates and production hours are not necessarily uncorrelated: the lowest labor rates are quite often in regions with less automation and infrastructure resulting in longer task times.

TABLE 3.1-1
Numbers of Conventional (Normal Conducting, NC) and Superconducting Magnets and Magnet Styles in ILC Areas

Magnet Type	Grand Totals		Sources			Damping Rings					2 RTMLs		2 Linacs		2 BDS	
	# of styles	total qty.	# of styles	e- total qty.	e+ total qty.	# of styles	e- DR total qty.	e+ DR total qty.	e- Inj/Ext total qty.	e+ Inj/Ext total qty.	# of styles	total qty.	# of styles	total qty.	# of styles	total qty.
Dipole	22	1356	6	25	157	2	126	126	8	8	6	716	0	0	8	190
NC quad	37	4165	13	76	871	4	747	747	76	76	5	1368	0	0	15	204
SC quad	16	715	3	16	51	0	0	0	0	0	0	56	3	560	10	32
NC sextupole	7	1050	2	0	32	2	504	504	0	0	0	0	0	0	3	10
SC sextupole	4	12	0	0	0	0	0	0	0	0	0	0	0	0	4	12
NC solenoid	3	50	3	12	38	0	0	0	0	0	0	0	0	0	0	0
SC solenoid	4	16	1	2	2	0	0	0	0	0	1	8	0	0	2	4
NC corrector	9	4016	1	0	840	3	540	540	0	0	4	2032	0	0	1	64
SC corrector	14	1374	0	32	102	0	0	0	0	0	0	84	2	1120	12	36
Kickers/septa	11	227	0	0	19	5	46	46	0	0	1	52	0	0	5	64
SC wiggler	1	160	0	0	0	1	80	80	0	0	0	0	0	0	0	0
NC oct/muon spoiler	3	8	0	0	0	0	0	0	0	0	0	0	0	0	3	8
SC octupole	3	14	0	0	0	0	0	0	0	0	0	0	0	0	3	14
SC undulator	1	27	1	0	27	0	0	0	0	0	0	0	0	0	0	0
Overall Totals	135	13190	30	163	2139	17	2043	2043	84	84	17	4316	5	1680	66	638
Totals w/o Correctors	112	7800														
Total NC	92	10872														
Total SC	43	2318														

3.2 VACUUM SYSTEMS

3.2.1 Overview

The ILC has over $\sim$80 km of beamlines which must be kept under vacuum to limit the beam-gas scattering and operate the RF cavities. Different areas of the machine present different challenges but fortunately, there is an experience base at existing accelerators for essentially all of the systems, to facilitate design and costing. The largest and most complex are the vacuum systems for the cryomodules containing superconducting cavities that accelerate the beam. There are $\sim$1680 cryomodules in the main linacs, electron and positron booster linacs and bunch compressors. There are also single cavity cryomodules in the damping rings and beam delivery systems. These cryogenic units require separate vacuum systems for the beam line, the insulating vacuum and the waveguides.

Other beamlines throughout the ILC pose particular challenges. The lifetime of the electron source photocathode requires a vacuum in the range of a pico-Torr. The superconducting undulator for the positron source is a warm bore chamber with a very small aperture. Chambers for bending magnets in the damping rings and elsewhere require antechambers and photon absorbers for the synchrotron radiation. The presence of electron cloud in the positron damping ring and ions in the electron damping ring can seriously impact performance and requires mitigation. Beam-gas scattering in the beam delivery must be limited to reduce backgrounds in the experimental detectors. The designs for each system and costing approach are discussed in more detail below.

3.2.2 Technical Issues

3.2.2.1 Linac Cryomodules

There are $\sim$20 km of cryomodules in the main linac and another $\sim$1.6 km of modules in the sources and bunch compressors. Each cryomodule has separate vacuum systems for the accelerating structures, the insulating vacuum and the transmission waveguides. The structure vacuum vessel holds the niobium cavities and is at 2K cryogenic temperature. This system must produce very low quantities of particulates as these can contaminate the cavities causing field emission and lowering the available gradient. The system must also be able to produce ultra-high vacuum at room temperature to eliminate the risk of residual gases condensing on the niobium walls during cooldown. The beamline vacuum is segmented into strings of 154.3 m. Each string has an insulating vacuum break and a port for valves and ion pumps. Every other string has additional valves, pumps, leak detection, and vacuum diagnostics. Each group of 4 strings (617 m) has cold vacuum isolation valves. A vacuum/diagnostics station is installed between every 16 strings (2.472 km). These stations have slow start turbo-molecular pumps, leak detection, clean venting systems, and warm isolation valves.

The insulating vacuum system must maintain a typical pressure of $\sim$ 0.1 mTorr, a regime where high voltage breakdown is a serious issue. It is complicated by the pump cabling from the main system which must pass through the insulating vacuum. The system is segmented into 154.3 m strings consistent with the beamline vacuum. Each string has valves, a turbo-molecular pump, and bypass valves. Every other string additionally has a leak detector and a large screw pump.

Much of the transmission waveguide vacuum is at room temperature, but it must transition to helium temperatures at the couplers. In addition, the rf power being transmitted is
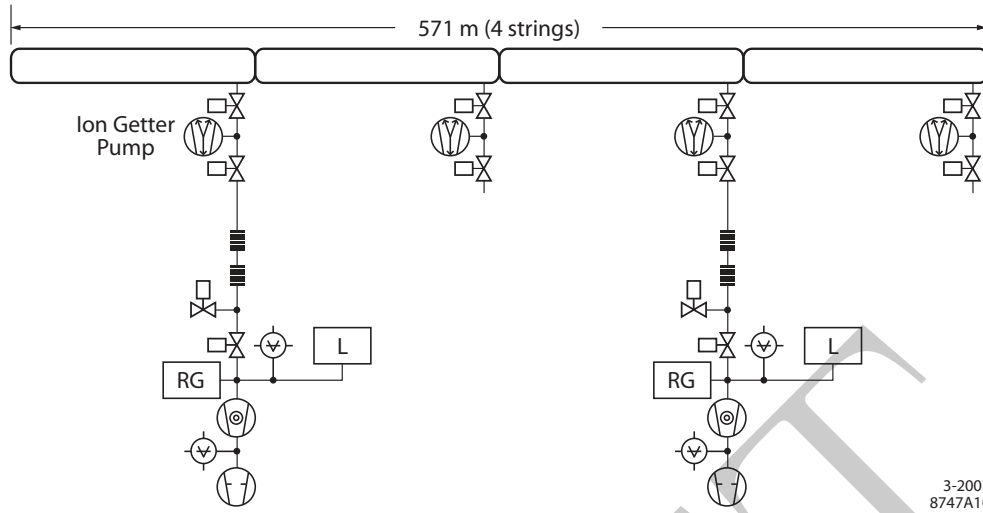
FIGURE 3.2-1. Beamline vacuum system – 2 turbo-molecular pumps (TMP) with high sensitivity leak detector (LD) and residual gas analyzer (RGA), safety, clean venting system, slow start pumping etc.

very high, so multipactoring and arcing must be considered in the design. There is a valve for each coupler. Every cryomodule has an ion pump and titanium sublimation pump, and every 3 cryomodules have a turbomolecular pump, a scroll fore pump and a leak detector.

While the cryomodule vacuum system is complex, costs can be estimated from work done for the TESLA TDR proposal and from recent projects such as SNS. Standard parts, were estimated from vendor quotations and from recent large quantity procurements.

3.2.2.2 Damping Ring and Beam Delivery Cryomodules

The damping ring accelerating rf is single 650 MHz cavities in individual cryomodules. The beam delivery also uses superconducting crab cavities with individual cryomodules. (See Sections 2.4 and 2.7.4.1 for a description of damping ring cryomodules and crab cavity cryomodules.)

3.2.2.3 Polarized Electron Source

The electron source is a DC gun with a laser illuminated photocathode similar to the electron guns at SLAC and Jefferson Lab. To maintain photocathode lifetime, the pressure must be <
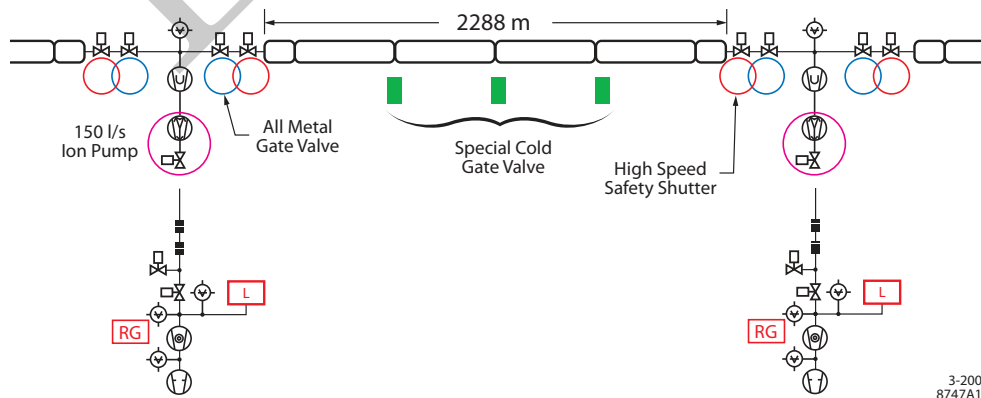
FIGURE 3.2-2. Beamline vacuum system gates and valves.
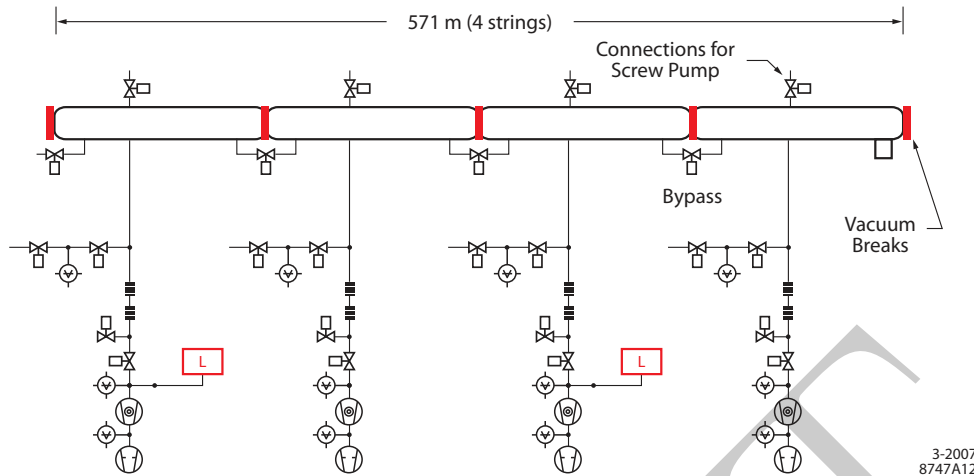
FIGURE 3.2-3. Insulating vacuum system – 4 TMP pumping units: 2 with LD (leak detector) + 2 large screw pump for fore pumping.

$3{\times}10^{-11}$ torr. This is achieved by incorporating large ion pumps and non-evaporable getter (NEG) pumps.

3.2.2.4 Positron Source

The positron source undulator and target vacuum systems are particularly challenging. Electrons are transported through a superconducting undulator to produce γ-rays. The superconducting undulator is a cold bore chamber with a small aperture. The γ-rays are then directed onto a target to produce positrons. The positron target has a very large power load deposted into the target and nearby structures.

3.2.2.5 Damping Ring

The most challenging issues for the damping ring vacuum systems are suppression of the electron cloud in the positron damping ring and ions in the electron damping ring. A variety of techniques are used, including low residual pressure, low SEY coatings, and possibly grooved chambers or clearing electrodes. Lifetime considerations require pressures of less than 1
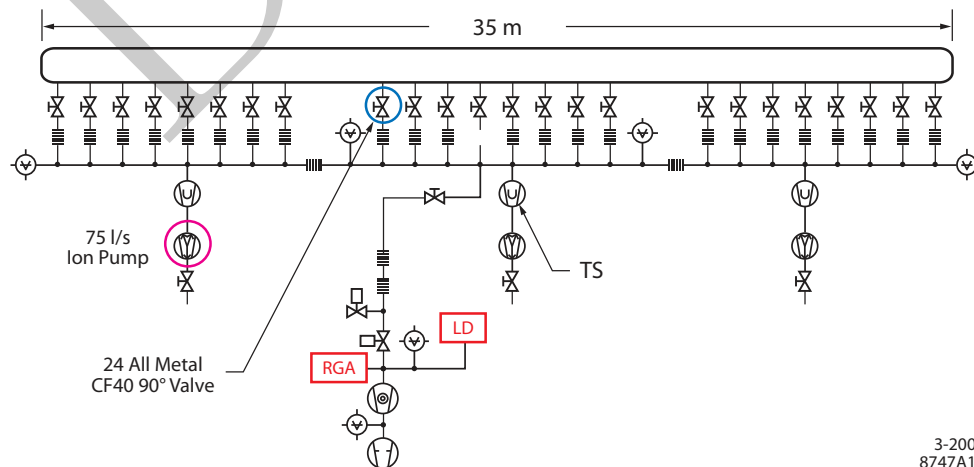
FIGURE 3.2-4. Waveguide and coupler vacuum system.

TABLE 3.2-1
Transport lines for the ILC Electron Source System. Vacuum specifications, beam aperture inner diameters, and lengths are noted. Except in the case of the accelerator sections, the vacuum chamber material is stainless steel.

Beamline	Max Pressure (nTorr)	Aperture Diameter (cm)	Length (m)	Number of Beamlines	Comments
Gun	10^{-3}	4	0.2	2	Integrated into gun design
Gun combining beam line	10^{-3} to 0.1	3	1	2	Differential pumping needed to protect gun vacuum
Transport through Bunching System	1	4	~15	1	
NC beam lines	10	4	~17.5	1	
SC RF	<1	7	~273	1	8 strings (of 3) cryomodules, adopt vacuum specification for Main Linac
Dump beam line	10	4	12	1	
ELTR	10	4	~140	1	Linac to Ring beam line

nTorr which is achieved with neg coated chambers. The bend magnet vacuum pipe requires an antechamber with a photon absorber to collect synchrotron radiation emitted. (For details see 2.4.)

The wiggler straight vacuum system for the ILC damping rings consists of separate chambers for the wiggler and quadrupole sections. The chamber is a machined and welded alu-

TABLE 3.2-2
Transport lines for the ILC Positron System. The reasoning behind the specification is noted and is subject to discussion. Vacuum specifications and aperture inner diameters are noted. Except in the case of the accelerator sections, the vacuum chamber material is stainless steel.

Beamline	Max Pressure (nTorr)	Aperture (cm)	Length (m)	Comments
Chicane 1	50	2	300	halo generation
Undulator	100	0.6	290	fast ion, Daresbury
Chicane 2	50	20	300	halo generation
Photon line	1000	4.5	500	
Positron transport	100	15	5,100	
NC RF	20	6 and 6-4.6	115	1.27 m and 4.3 m sections
SC RF	<1	7	280	12.6 m sections
Linac-to-Ring	50	2	80	
Other	100	6	300	

minum unit designed as a warm bore insert which is mechanically decoupled from the wiggler and cryogenic system. A NEG pumping system [109] and photon absorber are incorporated in ante chambers. Integral cooling is incorporated to minimize distortion of the chamber and thermal load on the wiggler cryostat during NEG regeneration. A NEG surface coating will be used on the main chamber bore to minimize secondary electron yield [110]. Clearing electrodes will also be incorporated to reduce the electron cloud.

The quadrupole chamber is welded aluminum, also incorporating NEG coating for secondary electron yield reduction. Bellows, a BPM assembly and an ion pump are incorporated. The quadrupole chamber is completely shadowed by the wiggler chamber photon absorbers and does not absorb any of the photon power from upstream wigglers.

3.2.2.6 Ring to Main LINAC

Each of the two Ring to Main Linac transport sections contains a room temperature transport line of ∼15 km length, superconducting RF sections of ∼0.5 km length, and additional room temperature beamlines of ∼1.0 km length. The vacuum level in the long room temperature transport line is set by requirements on the beam-ion interaction in the electron system to ∼20 nTorr. The vacuum level in the remaining room temperature beamlines is set by beam scattering requirements to 100 nTorr, at which level about 1×10^{-6} of the beam population is scattered out of the acceptance. The superconducting RF sections have vacuum requirements and system designs which are identical to those of the main linac, i.e., beamline and isolation vacuum systems. Although the RTML contains room temperature bending sections they are not expected to need photon stops or other photon power absorbers because the average current is low and the bending radii in the RTML are kept large to limit emittance growth from incoherent synchrotron radiation effects.

3.2.2.7 Beam Delivery System

The beam delivery system transport requires special attention to limit backgrounds in the experimental detectors. In order to reduce the residual beam-gas scattering to acceptable levels, the line pressure near the interaction region needs to be <1 nTorr. The design is complicated by the requirement for small chamber diameters. The small chamber diameter and the low pressure require close spacing of the ion pumps, bake-outs and the use of NEG coated chambers.

3.2.3 Cost Estimation

The main parts of the vacuum systems were obtained from quotations from vendors and from recent large quantity procurements. "Consumables," such as flanges, gaskets, bolts and nuts, cables, etc, were either not yet included or were estimated for quantity discounts of catalog items.

3.3 MODULATORS

3.3.1 Overview

The accelerating gradient for the ILC main linacs is supplied by superconducting 1.3 GHz cavities powered by 560 10 MW RF stations, each with a modulator, klystron and RF distribution system. Another 86 similar stations are used in the e$^+$ and e$^-$ Sources and RTML bunch compressors. The damping ring RF power is supplied by 650 MHz superconducting cavities powered by 1.2 MW peak power klystrons. These are fed from a DC supply and do not have pulsed modulators. There are also a few special purpose S-band RF stations for instrumentation and a 3.9 GHz RF station to power the crab cavities near the Interaction Point. This section describes only the 1.3 GHz modulators, Damping Ring HVPS system

TABLE 3.3-1
Modulator Specifications & Requirements Assuming Klystron μP=3.38, Effy=65%

Specification	Typical	Maximum
Charger input voltage kV RMS	7.67	8
Charger average power input kW	147.9	161.7
Charger efficiency	0.93	0.93
Charger DC output voltage = Modulator kV$_{in}$	10.8	11.3
Charger DC avg output current = Modulator A$_{in}$	13.26	13.26
Charger average power output @ 5 Hz kW	137.5	150.3
Modulator efficiency	0.94	0.94
Modulator pulse voltage output = Pulse Transformer kV$_{in}$	10.16	10.18
Modulator pulse current output = Pulse Transformer A$_{in}$	1560	1680
Modulator average power output @ 5 Hz kW	129.3	141.3
Pulse transformer step-up ratio	12	12
Pulse transformer efficiency	0.97	0.97
Pulse transformer voltage out = Klystron kV$_{pk}$	115.7	120
Pulse transformer current out = Klystron A$_{pk}$	133.0	140
Pulse transformer average power output @ 5 Hz kW	125.4	137.1
High voltage pulse duration (70% to 70%) ms	1.631	1.7
High voltage rise and fall time (0 to 99%) ms	<0.23	0.23
High voltage flat top (99% to 99%) ms	1.565	1.565
Pulse flatness during flat top %	$< \pm0.5$	±0.5
Pulse to pulse voltage fluctuation %	$< \pm0.5$	±0.5
Energy deposit in klystron from gun spark J	< 20	20
Pulse repetition rate, Hz	5	5
Klystron filament voltage V	9	11
Klystron filament current A	50	60

and associated components.

3.3.2 Technical Description

The 10 MW L-Band RF power stations for the ILC are installed in the support tunnel, spaced approximately 38 meters apart. The L-Band Modulator baseline design was developed for the TESLA Test Facility at DESY, and has been adopted for the European XFEL. Three FNAL units and 5 commercial units have brought online at DESY starting in 1993. The design has a series on-off solid state switch with partial capacitor discharge. The ILC unit varies from this design in two minor ways: (1) A new solid state redundant switch is employed to form the 1.7 msec output pulse, for better reliability; and (2) the input charger will operate from a voltage of 8 kV instead of 480 V to eliminate the AC input step-up transformer in the current design. The modulator specifications and requirements are summarized in Table 3.3-1.

The block schematic is shown in Figure 3.3-1. Photos of current prototypes are shown in Figure 3.3-2. Operation is straightforward: The charger delivers a DC voltage to the storage capacitors of approximately 11 kV. The modulator main switch is then triggered and held closed for 1.7 msec. Capacitor current flows through the switch to the step-up transformer input. At the same time, an auxiliary droop compensation "bouncer" circuit is fired to maintain the pulse top flat to within $\pm 0.5\%$ during the RF drive period. The slightly above 10 kV drive pulse (to compensate for Bouncer voltage) is delivered to the input of the pulse transformer in order to produce at least 115.7 kV 133.0 A to the klystron for rated 10 MW peak output.
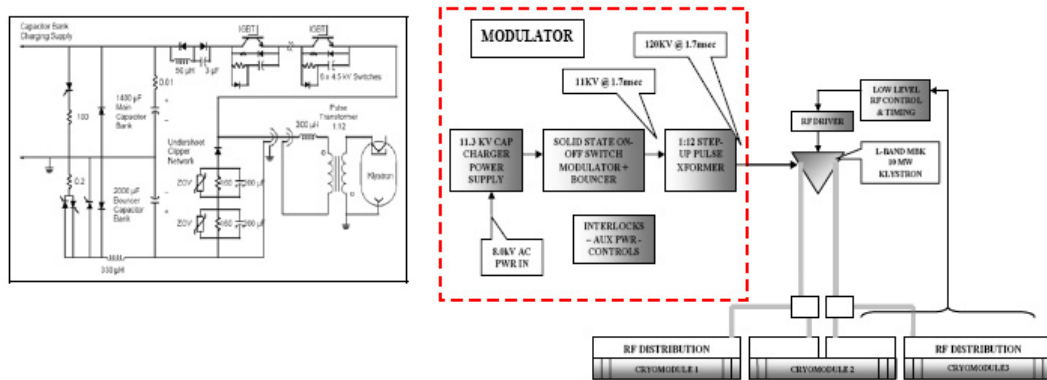
FIGURE 3.3-1. Modulator schematic and L-Band RF station block diagram (1 of 646).

The Damping Rings have 650 MHz CW stations using 1.2 MW peak power klystrons, 20 in total for 2 rings. Power is supplied from a DC supply of 2.0 MW delivering 50-75 kV at 17-10 A DC. The RF envelope is controlled by the low level RF and timing to maintain stability and clearing gaps as needed. The station block diagram is shown in Figure 3.3-3.
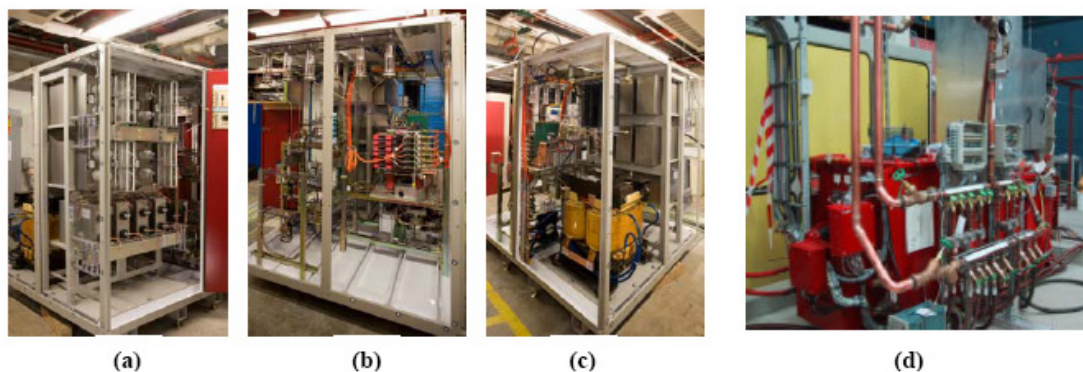
FIGURE 3.3-2. (a) Capacitor stack, (b) Dual IGBT switch, (c) Bouncer choke, (d) Pulse transformer.
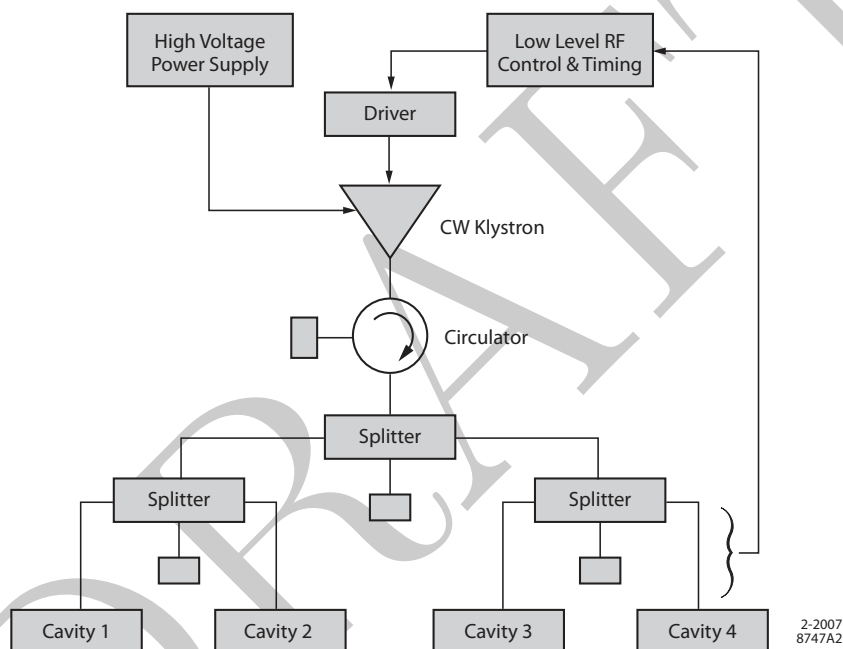
FIGURE 3.3-3. Damping Ring 1.2 MW RF station (1 of 20).

3.3.3 Technical Issues

3.3.3.1 L-Band

There are no major technical issues with the L-Band modulator as long as the entire system has sufficient overhead (redundancy) to compensate for a failed station. To achieve an acceptable availability, the linac energy and beam current parameters must be chosen to provide some RF spare stations. Redundancy of internal components such as IGBT switches and sectioning of chargers for N+1 redundancy[2] is also important. Currently this is only partially implemented in the prototypes.

---

[2]N+1 design segments a single unit such as a power supply into N parallel or series smaller modules components plus an additional spare so one module can fail without interrupting operation. N+1 design is used in stacked or parallel power supplies, capacitors and IGBT's. Such designs can achieve much higher overall Availability especially if modules can be exchanged without interrupting operation (Hot Swap capability). This is only possible in lower voltage units.

The present design which develops the drive pulse at low voltage and high current has larger losses than would be experienced with a higher voltage design. This is not a major technical issue, but a cost, size and weight issue. Installation and repair during operations will be more difficult with multi-ton components such as the transformer and main capacitor-switch multi-cabinet assembly.

An alternative modulator design is being investigated to address these issues, including the possibility of significant cost reduction. The design would reduce the overall footprint and eliminate the step-up transformer and other oil-filled components.

3.3.3.2   Damping Rings 650 MHz

The Damping Ring stations are modeled after similar stations in operation in Italy, Japan and the US. The power supply systems are very well understood. The only change desired would be to make them N+1 redundant internally for higher reliability. This will be investigated and will not have a large cost impact.

3.3.4   Cost Estimation

The L-Band modulator cost model was derived directly from the latest FNAL design, extrapolated as needed to fit the ILC specifications. A traditional bottom-up estimate was made and learning curves applied to first-unit costs for an estimated manufacturing cost. Both single and dual source factory models were examined, as well as sensitivity to learning curve assumptions. These costs were also compared with industrial estimates from both Europe and Japan. In general, the US estimated cost lies between the two offshore commercial estimates. Conservative learning curve exponents ("alphas"[3]) were used for both parts and labor. Profit and factory support costs were than applied, as well as the staging costs of preparing the units for installation and final system checkout. These costs were compiled in M&S and FTE's. The factory models were documented in detail for each Area subsystem and given to the responsible managers for the Area rollups.

The modulator and charger costs were based on recent fabrication of units at SLAC in partnership with LLNL. All parts were recently purchased or fabricated at outside shops, and small additional extrapolations were made for the total quantities.

The cost of the HV power supply for the Damping Ring CW tubes was estimated based on recently built PEPII stations at SLAC, and separate estimates from Italy and Japan. All estimates were in reasonable agreement. The CW power rating needed is 25% lower than for PEP but there will be some additional cost for the N+1 implementation. Again a conservative learning curve was applied for 20 units.

3.3.5   Table of Components

Table 3.3-2 shows the modulator component counts in various Areas.

---

[3] "Alpha" refers to the exponential decrease of costs with each doubling of manufacturing volume. For details see section 6.1.

TABLE 3.3-2
Modulator distribution by type and area.

Modulator type	Total	e^- Inj	e^+ Inj	e^- RTML	e^+ RTML	e^- Linac	e^+ Linac	e^- DR	e^+ DR
10 MW–1.3 GHz–5 Hz	646	13	39	17	17	282	278	0	0
1.2 MW–650 MHz–CW	20	0	0	0	0	0	0	10	10

3.4 KLYSTRONS

3.4.1 Overview

The accelerating gradient for the ILC main linacs is supplied by superconducting 1.3 GHz cavities powered by 560 10 MW RF stations, each with a modulator, klystron and RF distribution system. Another 86 identical klystron/modulator systems are used in the e^+ and e^- Sources and RTML bunch compressors. The damping ring RF power is supplied by 650 MHz superconducting cavities powered by 1.2 MW CW klystrons. These are fed from a DC charging supply and do not have modulators. There are also a few special purpose S-band RF stations for instrumentation and a 3.9 GHz RF station to power the crab cavities near the Interaction Point. This section describes the 1.3 GHz and damping ring klystrons.

3.4.2 Technical Description

3.4.2.1 L-Band Klystrons

The 10 MW L-band source in the ILC baseline design is a Multi-Beam Klystron (MBK), chosen as a result of ten years of R&D for TESLA and the European XFEL. The MBK is a design approach for linear beam tubes that achieves higher efficiency by using multiple low space charge (low perveance) beams. This allows MBKs to operate at a lower voltage yet with a higher efficiency than simpler single round beam klystrons, and provides a cost-effective and simplified design configuration for the ILC RF systems.
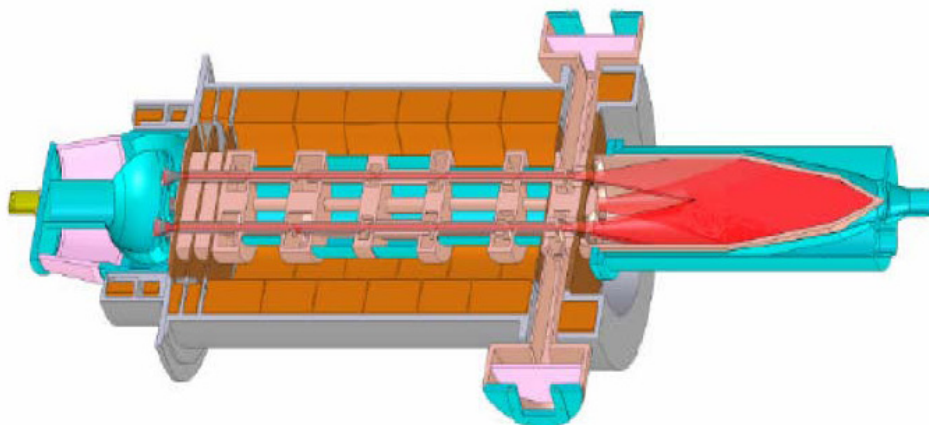
FIGURE 3.4-1. Toshiba E3736 Multi-Beam Klystron.

MBK prototypes have been successfully built for the XFEL by three major electron tube manufacturers: Thales, CPI and Toshiba. These prototypes were designed for essentially the same peak RF output power specifications as required at ILC, yet with nearly twice the duty cycle as required for the XFEL. All of these manufacturers have extensive past experience in bringing prototype klystrons of state-of-the-art designs into production models, and they are regarded as fully capable of ramping up and producing the required quantities of MBKs to meet the delivery schedule for the construction of the ILC. A summary of the MBK specifications is shown in Table 3.4-1.

TABLE 3.4-1
10 MW MBK parameters.

Parameter	Specification
Frequency	1.3 GHz
Peak Power Output	10 MW
RF Pulse Width	1.565 ms
Repetition Rate	5 Hz
Average Power Output	78 kW
Efficiency	65%
Saturated Gain	$\geq$47 db
Instantaneous 1 db BW	>3 MHz
Cathode Voltage	$\leq$120 kV
Cathode Current	$\leq$140 A
Power Asymmetry	$\leq$1%
Lifetime	>40,000 hours

3.4.2.2 Damping Ring Klystrons

The CW Klystron used in the damping rings is a frequency scaled version of the 1.2 MW 500 MHz CW klystrons currently operating reliably at SLAC and KEK [114]. Frequency scaling of klystrons is a common practice in industry, which has a thorough understanding of the engineering procedures to follow. Therefore, availability of the 650 MHz klystrons is not considered to be a technical concern.

3.4.3 Technical Issues

3.4.3.1 L-Band Klystrons

The RF design of the MBK klystron has matured through several iterations of design and testing, and today essentially all aspects of the electrical design are considered solved, in particular, the choice of resonant frequencies to use for the cavities within the klystron body, the beam focusing and others [114], [115], [116], [117], [118]. Test results for all three manufacturers are summarized in Figure 3.4-3.

The three most important technical issues for the MBK are lifetime, manufacturability, and reliability. Lifetime for linear beam tubes is dominated by cathode performance. Both the CPI and Toshiba MBKs have gun designs with cathode loading close to 2 A/cm^2. For an M-type dispenser cathode, this low current density corresponds to a lifetime in excess of 50,000 hours. However, this lifetime has to be confirmed by suitable long-term operation tests. The "lifetime" quoted in Table 3.4-1 is the time during which the klystron can operate at the design performance specifications.

Construction of the MBK is inherently more complex than that of single-beam klystrons due to the several linear beam tubes being built into a single vacuum envelope. The number of braze joints, the fixturing and tooling, and the processes required to successfully construct, bakeout, and test an MBK are issues that require attention in developing an efficient assembly procedure that reduces the unit cost.
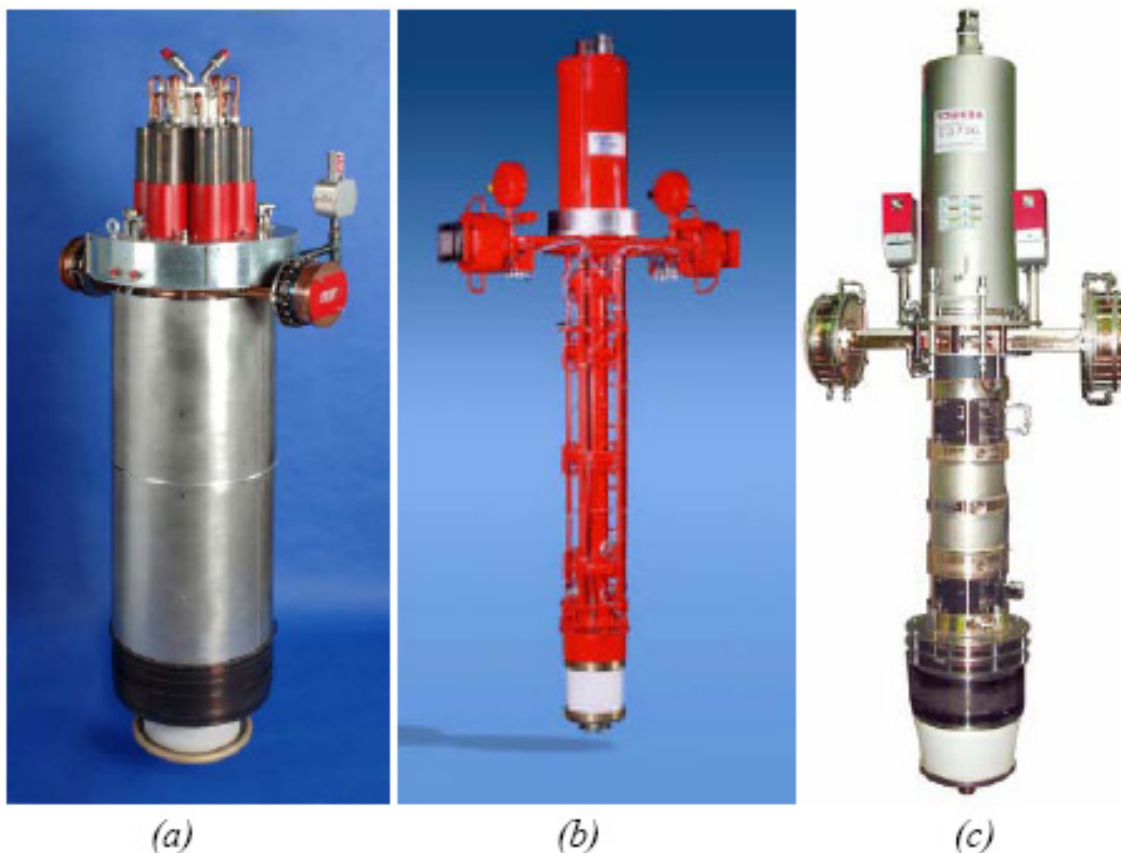
FIGURE 3.4-2. (a) CPI VKL-8301 (b) Thales TH1801 (c) Toshiba MBK E3736.

For reliable performance, a robust thermal design of the output circuit (output cavity, waveguide, and RF window) is important. Since ILC MBK klystrons are being built for the European XFEL, where they will operate at nearly twice the duty cycle of the ILC, there will be significant thermal/mechanical margin when operated for ILC specifications. The XFEL, however, does not require operation at full power, so reliability at 10 MW must also be demonstrated.

A remaining open issue is that the existing prototypes are vertical klystrons but a horizontal version is required for installation in the tunnel. While this is an engineering challenge, DESY is already working with the manufacturers to produce a horizontal klystron for the
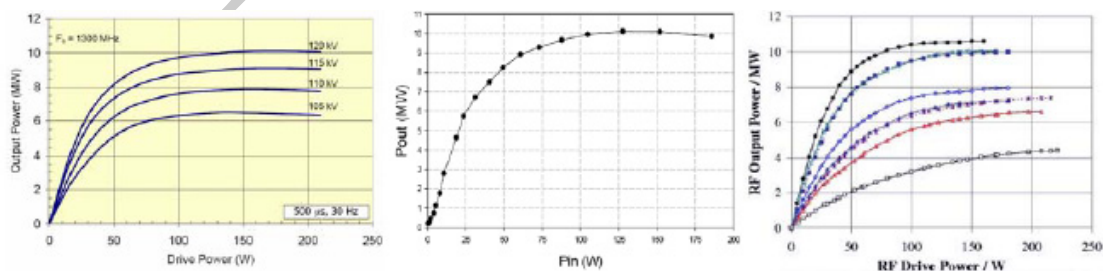
FIGURE 3.4-3. Test results for: (a) CPI VKL-8301 at reduced pulse width; (b) Toshiba MBK E3736 at full spec pulse width; (c) Thales TH1801 at reduced pulse width.

XFEL.

An alternate design is being developed to improve on the manufacturability and reliability of the MBK. The Sheet Beam Klystron (SBK) [118] has fewer parts and processes than an MBK. It is focused with a periodic permanent magnet (PPM) system and, as a result, is smaller and weighs less than an MBK.

3.4.4 Cost Estimation

The cost estimate for the MBKs was derived from cost estimates from the manufacturers themselves, from the actual costs of the prototypes, and from a bottoms-up factory model. The manufacturers' estimates have inherent in them a set of assumptions that are company specific and not transparent to an outside reviewer. These assumptions cover the spectrum from proprietary processes to corporate policy decisions regarding risk assessment. The actual costs of prototypes are useful to determine the characteristics of possible learning curves a company may have used for quantity discounting, and may be useful in benchmarking models such as those used in the bottoms-up factory model.

The bottoms-up factory model used for the MBK was derived from the model used for the NLC X-band klystron. It is a comprehensive factory model with explicit assumptions about variable costs such as yield and learning curves, and fixed costs, such as up-front costs of tooling and fixturing. Fixed costs are more than 50% of the total cost during the prototype and pre-production stage of manufacturing, and taper off to 10% during the years of maximum production rates. The range of estimates from all sources is well within the risk associated with those estimates.

The cost estimate for the Damping Ring klystrons was based on actual procurement costs for 1.2 MW klystrons already produced by industry.

3.4.5 Components

TABLE 3.4-2
Klystron requirements by area.

Klystron	Main Linac	RTML	e$^-$ source	e$^+$ source	DRs
1.3 GHz	560	34	13	39	0
650 MHz	0	0	0	0	10

3.5 RF DISTRIBUTION

3.5.1 Overview

The accelerating gradient for the ILC main linacs is supplied by superconducting 1.3 GHz cavities powered by 560 10 MW RF stations, each with a modulator, klystron and rf distribution system. Another 86 similar stations are used in the e^+ and e^- sources and RTML bunch compressors. The injector stations have slightly fewer cavities (24-25) per RF unit. This section describes the baseline design for distributing the high-power RF to the cavities.

3.5.2 Technical Description

The high-power L-band RF from each 10 MW klystron is brought to the accelerator cavity couplers through an RF distribution system (see Figure 3.5-1). The standard linac RF unit powers 26 nine-cell superconducting cavities filling three cryomodules. The upstream and downstream cryomodules contain nine cavities each, and the middle one contains eight, with a superconducting quadrupole magnet replacing the center cavity. This three cryomodule unit occupies 37.956 m and, at the nominal 31.5 MV/m cavity gradient, provides 846.6 MeV of acceleration (5° off-crest). With a 9 mA beam current, the total power needed in the cavities is 7.62 MW, so some overhead is included.
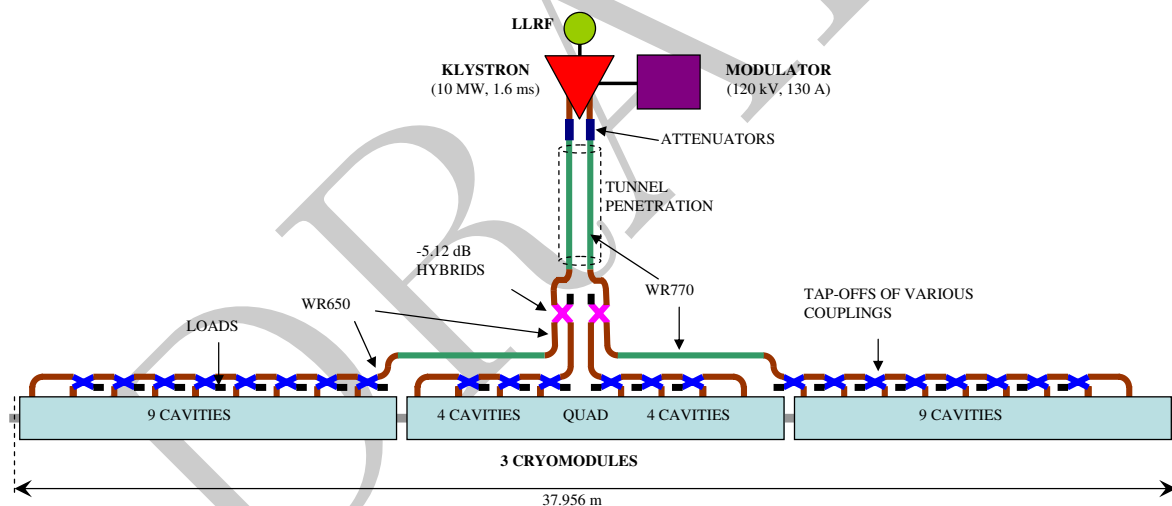
FIGURE 3.5-1. RF unit diagram showing the basic waveguide distribution layout between the klystron and 26 cavities in three cryomodules.

The dual outputs of the klystron feed into two waveguides, each carrying half the power, which run roughly 11 m to the linac through a penetration between the service tunnel and the main tunnel. High-power in-line attenuators allow more power to be sent through one arm than the other to accommodate different average gradient capabilities in the sets of cavities they feed. The penetration emerges approximately at the center of the middle cryomodule of the unit. Here, a hybrid splitter divides the power in each waveguide with a 4:9 ratio (-5.12 dB). The lower power output of each splitter feeds half the center cryomodule and the higher power output is carried approximately 6 m to one of the outer cryomodules.

Along each cryomodule, RF power is equally distributed among the cavities in a linear waveguide system, passing through a series of hybrid-style 4-port tap-offs. These tap-offs couple the appropriate sequential fraction (1/8, 1/7, ...1/2 or 1/4,1/3,1/2) of the power remaining in the line to all but the last cavity, which is directly fed the remainder. The nominal power required in each cavity is 293.7 kW. Between the tap-offs, the remainder of the 1.326 m coupler spacing is filled with modified straight waveguide sections whose width is symmetrically tapered, with 1/4-wave transformer matching steps, varying the guide wavelength to roughly yield the proper inter-cavity phasing.

Between each tap-off output and its associated cavity coupler are a circulator, a three-stub tuner, and a diagnostic directional coupler (see Figure 3.5-2). The three-stub tuner allows fine adjustment of both cavity phase and external coupling. The circulator, with a load on its third port (thus technically an isolator), absorbs RF power reflected from the standing-wave cavity during filling and emitted during discharge. It provides protection to the klystron and isolation between cavities. A couple of E-plane waveguide U-bends are also needed to keep the system compact and feed into the downward pointed coupler flange, and a short semi-flexible section is included to relieve stress and ease alignment tolerances.
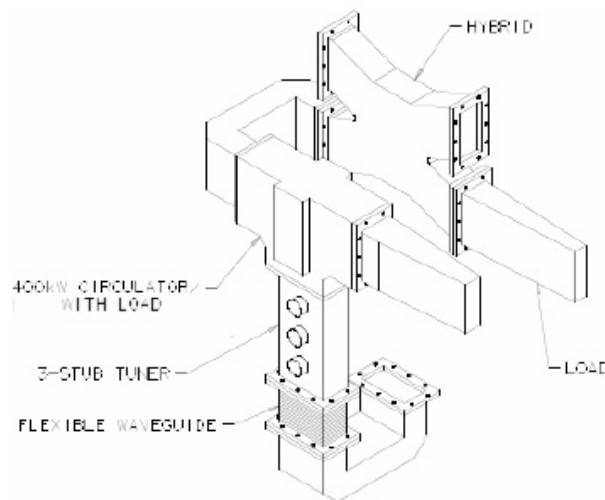
FIGURE 3.5-2. Waveguide circuit from tap-off hybrid to coupler input, showing the various components (except for the directional coupler).

3.5.3 Technical Issues

3.5.3.1 Waveguide

The bulk of the distribution system consists of aluminum WR650 waveguide (6.50" × 3.25") components. This is the standard rectangular waveguide for 1.3 GHz. Larger WR770 waveguide (7.70" × 3.85"), which has 32% lower attenuation, is used, with matched transition sections, for the long runs through the penetration and to the outer cryomodules in order to reduce system losses. The remaining loss, estimated at about 6.5%, may be further reduced by plating the inner walls of waveguide and/or components with copper, which is 22% less lossy.

The entire waveguide system, from the klystron window to the outer coupler window, is pressurized with dry nitrogen to a pressure of 3 bar absolute. This prevents RF breakdown at the klystron window and potential problems in the circulator or elsewhere. It requires thicker-walled (0.25") waveguide, but is more economical than evacuating the system and also avoids multipactoring. The option of using SF6 was considered undesirable due to safety regulations and the risk of corrosion. Gas loss due to an open connection provides a signal to disable RF operation as a safety measure during installation and maintenance.

Relative phase changes along an RF unit due to temperature change during installation, maintenance or operation are at most about 1.1° per degree Celsius. This can be easily controlled with water cooling and insulation on some waveguide runs and components. In addition to the water cooling required on the loads and circulators, this water removes heat from the system that would be more expensive to remove from the tunnel air.

As a cost-saving measure, electron-beam welding of waveguide joints is used in place of expensive waveguide flanges and gaskets where feasible. This will be particularly useful for the penetration waveguide, which cannot be put through in one piece, as it reduces the effective waveguide cross-section.

3.5.3.2 Components

The tap-offs are compact four-port hybrids with WR650 ports of the type used at TTF. Eight different designs are required, with various coupling fractions: four each with 1/4, 1/3, and 1/2, and two each with 1/9, 1/8, 1/7, 1/6, and 1/5. The 4/13 hybrids providing the 4:9 split of the power from each klystron arm may be of the same type. Alternatively, a "button type" hybrid with slight adjustability of the split ratio might be used to provide added flexibility to tailor the system for unequal cryomodule performance.

The circulators are ferrite-based, with a T-junction configuration that provides a needed H-plane bend. The third port of this device is matched into a water load, which absorbs power propagating backward, away from the cavity. In addition to being the most expensive components in the distribution system, circulators contribute the most loss (2% out of ~6.5%). R&D for an alternate distribution system aims at eliminating the need for them.

With three degrees of freedom, the three-stub tuner is a complicated tool to use. It is, however, compact and well tested in TTF. It may be desirable to replace it with an alternate phase shifter, with the movable coupler antenna providing Q_{ext} adjustment.

3.5.4 Cost Estimation

The cost estimate for the RF distribution system was derived from cost estimates from component manufacturers, from the actual costs of purchased components in small quantities, and from a bottoms-up factory model. The estimates from waveguide component manufacturers have inherent in them a set of company specific assumptions that are not transparent to an outside reviewer. However, it is possible to quantify high quantity discounts and learning curves from a manufacturer if small quantities of a component were already purchased. The actual costs of purchased components were used in two different ways: 1) to calculate learning curves and quantity discounts as mentioned above, and 2) to use in bottoms-up factory models. The bottoms-up factory model approach developed a cost for a single unit using information from previous experience in constructing components such as loads and couplers. These costs included material, labor and overhead, and fixturing costs. Once a

completed first unit cost was computed, a learning curve was applied for high quantities.

The difference between the manufacturers' estimates and the factory model was about 10%. Cost estimates for some components reflected a wide range in capacity and high-volume manufacturing experience among the three regions.

3.5.5   Components

Table 3.5-1 gives a rough part count for the components in the baseline RF distribution system of a single RF unit. There are a total of 560 L-Band RF units in the main linacs and approximately 86 more (some normal conducting) in the injectors and RTMLs.

TABLE 3.5-1
Component Count for a Single L-Band RF Distribution System to 26 Cavities.

Component	#/RF Unit	Component	#/RF Unit
Circulators w/loads	26	H-Plane bends	24
3-stub tuners	26	E-Plane bends	4
Directional couplers	32	E-Plane U-bends	52
Hybrids	24	Meters of WR770	34
Loads	24	Meters of WR650	4
Flex guides	30	WR650-770 trans.	8
Phasing sections	25	Gaskets	306

3.6 CAVITIES

3.6.1 Overview

The accelerating gradient in the ILC main linac is supplied by over 16,000 9-cell superconducting RF cavities, grouped into approximately 12.6 m long cryomodules. Another ~1200 9-cell cavities provide acceleration in the sources and bunch compressors. The baseline cavities use the TESLA design developed at DESY over the past 10 years. The cavities are qualified at 35 MV/m gradient in a vertical test and operated at an average gradient of 31.5 MV/m. At these gradients, piezo-electric tuners are required to compensate for Lorentz force detuning.

3.6.2 Technical Description

3.6.2.1 Cavity Design

The TESLA 9-cell superconducting cavity was chosen as the baseline design because it has achieved the highest qualification gradients to date for multi-cell cavities, approximately within the range required for ILC. There is significant operational experience with these cavities and it has been demonstrated with beam that accelerating gradients of greater then 30 MV/m are possible after full installation in a cryomodule. Figure 3.6-1 shows examples of the best vertical test performance for individual cavity structures at DESY (left) and results for a recent DESY cryomodule assembled with the best collection of high gradient cavities (right).
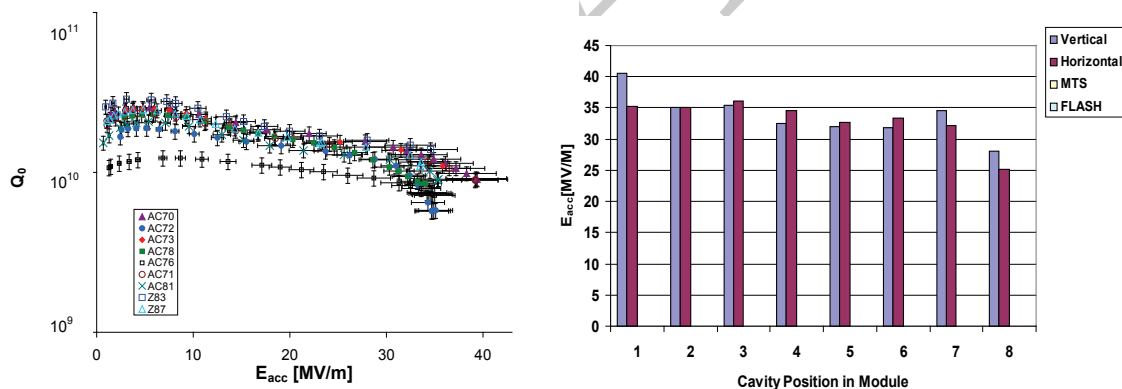
FIGURE 3.6-1. Q_0 vs. E Curves for The Best 9 Cell Vertical Qualification Tests at DESY (left) and Data for a High Gradient Cryomodule Assembled at DESY (right).

Each 9 cell cavity consists of nine accelerating cells between two end group sections. One end group has a port for coupling RF power from the power source into the structure, and the other end has a port for a field sampling probe used to determine and control the accelerating gradient. Each of these ports accepts an electric field antenna required for qualification and operation. Each end group also has a resonant higher order mode (HOM) coupler structure with a probe port and small electric field antenna for extracting HOM power and for diagnostics. In the process of building a cryomodule, these cavity structures are cleaned, tested and placed in a helium jacket for cooling together with additional peripheral

components assembled on them (dressing the cavity). A dressed cavity contains one 9-cell niobium cavity structure, coarse and fine tuners for adjusting the frequency of the structure, magnetic shielding material to minimize the cavity losses, a variable coupling high power input antenna for powering the cavity, an electric field sampling antenna and two higher order mode electric field antennas. Nine of these dressed cavities are usually connected into a string and are a subcomponent of a superconducting cryomodule. Figure 3.6-2 shows a TTF cavity undergoing clean assembly for RF qualification. The basic design parameters for this cavity are listed in Table 3.6-1.

FIGURE 3.6-2. A TTF cavity assembled and prepared for RF qualification testing.

3.6.2.2 Cavity Fabrication

The fabrication of high quality superconducting cavities starts with high quality niobium materials. The cavity accelerating cells and end group components are fabricated from high purity, high RRR niobium sheets. The RRR (residual resistivity ratio) value indirectly indicates the purity of the bulk metal as well as interstitial contamination that can affect the performance of the superconducting properties. An RRR value of 300 is considered desirable Table 3.6-2 shows the typical properties of niobium sheets considered suitable for ILC. The transition joints to the helium vessel are fabricated from a lower grade niobium sheet called "reactor grade" with a RRR value of around 40. The cavity flanges and transitions to the helium vessel are made from bar or round stock niobium alloy, typically NbTi55. The alloy is harder and stronger, and it prevents deformation near the vacuum seals and provides strong transition joints at the cavity connections.

As a final quality assurance check prior to use, the cell material is sometimes eddy-current scanned to a depth of 0.5 mm into the surface of the sheet material. Cavity cells are traditionally formed by deep drawing or hydro-forming methods where the sheets are pressed into dies to form the necessary shapes. These fabrication methods require machining of surfaces to form the weld joints. All cavity subcomponents are joined by electron beam welding in a vacuum chamber. This reduces the contamination at the welds and is considered the cleanest form of joining metals together. Prior to electron beam welding, all subcomponents are inspected, degreased then prepared typically by mechanical polishing of surfaces to be welded, as necessary. The welded components are degreased and chemically etched and rinsed to remove inclusions and surface contamination from the machining and welding steps. The

TABLE 3.6-1
ILC 9-Cell Superconducting Niobium Cavity Design Parameters.

Parameter	Value
Type of accelerating structure	Standing Wave
Accelerating Mode	TM_{010}, π mode
Fundamental Frequency	1.300 GHz
Average installed gradient	31.5 MV/m
Qualification gradient	35.0 MV/m
Installed quality factor	$\geq 1 \times 10^{10}$
Quality factor during qualification	$\geq 0.8 \times 10^{10}$
Active length	1.038 m
Number of cells	9
Cell to cell coupling	1.87%
Iris diameter	70 mm
R/Q	1036 Ω
Geometry factor	270 Ω
E_{peak}/E_{acc}	2.0
B_{peak}/E_{acc}	4.26 mT $MV^{-1}m^{-1}$
Tuning range	± 300 kHz
$\Delta f / \Delta L$	315 kHz/mm
Number of HOM couplers	2

completed cavity has both internal and external chemistry to further remove the damage layer from the fabrication steps of both welding and handling. A smooth outer surface is

TABLE 3.6-2
Typical properties of high-RRR Niobium suitable for use in ILC cavities.

Element	Impurity content in ppm (wt)	Property	Value
Ta	≤ 500	RRR	≥ 300
W	≤ 70	Grain size	≈ 50 μm
Ti	≤ 50	Yield strength	>50 MPa
Fe	≤ 30	Tensile strength	>100 MPa
Mo	≤ 50	Elongation at break	30%
Ni	≤ 30	Vickers hardness	
H	≤ 2	HV 10	≤ 50
N	≤ 10		
O	≤ 10		
C	≤ 10		

necessary to provide good thermal contact with the cryogenic bath.

In total about 150-250 μm of niobium material is removed from the interior RF surface of the cavity through several cleaning steps. After each of these acid etchings the cavity has a new superconducting RF surface and can have different RF performance and a different gradient limitation.

The two primary issues with cavity fabrication are quality assurance on the niobium materials and on the electron beam welds. Niobium materials must be scanned to detect and eliminate surface defects, and then protected with care throughout the manufacturing process. Defective material will ultimately limit the gradient performance of a completed cavity. As with the surface defects, impurities in the welds and heat affected zones next to welds will also limit the gradient performance. Welds must have a smooth under-bead and form no surface irregularities, in particular, sharp edges where the weld puddle meets the bulk material. Defects in the equator welds will limit the gradient by thermal quenches due to the high magnetic fields there. Thermal mapping of quench locations suggests that they are typically located at or near the equator region.

3.6.2.3 Cavity Processing

The current technology for preparing cavity surfaces consists of a series of process steps that: remove niobium material damage incurred during the fabrication process or handling; remove the chemical residues left over from the material removal steps; remove the hydrogen from the bulk niobium that has entered during the chemistry steps; remove any particulate contamination that entered during the cleaning and assembly steps; and close up the cavity to form a hermetically sealed structure. The following steps are typical of those used to qualify a cavity structure in a vertical RF test.

Mechanical Inspection: The cavity is mechanically measured with a coordinate measuring machine to compare dimensional measurements against mechanical tolerances identified on design drawings.

RF Inspection: The cavity fundamental frequency is measured. A bead is pulled through the beam axis of the cavity to determine and record the stored energy of each cell. The bead disturbs the fields in each cell as it passes through which changes the frequency by an amount equal to the stored energy in that cell.

Bulk Chemistry: Both the internal and external surfaces of the cavity are ultrasonically treated in hot de-ionized water to remove grease from the handling and surface particulates that have collected since fabrication. The cavity is then internally chemically etched with electropolishing to remove 150-250 μm of material. The cavity is placed horizontally into an alignment fixture, which levels the cavity and seals the openings while allowing the cavity to rotate. A high purity aluminum cathode rod is inserted on the beam axis to pump cooled electrolyte into each cell of the cavity through a series of holes in the cathode. The cathode is electrically connected to the negative contact of a DC power supply. The cavity itself is the anode and is typically connected on the cells to the positive contact of the DC supply. The electrolyte is a mixture of hydrofluoric and sulfuric acid in a 1:9 or 1:10 parts by volume respectively. At the start of the process, the cavity is filled to the 60% level covering the entire cathode with the cavity slowly rotating at $\approx$1 RPM. The DC power supply provides a current density of about 50 mA/cm^2 and the cavity is polished for approximately 6-7 hours for an etching depth of 150 μm. Temperatures are monitored during the process to control the current and etch rate which is 0.4 μm/minute at 30 degrees C. After etching, the cavity is

rinsed extensively with ultra pure water to remove any chemical residues or chemical safety hazards.

Heat treatment: After bulk chemistry the cavity is cleaned and dried before inserting into a vacuum furnace for heat treatment. The chamber is evacuated to $\approx 10^{-7}$ mbar and the bare cavity is heated to 800 °C and soaked at that temperature to remove any excess hydrogen gained during the chemistry. This additional hydrogen, if not removed, lowers the cavity Q-value due to formation of a niobium hydride during cool-down, that adds surface losses. The cavity is then cooled to room temperature and removed from the furnace.

RF Tuning: The cavity is tuned to the correct warm frequency and the stored energy (field flatness) in each cell equalized. The cells are measured with a bead pull and then plastically deformed by pulling or squeezing in a mechanical tuner. The cavity is mechanically adjusted to correct any alignment errors that would affect tuning for field flatness.

Final Chemistry: The final internal chemistry refreshes the niobium surface by electropolishing removal of 10-30 μm of material. The processing steps are the same as for the bulk chemistry although the processing time is much shorter. After the standard water rinsing, additional steps should be taken to remove any sulfur particulates from the surface and several methods are now under evaluation.

High Pressure Rinsing: The cavity is inserted vertically into the high pressure rinse (HPR) system where a wand is moved slowly through the beam axis of the cavity and the cavity is rotated. The head of the wand has small diameter nozzles tilted at angles through which high pressure ultra pure water is sprayed. A water pressure to the wand of 80-100 bar produces up to 40 N of force on the surface at impact. The wand is repeatedly moved up and down spraying all surfaces of the cavity with water to remove surface particulates which are attached on the cavity interior. The HPR process is considered the most effective cleaning method to remove surface contamination.

First Assembly: Assembly takes place in a Class 10 cleanroom, where the cavity has been left open to air dry over night. Once the cavity has dried, cleaned subcomponents are carefully attached to the cavity by hand. Each flange connection is sealed using a diamond shaped aluminum alloy gasket that is crushed between flange faces with high line loading forces. High strength bolts and nuts with washers provide the force necessary to crush the seal. All subcomponents are assembled to the cavity except the bottom beam-line flange to allow for the second high pressure rinse.

Second HPR: The second rinse is typically longer then the first rinse and is necessary to remove any additional particulates that have entered during the assembly steps, either from the personnel, the cleanroom environment, or the subcomponents. The cavity is removed from the HPR system after the rinse is completed and is moved to the Class 10 area to dry again overnight, this time with only the lower beam-line flange open.

Second Assembly: The bottom beam-line flange is connected to the cavity. It typically has an isolation vacuum valve with pump-out port and an RF input probe to power the cavity. The cavity is now hermetically sealed and ready for evacuation.

Cavity Evacuation: The cavity pump-out port is connected to a vacuum pump and evacuated. The pump system usually has a turbo molecular pump with a scroll type dry mechanical backing pump. The cavity is pumped overnight and the following day tested for vacuum leaks by spraying the cavity flange joints with helium gas and using a residual gas analyzer on the vacuum system to detect helium.

120°C Vacuum Bake: To improve the high field Q-value, the cavity is baked at 120 degrees C for 12-24 hours while actively being pumped by the vacuum system. After being

cooled to room temperature, the cavity is ready for RF testing.

RF Qualification Testing: The cavity is mounted vertically into a cryogenic test stand, RF cables are connected to the cavity probes and the stand is inserted into a cryogenic dewar. The dewar is cooled to 4.2 K by helium gas and liquid is collected to fill the dewar. The dewar is pumped down, lowering the temperature to 2.0 K where the cavity is RF tested to determine its gradient, Q-value and limitations. Once testing is complete, the dewar is warmed up to room temperature and the stand with cavity is removed. With existing technology and infrastructure, this cryogenic cycle usually takes about 2 days at DESY, and about 4 to 5 days at KEK.

3.6.2.4   Peripheral Components

The DESY variable input coupler has been chosen as part of the baseline cavity design. This coupler features two ceramic RF windows as wells as two bellows which allow the center conductor to be mechanically moved into or out of the cavity structure thus changing the RF coupling of klystron power to the cavity. Further R&D will focus on reducing the cost of construction and adapting it to large scale production in industry.

The ILC cavities have both a mechanical coarse tuner and a piezo electric fine tuner. There are several viable designs for both the mechanical and the piezo electric tuners such as the blade tuner (mechanical). Currently no tuner has been chosen for the baseline design, and R&D is required to determine the reliability and installed performance of current designs.

The ILC cavities use a DESY style helium vessel made from titanium, which is thermally matched to the cavity material to avoid distortion of the cavity shape during cool down.

3.6.2.5   Cavity Performance Requirements

The ILC cavities must meet specific requirements on accelerating gradient and Q-value, both in the vertical qualification test and after assembly in a cryomodule. For the vertical test, each cavity must achieve 35MV/m gradient with a Q-value of 0.8×10^{10} or greater. The Q-value is a ratio of the stored energy within the cell structure to the losses dissipated in the cell walls. Lower Q-values increase the heat load to the cryogenic system. A cavity assembled within a cryomodule must reach 31.5MV/m on average, with a Q-value of 1×10^{10}. The installed gradient and Q-value requirements are believed to be achievable with current fabrication and processing techniques. The vertical test gradient requirement is higher then that of the cryomodule in order to increase the success rate of assembled cryomodules. The performance of a cryomodule can be limited by additional system variability and administrative interlocks for the protection of peripheral components as well as from the cavity. The baseline design of ILC has been developed under the assumption that cavities qualified at 35MV/m will meet the requirement of 31.5MV/m on average once installed in a cryomodule, with overheard to compensate for microphonics and for limitations from weaker cavities powered by the same RF source.

With current fabrication and process procedures, cavities have a large spread in gradient and Q-value performance and do not reliably reach 35MV/m in the vertical tests. The primary issue is the magnitude and onset of field emission, which lowers the Q-value below specification. Field emission is typically caused by surface contamination located in regions of high electric field. Electrons emitted from the contamination site bombard other cavity surfaces, increasing surface heating and surface losses, thus lowering the cavity Q-value at

that gradient. Once field emission starts, it is typically stable and the Q-value continues to drop with increasing gradient.

When not dominated by field emission, the high gradient performance of a cavity is typically limited by a thermal magnetic quench of the niobium material. Quenches can be caused by a variety of surface defects such as bad welds, lossy oxides and imbedded materials entering during fabrication or handling, or even by field emitted electrons from surface contamination.

The highest priority for ILC accelerator cavity R&D is to increase the success rate in producing cavities that reach the required performance. Increased quality control of the processing and assembly steps is expected to address the field emission issues which currently appear to dominate the limitation and variation of cavity performance. Better control of the process variables are being pursued through a global R&D effort. Current emphasis is on understanding and improving the electropolishing process. To reach the desired gradient and Q-value, a high level of quality control must be implemented for the preparation of material used in cavity fabrication, throughout the fabrication of the structures, and during the cleaning and assembly processes.

FIGURE 3.6-3. A low loss nine cell prototype RF structure under development.

3.6.2.6   Alternative Cavity Designs

Alternative cavity shapes and fabrication materials are being studied that could potentially reduce the cost of fabrication or increase the achievable gradient. If successful, either could significantly reduce the ILC cost.

By slightly changing the shape of the cavity cell walls, it is possible to reduce the peak magnetic flux on the walls and allow the cavity to reach higher accelerating gradients before reaching a critical field limit on the niobium surface and starting to quench. New cavity shapes have been successfully tested as single cell structures up to gradients of 50MV/m at both Cornell University, with a reentrant shape, and at KEK with the "Ichiro" design. Figure 3.6-3. shows a low loss nine cell prototype RF structure. However, the cavity shape affects many other operational parameters such as the effectiveness of higher order mode damping, multipactoring, shunt impedance, peak electric fields, energy dissipation, beam impedance and mechanical properties since a different aperture size is to be adopted. These aspects must be reoptimized.

Recent niobium material studies at Jefferson Lab have led to new methods for cavity fabrication using either large grain or single crystal niobium. These new materials may lead to significant cost savings in cavity preparation as well as simplification of the processing procedures.

3.7 CRYOMODULES

3.7.1 Overview

The accelerating gradient in the ILC main linac is supplied by over 16,000 9-cell superconducting RF cavities. These cavities are grouped into approximately 1,700 12.7 m long cryomodules. Each cryomodule holds nine cavities, their supporting structure, thermal shields, associated cryogenic piping, and the insulating vacuum vessel. Every third cryomodule in the main linac contains a superconducting quadrupole/corrector/BPM package in place of the center cavity. Another 150 cryomodules are located in the e^+ and e^- sources and RTML bunch compressors. Most of these are the standard linac configuration of 9 cavities or 8 cavities plus quad. A few have special configurations of cavities and quadrupoles.

3.7.2 Technical Description

The cryomodule design is a modification of the type developed and used in the TESLA Test Facility (TTF) at DESY, with three separate vacuum envelopes. The ILC cryomodules contain either nine 9-cell cavities or eight cavities plus a quadrupole package, and have a uniform length of 12.652 m. The cavity spacing within this modified cryomodule is (6-1/4) $\lambda_0 = 1.327$ m. This facilitates powering the cavities in pairs via 3 db hybrids with reflection cancelation in an alternate distribution scheme that may allow the elimination of circulators. Present day accelerators with superconducting RF cavities typically have many separate cryogenic supply boxes and associated warm-to-cold transitions, which represent a significant fraction of the cost. The concept adopted for the ILC is to significantly reduce this number by having a single long continuous string of about 2.5km—called a cryogenic unit—which is connected to one cryogenic supply box at the beginning and one end box.
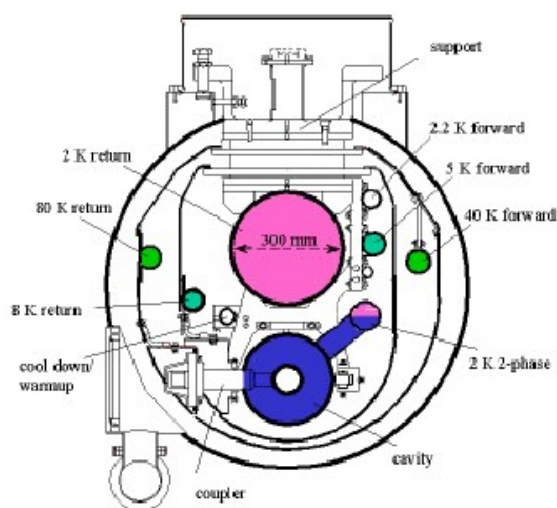
FIGURE 3.7-1. Representative Cryomodule Cross-Section

3.7.3 Technical Issues

3.7.3.1 The Cryomodule

Figure 3.7-1 shows a cross-section of an ILC cryomodule [**?**]. The 300 mm diameter helium gas return pipe (GRP) is the main support structure for the string of cavities and the quadrupole package. The GRP is supported from above by three posts which provide the necessary thermal insulation to room temperature. The posts are fastened to large flanges on the upper part of the vacuum vessel by adjustable suspension brackets, allowing the axis of the cavities and quadrupoles to be correctly aligned, independent of the flange position. The support system is designed to allow the GRP to contract/expand longitudinally with respect to the vacuum vessel during thermal cycling. The center post is fixed to the vacuum vessel, while the two end brackets can move in the axial (z) direction to accommodate differential shrinkage. A post consists of a fiberglass pipe terminated by two shrink-fit stainless steel flanges. Two additional shrink-fit aluminum flanges are provided to allow intermediate heat flow intercept connections to the 5-8 K and 40-80 K thermal shields; the exact location of these flanges has been optimized to minimize the heat leakage.

Each of the cavities is encased in a titanium helium vessel, supported by the GRP by means of stainless steel brackets connected to four titanium pads on the helium vessel itself; each bracket is equipped with a longitudinal sliding mechanism and adjusting screws and pushers for alignment. A mechanical, coaxial (blade) and a piezo-electric tuner are mounted to the vessel. The inter-cavity spacing—which accommodates RF- and HOM-couplers and a flanged interconnecting bellows—amounts to 291 mm. Manually operated valves required by the clean-room assembly terminate the beam pipe at both module ends. The valves are fitted with simple RF shields.

During cool down the two ends of the $\sim$12 m long gas return pipe move by up to 18mm toward the center of the module. To keep the cold input coupler head of each cavity fixed longitudinally within an accuracy of 1 mm, each cavity is anchored to a long invar rod attached to the longitudinal center of the gas return pipe. The beam pipe interconnection between the cryomodules consists of a 0.38 m long section that incorporates a Higher Order Mode (HOM) absorber, a bellows, and a vacuum pumping port; the latter connected to a flange in the vacuum vessel every ninth cryomodule.

The cryostat includes two aluminum radiation shields operating in the temperature range of 5-8K and 40-80K respectively. Each shield is constructed from a stiff upper part (divided into two halves), and multiple lower sections (according to the number of the cold active components, e.g. cavities, magnets). The upper parts are supported by the intermediate flanges on the fiberglass posts; they are screwed to the center post but can axially slide on the other two posts, to which they are still thermally connected. The 'finger welding' technique is used both to connect each thermal shield to its properly shaped aluminum cooling pipe, and the lower shield parts to the upper ones.

Blankets of multi-layer insulation (MLI) are placed on the outside of the 5-8 K and the 40-80 K shields. The 5-8 K shield blanket is made of 10 layers while the 40-80 K blanket contains 30 layers. In addition the cavity and quadrupole helium vessels, gas return pipe and 5-8 K pipes are wrapped with 5 layers of MLI to reduce heat transfer in the event of a vacuum failure.

The cryostat outer vacuum vessel is constructed from carbon steel and has a standard diameter of 38". Adjacent vacuum vessels are connected to each other by means of a cylindrical sleeve with a bellows, which is welded to the vessels during installation. Radiation shield

bridges are also provided. In the event of accidental spills of liquid helium from the cavity vessels, a relief valve on the sleeve together with venting holes on the shields prevent excessive pressure build-up in the vacuum vessel. Wires and cables of each module are extracted from the module using metallic sealed flanges with vacuum tight connectors. The insulating vacuum system is pumped during normal operation by permanent pump stations located at appropriate intervals. Additional pumping ports are available for movable pump stations, which are used for initial pump down, and in the event of a helium leak. The RF power coupler needs an additional vacuum system on its room temperature side; this is provided by a common pump line for all couplers in a module, which is equipped with an ion getter and a titanium sublimation pump.

The following helium lines are integrated into the cryomodules:

- The 2 K forward line transfers pressurized single phase helium through the cryomodule to the end of the cryogenic unit.

- The 2 K two phase supply line (made from titanium) is connected to the cavity and magnet helium vessels. It supplies the cavities and the magnet package with liquid helium and returns cold gas to the 300 mm GRP at each module interconnection.

- The 2 K GRP returns the cold gas pumped off the saturated He II baths to the refrigeration plant. It is also a key structural component of the cryomodule

- The 5-8 K forward and return lines. The 5K forward line is used to transfer the He gas to the end of the cryogenic unit. The 5-8 K return line directly cools the 5-8 K radiation shield and, through the shield, provides the heat flow intercept for the main coupler and diagnostic cables, and the higher-order mode (HOM) absorber located in the module interconnection region.

- The 40-80 K forward and return lines. The 40 K forward line is used to transfer He gas to the cryogenic unit end and cools the high temperature superconductor (HTS) current leads for the quadrupole and correction magnets. The 40-80 K return line directly cools the 40-80K radiation shield and the HOM absorber and, through the shield, provides an additional heat flow intercept for the main coupler and diagnostic cables.

- The warm-up/cool-down line connects to the bottom of each cavity and magnet helium vessel. It is used during the cool down and warm up of the cryostat.

The helium lines connected to the cavities and the magnets withstand a pressure of 4 bar; all other cryogenic lines withstand a pressure of 20 bar. The helium lines of adjacent modules are connected by welding, as was done for the HERA superconducting magnets. Transition joints (similar to those used in the HERA magnets) are used for the aluminum to stainless steel transition on the thermal shield cooling lines. The cryostat maintains the cavities and magnets at their operating temperature of 2 K. A low static heat load is an essential feature of the cryostat design; the total heat load is dominated by the RF losses, and is thus principally determined by cavity performance. Table 3.7-1 lists the heat loads for an RF unit scaled from the 12-cavity cryomodule heat loads calculated for TESLA and documented in the TESLA TDR. For the scaling to the ILC, it was assumed that the gradient is 31.5 MV/m, the cavity Q_0 is 1×10^{10}, and the beam and RF parameters are those listed in section 2.6.

Most losses occur at lower frequencies where the conductivity of the superconducting surfaces is several orders higher than that of normal conducting walls. Part of this power is extracted by input- and HOM-couplers, but high frequency fields will propagate along the structure and be reflected at normal and superconducting surfaces. In order to reduce the

TABLE 3.7-1
Heat loads for one RF unit of 3 cryomodules with 26 cavities. All values are in watts.

	2 K		5-8 K		40-80 K	
	Static	Dynamic	Static	Dynamic	Static	Dynamic
RF Load		22.4	4.2		97.5	
Supports	1.8	0.0	7.2		18.0	
Input coupler	1.6	0.5	4.4	4.0	46.5	198.2
HOM coupler (cables)	0.0	0.6	0.9	5.5	5.5	27.1
HOM absorber	0.4	0.0	9.4	1.6	9.8	32.6
Beam tube bellows		1.1				
Current leads	0.9	0.9	1.4	1.4	12.4	12.4
HOM to structure		3.6				
Coax cable (4)	0.2					
Instrumentation taps	0.2					
Diagnostic cable			4.2		7.4	
Sum	5.1	29.0	31.7	12.5	177.6	270.3

losses at normal conducting surfaces at 2 K and 4 K, the cryomodule includes a special HOM absorber that operates at 70 K, where the cooling efficiency is much higher. The absorber basically consists of a pipe of absorbing material mounted in a cavity-like shielding, and integrated into the connection between two modules. As the inner surface area of this absorber (about 280 cm^2) is small compared to that of all the normal conductors in one cryomodule, the absorber has to absorb a significant part of all the RF power incident upon it. In field propagation studies, which assume a gas-like behavior for photons, it has been shown that an absorber with a reflectivity below 50% is sufficient. Theoretical and experimental studies have suggested that the required absorption may be obtained with ceramics like MACOR or with artificial dielectrics.

The ambient magnetic field in the cavity region must not exceed 0.5 μT to preserve the low surface resistance. The magnetic field tolerance is achieved by demagnetizing the vacuum vessel before assembly of the cryomodule, and placing a passive shield made of Cryoperm around each cavity's helium vessel.

3.7.3.2 Quadrupole/Corrector/BPM Package

The quadrupole/corrector/BPM package is discussed in Section 2.6. An important feature that must be addressed is the package fiducialization and subsequent transfer of these features to reproducible, external cryomodule fiducials to assure the correct alignment of the package with respect to the cryomodule string.

3.7.3.3 Damping Ring and Beam Delivery Cryomodules

The damping ring accelerating RF is single 650 MHz cavities in individual cryomodules. The beam delivery also uses superconducting crab cavities with individual cryomodules. This system is discussed in Section 2.4.

3.7.3.4 Shipping of Cryomodules

To date, no engineering design to facilitate the shipping of completed cryomodules exists. It is essential that a reliable method be developed and incorporated into the ILC cryomodule deign.

3.7.4 Cost Estimation

The cryomodules represent nearly one third of the total ILC project cost. Cost studies have been conducted in all three regions , Americas, Asia and Europe. Much of the original effort relied on the TESLA TDR costing as a basis for comparison. However, independent regional studies and the cost study for the XFEL have proved useful in improving the reliability of the ILC cost numbers.

Significant effort has been expended to understand the cost drivers for cryomodules. The cavities are the largest item, with over 40% of the cryomodule cost for cavity fabrication, processing, dressing and qualification. The next largest items are the power couplers, the helium vessel fabrication, the quad package and the tuners, which represent another 30%. It is anticipated that joint studies between ILC engineers and designers and industrial partners utilizing design for manufacture methodology and value engineering principles will lead to significantly reduced cryomodule component and assembly costs.

3.7.5 Table of Cryomodule Types

The different cryomodule types and required quantities of each type are listed in Table 3.8-1. As can be seen in this table, there are basically four types of cryomodules required for the 1.3 GHz portion of the ILC.

3.8   CRYOGENIC SYSTEMS

3.8.1   Overview

With superconducting equipment throughout the ILC, cryogenic systems of extensive size and capacity will be required. Superconducting RF cavities operating at 2 Kelvin in the main linacs are the primary accelerating structures in the ILC and comprise the largest cryogenic cooling load. Although not as extensive, the positron and electron sources, damping rings, RTML, and beam delivery systems include a large number and variety of superconducting RF cavities. Table 3.8-1 summarizes the numbers of various types of superconducting RF modules in the ILC.

In addition to the RF modules listed in Table 3.8-1, there are a variety of superconducting (SC) magnets in the ILC. About one third of the 1.3 GHz cryogenic modules contain SC magnets. As part of the positron source, the electron linac includes about 150 meters of SC helical undulators in 2 to 4 meter length units. The Damping Rings have 8 strings of superconducting wiggler magnets, and there are special SC magnets in the sources, RTML, and beam delivery system.
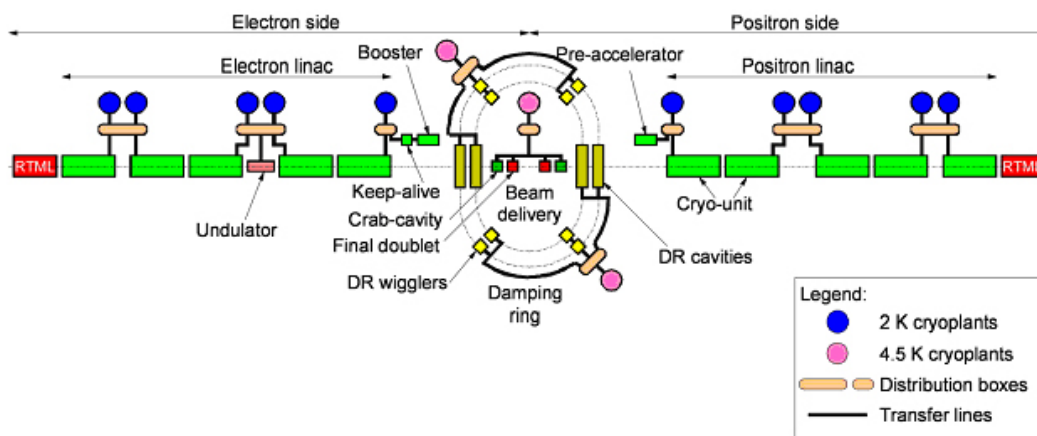
FIGURE 3.8-1. The Overall Layout Concept for the Cryogenic Systems

Figure 3.8-1 illustrates the concept for the cryogenic system arrangement in ILC. Ten large cryogenic plants with 2 Kelvin refrigeration cool the main linac, RTML and the electron and positron sources. Three smaller cryogenic plants with mostly 4.5 K loads cool the damping rings and beam delivery system.

3.8.2   Technical Issues

3.8.2.1   Cryogenic System Definition

The ILC cryogenic systems are defined to include cryogen distribution as well as production. Thus, components of the cryogenic system include the cryogenic plants, distribution and interface boxes, transfer lines, and non-magnetic, non-RF cold tunnel components. Although cryomodules, SC magnets, and production test systems also include significant cryogenics, those are not considered in this section of the RDR.

TABLE 3.8-1
Superconducting RF modules in the ILC, excluding the two 6-cavity energy compressor cryomodules located in the electron and positron LTRs

Cryomodules (cavities/cryomoule) (quads/cryomodule) (frequency, MHz)	8-C 1-Q 1300	9-C 0-Q 1300	8-C 2-Q 1300	6-C 6-Q 1300	Total 1300	1-C 650	2-C 3900
Main Linac e^-	282	564			846		
Main Linac e^+	278	556			834		
RTML e^-	18	30			48		
RTML e^+	18	30			48		
e^- source	24				24		
e^+ booster	12		6	4	22		
e^+ Keep Alive	2				2		
e^- Damping Ring						18	
e^+ Damping Ring						18	
Beam Delivery System							2
Total	634	1180	6	4	1824	36	2

3.8.2.2 Cryogenic Cooling Scheme for the Main Linac

Main linac cryogenic modules each containing eight (with magnet package) or nine (without magnet package) nine-cell niobium cavities, cold helium pipes, and thermal shields are the dominant load to be cooled by the cryogenic system. The magnet package, in one third of the cryomodules, includes a superconducting quadrupole and corrector magnets. The ILC cryomodule design for the 1.3 GHz RF is based on the TESLA Test Facility (TTF) type III design [1] which contains all the cryogenic pipework inside its vacuum enclosure. There are approximately 23 km of 1.3 GHz cryomodules including main linac, RTML, and sources.

Series architecture is mostly used in the cryogenic unit cooling scheme. Like for the TESLA cryogenic concept, saturated He II cools RF cavities at 2 K, and helium gas cooled shields intercept thermal radiation and thermal conduction at 5 - 8 K and at 40 - 80 K. A two-phase line (liquid helium supply and concurrent vapor return) connects to each helium vessel and connects to the major gas return header once per module. A small diameter warm-up/cool-down line connects the bottoms of the He vessels.

A subcooled helium supply line connects to the two-phase line via a Joule-Thomson valve once per string (typically 12 modules). The 5 K and 40 K heat intercepts and radiation screens are cooled in series through an entire cryogenic unit of up to 2.5 km in length. For the 2 K cooling of the RF cavities, a parallel architecture is implemented with the parallel cooling of cryo-strings resulting in operational flexibility. Consequently, each cryogenic unit is subdivided into about 14 to 16 cryo-strings, each of which corresponds to the 154 meter length elementary block of the cryogenic refrigeration system.

Figure 3.8-2 shows the cooling scheme of a cryo-string, which contains 12 cryomodules. The cavities are immersed in baths of saturated superfluid helium gravity filled from a 2 K two-phase header. Saturated superfluid helium is flowing all along the two-phase header for filling the cavities and phase separators located at both ends of the two-phase header.
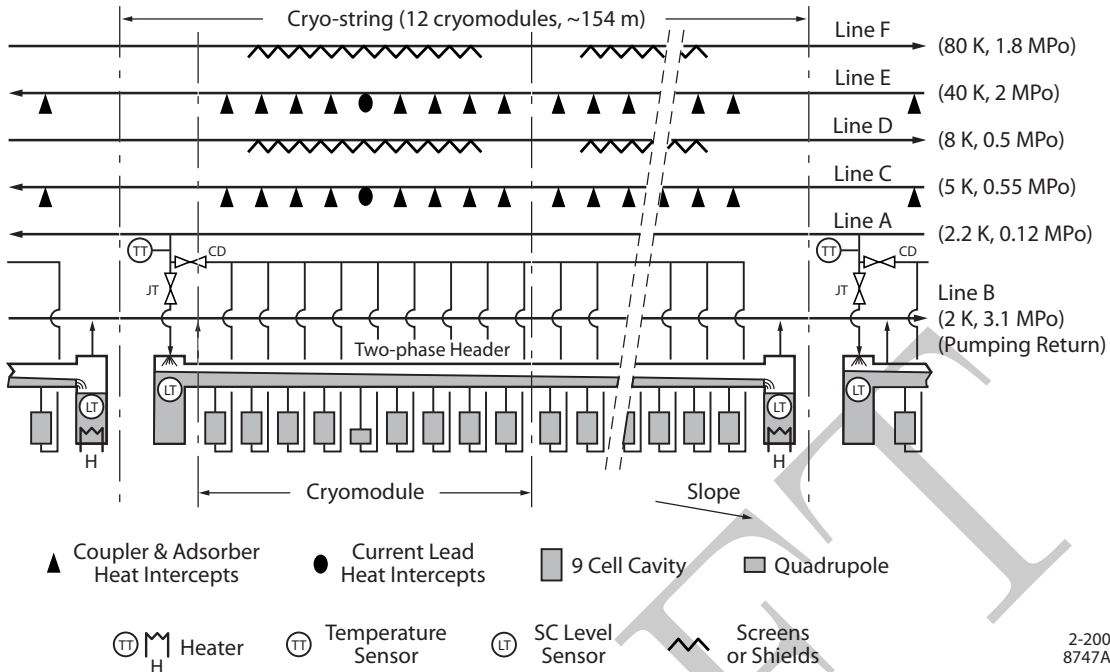
FIGURE 3.8-2. Cooling Scheme of a Cryo-String

The first phase separator is used to stabilize the saturated liquid produced during the final expansion. The second phase separator in used to recover the excess of liquid, which is vaporized by a heater. At the interconnection of each cryomodule, the two-phase header is connected to the pumping return line.

The division of the Main Linac into cryogenic units is driven by various plant size limits and a practical size for the low pressure return pipe. A cryogenic plant of 25 kW equivalent 4.5 K capacity is a practical limit due to industrial production for heat exchanger sizes and over-the-road shipping size restrictions. Cryomodule piping pressure drops also start to become rather large with more than 2.5 km distances. Practical plant size and gas return
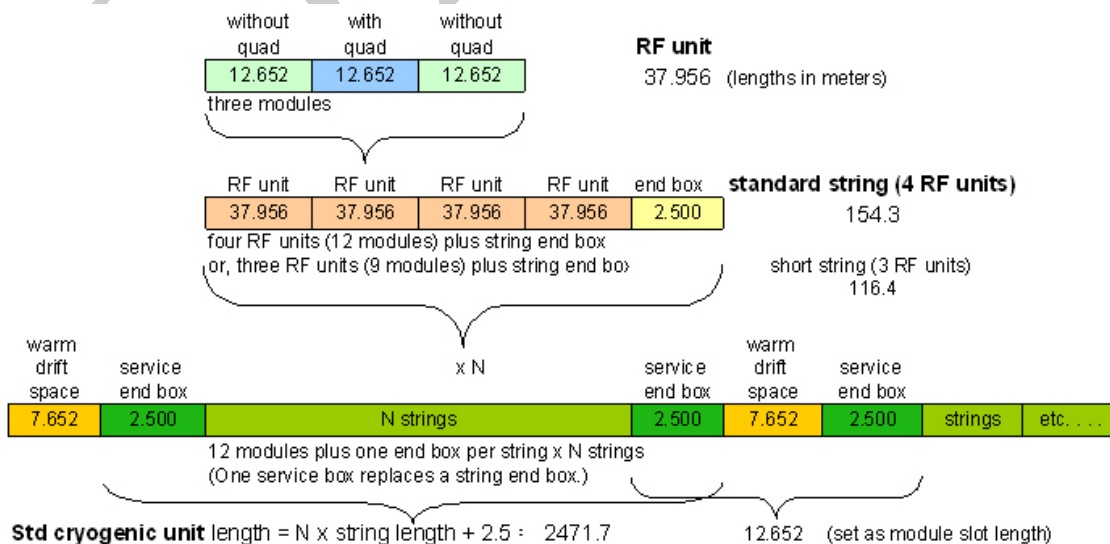
FIGURE 3.8-3. Lengths and Typical Arrangement of Modules in the Electron Main Linac
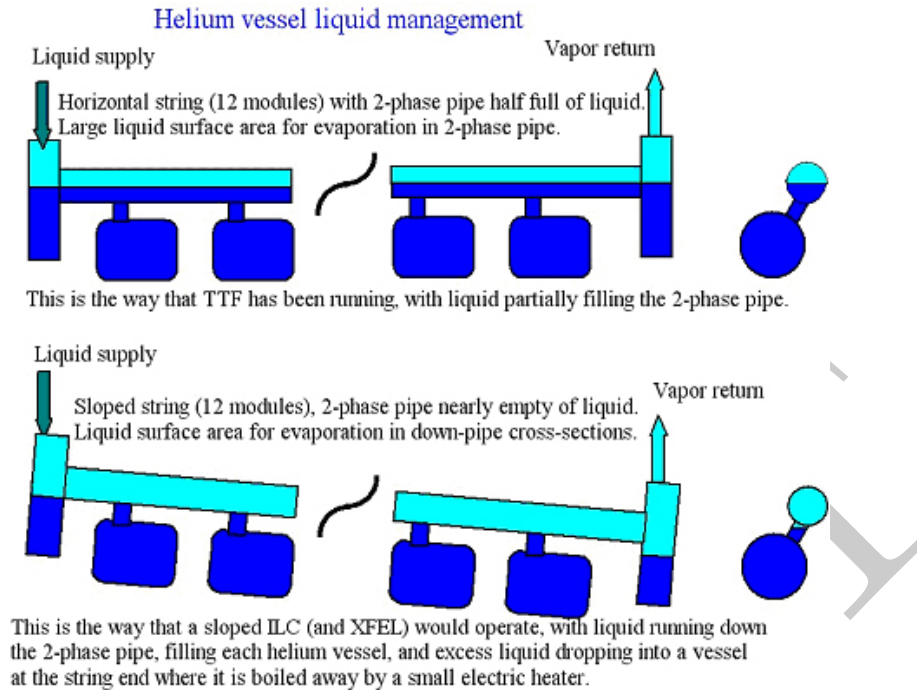
FIGURE 3.8-4. Two-Phase Helium Flow for Level and for Sloped Systems

header pressure drop limits are reached with 192 modules in a 16-string cryogenic unit, 2.47 km long. Five cryogenic units divide the main linac conveniently for placing the positron source undulators at 150 GeV. Figure 3.8-3, illustrates the division of the main linac into strings and units.

3.8.2.3 Liquid Helium Management in 1.3 GHz Modules

As the ILC site has not yet been selected, the cryogenic system concept must accommodate different configurations of tunnel and civil works. The tunnel may follow the earth's curvature or be laser-straight with a maximum slope of up to 0.6% creating large elevation differences. To avoid harmful instabilities, all fluid should ideally be transported over large distances in a mono-phase state. Local two-phase circulation of saturated liquid can be tolerated over limited lengths, within a controlled range of vapor quality. Figure 3.8-4 illustrates two methods of liquid management in the two-phase supply pipe for main linac cryogenic modules, one case for a sloped system and the other for a level system.

3.8.2.4 Sources, Damping Rings, and Beam Delivery Systems

As listed above in Table 3.8-1, electron and positron sources each include just over 20 SRF modules containing 1.3 GHz RF cavities cooled to 2 Kelvin. The sources also include several superconducting magnets, as well as about 150 meters of superconducting positron source undulators. These undulators are cooled by one of the cryogenic plants in the electron linac cryogenic system. The electron and positron source linacs are also cooled from main linac cryogenic plants, as illustrated in Figure 3.8-1.

Damping ring cryogenic loads include 4.5 K superconducting wigglers, 4.5 K 650 MHz cryomodules, associated cryogenic distribution systems, and 70 K thermal shields for all of these. Two cryogenic plants serve the damping rings.

TABLE 3.8-2
Main Linac Heat Loads and Cryogenic Plant Size

	40-80 K	5-8 K	2 K
Predicted module static heat load (W/mod)	59.19	10.56	1.70
Predicted module dynamic heat load (W/mod)	94.30	4.37	9.66
Modules per cryo unit	192	192	192
Non-module heat load per cryo unit (kW)	1.0	0.2	0.2
Total predicted heat per cryo unit (kW)	30.47	3.07	2.38
Efficiency (fraction Carnot)	0.28	0.24	0.22
Efficiency (Watts/Watt)	16.45	197.94	702.98
Uncertainty & overcapacity factor (Fo)	1.54	1.54	1.54
Heat Load per Cryo Unit including Fo (kW)	46.92	4.72	3.67
Installed power (kW)	771.7	934.9	2577.6
Installed 4.5 K equivalent (kW)	3.5	4.3	11.8
Percent of total power at each level	18.0	21.8	60.2
Total operating power for one cryo unit based on predicted heat (MW)	3.34		
Total installed power for one cryo unit (MW)	4.33		
Total installed 4.5 K equivalent power for one cryo unit (kW)	19.57		

The beam delivery system has one 3.9 GHz cryomodule (containing two cavities) on each side of the interaction point, superconducting final focus quadrupoles, and other special superconducting magnets spaced several hundred meters from the IR. One cryogenic plant serves both sides of the interaction region. This plant could also serve the cryogenic needs of the detectors, but that aspect of these cryogenic systems is not considered here.

3.8.2.5 Heat Loads and Cryogenic Plant Power

Table 3.8-2 shows the predicted heat load for a typical Main Linac Cryogenic Unit. This table lists a combined uncertainty and overcapacity factor, Fo, which is a multiplier of the estimated heat loads. The factor Fo is used to estimate a total required cryogenic plant capacity as follows. Installed cryogenic capacity = Fo × (Qd + Qs), where Fo is overcapacity for control, off design operation, seasonal temperature variations, and heat load uncertainty. Qd is predicted dynamic heat load, and Qs is predicted static heat load. Note also that cryogenic plant efficiency is assumed to be 28% at the 40 to 80 K level and 24% at the 5 to 8 K temperature level. The efficiency at 2 K is only 20%, however, due to the additional inefficiencies associated with producing refrigeration below 4.2 Kelvin. All of these efficiencies are in accordance with recent industrial conceptual design estimates.

A similar analysis has been done for the sources, damping rings, and beam delivery system in order to estimate size requirements for each. (RTML cooling is included with the main linac.)

Table 3.8-3, below, lists the estimated heat loads and required cryogenic plant size for the damping rings.

Table 3.8-4 summarizes the required capacities of the cryogenic plants for the different

TABLE 3.8-3
Damping Ring Cryogenics (per ring, two total)

	Units	Value
Total predicted 4.5 K heat	W	1660
Total predicted 4.5 K liquid production (for current leads)	grams/sec	0.80
Total predicted 70 K heat	W	5080
Uncertainity and overcapacity (total combined) Margin		1.54
Installed power	MW	1.13
Cryogenic plant capacity (converted to 4.5 K equiv)	kW	3.45

area systems. The maximum required plant capacities (equivalent at 4.5 K) are comparable with the present state of the art cryogenic plants used in the Large Hadron Collider [3]. Total installed power for the cryogenic system is 48 MW, with an expected typical operating power of 37 MW.

TABLE 3.8-4
ILC Cryogenic Plant Sizes (sources listed separately here, but may be combined with Main Linac)

Area	# of Plants	Installed Plant Size (each) (MW)	Total Installed Power (MW)	Operating Power (each) (MW)	Total Operating Power (MW)
Main Linac + RTML	10	4.35	43.52	3.39	33.91
Sources	2	0.59	1.18	0.46	0.92
Damping Rings	2	1.26	2.52	0.88	1.76
BDS	1	0.41	0.41	0.33	0.33
Total			47.63		36.92

If the tunnel is located near the surface, i.e. with depth of access shafts smaller than 30 m, the entire cryogenic plant can be installed above ground. If the tunnel is deep, certain components must be installed at tunnel level because of the hydrostatic pressure loss.

3.8.2.6   Helium Inventory

As illustrated in Figure 3.8-5, most of the helium inventory consists of the liquid helium which bathes the RF cavities in the helium vessels. The total helium inventory in ILC will be roughly equal to that of the LHC at CERN, about 650,000 liquid liters, or about 100 metric tons.

3.8.3   Cost Estimation

The cryogenic system cost estimate has been generated based on experience in procurement of cryogenic plants and equipment at Fermilab, CERN, DESY, and other laboratories.
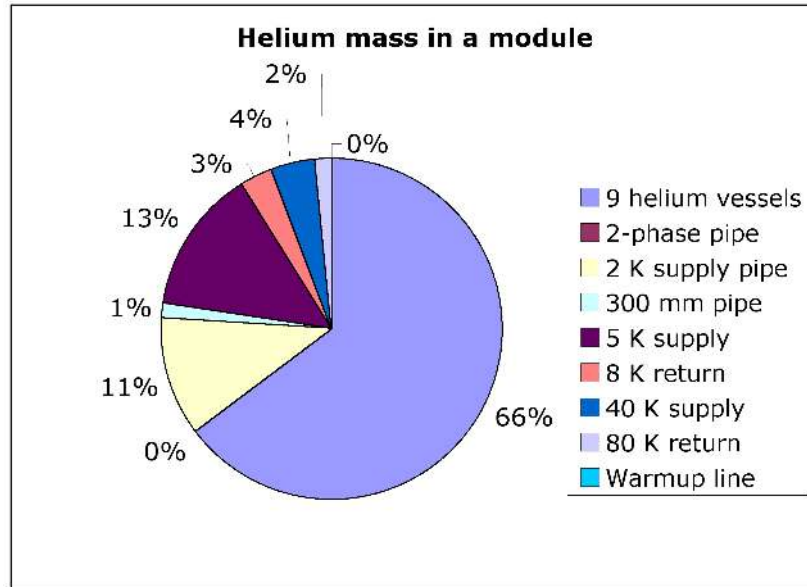
FIGURE 3.8-5. Helium Mass in a Module

TABLE 3.8-5
Main Linac Helium Inventory

Volumes		Helium (liquid liters equivalent)	Tevatron Equiv.	LHC Equiv.	Inventory Cost (k$)
One module		370			
String	12 modules	4,500	0.1		13.4
Cryogenic unit	14-16 strings	68,000	1.1	0.1	203.6
ILC Main Linacs	2x5 cryo units	680,000	11.3	0.9	2,037

3.9 LOW LEVEL RF CONTROLS

3.9.1 Overview

The Low-Level RF system (LLRF) controls the phase and amplitude of the RF cavities used to accelerate the beam, and is essential for stable and reliable beam operation. The LLRF includes feedback and feed-forward, exception handling and extensive built-in diagnostics with suitable speed and accuracy. Each of the ∼650 L-Band RF units in the main linacs, sources and bunch compressors have a LLRF controller, as do the damping ring RF stations. LLRF also controls the crab cavities in the beam delivery and various RF diagnostic devices.

A primary challenge for the ILC LLRF is the large number of cavities driven by a single klystron. The LLRF controls the vector-sum of all cavities as well as controlling the individual cavities. Most of the needed requirements have been demonstrated in the LLRF systems in operation at the FLASH facility at DESY [123]. The DESY LLRF uses state-of-the-art technologies for digital control of the operational parameters. Similar systems are being implemented at FNAL and KEK.

3.9.2 Technical Description

The performance requirements for the LLRF are set by the gradient desired from the cavities and by the stability required for beam parameters such as energy and energy spread, both bunch to bunch and pulse to pulse. There are also stringent requirements on the bunch compressor RF to set the arrival time of the beams at the IP, and on the crab cavity RF to fix the beam position at the IP.

Three issues of particular importance for the ILC LLRF are:

1. Lorentz force detuning: The radiation pressure of the electromagnetic field during the RF pulse deforms the cavity and pulls it off resonance. The static detuning (Δf) due to the Lorentz forces is proportional to the square of the accelerating field (E_{acc}) and is approximately 600 Hz [124] for operation at design gradient in the main linac (31.5 MV/m).

   To maximize the RF power efficiency, and to reduce the electric fields at the cavity input coupler, it is essential to cancel the Lorentz force detuning by a fast frequency tuner (for example, piezoelectric actuators).

2. Microphonics: External mechanical vibrations can be transferred to the cavities via the supporting system within the cryostat. Modulation of the resonant frequency due to microphonics is estimated to be ∼10 Hz rms. This modulation is not correlated to the macro pulse and and therefore can only be corrected by the feedback system.

3. Beam loading: The beam loading by individual bunches is about 0.15However, slow bunch charge fluctuations within the bandwidth of the RF system cause cavity vector disturbances that need to be controlled on the order of 0.05% at each station as the bunch charge fluctuations are correlated through the accelerator chain. Bunch charge is measured in the DRs and processed by the LLRF to create a correction feedforward term before beam is injected into the linac.

The RF systems in the main linacs and RTML require tight field control on the order of up to 0.07% for amplitude errors and 0.35° for the phase. Due to microphonics, the measurement of the vector sum must be calibrated to an accuracy on the order of 1% for amplitude and

TABLE 3.9-1
Summary of tolerances for phase and amplitude control. These tolerances limit the average luminosity loss to <2% and limit the increase in RMS center-of-mass energy spread to <10% of the nominal energy spread.

Location	Phase (degree)		Amplitude (%)		limitation
	correlated	uncorr.	correlated	uncorr.	
Bunch Compressor	0.24	0.48	0.5	1.6	timing stability at IP (luminosity)
Main Linac	0.35	5.6	0.07	1.05	energy stability $\leq 0.1\%$

1.0° for phase. The phases of crab cavities in the beam delivery system must be stabilized to better than 0.015°. Table 3.9-1 gives an overview of the regulation requirements of the Main Linac and RTML bunch compressor.

Besides field stabilization, the LLRF provides automatic beam-based system calibration and diagnostic signals to the accelerator control system. Exception handling is required to avoid unnecessary beam loss and to allow for maximum operable gradient.

Availability and maintainability are also critical considerations in the LLRF system design. Although most of the LLRF system components are located in the service tunnel, the large number of units requires a high availability design. Possible failure modes must be understood, their operational impacts examined, and mitigation measures developed and implemented. Adequate redundancy such as a simple feed-forward technique in the complex feedback scheme should be an integral part of the system design. Built-in diagnostics for both hardware and software are required to support preventative maintenance and increase reliability.

3.9.3 Technical Issues

3.9.3.1 Hardware Architecture

The most basic function of any LLRF control is a feedback that measures the cavity field vector and attempts to hold it to a desired set-point. The vector difference between the measured field and the set-point is filtered and amplified, then used to modulate the klystron drive and thereby the incident power to the cavities. The forward and reflected power signals are also processed to measure the resonant frequencies of the ILC cavities, for automated adjustment by slow motor-controlled tuners and fast piezoelectric actuators. The architecture of a typical LLRF control system is shown in Figure 3.9-1. The signal from the master oscillator, brought through the RF distribution system, is used as the RF reference.

The LLRF has to combat numerous perturbations with various time patterns and frequencies. Some of these perturbations recur at the machine repetition rate (5 Hz for ILC), like Lorentz force detuning and beam loading. An adaptive feedforward system is used to compensate for the average repetitive errors. The set-points for cavity fields are also implemented in a table to accommodate the time-varying gradient and phase during the cavity filling.
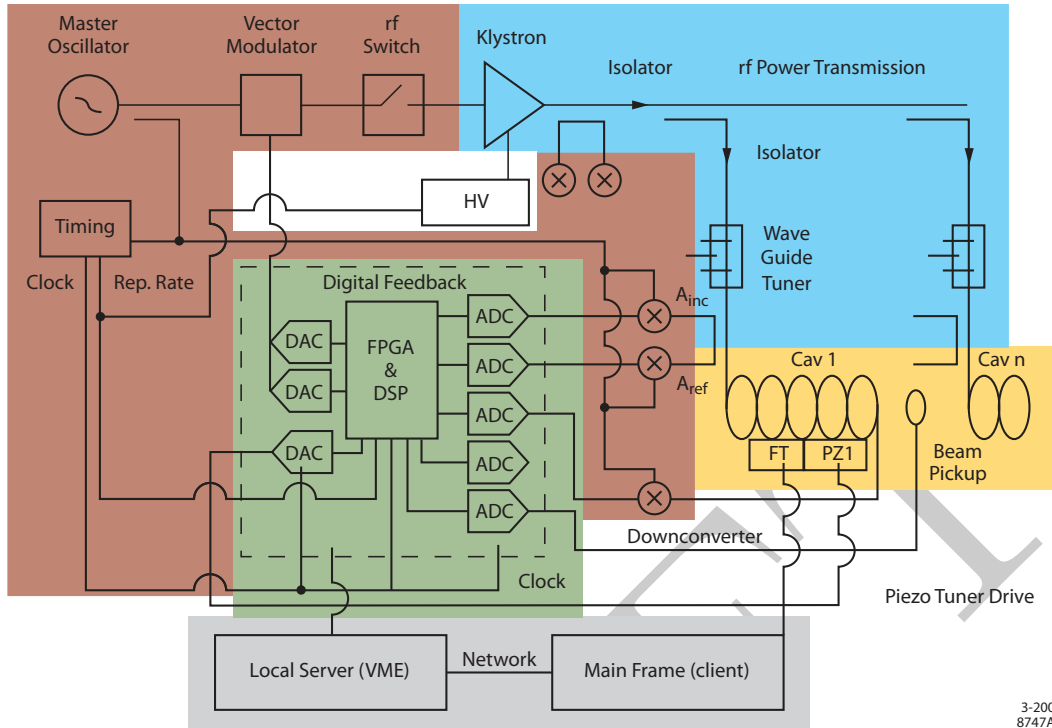
FIGURE 3.9-1. Typical configuration of an RF control system using digital feedback control.

3.9.3.2 Digital Technologies

The key technologies to be used are modern Analog to Digital Converters (ADCs), Digital to Analog Converters (DACs), as well as powerful Field Programmable Gate Arrays (FPGAs) and Digital Signal Processors (DSPs) for signal processing. Low latency can be realized, with time delays from ADC input to DAC output ranging from a few 100 ns to several μs depending on the chosen processor and the complexity of the algorithms. Gigabit links are used for the high speed data transfer between the large number of analog input and output channels and the digital processor as well as for communication between various signal processing units. Typical parameters for the ADCs and DACs are sample rates of 65-125 MHz and 14-bit resolution. The signal processing uses FPGAs with several million gates, including many fast multipliers. More complex algorithms are implemented on slower floating point DSPs

A down-converter module translates the 1.3 GHz RF cavity probe signal to the Intermediate Frequency (IF) where it can be digitized and processed further. The down converter can degrade overall performance if not properly designed. Problems with nonlinearities, thermal noise, phase noise and thermal stability must be addressed in order to maintain the integrity of the detected signal from the cavity. The up-converter module translates a digitally generated IF signal back to the RF in a process similar to that of the down converter. The up converter has less stability issues since it is within the feedback loop.

A fast piezoelectric actuator and a slow motor-driven tuner control the resonant frequency of each individual cavity. The frequency error of the cavity is measured during and after the flattop. This error can be reduced by suitable excitation of the piezoelectric actuator (fast tuner), or it can be compensated via additional RF power. The motor-driven tuner is only used to correct for long-term drifts. The station LLRF system must interface to High Level RF, beam transfer control, machine protection, sector and global energy and phase

regulation, and the control system. A control system IOC is built into the LLRF system to handle parameter and data collection.

3.9.3.3 Software Architecture

A major benefit of a digital RF feedback and feed-forward system is that it supports automated operation with minimal operator intervention. This is accomplished by deploying a number of algorithms to maintain best field stability (i.e. lowest possible rms amplitude and phase errors), to allow for fast trip recovery, and to support sophisticated exception handling. Beam-based feed-forward further improves the field stability. Figure 3.9-2 shows the basic functional diagram of the LLRF software system.
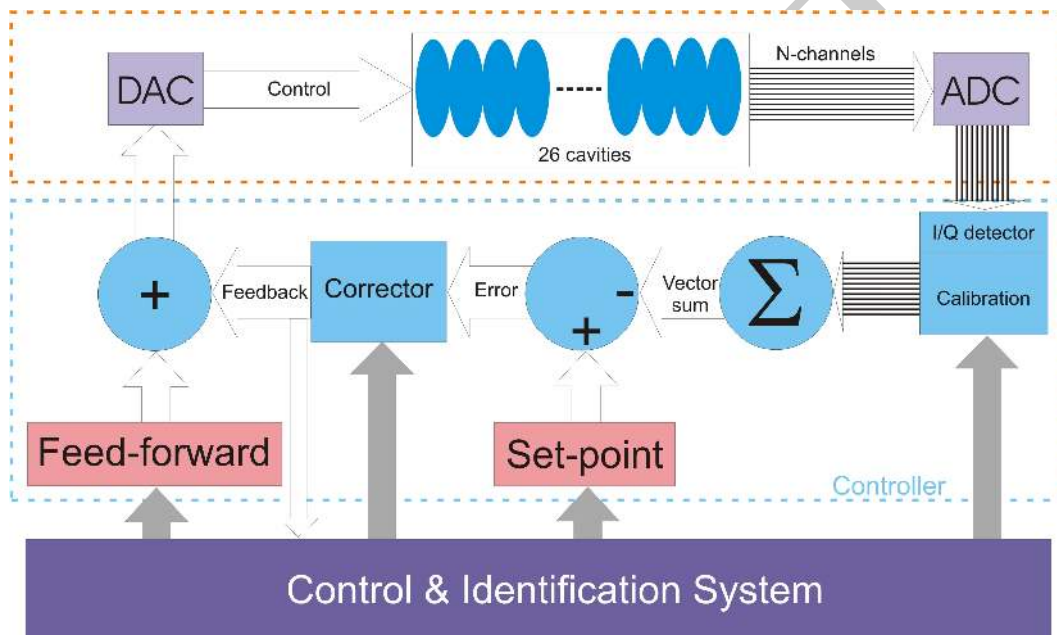
FIGURE 3.9-2. Basic functional diagram of the LLRF software system.

The software implementation of the RF control system must also support high availability. The main requirements for the algorithms are low latency for feedback, modularity to simplify interfacing, and support of a high degree of automation. Important applications include exception handling, built-in diagnostics and beam-based feedback.

subsubsectionSoftware Implementation

The massive parallel processing in the FPGAs provides low latency for the feedback algorithm. Complex algorithms requiring floating point calculations such as adaptive feed-forward can be also implemented.

The setting of system parameters and piezoelectric tuner control are implemented on floating point DSP processors since the latency requirements are not as stringent. Automated operation can also be implemented on a middle layer server CPU since the timing requirements are not as critical.

The distribution of the modular algorithms requires well-defined interfaces to ensure simplicity in performing trouble shooting, maintenance, and upgrades. Low latency links use in-house protocols while commercial protocols are available for links needing high bandwidth but not low latency.

System redundancy is achieved with algorithms, which calculate the key results from multiple signal sources. It is, for example, possible to calculate the cavity field from forward and reflected power although the measurement error is larger. Any discrepancy between the independently derived signals flags potential errors in hardware or algorithms.

Data storage is provided locally on most processor boards and is distributed to the central servers between pulses for further signal processing. With almost 15,000 cavities to control, automation is essential to ensure simplicity of operation and high availability. To support automation, the front-end hardware and software must as a minimum include the following features: field vector measurement, loop phase and loop gain, loaded Q and cavity detuning, beam phase and beam induced voltage, calibration of cavity field and phase, vector-sum calibration, calibration of forward and reflected wave, beam loading compensation (current and phase), klystron linearization, exception detection and handling, RMS field errors, warnings and alarms.

It is desirable to implement the algorithms as close a possible to the LLRF station controller to reduce network traffic. However, if the algorithms and applications are implemented in middle layer servers or as client applications, it can simplify the programming, facilitate later upgrades and improve maintainability.

3.9.4   Components

Table 3.9-2 gives a rough parts count for the components in the baseline LLRF system for a single RF unit in the main linac.

TABLE 3.9-2
Rough part count for the components in the baseline LLRF system for a single RF unit at the main linac.

Module	Specification	Quantity
Precision cable	1/2 Coax–low temp.coef.	94
Down converter	1300MHz to IF	95
ADC channel	14 bit, 65MHz or higher	95
FPGA & DSP	State of the art	3 to 10 each
DACs	16 bit, 100 MHz or higher	6

There are a total of 14,540 cavity modules in the main linacs, where 560 klystrons (i.e. 560 RF units) provide the drive power for 26 cavities each. The e^- source, e^+ source, RTMLs have 11, 39 and 36 RF units, respectively. The e^- and e^+ damping rings have 10 klystrons driving 36 superconducting cavity modules in total. Each of these cavity modules has three signals monitored by the LLRF, a cavity field probe, and a forward and reflected power signal. Each signal is routed in temperature-stabilized coaxial cable.

3.10   INSTRUMENTATION

3.10.1   Overview

To deliver high luminosity, the ILC must produce very low emittance beams in the damping rings, preserve that low emittance through more than 20 kilometers of beam transport, bunch compression and acceleration, to finally focus the beams to a few nanometers at the collision point. This requires extensive beam instrumentation with requirements at or often beyond the current state-of-the-art. Most of the beam instrumentation in the linac and beam delivery requires single-pass, bunch-by-bunch signal processing and data acquisition. The damping ring requires turn-by-turn or multi-turn measurements similar to modern storage rings. Beam instrumentation is a critical component of:

- diagnostic systems characterizing machine performance, beam properties and collision parameters,
- beam-based feedbacks,
- machine protection system.

The beam position monitors (BPM), beam profile monitoring systems and feedbacks are particularly challenging, and include devices based on RF cavities or lasers. In many cases, individual devices have been built that satisfy the minimal requirements, but these must be integrated into large, highly reliable systems to achieve the required levels of beam monitoring and control.

3.10.2   Technical Description

Instrumentation includes all direct *beam* monitors, e.g. beam position, profile, bunch length and bunch charge monitors, as well as beam feedbacks, but not general machine infrastructure monitoring systems such as RF control and protection interlocks, temperature and pressure monitors, flow meters, etc. Near the interaction point (IP), there is also specialized beam instrumentation, e.g. luminosity and background monitors, energy spectrometers and polarimeters, that is not within the scope of the instrumentation technical system.

In both physical and cost terms, the largest instrumentation systems are the beam position monitors (BPMs) and the laser-based beam profile monitors (*laser-wires*). The BPM systems consist of ∼4500 beam pickups of two basic types, i.e. resonant cavity-sytle and broadband button (or stripline) style, with associated analog front-end electronics, digital signal processing, and related infrastructure such as cables, power-supplies, racks, crates, etc., distributed along the beamlines. The laser-wires include 68 laser/beam Interaction Points, fed by 17 lasers with 29 Compton gamma detectors.

3.10.2.1   Beam Position Monitors

The beam position monitor systems in the ILC accelerator complex are the most essential and most extensive beam instrumentation tool. Four different types of beam position monitors (BPMs) are used throughout the ILC. Broadband BPMs of *stripline* or *button* style (Fig. 3.10-1, left) are used for applications requiring medium or lower resolution, ∼10-30 μm RMS (single bunch). Button pickups are used in the gun region, in the damping rings and in other space critical areas. Stripline pickups are used in most warm sections of the sources
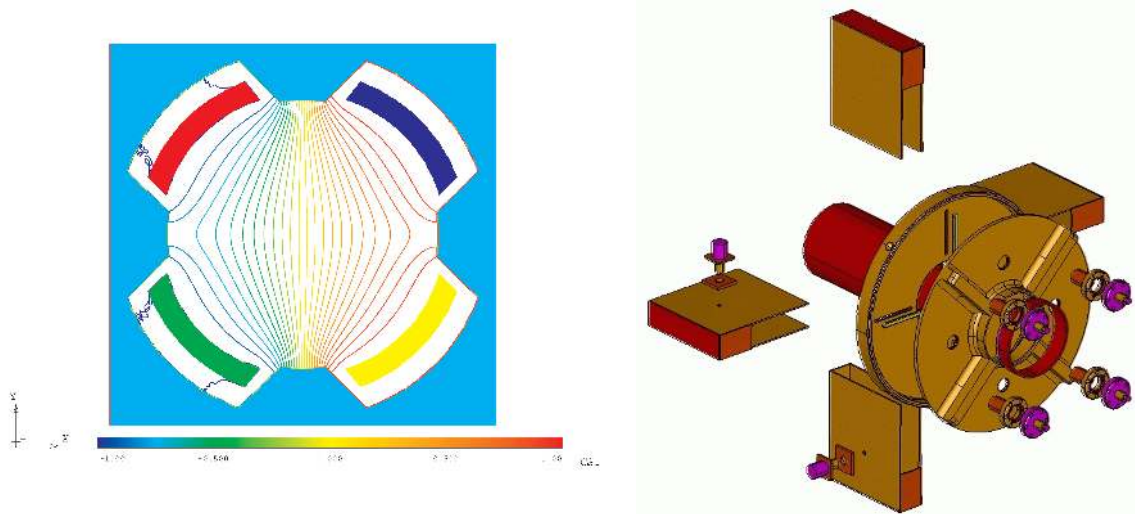
FIGURE 3.10-1. Broadband (left: hor. equipotentials of the ATF damping ring button BPM) and resonant BPM pickups (right: exploded view of the L-Band cavity BPM)

and in the BDS. Cavity BPMs are used for higher resolution applications, where few- or sub-micron RMS single-bunch resolution is required (see Table 3.10-2). Three different basic styles, C-Band, S-Band and L-Band, are used according to the needs of different beam pipe apertures. A "cold" version of the L-Band cavity BPM is used in the cryostats of the Main Linacs, RTMLs and Sources (Fig. 3.10-1, right). "Warm" cavity BPMs of all styles are used thoughout the ILC accelerator complex downstream of the damping rings.

Except for the damping rings, all BPM systems are designed to be able to provide the beam position of each bunch in the macropulse (bunch-by-bunch). This requires a measurement or integration time smaller than the bunch-by-bunch time spacing (369 ns, nominal) for all BPM system components. The damping ring BPMs have to time resolve the beam position on a turn-by-turn basis ($t_{rev} \sim 20\ \mu s$) or measure in a narrow-band (BW ~ 1 kHz) averaging mode. A common set of readout, timing and auxiliary hardware and software is used for all BPMs, apart from the RF analog signal processing front-end section. This minimizes cost, and simplifies commissioning, maintenance and troubleshooting. A beam position monitor consists of:

- A pickup detector, which detects the beam's electromagnetic field and converts it to an electrical signal, usually in the range of RF or microwave frequencies.
- A set of analog and digital read-out electronics, which processes the pickup signals to extract the required beam displacement information.
- Trigger and timing hardware to time-resolve position data for individual bunches or turns.
- A system for calibration and self-diagnosis tests.
- Digital data acquisition and control hardware and software, including a control system interface.
- Auxiliary systems and components (racks, crates, power supplies, cables, etc.).

There are a variety of R&D activities for ILC BPMs at the laboratories, mostly including university collaboration. Warm cavity BPMs studied under ILC-like beam conditions (nanoBPM collaboration) at the KEK Accelerator Test Facility (ATF) have achieved a

single-bunch position resolution of ∼20 nm. The ATF damping ring is also developing high resolution BPMs based on a digital receiver readout system [127]. The DESY FLASH linac has a variety of button and stripline-BPMs, and uses RF-signals from the HOM-couplers of the accelerating structures for beam position and alignment studies (HOM collaboration) [128]. S-Band cavity BPMs tested in SLAC "End Station A" (ESA) achieved a single bunch resolution well below 1 μm [129]. A "cold" L-Band cavity-BPM for use in the cryomodule is being built at FNAL using a read-out digitizer based on the high availability ATCA standard [130].

3.10.2.2 Beam Profile Monitors
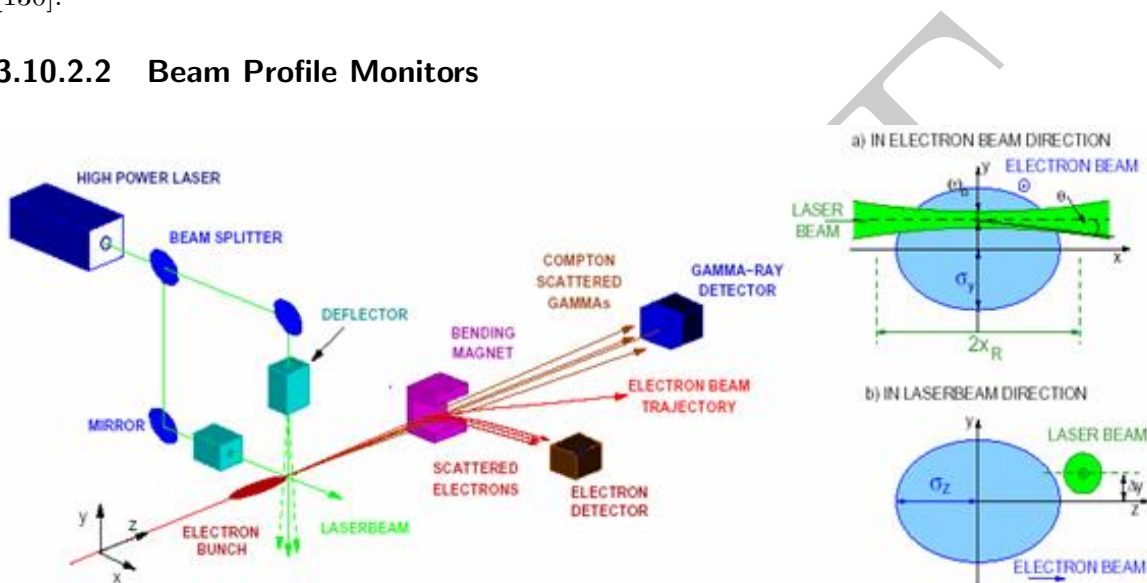
FIGURE 3.10-2. Schematic of a laser-wire beam profile monitor

A variety of beam profile monitors are used throughout the ILC. Conventional wire scanners are used for beam transverse emittance measurements in upstream low-energy sections, i.e. the electron and positron sources. However, in the damping rings and downstream areas of the machine the low emittance beam would destroy any conventional wire scanner. In these areas laser-wires must be used for any measurements of the beams transverse dimensions.

The laser-wire (Fig. 3.10-2) operates by scanning a finely focussed beam of laser light across the electron/positron bunches. The resulting rate of Compton scattered photons is measured in a downstream detector, as a function of relative position of laser and beam. The laser-wire is a relatively non-invasive device and can be used to measure the beam properties continuously during ILC operations. Prototype laser-wire systems are being developed at PETRA [131] and ATF [132] [133]. In the latter case the key R&D challenge is to push the spatial resolution to the micron level, as required for ILC.

Other optical beam monitors are used to analyze transverse and longitudinal beam parameters, and beam energy. There are OTR (optical transition radiation) and OTRI (OTR interferometer) screen monitors for beam emittance and energy measurements in the sources, RTML and BDS. Screen monitors are also used in other ways (e.g. YaG, slits, etc.) X-ray synchrotron light monitors are used for transverse and longitudinal beam imaging in the positron source, damping rings, RTML and BDS. In the damping rings they can image the 3D parameters of a bunch on a turn-by-turn basis (as done at LEP). Other optical-based

beam monitor systems, currently not in the RDR baseline, may be required (e.g. bunch length measurements based on elecro-optical sampling (EOS), optical diffraction radiation (ODR) monitors, interferometers, etc.). As these are lower cost single system installations, they would not affect significantly the overall instrumentation costs and requirements.

3.10.2.3   Bunch Length Monitors

The electron and positron sources and RTMLs have Deflecting Mode Cavity (DMC) or *LOLA* [134] structures, based on normal-conducting technology to measure bunch length and longitudinal charge distribution. A pair of DMCs based on superconducting technology are located near the crab-cavity bunch rotation system just upstream of the IP. Streak cameras are used for beam imaging in the damping rings.

3.10.2.4   Beam Current Monitors

There are a variety of beam current monitors used to measure the bunch charge, including toroids, wall current monitors (WCM), Faraday cups and DC Current Transformers (DCCT). The WCM and Faraday cups are located in the sources, and the DCCTs in the damping rings. These monitors measure the charge of every bunch in the macro pulse. Like the BPMs, the measurement time has to be < 369 ns to time resolve the charge of individual bunches. Monitors with higher bandwidth are required in the damping rings where the bunch-to-bunch spacing is 6 ns. Synchronized bunch charge measurements also quantify the injection/ejection efficiency to/from the damping rings, and are used to detect beam losses as part of the machine protection system (MPS). For luminosity monitoring, a high precision bunch charge measurement is required in both Beam Delivery Systems. All of these devices are commonly available and require little or no R&D.

Toroids are the simplest and most reliable detector for bunch charge measurements, with medium to high bandwidth (100...1000 MHz), and a cut-off frequency as low as 10 Hz. Toroids for accelerator applications are offered by several smaller companies but are also developed in-house at some laboratories (eg. DESY, CERN).

Faraday cups are used in the electron source at the end of the low-energy spectrometer and in the gun region. As they physically collect the particles, they have a very high sensitivity and can also be used for dark current investigations. The bandwidth is sufficient to resolve the charge of individual bunches.

The wall current monitor (WCM) is a broadband beam current / bunch charge monitor which offers very high bandwidth (typically 5-10 GHz). It is used in the electron and positron sources as an excellent source of bunch timing signals and as a diagnostic for issues in the timing and trigger distribution system, e.g. filled neighbor buckets (parasitic bunches), time-of-flight measurements, etc.

A DCCT monitor in each damping ring measures the DC beam current component with high resolution. The system can also serve for diagnostic purposes and machine development studies, e.g. beam lifetime studies.

3.10.2.5   Beam Phase Monitors

Beam phase monitors are used in the electron and positron sources, RTMLs and BDS. The precise measurement of the phase or time of the bunch center (or the average of all bunches)

with respect to the 1.3 GHz RF-drive signal, is crucial for successful ILC operation (see Section 3.9). The beam phase can be used to diagnose numerous machine performance issues, such as unwanted signal content generated in the different sections of the RF sources and distribution (noise, jitter, wrong set points, problems in feedback, feed-forward or state machine systems), problems in the related auxiliary systems (water cooling, power distribution), in the accelerating cavities (slow tuners, Lorenz force compensation), and finally issues driven by the beam itself (beam loading, wakefields). The resolution requirements for a beam phase monitor ranges from 0.1-0.01° of 1.3 GHz (equivalent to ~200-20 fs). In many instances, an average beam phase measurement is sufficient, but in some cases, a bunch-by-bunch beam phase gives additional, valuable information. Two or more broadband detectors can provide a time-of-flight (TOF) measurement of particular interest in the bunch compressors. DESY is currently developing two beam phase measurement methods, relevant for ILC.

- A broadband, bunch-by-bunch beam phase and TOF measurement system is based on an electrical pickup (similar to a button BPM) read-out by an optical Terahertz sampler. Beam tests show a bunch-by-bunch resolution of 30 fs RMS. This method is used in several locations in the sources, RTML and BDS areas of the ILC.

- A broadband read-out (oscilloscope based) of the HOM signals is used for a high resolution (0.08 degree RMS, equivalent 170 fs) measurement of the beam phase, by comparing the signal of the RF-driven fundamental TM010 mode (1.3 GHz) with the beam-driven first higher monopole mode TM011 mode. This technique is used in the RF cryomodules to measure the average beam phase of all bunches.

3.10.2.6 Beam Loss Monitors

Two types of beam loss monitors are used throughout the entire machine complex. Long ion-chambers (LION) run along the tunnel sections and photo-multiplier tube (PMT) based beam loss monitors are attached to scintillation paddles or aluminum foils. Both systems are used for machine commissioning and for the machine protection system (MPS). A reliable detection of low beam losses <0.01 % of the total beam intensity is required, along with good calibration and linearity.

3.10.2.7 Beam Feedback Systems

Beam based feedback systems stabilize the beam current, energy and trajectory throughout the machine. There are slow, pulse-to-pulse (5 Hz), and bunch-to-bunch (intra-train) feedbacks. Only beam-based feedback systems are discussed here, all of which employ instrumentation such as beam position monitors (BPMs) and fast kickers. Other feedback and feed-forward systems (including non-beam based), such as adaptive LLRF control loops, cavity temperature control, etc. are covered elsewhere. A partial list of feedback loops is given in Table 3.10-1.

Damping ring orbit stability requirements are similar to those for existing storage rings such as B factories and synchrotron light sources. Orbit feedback based on a response matrix method takes position measurements from multiple BPMs around the ring, and corrects the orbit with multiple distributed correctors, using algorithms and technology that are well established.

A turnaround in the Ring to Main Linac (RTML) allows bunch-by-bunch trajectory measurements to be fed forward over a shorter path length to two fast correctors/kickers per

TABLE 3.10-1
Partial list of feedback loops.

Damping Ring	
Injection and extraction trajectory control	5 Hz
Dynamic orbit control	10-20 KHz
Bunch-by-bunch transverse feedback	
Ring to Main Linac	
Pre- and post-turnaround emittance correction	5 Hz
Turnaround trajectory feed-forward	bunch-by-bunch
Beam energy at bunch compressor	two stages
Main Linac	
Trajectory Feedback (several cascaded loops)	5 Hz
Dispersion measurement and control	
Beam energy (several cascaded sections)	5 Hz
End of linac trajectory control	bunch-by-bunch
Positron Source	
Beam energy at undulator	5 Hz
Beam Delivery System	
Trajectory feedback	5 Hz
Interaction Point collision feedbacks	5 Hz and bunch-by-bunch

plane, separated by 90 degree phase advance. Processing time is critical as the turnaround length is only 170 m, which allows less than 0.5 μsec to measure, process, and apply the kick angle correction.

All trajectory feedback, except the RTML feed-forward, has the same basic elements, the same algorithm, and similar or identical hardware. The algorithm is based on response matrices, but most of the trajectory correction loops operate synchronously at the 5 Hz ILC pulse rate. BPM measurements are processed locally, and read by the middle-ware layer of the control system, which then calculates corrector magnet settings for the subsequent ILC pulse, and distributes the corrector setpoints synchronously.

Several cascaded feedback loops provide position and energy control in the sources, bunch compressor, main linac, and beam delivery system. In addition to the trajectory feedback, two BPMs in each section are used to measure beam energy and provide local feedback using klystron phase/amplitude control. There is a 5 Hz BDS trajectory feedback system that may be cascaded with the linac 5 Hz systems, and/or augmented with feed-forward information from upstream in the machine (i.e. from the linacs and/or the damping rings). In addition, there is a 5 Hz interaction-point (IP) feedback system. All of these systems will use similar hardware software based on state space analysis and adaptive feedback algorithms.

For collision optimization, and luminosity stabilization, there is an intra-train (bunch-to-bunch) feedback system at the IP. A BPM sensor several meters downstream of the IP measures the position of the outgoing bunches, and a kicker several meters upstream of the

IP corrects the incoming bunches. Such a system can *lock in* within ∼100 bunch crossings to achieve roughly 80% of the luminosity attainable if the beams were in perfect collision. Additional upstream BPM-kicker sets provide angle correction. An intra-train position/angle scan(s) is used to optimize a bunch-by-bunch luminosity signal from the detector. Inputs to the feedbacks from additional diagnostics such as beam charge, transverse size, and bunch length monitors allow adaptive gain control as collision conditions change.

3.10.3 Technical Issues

3.10.3.1 Feedback Hardware

The relatively low correction rates and the distributed nature of many of the monitors and actuators make it possible to implement the 5 Hz feedback in the integrated controls infrastructure without requiring dedicated hardware and interfaces. Dedicated local systems are required for intra-bunch feedback systems that must operate at the bunch rate of ∼3 MHz, such as the RTML turnaround trajectory feed-forward control, and intra-bunch trajectory control at the IP. In addition, a fast synchronous infrastructure will allow implementation of delayed bunch-to-bunch feedback/feed-forward along the length of the linac.

Modern storage rings have refined orbit correction systems to the level likely required for the ILC damping ring. Ongoing advances in digital processor performance and fast high performance analog to digital conversion chips has allowed the conversion from the analog to digital domains to be performed much earlier in the signal chain. Most challenging are systematic effects in beam position monitoring when required resolutions are at or below the few micron level.

Fast intra-bunch trajectory control for the IP is presently being developed by the FONT collaboration, with the latest implementation being (FONT-4) [135] aiming to demonstrate feedback with 100 ns latency in the electronics, and stabilization at μm level.

3.10.3.2 Layout

A generalized schematic of an Instrumentation system is shown in Fig. 3.10-3. While the pickup monitors of the beam instruments are located in the accelerator tunnel (in most cases they are part of the vacuum system), the read-out electronics are typically installed in an accessible service tunnel or in service buildings. Pickup stations and electronics are connected by cables through the penetrations between the parallel tunnels. Most of the signal processing is done in the digital domain, if applicable. Standardized, common hardware (e.g. ATCA, VME) is used over the entire system complex. Data management, collection and distribution are part of the Control system. Auxiliary systems for trigger and clock signals (timing), AC power and cooling and the infrastructure for racks, crates, cabling, etc. are required.

3.10.4 Table of Components

3.10.5 Cost Estimation Methodology

For beam monitors the Instrumentation cost estimation covers:

- all pickup stations, as part of the vacuum system;
- scintillators, PMTs, laser systems, calibration systems;
- RF systems and infrastructure for the DMC-based bunch length monitors;
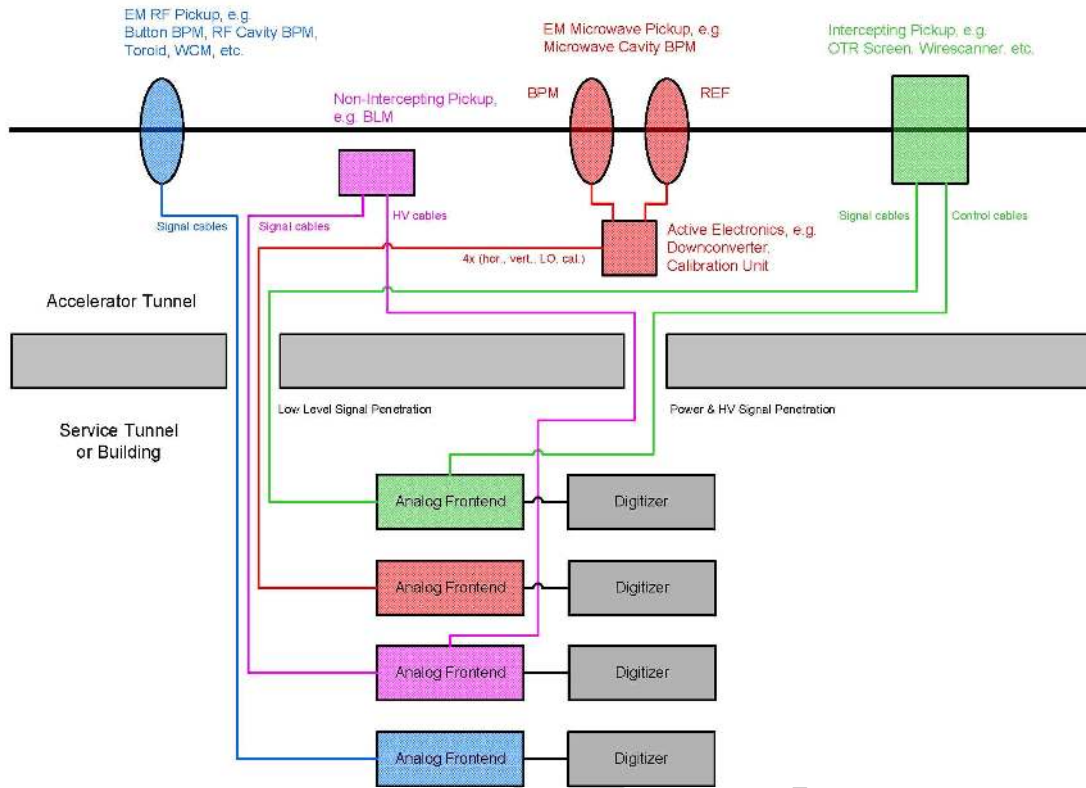
FIGURE 3.10-3. Generalised Schematic of Beam Pickups and Read-Out Systems

- associated motors, switches, and mechanical set-up;
- signal and control cables, connectors, patch-cables, etc.;
- dedicated read-out electronics (analog & digital), control units, local timing electronics, calibration electronics, local software and firmware.

Except for special cases, e.g. certain feedback systems, data acquisition infrastructure is covered by the control system cost estimation. Controls includes global trigger and clock signals, global electronics infrastructure (racks, crates, power supplies, cabling), global communication and data acquisition hardware, firmware and software.

For costing purposes, instrumentation was classified into 17 different *systems*. Core cost and manpower information was estimated for each individual component of an instrumentation system and its subcomponents, including the cost reductions due to volume or/and technology advances. Counts for each type of instrumentation were supplied by the Area Systems. No spares were included. Counts of control racks required for data acquisition were generated form the above data. Labor information (in person years) was estimated separately for Prototyping, Testing and Installation. The Installation labor was then incorporated into the Installation estimate and not included in Instrumentation.

TABLE 3.10-2
Counts of Beam Instrumentation System Installations in the ILC Accelerator Complex (along with some basic requirements). (The BPMs and the laser-wires are the cost-drivers)

INSTRUMENT requirements (e.g. resolution)	AREA						
	e⁻ source	e⁺ source	DR	RTML	ML	BDS
Button/stripline BPM	69	400	2 × 747			
resolution (μm)	10-30	10-30	<0.5			
C-Band Cavity BPM (warm)		109		2 × 649		262
resolution (μm)		<0.1-0.5		<0.1-0.5		<0.1-0.5
S-Band Cavity BPM (warm)						14
resolution (μm)						< 0.1-0.5
L-Band Cavity BPM (warm)				2 × 27		42
resolution (μm)				<1-5		<1-5
L-Band Cavity BPM (cold)				2 × 28	2 × 280	
resolution (μm)				~0.5-2	~0.5-2	
Laser-wire IP	8	20	2 × 1	2 × 12	2 × 3	8
resolution (μm)	<0.5-5	<0.5-5	<0.5-5	<0.5-5	<0.5-5	<0.5-5
Wirescanner	12	8				
Optical Monitors	6	17	2 × 2	2 × 8		11
DMC	3	4		2 × 2		2 (cold)
Beam Current Monitors	7	11	2 × 1	2 × 2	2 × 3	11
resolution ΔE ~0.1% / s_z ~100 μm						
Beam Phase Monitor	4	2		2 × 3		2
BLM (PMT/IC)	60/2	400/20	2 × 40/4	2 × 25/2	2 × 325/10	100/10
Feedback System	5	10	2 × 2	2 × 1	2 × 10	12

3.11 DUMPS, COLLIMATORS, AND STOPPERS

3.11.1 Overview

The ILC requires a total of 26 beam dumps, each of which must be capable of absorbing its rated beam power indefinitely without failing. Most of these dumps are used primarily during personnel access, during invasive beam tuning, or as locations where the beam can be extracted in the event of a machine protection system (MPS) fault. There are also 2 main beam dumps near the interaction point and 1 photon dump in the positron source which are used during normal luminosity delivery. Almost all of the dumps require water cooling.

In addition to the dumps, there are 25 beam stoppers in the ILC. These stoppers are never intended to see beam during normal operation, but are only used as backups to other devices and/or systems which are expected to contain the beam power. The stoppers are thus designed as sacrificial devices, which are expected to be damaged if struck by the beam. Their failure then cause a beam abort. Stoppers are used as part of the Personnel Protection System (PPS) as well as MPS.

The ILC collimators are required to absorb a fixed fraction of the beam power indefinitely without failing. In general, this fraction is between 0.1% and a few percent. The collimators are used to reduce detector backgrounds, to protect downstream devices and apertures from damage, and to limit radiation deposition and activation to specific regions of the beamline, which can then be shielded locally. The ILC has 113 collimators with adjustable apertures and 85 collimators with fixed apertures.

3.11.2 Technical Description

The design of each beam dump, collimator or stopper is determined by the peak incident power, power density, beam energy, and particle type. Electron and positron beam dumps and collimation devices that absorb from 0-25 W of power can be made of uncooled metal; this category of devices includes the abort dumps in the damping rings, which are only used in the event of a hardware failure in the rings themselves, and the faraday cups at each electron source. Devices which are required to absorb from 25 W to 40 kW can also be made of metal, with peripheral cooling that is provided by the facility's low conductivity water (LCW) system; this category of devices includes the low-power tune-up dumps in the BDS, and the full power dumps at low-energy (100-400 MeV) locations in the electron and positron sources. For beam power in the range of 40 kW to 600 kW, the dump contains aluminum balls immersed in water; this category of devices includes the tune-up dumps at the 5 GeV end of the electron and positron sources, the tune-up dumps in the RTML, and the tune-up dump in the positron production undulator hall. Beam power above 600 kW requires water as the absorbing medium; this category of devices includes the main beam dumps and the tune-up dumps in the BDS. The photon dump downstream of the positron production undulator is also a pure-water dump.

The ILC collimation system includes devices with fixed apertures and devices which are adjustable, either in one plane or in two. There are 6 fixed-aperture collimators in the post-collision extraction lines which require water-cooled aluminum balls as their primary absorber; the remainder of the collimators are solid metal with peripheral cooling. In many locations, a thin (0.6-1.0 X_0) collimator (or "spoiler") is placed in front of a thick ($> 20\ X_0$) collimator (or "absorber"); if the primary beam leaves the collimation acceptance, the spoiler

expands the beam size via multiple Coulomb scattering to reduce the power density on the absorber. This approach is used to improve the survivability of collimators in some locations, most notably the collimators downstream of the damping ring and upstream of the final focus.

Beam stoppers that are part of the ILC Personnel Protection System (PPS) are low power devices that self-destruct when struck by the beam, such that the loss of beamline vacuum causes the beam to be shut off; they are inserted into the beam path during access periods as insurance against the failure of the primary beamline components that protect the area under access. Beam stoppers that are part of the ILC Machine Protection System (MPS) have fixed or adjustable apertures; if the beam violates the defined aperture their burn through monitors protect the remainder of the beamline by spoiling the vacuum and shutting down the beam.

For dumps and absorbers that bring water into direct contact with ionizing radiation, underground plumbing must be provided to safely remove or contain the radiolytically evolved gases or isotopes while providing adequate cooling. All dumps and collimators require local steel and concrete shielding to protect equipment and personnel from residual radiation from the activated devices. If the site chosen for the ILC tunnels is not dry, additional shielding to protect ground water from tritium activation will be required.

3.11.3   Technical Issues

3.11.3.1   18 MW Beam Dumps

The four linac tune-up and main beam dumps are sized for a peak power at nominal 1 TeV beam parameters of 18 MW. These dumps (Figure 3.11-1) consist of 1.5 m diameter cylindrical stainless steel high pressure water vessels with a 30 cm-diameter 1 mm-thick Ti window; they, their shielding and associated water systems represent most of the cost of the Beam Delivery System dumps and collimators. The design is based on the SLAC 2.2 MW water dump [136][137] that has been used without problems for over 40 years.

The dumps absorb the energy of the electromagnetic shower cascade in 6.5 m (18 X_0) of water followed by 1 m of water cooled Cu plates (22 X_0). Each dump incorporates a beam sweeping magnet system to move the charged beam spot in a circular arc of 3 cm radius during the passage of the 1 ms long bunch train. Each dump operates at 10 bar pressure and also incorporates a vortex-flow system to keep the water moving across the beam at 1.0-1.5 m/s. In normal operation with 250 GeV beam energy, the combination of the water velocity and the beam sweepers limits the water temperature rise during a bunch train to 40°C. The pressurization raises the boiling temperature of the dump water; in the event of a failure of the sweeper, the dump can absorb up to 250 bunches without boiling the dump water. The power which is absorbed in the dump is finally removed by a heat exchanger system with a capacity of 2300 gallons per minute.

The integrity of the dump body and dump window, the management of radionuclides, the processing of the radiolytically evolved hydrogen and oxygen, and containment of the activated water are important issues for the 18 MW dumps.

3.11.3.1.1   Mechanical Failure of Dump or Dump Window   The main vessel is welded using low carbon stainless steel (316L) and all welds radiographed to ensure quality; the 10 atmosphere radioactive water cooling system is closed but communicates with the atmosphere via a small diameter tube from the gas space on top of the surge tank to avoid it being

FIGURE 3.11-1. Schematic of the 18MW water dump

classified as a nuclear pressure vessel. Several materials are under consideration for use in the dump window: 316L stainless, Ti-6Al-4V, and Inconel (A601,718,X750). All of these materials have been extensively used in nuclear reactors; their mechanical properties, thermal properties, and reaction to radiation damage have been thoroughly studied. As described above, the bunches in each train are swept in a circle to further reduce the thermal stress and radiation damage to the dump windows; the windows also have additional water cooling from multiple water jets in a separate cooling loop from the main vessel. Each dump incorporates a remote controlled mechanism for exchanging the highly activated windows on a regular schedule driven by integrated specific dose, along with local temporary storage for all tritiated water. As a final backup to guarantee environmental safety in the event of a failure of the dump body or dump window, the dump enclosure is air tight and incorporates adequate sump volume and air drying capacity to prevent the release of tritiated water even in the case of catastrophic dump failure. Since a failure of the window could create a catastrophic water-to-vacuum leak with highly radioactive tritated water, a pre-window, with peripheral and gas cooling, isolates the beamline vacuum system and provide secondary containment. Storage space for a damaged dump and a removable cavern wall are provided for dump replacement.

3.11.3.1.2 Water Activation Products   Activation products are primarily the result of photo-spallation on ^{16}O, primarily ^{15}O, ^{13}N, ^{11}C, ^{7}Be and ^{3}H (tritium). The first three radionuclides have short half lives and decay after ~ 3 hours. ^{7}Be is removed from the system by filtering it out in a mixed bed ion exchange column located in the dump support cavern. Tritium, a ~ 20 keV emitter with a half life of 12.3 years builds up in the water to some equilibrium level; the tritium is contained by the integrity of the dump system and the backup measures described in the preceding section.

3.11.3.1.3 Radiolysis and Hydrogen and Oxygen Evolution   Hydrogen is produced via the reaction $H_2O \rightarrow H_2 + H_2O_2$ at the rate of 0.3 l/MW-s, or 5.4 l/s at 18 MW beam power. The lower explosive limit (LEL) of hydrogen in air is $\sim 4\%$. Experience at SLAC [138] indicates that a catalyst consisting of a high-nickel stainless steel ribbon coated with platinum and palladium, in the form of a 46 cm diameter 6.4 cm thick mat, will reduce the H_2 concentration to the 25% of the LEL in one pass. Other types of higher density catalyst are also available. The gases released in a surge tank are heated to 65° C and are pumped through the catalyst, which does not need replacement or servicing.

3.11.3.1.4 Shielding and Protection of Site Ground Water   Assuming a dry rock site, as in the baseline configuration, 50 cm of iron and 150 cm of concrete shielding are needed between the dump and other areas of the tunnel enclosure to protect equipment from radiation damage. If the chosen site is not dry, the area surrounding the dump must be enveloped by an additional 2 m thick envelope of concrete to prevent tritium production in the ground water.

3.11.3.2 Undulator Photon Dump

The dump that absorbs non-interacting undulator photons from the positron production target must absorb 300 kW continuously. The photon energy spectrum spans the range 0-140 MeV, with an average energy of 10 MeV; 300 kW corresponds to 1.9×10^{17} photons/sec. The photons are transported 500 m to the rapidly rotating 1.4 mm Ti positron production target and then 150 m to a stationary dump. The important issues are the energy density and temperature rise in the dump window and in the body of the dump absorber. The cross section of the photons is such that aluminum balls cannot be used despite the relatively low total power; the primary absorber in this case must be water. With the current undulator-dump separation the power density on a 1 mm Ti window is 0.5 kW/cm² and the resultant temperature rise after the passage of one bunch train is 425° C. This is to be compared with a limit of 2 kW/cm² and a fracture temperature of 700° C. In the core of the beam the rise in the water temperature would be 190° C. With this geometry a compact (10 cm diameter by 100 cm long) pressurized (12 bar) water vessel and Ti window, with a radioactive water processing system, is required. Lengthening the target to dump distance by several hundred meters would result in a less technically challenging and less expensive system, but with the added expense of boring a longer hole for the undulator photon transport.

3.11.3.3 Aluminum Ball Dumps

The water-cooled aluminum ball dump [139] consists of a 40 cm diameter by 250 cm long stainless vessel which is filled with 10 mm aluminum balls and water. The water is circulating with a flow rate of approximately 30 gallons per minute. The dump is backed up by a short length of peripherally-cooled solid copper. The aluminum ball dumps have technical issues which are qualitatively similar to some of those of the all-water main dumps: generation of hydrogen and oxygen, activation of the water, and local shielding. Because of the much lower power levels and the use of aluminum as the main absorbers, all of these issues are much less severe.

3.11.3.4   Stoppers and Collimators

The stoppers and collimators are largely based on well-understood designs in regular use at accelerator laboratories all over the world. The technical issues in these devices are not considered important, with two exceptions.

The first exception is the collimators in the extraction lines, which use water-cooled aluminum balls to absorb the beam power. This system has similar issues to the main dumps in terms of activation and risks of water-to-vacuum leaks, although on a much smaller scale. These collimators share the radioactive water system of the nearby main dumps.

The other exception is limiting the deleterious effects of wakefields in the collimators, in particular the geometric wakes of the short spoilers and the resistive-wall wakes of the long absorbers. The wakes are limited by the use of copper coatings on all surfaces in the vacuum system, and by longitudinal tapering of the apertures to limit geometric wakes.

3.11.4   Cost Estimation

The systems that put water into direct contact with the beam dominate the cost estimate of this technical system. For the main 18 MW dumps, the cost estimate is based on industrial studies [140] [141] by two German companies expert in nuclear reactor technology. Their estimates have been examined by the staff responsible for the ISIS neutron spallation target and adjusted, for example, to add the costs of the remote controlled window replacement system and air drying systems. For the aluminum ball dumps that do not operate at high pressure, the cost of the 2006 ISIS target cooling system was used as the basis of estimate.

Items with peripheral cooling supplied by the tunnel low conductivity water (LCW) system have only mechanical design and construction costs. Whether for collimators or solid dumps, these costs are estimated based on the production costs of similar devices in use at SLAC.

3.11.5   Table of Components

TABLE 3.11-1
Dump types and locations

Item	#	Locations
Beam Dumps		
10 MW 10 atm water	4	Ends of linacs and BDS dumplines
300 kW undulator photon	1	Behind positron production target
250 kW aluminum ball	9	DR injectors (2) RTML (6) positron production undulator chicane (1)
Fixed 10 kW solid metal, peripherally cooled	6	100 MeV points in e- sources (2), 114 and 400 MeV points in e+ sources (4)
Insertable low power tuning dumps	2	Final focus
Faraday cups	2	Electron guns
Uncooled aluminum blocks	2	DR abort dumps
Adjustable Aperture Collimators		
Short 2 jaw (H,V) tapered uncooled beam spoilers	60	RTML (36) BDS Collimation (24)
Long 2 jaw (H,V) cooled beam absorbers	43	BDS Collimation (32) BDS FF SR masks (4) Electron sources (2) Positron 5 GeV point (5)
Short 2 jaw uncooled collimator	10	Positron sources
Fixed Aperture Protection Collimators		
30 cm cooled solid metal with circular aperture	74	RTML (52) BDS (22)
High power water cooled aluminum balls	6	BDS extraction lines
Single jaw cooled device	2	BDS collimation
Uncooled block with rectangular aperture	2	BDS Crab Cavities
Photon collimator	1	Undulator / positron source
Beam Stops with Burn Through Monitors		
PPS stoppers	14	Positron source (2) RTML (6) BDS(6)
Fixed aperture MPS Stoppers	9	Positron source (3) BDS (6)
Variable aperture MPS	2	BDS Tuneup Dump Line

3.12   CONTROL SYSTEM

3.12.1   Overview

Rapid advances in electronics and computing technology in recent decades have had a profound effect on the performance and implementation of accelerator control systems. These advances will continue through the time of ILC construction, when network and computing capabilities will far surpass that of equipment available today. Nevertheless, a machine of the scope of an ILC presents some unique control system challenges independent of technology, and it is important to begin the process of determining functional requirements for the ILC control system.

This chapter discusses the control system requirements for the ILC, and describes a functional and physical model for the system. In several places implementation details are described, but this has been done largely as a means to describe representative technologies, and in particular, to establish a costing model. Regardless of the final technology implementation, the control system model described in this chapter contains a number of architectural choices that are likely to survive.

3.12.2   Requirements and Technical Challenges

The broad-scope functional requirements of the ILC control system are largely similar to those of other modern accelerator control systems, including control and monitoring of accelerator technical systems, remote diagnostics, troubleshooting, data archiving, machine configuration, and timing and synchronization. However, several features of the ILC accelerator push implementation beyond the present state of the art. These are described below.

3.12.2.1   Scalability

The ILC has an order of magnitude more technical system devices than other accelerators to date. The primary challenges of scalability in relation to existing accelerator control systems are the physical distances across the accelerator, the large number of components and number of network connections, and the implied network bandwidth. Real-time access to control system parameters must be available throughout the site, and by remote access. These challenges are also present in the commercial domain, notably in telecommunication applications, and lessons learned there are almost certainly applicable to the ILC control system.

3.12.2.2   High Availability

Requirements for high availability drive many aspects of the ILC control system design and implementation. These requirements were derived from accelerator-wide availability simulations. The control system as a whole is allocated a 2500 hour MTBF and 5 hour MTTR (15 hours downtime per year). This translates to control system availability between 99% and 99.9% (2-nines and 3-nines). A detailed analysis of how control system availability relates to beam availability is complicated. However, a coarse analysis shows that if the control system comprises some 1200 controls shelves (electronics crates), then each shelf must be capable of providing 99.999% (5-nines) availability. Such availability is routinely implemented

in modern telecom switches and computer servers, but has not been a requirement of present accelerator control systems.

3.12.2.3 Support extensive automation and beam-based feedback

A very complex series of operations is required to produce the beams and deliver them to the collision point with the required emittance. The control system must provide functionality to automate this process. This includes both getting beam through the entire chain and also tune-up procedures to maximize the luminosity. Beam-based feedback loops are required to compensate for instabilities and time-dependent drifts in order to maintain stable performance. Inter-pulse feedback should be supported in the control system architecture to minimize development of custom hardware and communication links. The automation architecture should have some built-in flexibility so procedures can easily be changed and feedback loops added or modified as needed. Automation and feedback procedures should incorporate online accelerator models where appropriate.

3.12.2.4 Synchronous Control System Operation

The ILC is a pulsed machine operating at a nominal rate of 5 Hz. Sequences of timing events must be distributed throughout the complex to trigger various devices to get beam through the accelerator chain. These events are also used to trigger acquisition of beam instrumentation and other hardware diagnostic information so that all data across the machine can be properly correlated for each pulse.

3.12.2.5 Precision RF Phase Reference Distribution

The control system must generate and distribute RF phase references and timing fiducials with stability and precision consistent with the RF system requirements.

3.12.2.6 Standards and Standardization, Quality Assurance

A critical aspect of implementing a high availability control system will be the use of consistent ("best") work practices and a level of quality assurance process that is unprecedented in the accelerator controls environment. Additional technical solutions to HA will rely on this foundation of work practices and quality assurance processes. Commercial standards should be used wherever they can meet the requirements, for such things as hardware packaging and communication networks.

The control system must specify standard interfaces between internal components and to all other systems. This makes integration, testing, and software development easier and more reliable. Standard interfaces allow parts of the system to be more easily upgraded if required for either improved performance or to replace obsolete technologies.

3.12.2.7 Requirements on Technical Equipment

Technical equipment comprises field hardware such as power supply controllers, vacuum equipment, beam instrumentation, and motion control devices. These systems are the responsibility of the technical groups. However, they must interface to the control system in a coherent way to allow equipment to be accessed via a common interface for application

programming, data archiving, and alarms. In order to meet the very stringent requirements for overall system reliability, as well as provide for more efficient R&D and long-term maintenance, standards must be applied to the technical equipment for packaging, field bus, communication protocol, cabling, and power distribution.

3.12.2.8 Diagnostic Interlock Layer

A Diagnostic Interlock Layer complements normal self-protection mechanisms built into technical equipment. The DIL utilizes information from diagnostic functions within the technical equipment to monitor the health of the equipment and identify anomalous behavior indicative of impending problems. Where possible, corrective action is taken, such as pre-emptive load balancing with redundant spares, to avert or postpone the fault before internal protective mechanisms trip off the equipment.

3.12.3 Impact of Requirements on the Control System Model

In order to meet the high availability requirements of the ILC, a rigorous failure mode analysis must be carried out in order to identify the significant contributors to control system downtime. Once identified, many well-known techniques can be brought to bear at different levels in the system, as well as system wide, and at different time scales (i.e. bunch-to-bunch, macro pulse, process control) to increase availability. The techniques begin with relatively straightforward, inexpensive practices that can have a substantial impact on availability. A careful evaluation and selection of individual components such as connectors, processors, and chassis are crucial. Administrative practices such as QA, agile development methodology, and strict configuration management must also be applied. Other techniques are much more complex and expensive, such as component redundancy with automatic detection and failover [142]. The control system must be based on new standards for next-generation instrumentation that

1. are modular in both hardware and software for ease in repair and upgrade;

2. include inherent redundancy at internal module, module assembly, and system levels;

3. include modern high-speed, serial, inter-module communications with robust noise-immune protocols; and

4. include highly intelligent diagnostics and board-management subsystems that can predict impending failure and invoke evasive strategies.

The Control System Model incorporates these principles through the selection of the front-end electronics packaging standard and component redundancy.

In addition to its intrinsic availability, the control system is responsible at the system level for adapting to failures in other technical systems. For example, the feedback system is responsible for reconfiguring a response matrix due to the loss of a corrector, or switching on a spare RF unit to replace a failed station.

Scalability requirements are met through a multi-tier hierarchy of network switches that allow for the flexible formation of virtual local area networks (VLANs) as necessary to segment network traffic. Control system name-servers and gateways are utilized extensively to minimize broadcast traffic and network connections. These software components manage the otherwise exponential growth of connections when many clients must communicate with many distributed control points.

Automation and flexible pulse-to-pulse feedback algorithms are implemented by a coordinated set of software services that work together through global coordination and distributed execution. The distributed execution is synchronized with the machine pulse rate via the timing event system which can produce software interrupts where needed. The network backbone accommodates the distribution of any sensor value to any feedback computation node. This distribution can be optimized to allow for efficient local as well as global feedback.

3.12.4 Control System Model

The model of the ILC control system is presented here from both functional and physical perspectives. This model has served as a basis for the cost estimate, as well as to document that the control system requirements have been satisfied. Functionally, the control system architecture is separated into three tiers, as shown in Figure 3.12-1. Communication within and between these tiers is provided by a set of network functions. A physical realization, as applied to the Main Linac, is shown in Figure 3.12-2. The remainder of the chapter describes the functional and physical models in more detail.
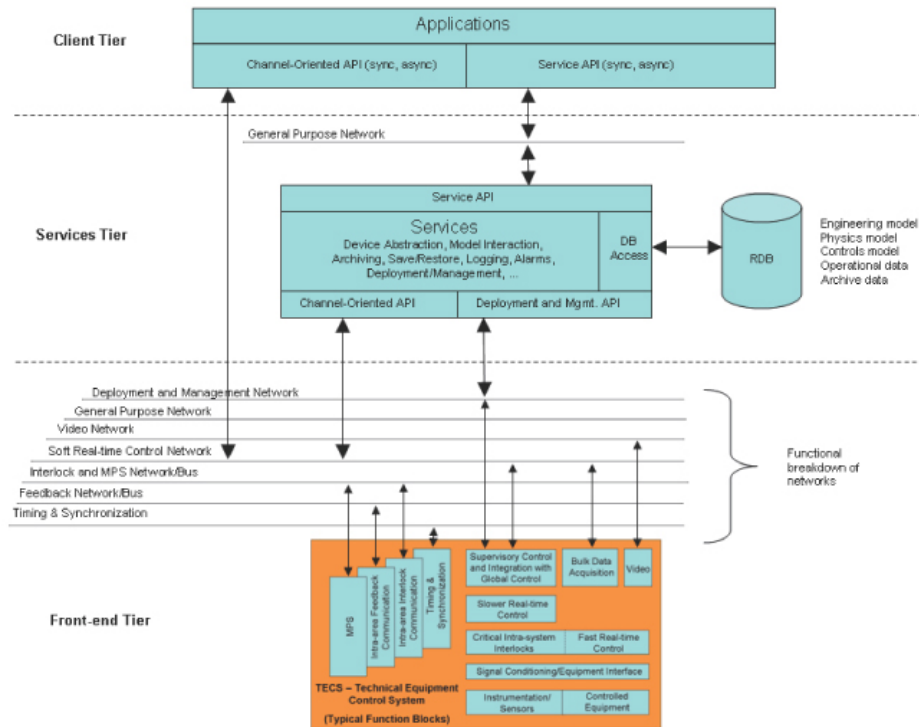
FIGURE 3.12-1. Control System Functional Model.

3.12.4.1 Functional Model

The control system model is functionally composed of three distinct tiers, as shown in Figure 3.12-1. The 3-tier model includes a middle tier that implements significant portions of
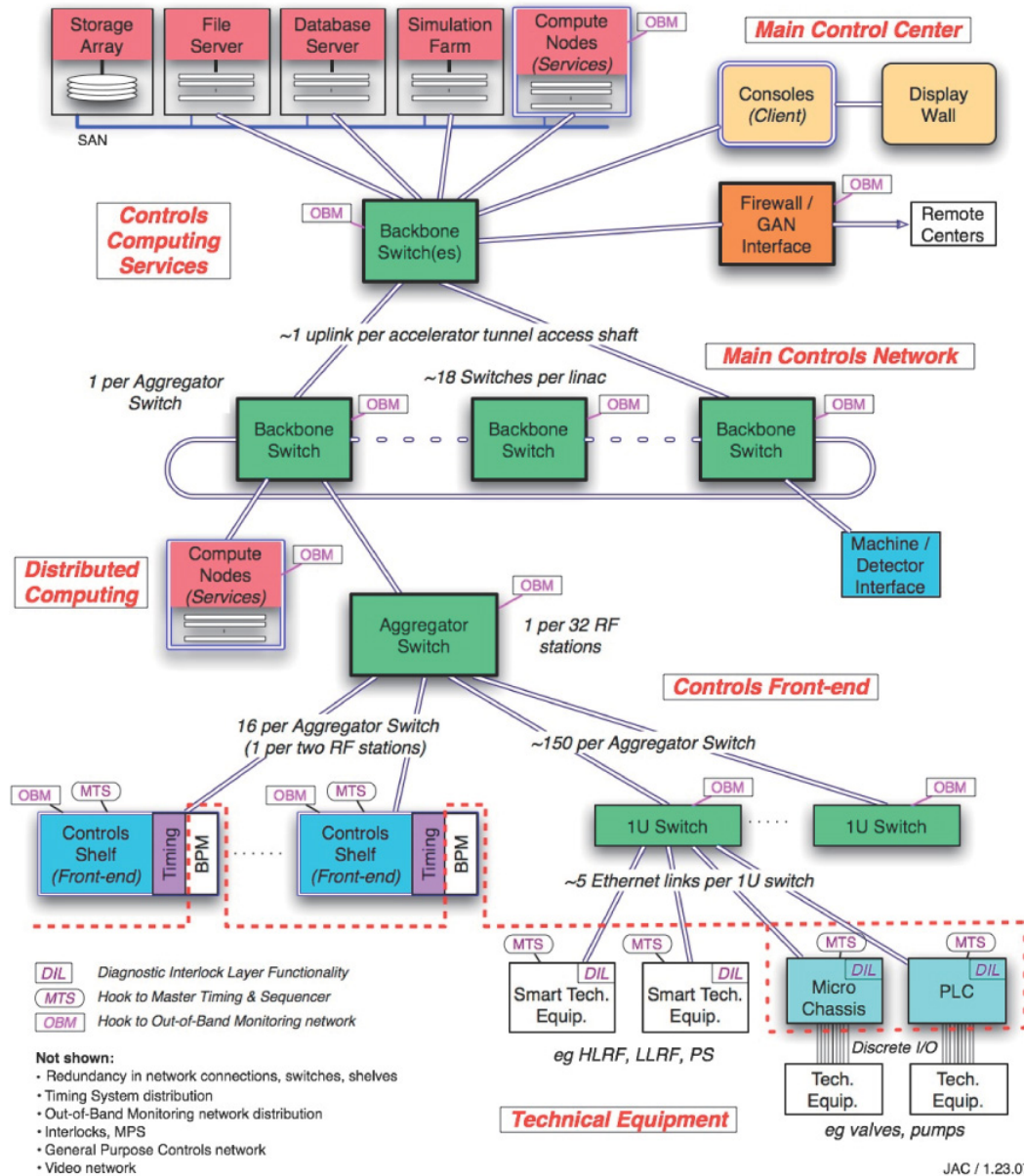
FIGURE 3.12-2. Control System Functional Model.

the logic functionality through software services that would otherwise reside in the client tier of a 2-tier system [143]. The three tiers are described in more detail below:

Client Tier: Provides applications with which people directly interact. Applications range from engineering-oriented control consoles to high-level physics control applications to system configuration management applications. Engineer-oriented consoles are focused on the operation of the underlying accelerator equipment. High-level physics applications require a blend of services that combine data from the front-end tier and supporting data from the relational database in the context of high-level device abstractions (e.g., magnets, BPMs).

Services Tier: Provides services that coordinate many activities while providing a well-defined set of public interfaces (non-graphical). Device abstractions such as magnets and

BPMs that incorporate engineering, physics, and control models are represented in this tier. This makes it possible to relate high-level machine parameters with low-level equipment settings in a standard way. For example, a parameter save/restore service can prevent two clients from simultaneously attempting to restore a common subset of operational parameters. This centralization of control provides many benefits in terms of coordination, conflict avoidance, security, and optimization.

Front-end Tier: Provides access to the field I/O and underlying dedicated fast feedback systems. This tier is configured and managed by the services tier, but can run autonomously. For example, the services tier may configure a feedback loop in the front-end tier, but the loop itself runs without direct involvement. The primary abstraction in this tier is a channel, or process variable, roughly equivalent to a single I/O point.

3.12.4.2   Physical Model

The ILC control system must reliably interact with more than 100,000 technical system devices that could collectively amount to several million scalar and vector Process Variables (PVs) distributed across the many kilometers of beam lines and facilities at the ILC site. Information must be processed and distributed on a variety of timescales from microseconds to several seconds. The overall philosophy is to develop an architecture that can meet the requirements, while leveraging the cost savings and rapid evolutionary advancements of commercial off-the-shelf (COTS) components.

3.12.4.2.1   Main Control Center   The accelerator control room contains consoles, servers, displays, and associated equipment to support operations of the ILC accelerator from a single location. Operators and technical staff run the accelerator and interact with technical equipment through Client Tier applications that run in the Main Control Center.

3.12.4.2.2   Controls Computing Services   Conventional computing services dedicated to the control system include storage arrays, file servers, and compute nodes. A separate simulation farm is anticipated for offline control system modeling and simulation, and for potentially performing model-reference comparisons to dynamically detect off-normal conditions. Enterprise-grade relational databases act as a central repository for machine-oriented data such as physics parameters; device descriptions; control system settings; machine models; installed components; signal lists, and their relationships with one another.

3.12.4.2.3   Controls Networks and Distributed Computing

Main Controls Network   Data collection, issuing and acting on setpoints, and pulse-to-pulse feedback algorithms are all synchronized to the pulse repetition rate. The controls network must therefore be designed to ensure adequate response and determinism to support this pulse-to-pulse synchronous operation, which in turn requires prescribing compliance criteria for any device attached to this network. Additionally, large data sources must be prudently managed to avoid network saturation.

For example, in the Main Linac, waveform capture from the LLRF systems likely dominates linac network traffic. Full-bandwidth raw waveforms from individual RF stations could be required for post-event analysis and therefore must be captured on every pulse. However,

only summary data is required for archiving and performance verification. By grouping multiple RF stations together (notionally into groups of 32), full-bandwidth waveforms can be locally captured and temporarily stored, with only summary data sent on.

Dedicated compute nodes associated with each backbone network switch run localized control system services for monitoring, data reduction, and implementing feedback algorithms.

Other Physical Networks   To accommodate communication functions that are not compatible with the Main Controls Network, several other physical networks are envisioned, namely: a *General-purpose controls network* for general controls network access, including wireless access and controls network access to non-compliant devices; an *Out-of-band monitoring network*: to provide independent means to access and configure all Network switches and Controls Shelves; a *Video network* to distribute video data streams facility wide. A *Technical Equipment Interlock Network* provides a means to distribute interlock signals. Functionally, this has similarities with the Machine Protection System described elsewhere. Technical equipment may report equipment or sensor status for use by other systems or utilize status information provided by other technical systems.

Based on initial assessments, commodity-computing equipment (e.g. 10-GB redundant Ethernet) is adequate to meet the requirements for all the networks.

3.12.4.2.4   Controls Front-end   The control system model front-end comprises the following three main elements:

1U Switch: Aggregates the many Ethernet controlled devices in a rack or neighborhood of racks. Some of these devices speak the controls protocol natively, while others have proprietary protocols that must be interfaced to the control system. It is assumed these 1U switches reside in many of the technical equipment racks.

Controls Shelf: Consists of an electronics chassis, power supplies, shelf manager, backplane switch cards, CPUs, timing cards, and instrumentation cards (mainly BPMs). The Controls Shelf serves several purposes: (1) hosts controls protocol gateways, reverse gateways, and name servers to manage the connections required for clients to acquire controls data; (2) runs the core control system software for managing the various Ethernet device communication protocols, including managing any instrumentation (BPM) cards in the same shelf; (3) performs data reduction, for example, so that full-bandwidth RF/BPM waveforms need not be sent northbound in the control system. The control system physical model references the commercial standard AdvancedTCA (ATCA) for the Controls Shelves. This is a specification that has been developed for the telecommunications industry [144], and has applicability for the ILC control system in part because of its high availability feature set.

Aggregation Switch: Aggregates network connections from the 1U switches and Controls shelves and allows flexible formation of virtual local area networks (VLANs) as needed.

3.12.4.2.5   Technical Equipment Interface   It has been common practice at accelerator facilities for the control system to accommodate a wide variety of interfaces and protocols, leaving the choice of interface largely up to the technical system groups. The large scale of the ILC accelerator facility means that following this same approach would almost certainly make the controls task unmanageable, so the approach must be to specify a limited number of interface options. For the purpose of the conceptual design and for the costing exercise, two

interface standards were chosen: a Controls-shelf compliant electronics module for special sensor signals and specific beam instrumentation applications such as BPM electronics; a controls compliant redundant network for all *smart* technical systems. While not explicitly part of the control system model, it is assumed that discrete analog and digital I/O can be provided through micro-controller chassis or PLCs.

In addition to conventional interfaces for controls purposes, the control system provides functionality for remote configuration management of technical equipment for micro- controllers, PLCs, application oriented FPGAs, etc.

3.12.4.3 Pulse-to-Pulse (5 Hz) Feedback Architecture

Many of the beam-based feedback algorithms required for ILC apply corrections at the relatively low machine pulse rate (nominally 5 Hz). This low correction rate and the distributed nature of many of the monitors and actuators make it desirable to use the integrated controls infrastructure for these feedback systems.

Using the integrated control system architecture to implement the feedback algorithms offers many advantages, including:

- Simpler implementation, since dedicated interfaces are not required for equipment involved in feedback loops.
- Higher equipment reliability, since there are fewer components and interfaces.
- Greater flexibility, since all equipment is inherently available for feedback control, rather than limited to predefined equipment.
- Simplified addition of ad hoc or un-anticipated feedback loops with the same inherent functionality and tools. This could significantly enhance the commissioning process and operation of the ILC.

Referring to Figure 3.12-2, feedback algorithms are implemented as services running in both distributed and centralized compute nodes. Design and implementation of feedback algorithms is enhanced through high-level applications such as Matlab [145] integrated into the Services Tier shown in Figure 3.12-1.

Implementing feedback at the machine pulse rate demands synchronous activity of all involved devices and places stringent compliance criteria on technical equipment, control system compute nodes, and the main controls network.

3.12.5 Remote Access / Remote Control

It is becoming commonplace for accelerator-based user facilities to provide means for technical experts to remotely access machine parameters for troubleshooting and machine tuning purposes. This requirement for remote access is more critical for the ILC because of the likelihood that expert personnel are distributed worldwide.

3.12.6 Timing and RF Phase Reference

Precision timing is needed throughout the machine to control RF phase and time-sampling beam instrumentation [146]. The timing system emulates the architecture of the control system, with a centrally located, dual-redundant source distributed via redundant fiber signals to all machine sector nodes for further local distribution. Timing is phase-locked to the RF system.

3.12.6.1   RF Phase Reference Generator

The RF phase reference generator is based on dual phase-locked frequency sources for redundancy. It includes fiducial generation (nominally at 5 Hz) and line lock. The macro-pulse fiducial is encoded on the distributed phase reference by a momentary phase shift of the reference signal. Failure of the primary frequency source can be detected and cause an automatic failover to the backup source.

3.12.6.2   Timing and RF Phase Reference Distribution

The phase reference is distributed via dual redundant active phase stabilized links. Figure 3.12-3 shows an overview of dual redundant phase reference transmission and local, intra-sector distribution.
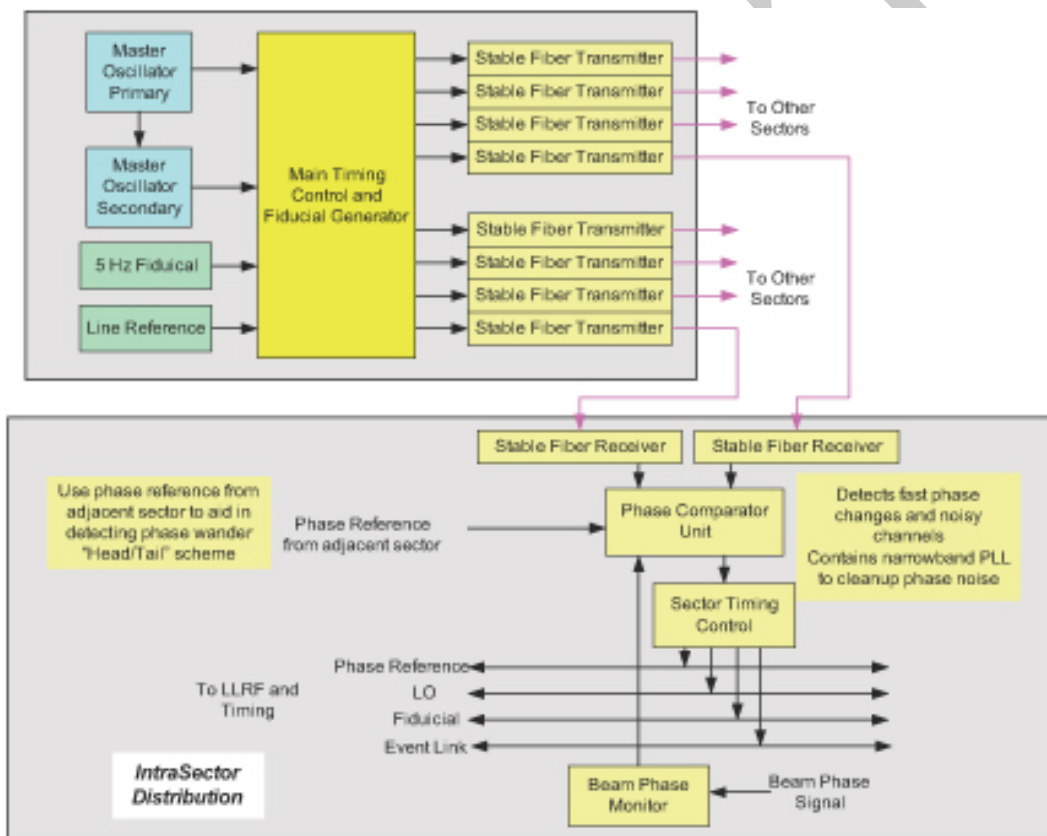
FIGURE 3.12-3. Timing System Overview showing redundant phase reference distribution and local intra-sector timing distribution.

The Phase Comparator unit detects failures in the primary phase reference link and automatically fails over to the secondary link. Both the Phase Comparator unit and the Sector Timing Control units are fault tolerant. A local DRO or VCXO is phase-locked to the phase reference to develop a low phase noise local reference for distribution within an RF sector of the main linac.

Figure 3.12-4 shows a block diagram of a single active phase-stabilized link. A portion of the optical signal is reflected at the receiving end. The phase of the reflected optical signal is compared with the phase of the frequency source. The resulting error signal controls the

temperature of the shorter series section of fiber to compensate for environmentally induced phase shifts [147].
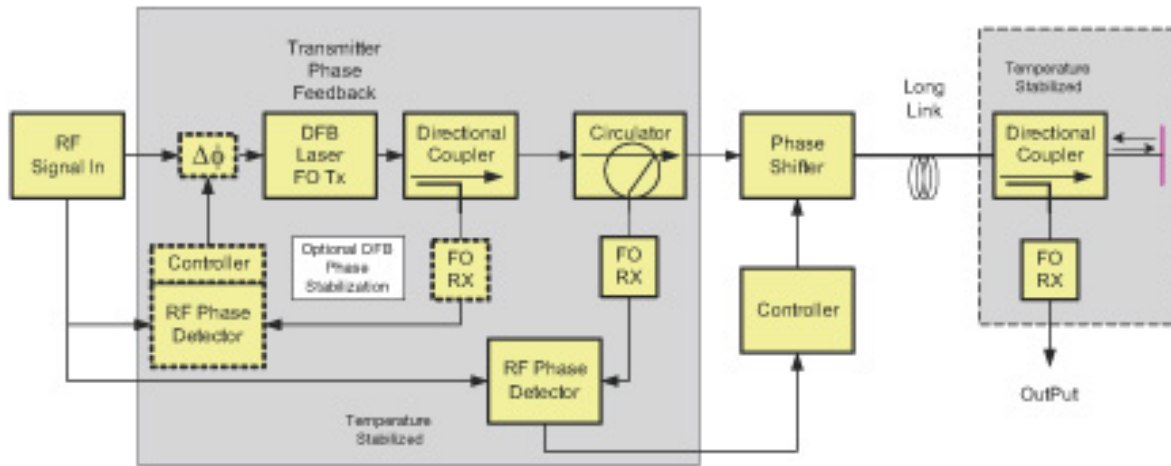
FIGURE 3.12-4. Phase stabilized reference link.

3.12.6.3 Timing and Sequence Generator

An event stream is distributed via dual redundant links in a star configuration. The system automatically fails over to the redundant link upon detection of a failure. The event system provides a means for generating global and local sequences, synchronizing software processing to timing events, and generating synchronous time stamps.

3.12.7 Beam-based Feedback

Beam-based dynamical feedback control is essential for meeting the high performance and luminosity needs of the ILC. Feedback systems stabilize the electron and positron trajectories throughout the machine, correct for emittance variations, and provide measurement and correction of dispersion in the Main Linac. Two timescales of beam-based feedback are anticipated, namely pulse-to-pulse feedback at the 5 Hz nominal pulse repetition rate, and intra-train feedback that operates within the macropulse containing ∼3000 bunches spaced at ∼300ns intervals.

3.12.7.1 Architecture for Intra-Bunch Feedback Systems

Unlike pulse-to-pulse feedback, which is implemented through the control system, dedicated systems are required for intra-bunch feedback. These must operate at the bunch rate of ∼3 MHz, and include the RTML turnaround trajectory feed-forward control and intra-bunch trajectory control at the IP. Orbit feedback in the damping ring is synchronized to the damping ring revolution frequency.

Local input/output processors acquire beam position, cavity fields, beam current, and other local beam parameters at the full 3 MHz bunch rate and distribute that information to a fast synchronous network. Local interconnections with the low-level RF systems provide opportunities for local feedback loops at the full 3 MHz bunch rate. Dedicated processing

crates provide both dedicated real-time bunch-to-bunch control, such as RF cavity fields, and dispersion-free steering, while additional uncommitted crates could provide feedback systems to be implemented as required.

3.12.7.2 Hardware Implementation

Most of the feedback processing requirements described in this section can be met using commercial hardware, including dynamic orbit control in the damping ring. Custom hardware solutions are required in cases where low latency or unique capabilities are required, such as for the RTML turnaround trajectory feed-forward and the IP intra-bunch trajectory feedback. High availability solutions are implemented as appropriate, using the same standards and approach as for other instrumentation and control system equipment.

3.12.8 Information Technology (IT) Computing Infrastructure

The ILC requires an Information Technology infrastructure. For the purposes of the RDR, this infrastructure is costed assuming that it resides at the ILC site. Equivalent functionality can be achieved by outsourcing many of the required services, but it is expected that the cost is similar. There is a central computing building to house the machines and network infrastructure, a network internal to the laboratory, a connection to the wide area network, computer hardware and software for business computing, computing tools for engineering support (excluding civil engineering), basic services (web, email, file servers, databases, back-ups, help desk, accounts), and computer security that complies with regulations and allows for secure access to and dissemination of information.

3.12.9 Cost Estimation, Bases of Estimates

An inherent assumption is that the control system hardware model can be implemented largely using COTS equipment.

Manpower estimates were developed top down, using assumptions about the level of effort required to implement a control system for ILC, and were compared with levels of effort from recent accelerator projects. It is assumed that the ILC control system software framework is founded on an existing framework, rather than developing a new framework from the ground up. Assumptions were made on the level of extra effort needed to implement high availability control system hardware and software.

Materials and Services cost estimates were derived from a bottom-up assessment of the controls requirements from each accelerator area and technical system. Costs for computing infrastructure (servers, networking, storage) were based on current commodity computing vendor prices, with an inherent assumption that technology advances will bring commodity computing to the level of performance required for the ILC by the time of project construction. Estimates for RF phase reference distribution were developed from a reference design and vendor quotes. Estimates for ATCA front-end electronics were based on technically comparable components in other electronics platforms since equivalent components are not yet available (or at least not in quantity) for ATCA.

The IT infrastructure estimates were based on actual costs for building and running IT infrastructure at Fermilab, assuming that an ILC laboratory requires equivalent functionality at approximately the same scale.

3.12.10   Table of Components

The following table shows a snapshot of the counts of the major control system elements.

TABLE 3.12-1
Snapshot counts of the major control system elements.

Component	Description	Quantity
1U Switch	Initial aggregator of network connections from technical systems	8356
Controls Shelf	Standard chassis for front-end processing and instrumentation cards	1195
Aggregator Switch	High-density connection aggregator for 2 sectors of equipment	71
Fiber Channel RAID Disks	Controls computing high performance disk storage	350 Terabytes
Tape Library	Automated tape system for backup & retrieval, plus front-end disk cache	1
Controls CPU	Controls computing CPUs (other than real-time front-end processors)	452
Database CPU	CPUs for running development, staging, and production databases	30
Controls Backbone Switch	Backbone networking switch for controls network	126
General Purpose Backbone Switch	Backbone networking switch for general purpose network	126
Monitoring Backbone Switch	Backbone networking switch for monitoring (SNMP, IPMI) network	126
Video Backbone Switch	Backbone networking switch for video distribution network	126
Phase Ref. Link	Redundant fiber transmission of 1.3-GHz phase reference	68
Phase Comparator	Phase comparison of dual phase references and adjacent sector	68
Sector Phase Ref. Timing Control	Local sector receiver of phase ref. and fiducial	68
Event System Link	Fiber link for event code distribution	68
Local Timing Card	Controls shelf timing receiver and intra-shelf timing distribution	1134
Controls Rack	Standard rack populated with one to three controls shelves	753
LLRF Controls Station	Two racks per station for signal processing and motor/piezo drives	668

CHAPTER 4

Conventional Facilities and Siting

4.1 OVERVIEW

This section provides an overview of the ILC Conventional Facilities and Siting (CFS) which has been adopted as the basis of the RDR cost estimate. A more detailed description can be found in [148]. In the absence of a specific ILC site, three reference sites one in each region have been developed in parallel by the CFS Group. The reference sites (described in Chapter 5) are all deep-tunnel sites, but have varying geologies and topographical constraints. An evaluation of an optimized shallow site (either a shallow tunnel or 'cut and cover') was beyond the scope of the current RDR activities, but will be done in the near future. While the focus of the CFS design work has been on the 31 km long 500 GeV machine, the sites are required to support the footprint of the 1 TeV upgrade, both in terms of space and available infrastructure (e.g. power).

The CFS Sample Site designs were generated using criteria provided by each of the ILC Area Systems. Overall tunnel lengths were specifically determined by the machine parameters. However, the size of tunnels, shafts, underground caverns and surface buildings, as well as the related CFS systems, have been developed to accommodate specific equipment installation, maintenance and personnel access and egress requirements. For all these systems, the original criteria have been iterated in order to minimize overall costs while meeting the requirements of the present state of the ILC design. Specific examples include the reduction of Service and Beam tunnel diameters, the number and size of shafts, electrical power and process cooling loads.

Figure 4.1-1 indicates the basic scope of the civil construction of the ILC layout:

- Two parallel 31 km long 4.5m diameter underground tunnels house the main accelerators and the Beam Delivery Systems (Beam Tunnel), and their associated support hardware (Service Tunnel, containing klystrons, modulators, power supplies, controls and instrumentation electronics etc.). The tunnels are generally separated horizontally by ∼11 m (center-to-center), and are connected via small diameter penetrations every 12 m supporting cables, waveguides etc. Personnel access connection tunnels (primarily for safety egress) are located every 500 m.

- A total of 13 shafts along the length of the machine provide access to underground caverns linking to the tunnels. They primarily support the large cryogenics plants required for the superconducting linacs.
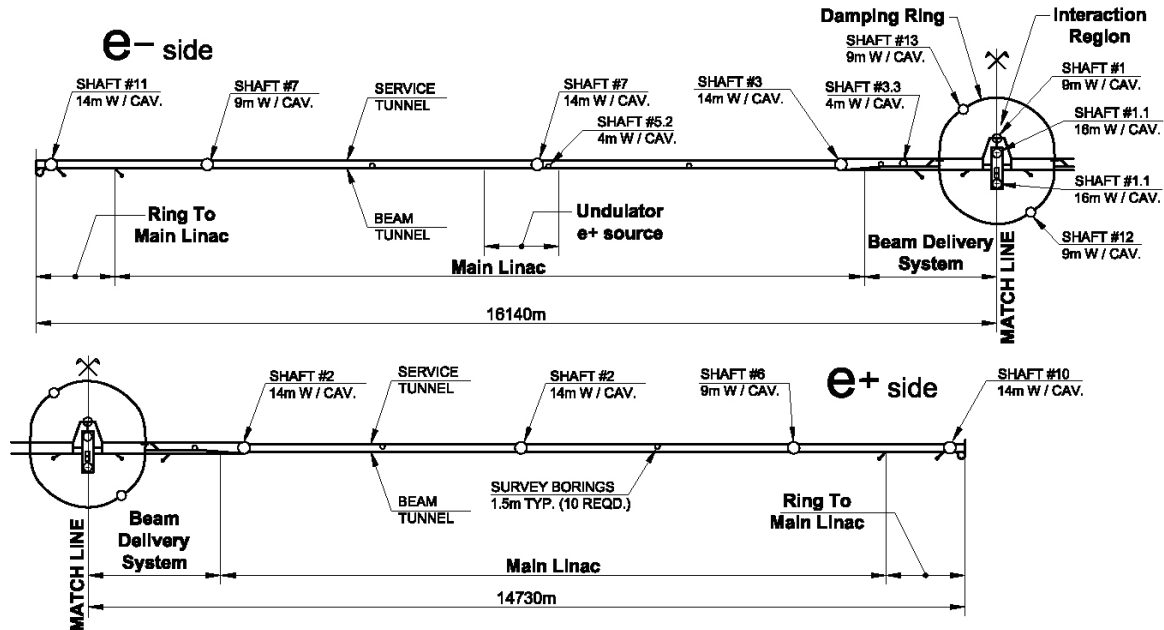
FIGURE 4.1-1. Layout of the Civil Construction, Indicating the Position of Shafts and Caverns

- A single collider hall at the Interaction Region (IR) is large enough to support two physics detectors in a push-pull configuration.

- A single 5 m inner-diameter ~7 km approximately circular tunnel located around the central IR region and ~10 m above the BDS elevation houses both the electron and positron Damping Rings in a stacked configuration.

- Several additional tunnels and service shafts house the electron and positron sources and injector linacs (injection into the Damping Ring), and connect the damping ring to the main accelerator housing.

Civil Engineering, Electrical, and Process Cooling Water comprise greater than 90% of the total cost of the CFS. The Civil Engineering portion of the project is almost two thirds of the total CFS cost, with the Underground Facilities equating to 75% of Civil Engineering. The more than 72 km of tunnel is the single largest cost element. Although formal value engineering has not yet been accomplished, the designs have been reiterated with the project team several times to develop a cost efficient, workable design.

4.2 CIVIL ENGINEERING AND LAYOUT

4.2.1 Main Accelerator Housing

The largest underground structures are the two parallel 4.5 m diameter tunnels, which effectively run for the entire length of the machine footprint (∼31 km). One tunnel (the Beam Tunnel) contains the beamline components (SCRF accelerator cryomodules, magnets, vacuum systems etc.) The second so-called "Service' Tunnel houses the entire support infrastructure: RF power sources (klystrons, modulators, pulse transformers); dc magnet power supplies; radiation-sensitive instrumentation and controls (electronics). Unlike the Beam Tunnel, the Service Tunnel is designed to be accessed during beam operation, allowing in-situ repairs and adjustment of equipment during running.

Figure 4.2-1 shows a cross-section of the Main Linac twin-tunnel, with the Beam Tunnel on the left. The 4.5 m inner diameter accommodates the cryomodules and RF distribution (waveguides), at the same time as allowing space for cryomodule installation (or removal), while maintaining a minimum "clear passage" for emergency egress (see Figure 4.2-1 left). The Cryomodules and other floor standing components are placed on short stands mounted to a concrete floor. The beam is centered 1.1 meters above the floor and 0.8 meters away from the wall, which is considered sufficient to allow for cryomodule installation (welding) and the installation of the RF waveguides. Space needed for the survey lines of sight has also been considered. The outer positioning of the cryomodules allows for clear access to the egress passageways connecting the two tunnels, spaced at 500 meter intervals (not shown).
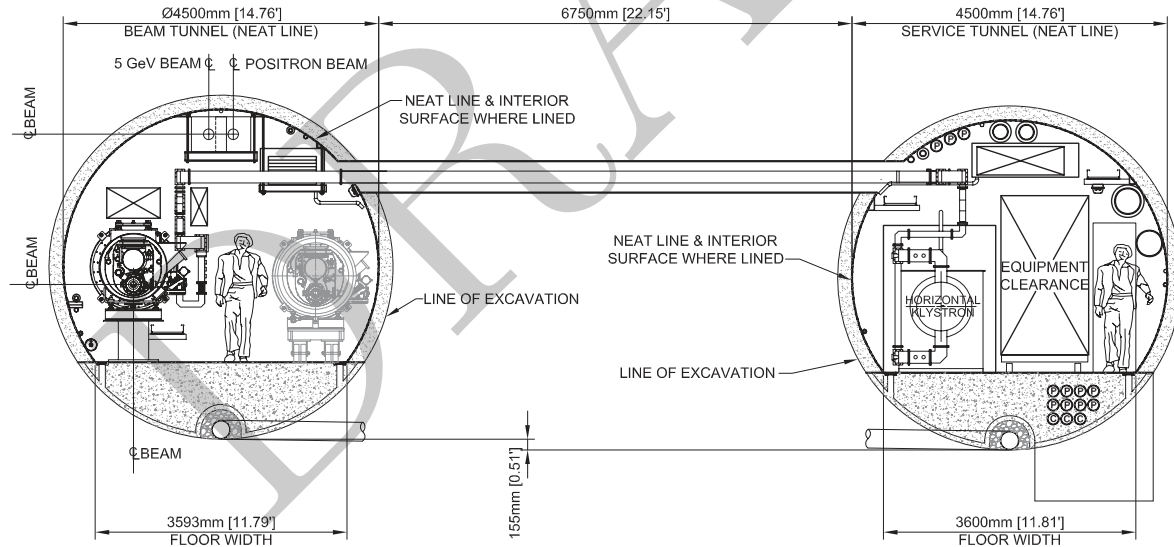
FIGURE 4.2-1. Cross-section of the Main Linac Housing (Beam Tunnel, left) and Service Tunnel, Showing the Connecting Waveguide Penetration

The lateral separation of the tunnels is ∼11 m (center to center). The ∼7 m rock and concrete separation between the Service Tunnel and Beam Tunnel is required for structural reasons and to provide the required radiation shielding mass allowing workers to enter the Service Tunnel while the accelerator is operating. Penetrations between tunnels have been sized and configured to provide the required radiation shielding.

TABLE 4.2-1
Main Service Tunnel Equipment for a Single RF Unit

Item Name	Size (Meters)	Comments
Klystron	1. × 3.38	
Pulse transformer	1.34 × 1.25	
Modulator	1 × 4.27	
Electronic racks	9 0.80 × 1.1	Self Contained w/ integral cooling
LCW & CW skids	1.22 × 2.06	
RF transformer	1.353 × 1.499	Plus 800 Amp Panel
Charging supply transformer	1.22 × 2.44	
Conventional transformer	1.575 × 1.245	Plus 800 Amp Panel
Emergency transformer	1.575 × 1.245	

The regions of superconducting RF (accelerator) dominate the length of the main accelerating housing. These sections are made up of many consecutive identical RF units. An RF unit is approximately 38 m long (three cryomodules), and is supplied from the Service Tunnel by three cross penetrations at intervals of approximately 12 m: one for the RF waveguides, and two additional ones for cables and signals. The main RF unit components housed in the Service Tunnel and their approximate space requirements are given in Table 4.2-1. For the 'warm'sections of the Ring-to-Main-Linac (RTML) as well as the Beam Delivery System (BDS), the Service Tunnel accommodates the many independent magnet power supplies, as well as electronics for controls and instrumentation.

In addition to the RTML, Main Linac and BDS beamline components, the Beam Tunnel also houses the 5 GeV low-emittance transport line (part of the RTML) which transports the beam from the central Damping Rings to the far ends of the machine. The RTML 'turnarounds'at the ends of the machine are housed in a 4.5 m diameter looped tunnel with an average bending radius of ∼30 m in the horizontal plane. The length of each loop is approximately 140 m. On the electron linac side, a third beamline from the undulator-based positron source (nominal 150 GeV point) is required to transport the 400 MeV positrons from the source to the Damping Rings. Both the long 5 GeV low-emittance and the 400 MeV positron transport lines are supported from the Beam Tunnel ceiling, and are positioned towards the center of the tunnel to allow for installation and replacement without removing a cryomodule. Power and cooling services for these elements are provided from equipment in the Service Tunnel.

The BDS and RTML bunch compressor tunnels (a total of ∼5.3 km and ∼2 km, respectively) lie in a plane, while the Main Linac tunnels (47.8 km) and associated beamline components, including the long RTML transfer lines, follow the Earth's curvature.

The large cryogenic plants (see Section 3.8), required primarily for the SCRF RF cryomodules, are housed in eight underground caverns connected to the surface via shafts (four per side, spaced approximately 5000 m apart): shaft nos. 2, 3, 4, 5, 10 and 11 are 14 m in diameter, while shaft nos. 6 and 7 are 9 m diameter (see Fig. 4.1-1 for shaft locations). Figures 4.2-2 , 4.2-3 shows a schematic of a typical 9 m shaft and cavern. In addition to housing the cryogenic plants, these shafts are also used for: installation of machine components (including cryomodules at the 14 m shafts); normal and safety egress from the tunnels; and

for supporting all services such as cooling water, power etc. The 14 m shafts are also used to lower, assemble and prepare the Tunnel Boring Machines (TBM) which are used extensively for tunnel excavation.
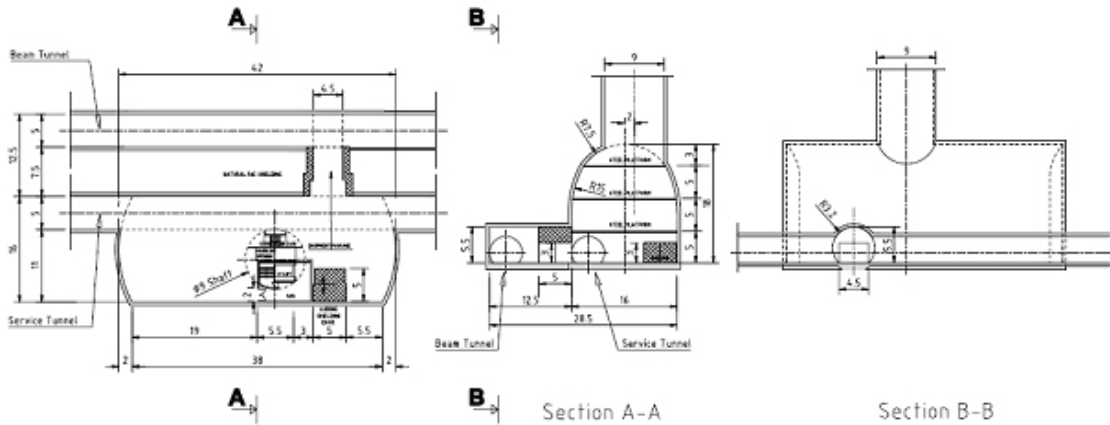
FIGURE 4.2-2. Example of a 9 m Shaft with Underground Cavern, Service and Beam Tunnels (European Sample Site)
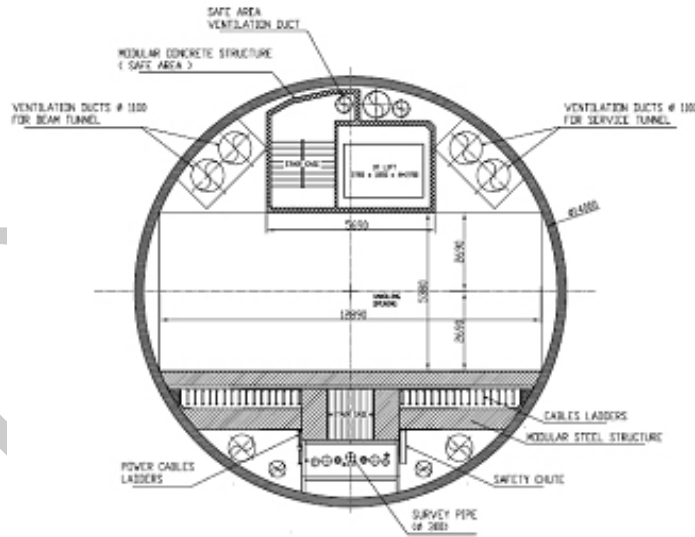
FIGURE 4.2-3. Detailed View of 14 Meter Shaft

Temperature neutral air is routed through the tunnel from the shafts, no additional heating or cooling is required in the Beam Tunnel. Where needed there is dehumidification equipment installed to maintain humidity levels below the dew point. Seepage is directed to a drain and routed to the sumps located at the shaft caverns.

A special underground cavern is required to service the undulator-based positron source, located at the nominal 150 GeV point in the Main Electron Linac. A 4 m vertical shaft is

provided for removal and installation of 'hot'targets.

4.2.2   Central Injectors

The central injector systems include: the 6.7 km circumference Damping Rings; the polarized electron source; the positron Keep Alive Source (KAS); and the electron and positron 5 GeV SCRF injector linacs. Figure 4.2-4 shows the primary tunnel and shaft arrangements.
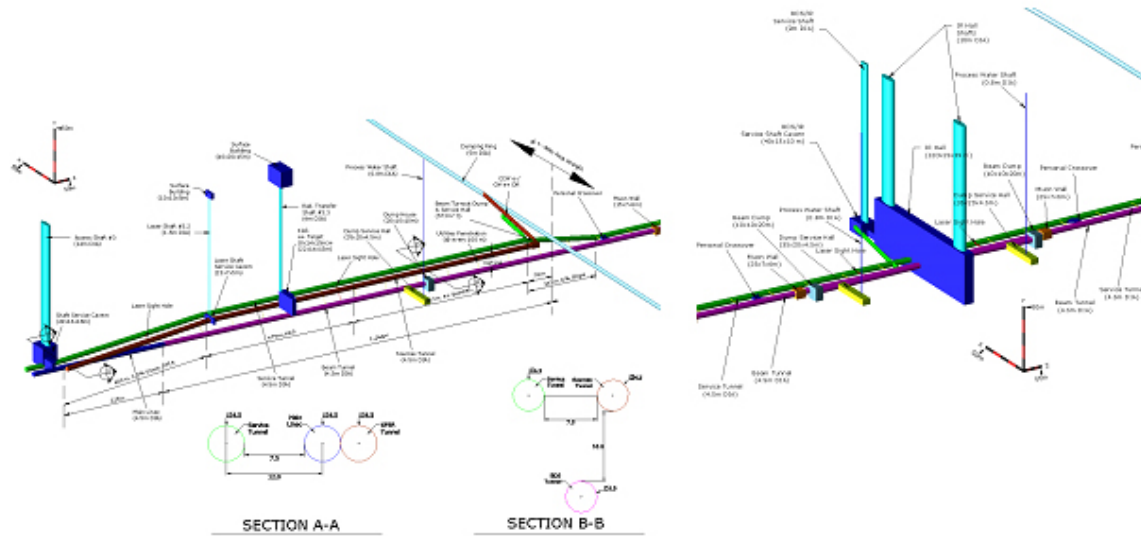
FIGURE 4.2-4. Layout of the Central Injector Complex (electron side)

The electron and positron Damping Rings are housed in a single 5 m inner-diameter quasi-circular tunnel with a total circumference of 6704 m. The tunnel is located in the horizontal plane, approximately 10 m above the plane of the BDS. The ring is made up of six arc sections, two long straight sections for injection and extraction and four short straight sections containing the superconducting damping wigglers and RF. The DR tunnel is connected to the injection tunnels from the sources in the middle of the long straight sections (see Fig. 4.2-4). The tunnel has 6 alcoves in total, located in the middle of the straight sections. Two main alcoves are accessed via two 9 m diameter shafts, and are used to house the cryogenic plants and RF power sources for the wigglers and RF cavities (and are also used for installation). The four smaller alcoves in the remaining straight sections are not connected to the surface, but two of them are vertically connected to the BDS portion of the Service Tunnel 10 m below to allow personnel access. As there is no separate service tunnel for the DR, all service and support equipment are housed in the two shaft caverns and the four smaller alcoves. A cross-section of the Damping Ring tunnel is shown in Fig. 4.2-5; the 5 m inner diameter is required to house the two rings (vertically stacked), and the emergency egress passage, while allowing enough space for component installation.

The electron and positron 5 GeV injector linacs are each housed in 4.5 m diameter tunnels, and share the main Service Tunnel with the BDS. The sources also make use of the 14 m diameter shafts located directly at the end of each Main Linac, where the connecting tunnel to the Damping Rings has a 2% slope to accommodate the 10 m vertical offset between the
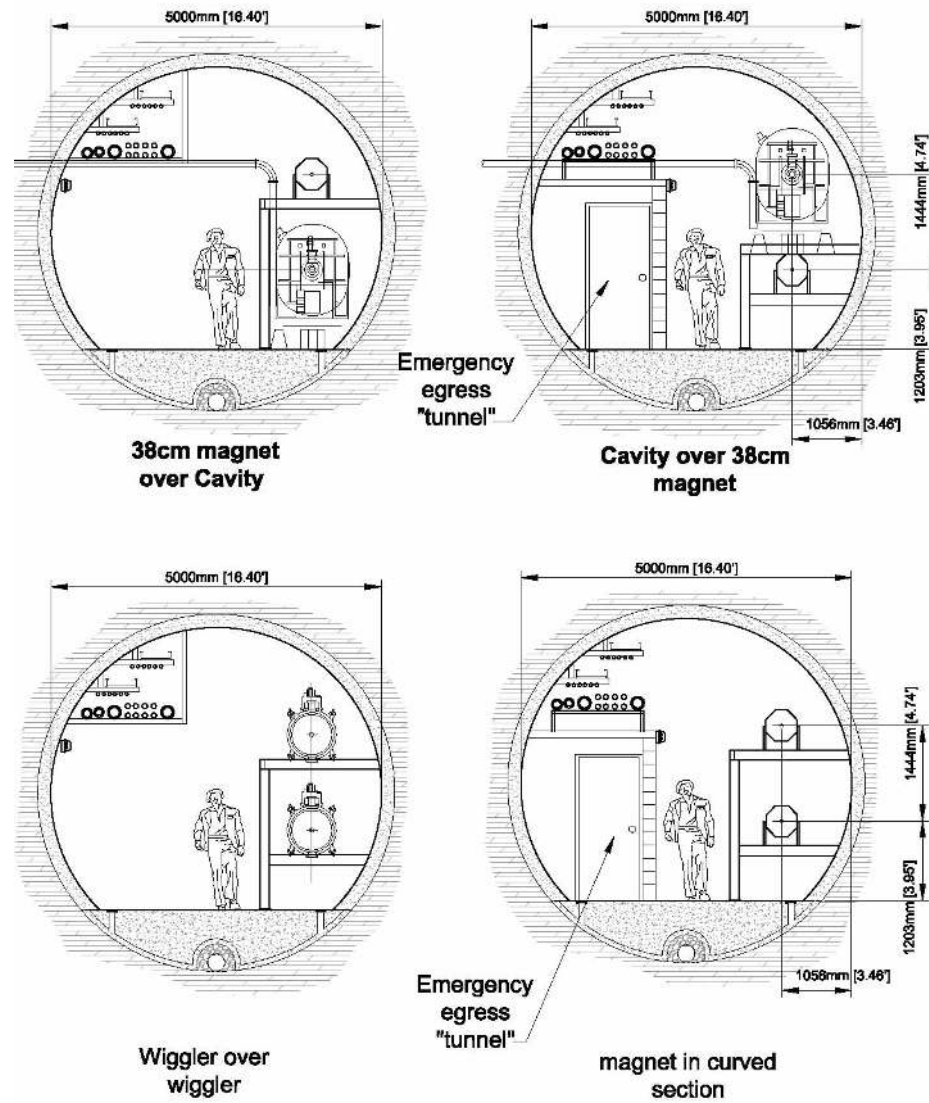
FIGURE 4.2-5. Cross-Sections of the 5 m Diameter Damping Ring Tunnel Showing Vertical Stacked Rings at Several Locations

Damping Ring and Main Accelerator Housing. The KAS source requires an underground cavern similar to the positron production vault in the electron Main Linac, again with a 4 m diameter vertical shaft for removal and installation of the hot target.

4.2.3 Interaction Region and BDS

The Physics Detector Hall is the largest cavern in the project. It is sized to accommodate two Physics Detectors in a Push Pull type configuration assuming surface assembly of each detector. The hall is connected to the surface assembly buildings via two 16 m diameter shafts, one for each Detector. It is also connected to the Beam Tunnel, to a service cavern through a passageway, and to the survey galleries. The floor slab is thick enough to accommodate the weight of the two Detectors and the weight of the movable shielding wall (2 pieces) in between the Detectors. The walls of the hall are equipped with 3 to 5 levels of steel platforms to be used for services and access at various levels to the Detectors. The hall also has beams

FIGURE 4.2-6. Schematic of Physics Detector Hall, showing BDS Service Cavern Arrangement

and rails for one 400 ton crane and two 20 ton cranes, assuming the surface pre-assembled Detector elements weigh 400 tons at most.

An additional service cavern for the BDS is located next to the Detector Hall (see Fig. 4.2-6). It houses all the equipment needed for the running of the Detectors and ancillary facilities, which need to the shielded from radiation or the magnetic field of the detectors. It has two steel platforms as intermediate floors for equipment, and is connected to the Detector Hall through a shielded passage for personnel and goods, and to the BDS service tunnel on both sides. The service cavern is accessible from the surface via a 9 m diameter vertical shaft, which supports all services, houses a safe staircase and lift for personnel and equipment, and leaves space for lowering all components to be installed in the service cavern.

There are four full-powered Beam Dump facilities in the BDS System, two on each side. For each one there is a cavern which houses the high-pressure water dump itself, and a service cavern located $\sim$30 m away to house all electrical, control and cooling equipment.

The inner diameter of the BDS beam tunnels are locally enlarged at four locations (two per side) to house the large magnetized toroids (so-called Muon spoilers) for reducing the muon background to the experimental hall.

4.2.4 Surface Buildings

A total of 120 surface buildings are estimated for the project. The type, number and dimensions of the buildings include only those surface facilities required for construction, installation and operation of the project. Additional infrastructure such as seminar rooms, guest-houses, restaurants, administrative facilities etc. are assumed to be supplied by a nearby (host) laboratory, and are not included in the cost estimate. The Asian sample site does not have a nearby laboratory and that estimate does include such central campus facilities.

Types of surface buildings considered included: surface equipment buildings, including cooling towers and pump stations; shaft head buildings; storage areas; local workshops and

assembly areas, local technical offices etc. The majority of these buildings are concentrated at the "central campus" and specifically at the Interaction Region. The remaining buildings are located at the shafts positioned along the Main Accelerator Housing. Concrete construction with acoustic absorbent material is used for buildings which contain "noisy" equipment; the remaining buildings have steel structures and insulated steel "sandwich" type panels for roof and wall cladding on concrete foundations. In all cases, the design of the buildings takes into account the local climatic loads, seismic load (according to local standards) and fixed or moving loads linked to the use of that building. The requirements for each building type have been considered in making the cost estimate. Overhead cranes, gantries, elevators and other lifting gear with appropriate capacity are included where necessary in surface and underground structures. A detailed breakdown of the surface buildings can be found in [148].

4.2.5   Site Development

For the areas where surface buildings are located (central campus, shaft positions), the following items have been included in the cost estimate:

- fences and gates;
- roads and car parks within fences and from fence to existing road network;
- pedestrian walkways;
- lighting for the above and around buildings including buried electrical connections;
- all necessary drains along roads, car parks, including sumps, water treatment facilities and connections to existing mains;
- all necessary water supply pipes, tanks and connection to existing water supply network;

- landscaping and planting of trees, bushes, seeding of grass as required;
- spoil dumps (where applicable) created close to the building areas, including landscaping.

All temporary facilities needed for the construction works as well as the necessary site preparation before start of the works are also included in the cost estimate.

4.2.6   Regional Variants

Both the Americas and European sites are similar deep tunnel sites and both utilize vertical shafts for access as described in the sections above. These shafts are respectively 135-100 m deep. The Asian site is somewhat different, in that it is located along the side of a mountain. With the exception of the two central shafts for servicing the Detector Hall at the IR, long almost horizontal access tunnels are used instead of vertical shafts. The lengths of these access tunnels range from 700 m to 2000 m. Other variants which are due to construction methods depending on local geology are covered in Chapter 5.

4.3 A.C. POWER DISTRIBUTION

Electrical power is categorized by three major systems:

- RF power (modulators);
- conventional power (normal conducting magnet power supplies, cryogenic plants, electronic racks, surface water plant systems and infrastructure components);
- emergency power provided by back-up generators (emergency lighting, sump pumps and ventilation systems for sub-surface enclosures).

The power requirements are dominated by the RF system (modulators) located in the Service Tunnel along the length of the Main Linac. Table 4.3-1 gives an overview of the estimated *nominal* [1] power consumption for 500 GeV center-of-mass operations, broken down by system area and load types. The cost estimate is based on a total nominal power requirement of 216.3 MW. The additional required power for a potential upgrade to 1 TeV centre-of-mass is not included in the current power load tabulation.

TABLE 4.3-1
Estimated Nominal Power Loads (MW) for 500 GeV Centre-of-Mass Operation

| Area System | RF Power | Conventional Power | | | | Emer Power | Total (by area) |
		Conv	NC Magnets	Water Systems	Cryo		
Sources e$^-$	1.05	1.19	0.73	1.27	0.46	0.06	4.76
Sources e$^+$	4.11	7.32	8.90	1.27	0.46	0.21	22.27
DR	14.0	1.71	7.92	0.66	1.76	0.23	26.29
RTML	7.14	3.78	4.74	1.34	0.0	0.15	17.14
Main Linac	75.72	13.54	0.78	9.86	33.0	0.4	134.21
BDS	0.0	1.11	2.57	3.51	0.33	0.20	7.72
Dumps	0.0	3.83	0.0	0.0	0.0	0.12	3.95
Totals (by system)	102.0	32.5	25.6	17.9	36.9	1.4	216.3

High voltage (HV) connections to the utility system varies by region, ranging from 275kV (Asia), 345kV (America) and 400kV (Europe). All regions provide for a main substation located at or near the Interaction Region/Central Damping Ring for connection to the utilitys high voltage transmission system. Standards for high voltage transmission, and medium (MV) and low voltage (LV) distribution vary across regions; consequently the approach to distributing the power to the machine components is slightly different for the three sample sites. However, the salient features remain the same:

- Connection to the utilitys HV transmission system via a main substation located at the central campus;
- HV transmission voltage is transformed to medium voltage (MV; 34-69 kV) for distribution across the site to remote shafts (access points);

---

[1] *Nominal* electrical power requirements have been developed (as much as practical) as *continuous power* , sometimes denoted as *wall power* . *Installed* power may be 75-100% higher.

- From the remote shaft locations, power is further transformed and distributed to the Service Tunnel. For the Main Accelerator Housing, this implies a distribution of approximately ±2.5 km (in both directions) from the shaft locations. Medium voltage is distributed directly to RF stations (modulators). Low-Voltage transformers located along the Service Tunnel tap-off the MV distribution system to provide power to the LV systems and components.

An optimized engineering solution for the power distribution is heavily influenced by site selection, including: availability and location of utilitys substations; regional voltage standards and regional safety regulations. The design work for this report was developed globally by identifying site-dependent and site-independent infrastructure requirements, the former being developed by the regions and the latter being based on a European estimate. Details can be found in [148]. In the following sections, the European solution is presented. Important regional variations are briefly described in Section 4.3.6.

4.3.1 System Configuration

Voltage levels selected for the MV distribution systems are 66/6 kV, 36 kV and 69/34 kV for the Asian, European and Americas regions, respectively. LV distribution systems for all regions are in the magnitude of hundreds of volts. Standardized switchboards powered from the LV transformers are used to locally distribute LV power.

All HV and MV substations - including the one at the central campus - are provided with a bus-tie-bus configuration (RF bus system and conventional bus system). The HV and MV protection systems are based on numerical relays with facilities for programming automated sequences, and for recording network perturbations; thus allowing every major electrical system to be monitored by a Supervisory Control and Data Acquisition system (SCADA)

4.3.2 Distribution for the Main Accelerator Housing

Two MV cable lines are routed along those sections of Service Tunnel containing SCRF cryomodules (Main Linac and RTML):

- One MV system provides power to the RF (Modulator) system, with a ring main unit (RMU) installed at every RF unit (∼38 m) connected directly to the RMU.
- The second MV system provides power for conventional services, with a RMU and 500 kVA transformer located at every fourth RF unit (∼152 m). A LV switchboard is powered from the 500 kVA transformer and located near the transformer in the Service Tunnel. The switchboard supplies LV power to ∼152 m of both the Beam and Service Tunnels.

In those sections of the Main Accelerator Housing where there are no RF units (warm sections of RTML and the BDS), only the conventional services MV system components are installed. The same 152 m module structure is used in these areas. For the BDS sections, individual transformers are rated 1000 kVA (each) in lieu of 500 kVA due to the higher density of the load (larger number of normal conducting magnets)

LV power is supplied to the Beam Tunnel via the connecting penetrations, spaced approximately 12 m apart (12 per 152 m distribution unit).

4.3.3 Distribution for the Central Injectors

Power for the central injectors (damping rings, sources and injector linacs) is derived from the main substation located at the central campus.

The SCRF is responsible for about two-thirds of the total power requirement for the Damping Rings, the remaining third being the normal conducting magnets and superconducting wigglers. Due to the restricted tunnel cross section, the MV systems are installed partly on the surface and partly in the tunnel alcoves (see Section 4.2.2). The Damping Ring tunnel is supplied from a MV loop system originating at one of the two Damping Ring service shafts. A distribution substation is installed on the surface, fed directly from the central area via a MV system. The surface equipment at the second service shaft completes the closed loop. A LV transformer provides power in the shaft base alcoves. RF and other large power consumers are fed via RMUs and the dedicated MV system at the surface.

For the remaining four subterranean alcoves located in the Damping Ring straight sections, an underground substation is powered utilizing RMUs. The LV distribution in the Damping Ring tunnel uses multiple LV switchboards. The LV in the tunnel provides general power to lighting, outlets, and possibly minor machine system loads. Switchboards are generally located in the alcoves together with the substation and RMU.

The sources are essentially concentrated in short tunnels and caverns. The equipment for each of the sources is fed from a short MV system with RMUs. Dedicated LV transformers are installed for the RF for the source capture sections and SCRF injector linacs. The remaining part of the electrical load is powered from the conventional power distribution system.

4.3.4 Interaction Region

The power requirements of the detectors are currently not known. The current design is estimated based on a detector load requirement of 3 MVA, scaled down from CMS. A MV cable system, RMUs, LV transformers and switchboards has been reserved for the detectors.

4.3.5 Emergency Supply Systems

The emergency supply system is based on stand-by diesel generator systems. Each generator set supplies a protected substation, which is normally supplied by the utility power. During a utility power interruption, the diesel engines start automatically and transfer the critical load when ready. On return of utility power, the diesel generator systems synchronize to the utility power system and the load is re-transferred back to the utility power system, after which the diesel generator systems shut down.

Due to voltage drop considerations, the generator output voltage must be transformed up to a MV level. The Main Linacs and the RTML zones are equipped with a MV system with RMUs at regular spacing. The Damping Ring tunnel is also equipped with a MV system, originating at one access shaft with a RMU in each alcove or cavern. Each MV system is completed by exiting the adjacent access shaft to the surface. Each of the RMUs feeds the critical load through a LV transformer and switchboard. Any critical system which cannot accept any power interruption is provided with an Uninterruptible Power Supply (UPS) system, or no-break systems.

TABLE 4.3-2
Various Voltage Levels Utilized by Regions. Note that there are two levels of HV distribution utilized for the Americas and Asian sample sites

Voltages	Europe	America	Asia
Transmission	400 kV	345 kV	275 kV
Distribution	36 kV	69 kV	66 kV
Distribution	36 kV	34 kV	6.6 kV
Distribution	400/230 V	480/277 V	400/200 V

4.3.6 Miscellaneous Technical Issues

Power quality considerations A separation of pulsed and non-pulsed systems may be needed to avoid interference between certain loads. Reactive power compensation and harmonics filtering may also be needed, depending on the non-linear load and the dynamic behaviour of the load, especially the RF (Modulator) system.

4.3.7 Regional Variations

Table 4.3-2 gives an overview of the various voltages assumed for the different regions.

European Sample Site: The description of the power distribution given above is primarily that adopted for the European site (and the cost estimate). The utility voltages are 400 kV, with the MV levels set to 36 kV. LV levels are typically 400 V (three phase) and 220-240 V (single phase).

Asian Sample Site: The distribution of power is slightly different to that documented above. The utility voltage is 275 kV, and is transformed to 66 kV and distributed via the Service Tunnel to the secondary substations located in each access base caverns. Secondary substations transform the voltage to 6.6 kV which is then distributed to local LV transformers. A LV system of 400 V (three-phase) and 100-200 V (single-phase) is supplied via local transformers from the 6.6 kV system. The system applies to power transport and distribution in the entire underground areas.

Americas Sample Site: The Americas distribution also varies slightly in that the utility voltage of 345 kV is first transformed to 69 kV at the master substation. The 69 kV is routed through the tunnel to each shaft, and then up the shaft to where it is stepped down to the medium distribution voltage (34.5 kV).

4.3.8 Information Network

Site-wide communications are in general supported via a fiber-optic based LAN system. For the underground areas, local LAN racks are located in the tunnel at an interval of approximately 200 m, which serve as the primary connection point to the end equipment (via electrical cables). From here the signals are sent to sub-center LAN racks located in the Shaft Bases, and finally to the main control center.

The LAN supports the following equipment:

- General digital data transfer.
- Telephone system: 1,800 cordless lines and 240∼360 fixed lines are assumed. Cordless telephones are supported in the underground areas via IP transmitters.

- Public address system (including safety address system): for the underground areas, speakers are mounted every 10 m of tunnel.

- Security CCTV and other video monitoring where needed (both surface buildings and underground areas).

- Fire alarms, smoke detectors etc.

In the case of the critical safety-related systems, emergency back-up power is supplied from the standby generator in case of power failure.

4.4 AIR TREATMENT EQUIPMENT

Figure 4.4-1 shows the air-flow and treatment for a typical section of Main Linac. Conditioned ventilation airflow of 68,000 m³/hr is ducted down every major shaft and routed into the Service Tunnel at the base of the shaft or Access Cavern in both directions. Air flows through the Service Tunnel to the midpoint between the major shafts (∼2.5 km) where it is directed through a protected air passageway into the Beam Tunnel and returned back to the shaft area. The return air is ducted to the surface where 15% (10,200 m³/hr) of the stale air is vented to the outdoors, and an equivalent amount of fresh conditioned outside air is mixed back in with the remaining circulated air. While at the surface, the air is cooled, dehumidified and/or heated as needed to achieve a neutral dry condition approximately 24-27°C dry bulb and 40% relative humidity. The supply air is then ducted back to the Service Tunnel. This air flow pattern requires evaluation by radiation safety personnel.

The conditioning units are located on the surface and reject tunnel heat and moisture to the ambient air. Air is supplied to the tunnel at a flow rate of approximately 27 m/min; this provides one complete air exchange every 6 hours in the entire tunnel volume. Additional non-conditioning exhaust and supply fans are provided at each shaft to double and/or reverse the airflow during emergency operation. Common ducts are used for both systems separated by configuration control dampers. Elevator shafts and exit vestibules are provided with separate air systems for control and pressurization during emergency operation.

TABLE 4.4-1
HVAC Requirements

Location	Temperature (drybulb)	Dewpoint	RH	Air Flow
e- Source	29°C	<13°C	<35%	27 m/min
Damping Ring	40°C	<13°C	<20%	27 m/min
Main accelerator service tunnel	29°C	<13°C	<35%	27 m/min
Main Linac beam tunnel (not contr.)	>30°C	<13°C	<35%	27 m/min
BDS beam tunnel	29-32°C	<13°C	<35%	27 m/min
IR hall	29-32°C	<13°C	<35%	27 m/min

4.4.1 Controls

The temperature and humidity in the Service Tunnel are primarily set by regional standards for allowing personnel to be in the tunnel at moderate work levels with no required rest periods. The requirements for the tunnels in each of the system areas are summarised in Table 4.4-1. In general, air temperature in the Service Tunnel is controlled at 27-29°C using chilled water Fan Coil Units (FCU), as described in Section 4.2.5. In the Main Linac sections, the FCUs are located at every RF unit.

Temperature control in the Main Linac Beam Tunnel is not provided because of the relatively low heat loads. The humidity level is maintained by the air circulation from the Service Tunnel and by packaged dehumidification units located approximately every 100 meters. Beam Tunnel temperatures in the BDS are maintained locally at 40-43°C by FCUs.
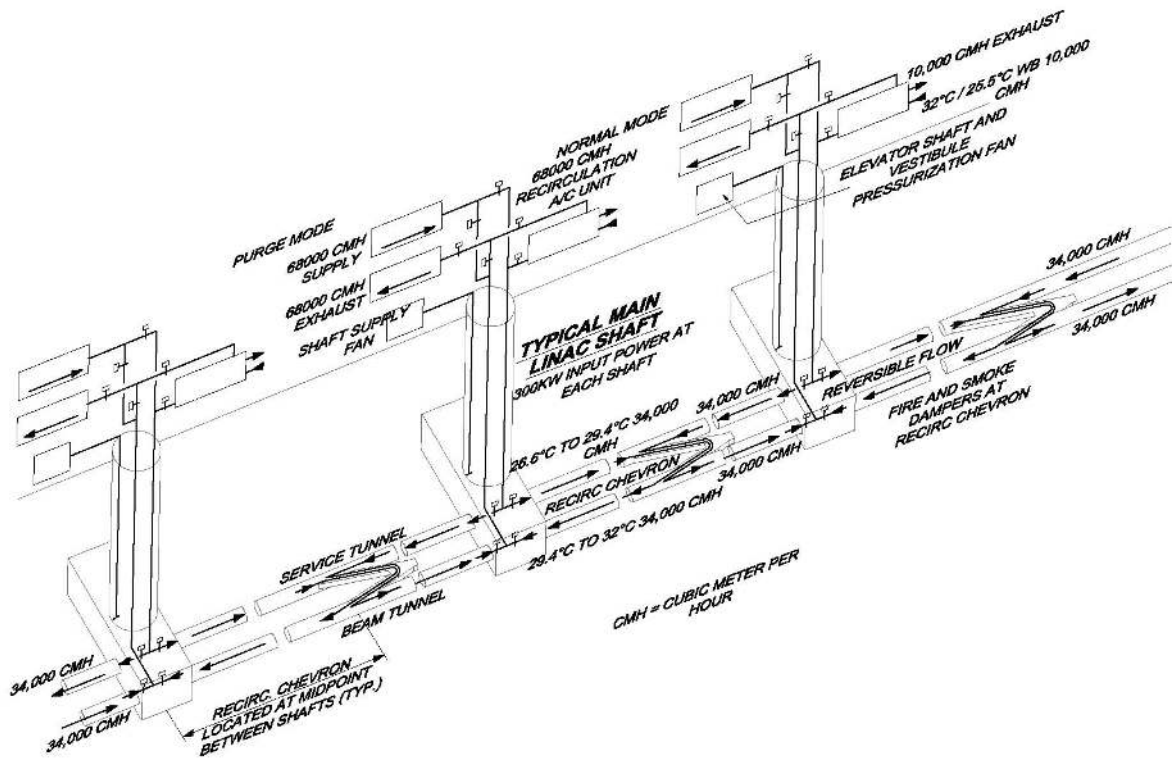
FIGURE 4.4-1. Air Treatment Concept for the Main Accelerator Housing.

4.5   PROCESS COOLING WATER

Cooling water is required as a heat rejection medium for technical components such as the water cooled RF components, water cooled magnets, and water dumps in the BDS. The majority if not all of these require low conductivity/deionized water (LCW). Further study is needed to establish water quality requirements. The following descriptions present a reference solution that is generally applicable for all regions, ignoring minor regional site differences.

4.5.1   Heat Loads

Table 4.5-1 summarizes the estimated heat-loads broken down by Area Systems. Of the total load of ~182 MW, over half is attributed to the Main Linac. Table 4.5-2 lists the heat loads for the Main Linac RF unit.

TABLE 4.5-1
Summary of Heat Loads broken down by Area System

Area System	LCW (MW)	Chilled Water (MW)	Total (MW)
Sources e$^-$	2.880	1.420	4.300
Sources e$^+$	17.480	5.330	22.810
DR e$^-$	8.838	0.924	9.762
DR e$^+$	8.838	0.924	9.762
RTML	9.254	1.335	10.589
Main Linac	56.000	21.056	77.056
BDS	10.290	0.982	11.272
Dumps	36.000	0.000	36.000
Total Heat Load (MW)			182

4.5.2   System Description

There are two water cooling systems; Process Water and Chilled Water. Chilled Water is used for water cooled racks in each RF area and for fan coils that remove the heat rejected to the tunnel air. The Process Water handles the water cooled technical components. The scope of the Process Water cooling included in conventional facilities includes the surface cooling towers, pumps, controls, cavern heat exchangers, skids and piping headers, and distribution and valving up to the water cooled components. Final hose connections to each water-cooled technical component are included in the relevant Technical System. The tower system for the cryogenics is considered part of the Cryogenics Technical System.

All water systems are closed loop. The cooling tower type is a closed circuit cooler similar to a dry cooler. The tower works dry by releasing the heat directly to the air during most of the year. During hot periods in the summer seasons, the towers/coolers are wetted with water in order to guarantee the supply temperature. This setup minimizes and conserves water and treatment chemicals and associated cost, as compared to typical open type towers. The closed circuit coolers also minimize plume from the tower. The make-up water to the

TABLE 4.5-2
Typical Main Linac RF Component Heat Loads

Components	Tunnel	Total (KW)	Average (kW)	To Water (KW)	To Air (KW)
RF Charging Supply 34.5 KV AC-8 KV DC	service	4.0	4.0	2.8	1.2
Switching power supply 4kV 50kW	service	7.5	7.5	4.5	3.0
Modulator	service	7.5	7.5	4.5	3.0
Pulse transformer	service	1.0	1.0	0.7	0.3
Klystron socket tank / gun	service	1.0	1.0	0.8	0.2
Klystron focusing coil (solenoid)	service	4.0	4.0	3.6	0.4
Klystron collector/ body/windows	service	58.9	47.2	45.8	1.4
Relay racks (instrument racks)	service	10.0	10.0	0.0	-1.5
Circulators, attenuators & dummy load	beam	42.3	34.0	32.3	1.7
Waveguide	beam	3.9	3.9	3.5	0.4
Subtotal Main Linac RF unit (KW)			120		

system and tower is supplied from a well with proper water treatment, from each surface water plant.
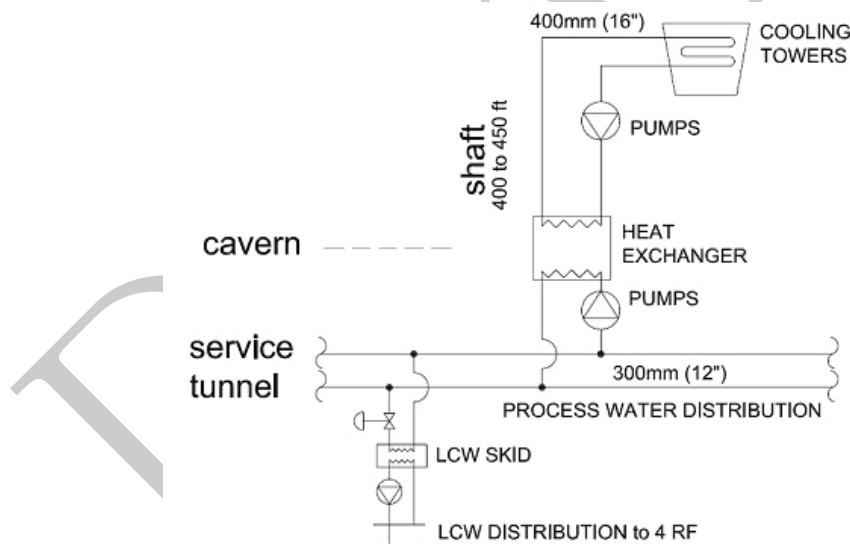
FIGURE 4.5-1. Process Water System at Shaft 7 Plant.

Figure 4.5-1 shows a schematic of a typical Process Water Plant. The Process water system has three closed water loops:

- The first is a water/glycol mixture loop from the surface cooling tower to the cavern heat exchanger at 29.4°C supply temperature.
- The second is a process water loop from the cavern heat exchanger at 32.2°C supply temperature to the LCW skid in the Service Tunnel. The heat exchanger in the cavern is needed to offset the effect of the static head on system pressure due to the tunnel depth.

- The third is the demineralized/LCW water from the skid at 35°C supply temperature.

The supply water temperature has a tolerance of ±0.5°C. The basis for pipe sizing and costing is for a ΔT ~11°C water system. The return pipe is thermally insulated to reduce the heating of the tunnel air. This setup is applicable for the Main Linac; a variation of this scheme is used for other areas. In the case of the Process Water supply to the large BDS (main) beam dumps, a near surface buried piping distribution from a surface plant at the IR location is fed into each dump cavern hall through individual drilled shafts. (The cooling system for the main high-powered beam dumps is discussed elsewhere.)

The Chilled Water system provides ~6.6°C supply temperature water to fan coils and to the water skid for racks. The water skid, in turn, regulates and provides the proper temperature (above dew point) to the water cooled RF racks. The major components for this system are the same as for the Process Water except for the addition of Chillers on the surface. All chilled water piping is thermally insulated (see Fig. 4.5-2).
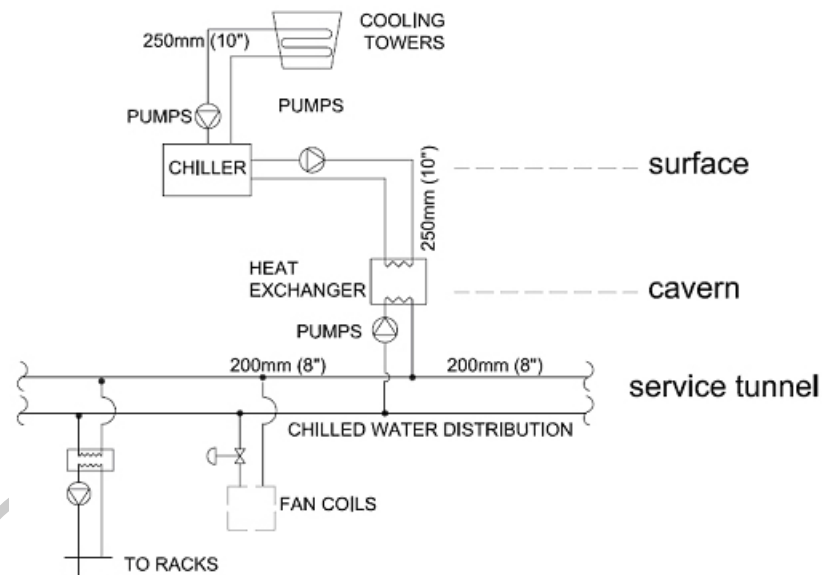
FIGURE 4.5-2. Chilled Water System at Shaft 7 Plant.

4.5.3 Locations and Distribution

The main distribution of the Process Water system follows the major shaft and cryogenic distribution locations. There are twelve surface water plants. For the reference solution, the distribution is simplified to minimize the number of area systems served by each water plant (considered consistent with the current estimate). Only the Main Linac RF system has been considered in any detail. Estimates for other areas have been scaled from the Main Linac model based on their respective loads.

One Low Conductivity Water (LCW) skid is used for cooling all the water cooled technical components for every four Main Linac RF units. Each LCW skid includes one stainless steel centrifugal pump (with no standby), one plate heat exchanger, controls, stainless steel expansion tanks, and miscellaneous fittings and accessories.

Similar to the LCW skid, one chilled water skid for racks is provided for every 4 RF units. This skid is a commercially available package coolant modulating unit typically used in data center rack applications. Each skid includes a multi-stage centrifugal pump, brazed plate heat exchanger, 3-way control valve, expansion tank, flow switch and integrated controls.

4.6 SAFETY SYSTEMS

4.6.1 Radiation safety

The radiation safety systems are described in Section 2.9.4.

4.6.2 Fire Safety

Because there are no existing laws and standards in any region which directly and compre-
hensively stipulate the safety measures for a facility like ILC, the currently planned safety
measures are based on examples of existing accelerator tunnels and the regulations for build-
ings and underground structures of various types. The final plan will be subject to the
approval of the competent authority that has jurisdiction over the selected site.

Evacuation of the underground Service Tunnel is the primary concern, due to the relatively
high level of cables. In the event of a fire in the Service Tunnel, personnel can escape to the
safety of the Beam Tunnel via the Beam-Service Tunnel personnel cross-overs, located every
500 m (see Figure 4.6-1). Egress to the surface is only possible at the shafts, located every 5
km. Assuming a walking speed of 1 m/s, 500 m between emergency egress points is considered
acceptable (~8 minutes maximum). During beam operations, triggering of a fire alarm will
immediately de-energize the machine, making it safe for personnel to enter the Beam Tunnel.

During access periods or installation, when personnel are present in the Beam Tunnel,
emergency egress can be either to the Beam or Service Tunnel, depending on the location of
the fire.
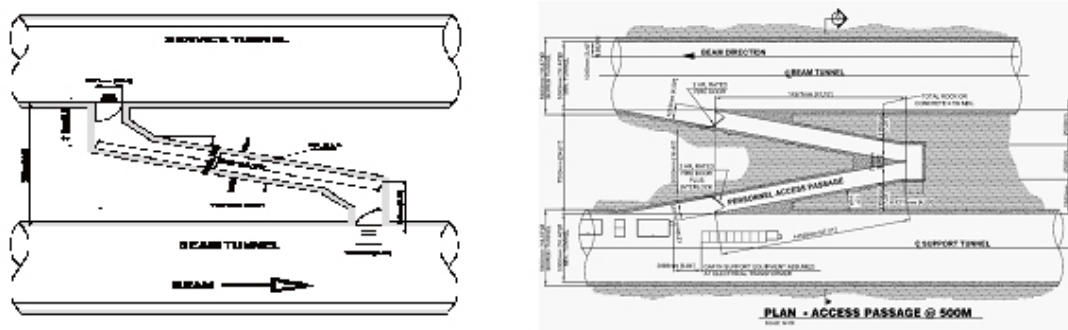
FIGURE 4.6-1. Examples of the personnel cross-connection passages between the Service and Beam
Tunnels (left Asia and Europe, right Americas). The geometry of the passage is designed to reduce the
radiation levels in the Service Tunnel to acceptable levels.

For the Damping Rings (during installation and maintenance), emergency egress is to a
separate safety enclosure behind a fire wall within the tunnel (see Section 4.2.2).

In all cases, personnel can either safely escape to the surface via the nearest shaft, or
remain in a fire-safe area until the emergency services respond.

Smoke detectors are installed in all underground tunnels and halls at intervals of 30 m.
Manual alarms (buttons) are located at intervals of 100 m. Alarm bells are also installed at
intervals of 100 m. A smoke exhaust fan of 60,000 m^3/hr is installed at each Shaft Access

Building on the surface. 1.2 m^2 ducts are installed in the Access Shafts/Tunnels to connect the fans and the Access Hall.

No emergency smoke exhaust system is installed in the tunnels. Instead, movement of the smoke is retarded by 1.5 m high walls mounted to the top of the tunnels at intervals of 50 m. Simulations using software developed and widely used in Japan indicate this solution is more effective than a mechanical exhaust system

Provisions for the required emergency fixtures are also included in the current estimate:

- emergency lighting located every 8 m
- illuminated exit signs installed above every exit door in the underground spaces
- illuminated exit direction signs installed at intervals of 20 m in the underground spaces

- portable chemical powder fire extinguishers (3.0 kg) placed every 30 m in the Service Tunnel, Beam Tunnel and for Asia Site the Access ramps
- large size fire extinguishing equipment (30 kg) located every 200 meters in the Access Halls and the Experimental Hall.

Sprinklers, hydrants and water curtains have not been specified to avoid possible water damage to the machines.

4.6.3 Safety Access Control

Access control equipment such as a card lock is installed at the entrances to the radiation control areas as required by the radiation safety plan.

4.6.4 Safety for Helium

The helium supply system is equipped with an oxygen meter which activates an alarm and stops the gas supply in case of oxygen deficiency. Air in the Beam Tunnel is automatically pressurized.

4.7 SURVEY AND ALIGNMENT

Survey and alignment covers a very broad spectrum of activities, starting from the conceptual design of the project, through the commissioning of the machines, to the end of operations. The cost estimate developed covers the work necessary until successful completion of the machine installation. It includes equipment needed for the tasks to be performed, and equipment for a dedicated calibration facility and workshops. It also includes the staff that undertake the field work, and the temporary manpower for the workshops. Full time, regular staff is considered to be mainly dedicated to organizational, management, quality control, and special alignment tasks. The cost estimate is mostly based on scaling the equivalent costs of the LHC to the ILC scope.

4.7.1 Calibration Facility

A 100 m long calibration facility is needed for the calibration of all the metrological instruments. The facility is housed in a climate controlled and stable building. Due to the range limit of current day commercial interferometers against which the instruments are to be compared the facility has been restricted to 100 m. A mechanical and an electronic workshop are also needed during the preparation phase and throughout the entire project. They are used for prototyping, calibration, and maintenance of the metrological instruments.

4.7.2 Geodesy and Networks

A geodetic reference frame is established for use across the whole site, together with appropriate projections for mapping and any local 3D reference frames appropriate for guaranteeing a coherent geometry between the different beam lines and other parts of the project. An equipotential surface in the form of a geoid model is also established and determined to the precision dictated by the most stringent alignment tolerances of the ILC.

The geodetic reference frame consists of a reference network of approximately 80 monuments that cover the site. These monuments are measured at least twice, by GPS for horizontal coordinates, and by direct leveling for determining the elevations. The first determination is used for the infrastructure and civil engineering tasks. The second, and more precise determination, is used for the transfer of coordinates to the underground networks prior to the alignment of the beam components. A geodetic reference network is also installed in the tunnel and in the experimental cavern. For costing purposes it is assumed that the reference points in the tunnel are sealed in the floor and/or wall (depending on the tunnel construction) every 50 m. In the experimental cavern, the reference points are mostly wall brackets. The underground networks are connected to the surface by metrological measurements through vertical shafts. The distance between two consecutive shafts does exceed 2.5 km in most cases.

4.7.3 Civil Engineering Phase

The layout points which define the tunnel locations and shapes are calculated according to the beam lines in the local 3D reference frame. The tunnel axes are controlled as needed during the tunnel construction. All tunnels, including profiles, are measured in 3D using laser scanner techniques when the tunnels are completed. The same process is applied to the experiment

cavern(s) and other underground structures. The buildings and surface infrastructure are also measured and the as-built coordinates are stored in a geographical information system (GIS).

4.7.4   Fiducialization

Systematic geometrical measurements are performed on all beamline elements to be aligned prior to their installation in the tunnels. The alignment of elements installed on common girders or in cryomodules is first performed, and the fiducial targets used for the alignment in the tunnels are then installed on the girders (cryomodules) and all individually positioned elements. The positional relation between the external markers and the defining centerlines of the elements are then measured. For this report, an estimated 10,000 magnetic elements were assumed to need referencing. It is also assumed that most corrector magnets do not need fiducialization. This number does not account for instrumentation, collimators, or other special beam elements.

4.7.5   Installation and Alignment

The trajectories of all the beamlines are defined in the local 3D reference frame which covers the entire site. The location of reference markers at the ends of each beam line element to be aligned are defined in this reference system, together with the roll angle giving a full 6 degrees of freedom description of element location and orientation. Likewise the position of all geodetic reference points is determined in this reference frame.

Prior to installation, the beamlines and the positions of the elements are marked out on the floors of the tunnels. These marks are used for installing the services, and the element supports. The supports of the elements are then aligned to their theoretical position to ensure that the elements can be aligned whilst remaining within the adjustment range of the supports.

After installation of services such as LCW and cable trays, the tunnels are scanned with a laser scanner. The point clouds are then processed, and the results inserted into a CAD model. A comparison with theoretical models is used by the integration team to help identify any non-conformity and prevent interference with the subsequent installation of components. The current requirements for the one sigma tolerances on the relative alignment of elements or assemblies are given in Table 4.7-1.

The components are aligned in two steps:

- A first alignment is performed to allow connection of the vacuum pipes or interconnection of the devices. This is done using the underground geodetic network as reference.

- After all major installation activities are complete in each beamline section, a final alignment, or so-called smoothing, is performed directly from component to component in order to guarantee their relative positions over long distances.

To reach and maintain the positioning tolerances of the final doublets in the BDS IR, a 150 m straight reference line is set up as close as possible to the beam components. This line, consisting of a laser or stretched wire and hydrostatic levels, is housed in a dedicated gallery built parallel to the beam tunnel, and goes through the experimental cavern. This allows for the geometrical connection between the beam lines and the detector.

TABLE 4.7-1
Component Alignment Tolerances

Area	Type	Tolerance
Sources, Damping Rings and RTML	Offset	150 μm (horizontal and vertical), over a distance of 100 m.
	Roll	100 μrad
Main Linac (cryomodules)	Offset	200 μm (horizontal and vertical), over a distance of 200 m.
	Pitch	20 μrad
	Roll	
BDS	Offset	150 μm (horizontal and vertical), over a distance of 150 m around the IR.

4.7.6   Information Systems

The theoretical positions of all the components to be aligned on the beam lines is managed in a dedicated database. This database is also used for managing all the geodetic and alignment measurements and the instrument calibrations. All measurement data are captured and stored electronically and subsequently transferred to the database. Pre-processing of the measurements are carried out in the database and then dedicated software for data analysis is used to calculate the best fit position of the elements and components. These results are also stored in the database where they can be accessed for further post-processing, analysis and presentation. A geographic information system (GIS) is set up for managing all location data.

4.8 CFS COST METHODOLOGY

The cost for the ILC CFS has been developed internationally with teams in each of the three regions (Americas, Asia and Europe). These teams have worked closely together to optimize the CFS design, based on the requirements supplied by the Area and Technical Systems.

To make use of the available resources for the design and cost work, a detailed WBS for the project was produced, containing up to 5 levels of detail. This WBS was then broken down into site-dependent and site-independent sections. For the site-dependent estimates, the CFS group established a set of uniform definitions for underground construction unit costs. This ensured consistency across all three regions. Estimates for each unit cost were independently produced by experts and consultant engineering firms in each of the three regions (the Civil Engineering falls into this category, for example) and then used to develop each site-dependent design. The remaining site-independent parts were then divided up amongst the regional teams to produce single estimates as follows:

Civil Construction	Regionally developed
Electrical: site-dependent	Regionally developed
Electrical: site-independent	European estimate used
Air treatment facilities	Americas estimate used
Process cooling water	Americas estimate used
Handling equipment	European estimate used
Safety systems	Asian estimate used
Survey and Alignment systems	European estimate used

Cost estimates in all three regions were developed using the same criteria and drawings. information was drawn from consultant engineers, historical data from other accelerator or similar projects, industry standard cost estimating guides, and where applicable the scaling of costs from similar systems. In all cases, the estimates reflect a median value for the work based on the criteria provided to date and the pre-conceptual level of design maturity. There are no factors for contingency contained in any of the CFS costs estimates. Costs for activities that take place prior to the construction start are explicitly not included in the estimate. Some examples of such costs are A/E Services before the start of construction, development costs for geotechnical and environmental investigation, land acquisition costs and cost incurred for compliance with local governmental statutes and regulations. These costs cannot be accurately identified until a specific site selection is made.

4.9   INSTALLATION PLAN

4.9.1   Overview

The baseline ILC covers a large geographical area over 30 kilometers long that includes a complex network of $\sim$72 km of underground tunnels at a depth of approximately 100 m. An overall schematic layout of the ILC is shown in Figure 4.9-1. These tunnels house most of the technical equipment needed to operate the accelerator. There are $\sim$2,000 cryomodules, over 13,000 magnets and approximately 650 high level RF stations to be installed. These and other technical components are described in the Area and Technical System sections of this report. The schedule for construction of the ILC is assumed to be 7 years as described in Section 6.3. This section describes the model that was developed and costed for the installation of all components on an appropriate schedule.
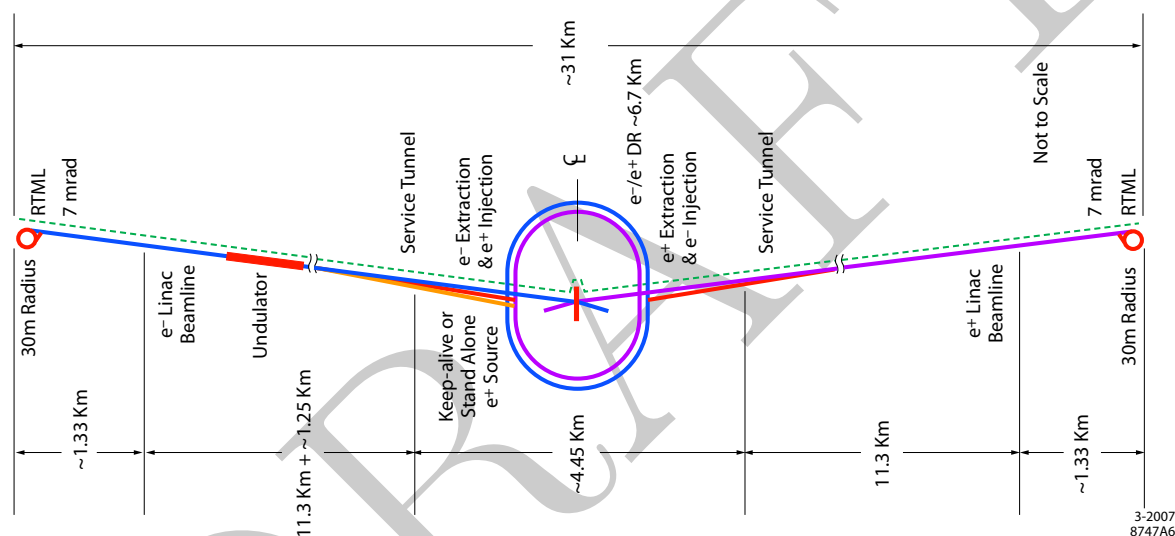
FIGURE 4.9-1. Schematic layout of ILC.

4.9.2   Scope

The installation plan covers all activities required to prepare, coordinate, integrate, and execute a detailed plan for the complete installation of the ILC components as well as associated site-wide logistics. It includes all labor, incidental materials and equipment required to receive, transport, situate, affix, accurately position, interconnect, integrate, and checkout all components and hardware from a central storage or subassembly facility to their operational location within the tunnels. The premise is that installation recieves fully tested assemblies certified for in-tunnel installation. It does not include component fabrication, assembly, quality control or commissioning. It also does not include the basic tunnel utilities provided by conventional facilities, such as ventilation, air conditioning, fire prevention, high voltage electrical and low-conductivity water distribution.

4.9.3 Methodology

For the RDR, the goal was to understand and define the scope of installation work sufficiently to develop a reasonable model for a first stage of planning and costing. The model was based on a work breakdown structure (WBS) that listed all of the activities required for installation of the technical systems, including the management, planning, and engineering support.

The installation WBS was broken down into two major level-of-effort categories, General Installation and Area Systems Installation. General Installation included all common activities and preparations and associated logistics on the surface. Area System Installation included all efforts required for complete installation of the components underground. General Installation was further broken down into logistics management, engineering support, equipment, vehicles, shipping-receiving, warehousing, and transportation. Area System Installation covered the six machine areas, electron source, positron source, damping rings, RTML, main linac and beam delivery. Each element of the WBS for both General and Area System was then extended two levels of effort further and populated with required labor as well as incidental material and equipment costs, as described below. Table 4.9-1 shows the top-level installation WBS.

TABLE 4.9-1
Top-Level WBS Installation.

WBS					Component
1	7	3			Installation
1	7	3	1		General Installation
				1	Logistics management
				2	Engineering support
				3	Equipment
				4	Vehicles
				5	Shipping & receiving
				6	Warehousing
				7	Surface transport
1	7	3	2		Area System Installation
				1	Sources e$^-$ area installation
				2	Sources e$^+$ area installation
				3	Damping Rings area installation
				4	RTML area installation
				5	Main Linac area installation
				6	Beam Delivery area installation

The installation cost estimate for the "Cold" Linear Collider from the 2003 US Technology Options Study was used as a starting point for developing the ILC WBS. This was adjusted for the differences between that design and the ILC as well as for lessons learned from other projects. Available information from the WBSs developed for NLC and TESLA was incorporated wherever possible, as was pertinent material from similar installation projects at APS,

FNAL Main Injector, KEKB, LHC, PEP-II, SLC and SPEAR-III, as well as installation plans for SSC and the European XFEL. The scope, complexity and salient features of these other machines were compared with the ILC.

To populate the WBS, a comprehensive list of components was compiled and interfaces and boundaries with the technical systems carefully defined. As an example of such cost/scope definition, it was assumed for magnet installation that fully tested and measured magnets complete with supports, anchor bolts, and other required materials were delivered to a surface staging area, along with any special instrumentation or handling equipment. The installation group transported the device to the proper location, arranged for alignment, installed the device and instrumentation, and connected it to the local power, water and cryogenic systems. Details of which group supplied the cables, hoses or fittings were explicitly specified, as were testing responsibilities.

The estimates for labor and equipment required to install the components came from a wide variety of sources. For conventional components, like beampipes and magnets, the technical systems provided estimates, based on experience with other projects. Visits to CERN and DESY provided data on installation of cryomodules, LHC magnets and the CMS detector as well as the opportunity to observe actual installation procedures. RSMeans 2006 cost data (North America's leading supplier of construction cost information) was used in estimating total work-hours needed for installing equivalent size/weight equipment under similar conditions. Since the main linac is a major cost driver, the installation of cryomodules and RF sources was modeled in detail. This is described in the next section. For other systems where there was not an appropriate experience base, the estimates were scaled from similar installation tasks based on an assessment of complexity.

The resulting estimates were subjected to a variety of cross-checks and reviewed for completeness and appropriateness by technical and area system leaders. The estimates were compared with individual estimates from other sources, and with the actual manpower used for the installation of recent accelerator projects. The labor estimate for the particular cryomodule installation tasks was also independently calculated by a second engineering team, and the results were in agreement to within 13%. An additional check was that the overall installation costs were 7% of the total level of effort. This is consistent with the estimate from the 2003 Options Study where the installation effort was 7% and with the installation costs for other projects studied which also averaged 7%.

Figure 4.9-2 shows the distribution of installation effort between General and Area Systems and between the various Area Systems, where the Main Linac accounts for almost half of the effort.

4.9.4 Model of Main Linac Installation

At this stage of the ILC design, it is too early for a complete model of the entire installation sequence. The Main Linac cryomodules and rf sources represent a major installation effort so a bottoms-up model for their installation was developed. The model was derived from that in the TESLA TDR. Installation was assumed to take place over a period of 3 years with half a year ramp up time. Labor productivity was taken to be 75%, or 6 hours per shift, given transport distances and handling difficulty.

Before starting installation, the section of the main linac beam and support tunnels must be completely ready for joint occupancy, along with one large and two small associated access shafts. The installation sequence was first to fix the cryomodule supports, then to move
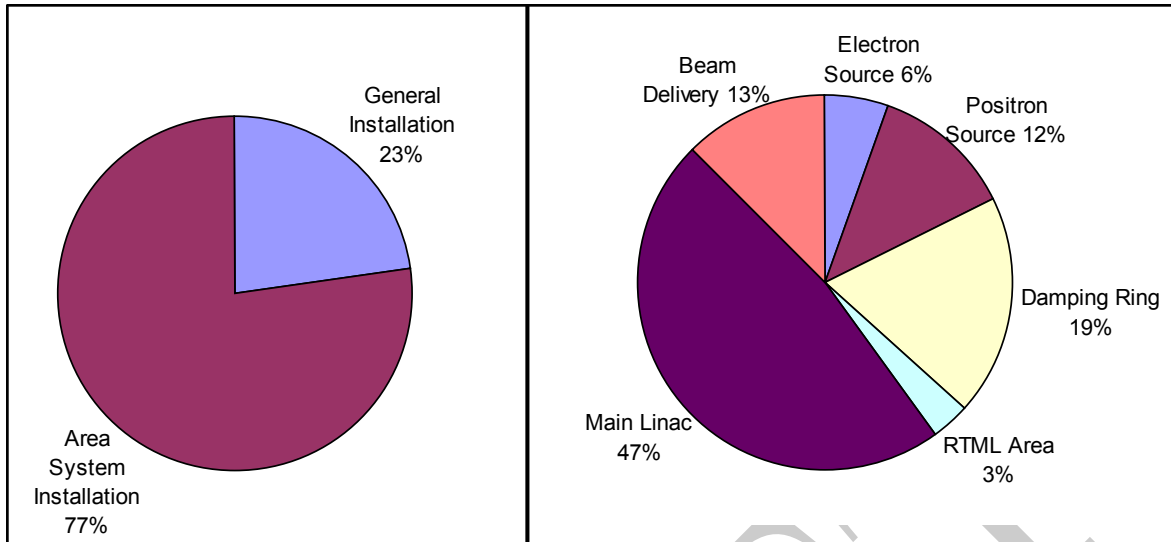
FIGURE 4.9-2. Distribution of effort between General and Area Systems and between Areas.

the cryomodules from the access shafts, install the cryomodule and complete the cryogenic, vacuum and rf connections. Figure 4.9-3 is a schematic of the cryomodule indicating the number of connections to be made. The installation rate was three cryomodules (one RF unit) and associated services per day for each crew. The model included the number and size of equipment, distances to installation, speed of transportation and estimates of number of staff and hours for each task.
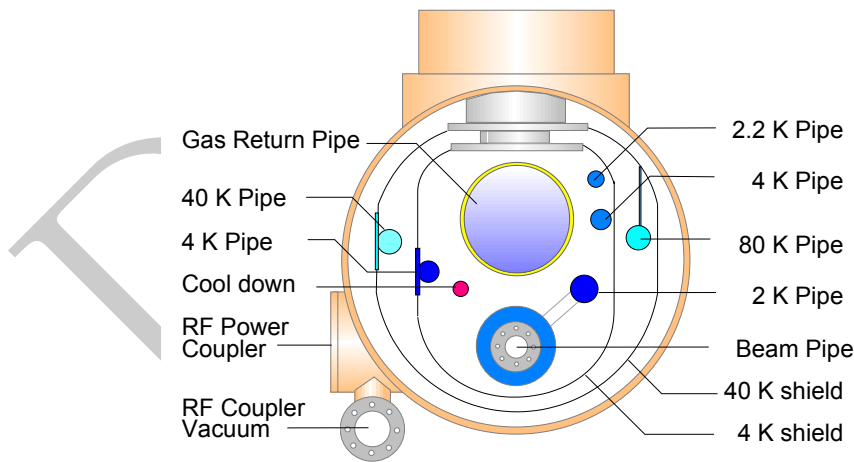
FIGURE 4.9-3. Schematic of the cryomodule showing multiple connections.

The study concluded that a total of 72 person-days are required to install 3 cryomodules. This labor includes engineers and technicians from a variety of specialties. The 3 cryomodules account for only about 20% of the effort to assemble an entire RF unit (and everything in this 38 m length of beam and support tunnels) so the installation estimate for an entire RF unit was taken to be 5 times the cryomodule estimate. The other components include, klystrons, modulators, control racks, cable trays, control cables and RF waveguides. Such a section of

the tunnels and components are shown in Figure 4.9-4.
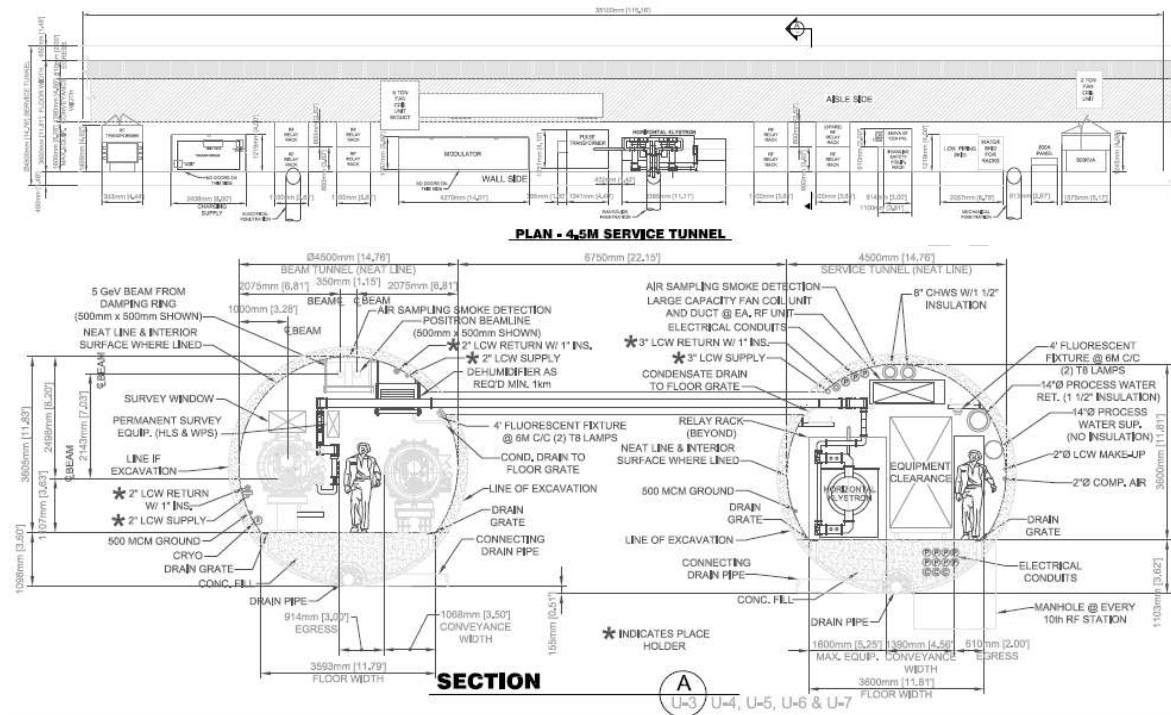
FIGURE 4.9-4. Plan view of service tunnel components in Main Linac (upper). Cross section of two Main Linac tunnels (lower).

4.9.5 Modelling

Installation planning of the large and complex ILC machine requires the creation of 3-D computer models of all the major components as well as the underground facilities. To create a cost effective, timely and safe installation plan, certain facility conditions must be assumed to exist prior to installation. Some examples include the availability of utilities, communication systems, above ground warehousing and equipment staging areas. Below ground, the personnel access rules, including safety and emergency considerations, must be defined and the schedule of equipment and tunnel availability must be known. Once these and the details of the technical components are known, a very general model, both in time and 3-D space, can be developed as is shown below for the main linac (see Figure 4.9-5).

Here the 72 man crew is working in a (moving) 1 km section of the tunnels at the 3 cryomodule per day rate, showing the different activities which spread over a 6 week time span. Two crews are working independently starting at shafts 2 and 6 and working towards shaft 4. Similar activities and crews will be working in other sections of the linac tunnels when they become available. This is also true for the central complex of injectors and damping rings.
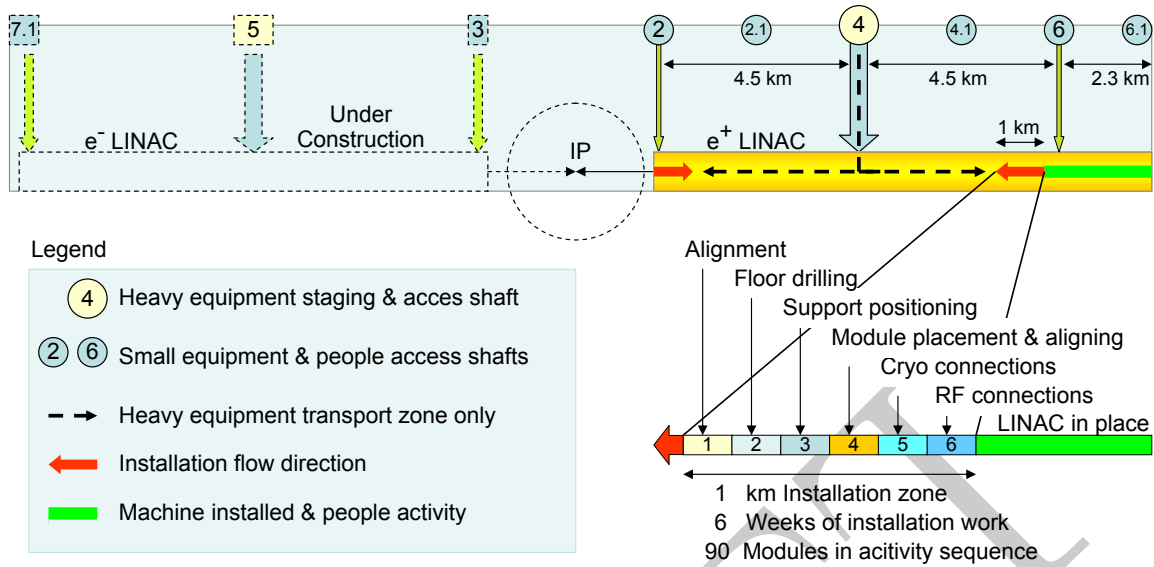
FIGURE 4.9-5. Installation model for main linac component installation in underground segment.

The RDR estimate assumed a 3 year installation schedule, a six month period of ramp up and on the job training, and a 75% efficiency. In tunnel activities are concentrated on day shift, with transport and staging on swing shift. Figure 4.9-6, shows a model of multishift manpower versus time, indicating the total manpower necessary to fit all of the installation activities into that 3.5 year period. During the peak 3-year period, there are over 500 people on day shift and another 300 on swing shift in various parts of the tunnel. There are also about 100 people involved in surface logistics.
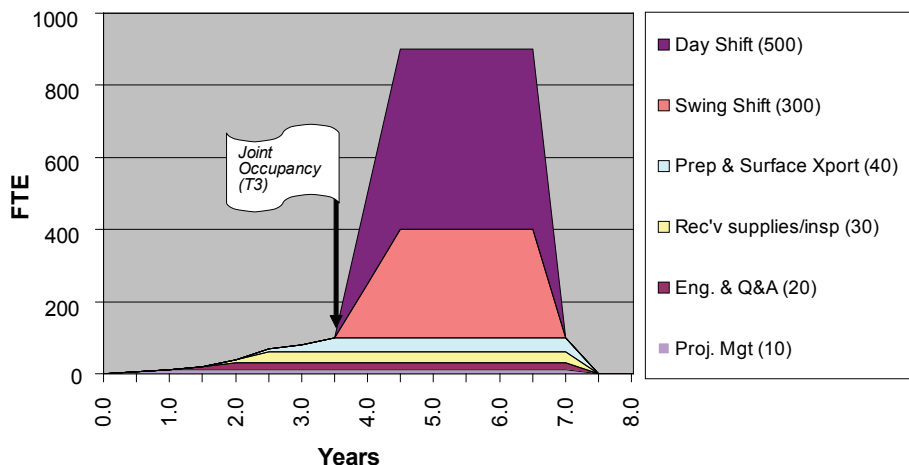
FIGURE 4.9-6. Required human resources versus time for the installation effort.

In the absence of a detailed fabrication plan for the major machine components, a very top level installation schedule was developed to integrate with a 7 year construction schedule. This will continue to be refined as more information on fabrication schedules become available.

CHAPTER 5

Sample Sites

5.1 INTRODUCTION

For this reference design, three 'sample sites for the ILC were evaluated. Each site was required to be able to accommodate all the conventional facilities for the 500 GeV CM machine; in addition, the sites needed to have the sufficient length to support an upgrade of the machine to 1 TeV CM, assuming the baseline main linac gradient. There were two reasons for the use of three sample sites for this reference design:

- This procedure demonstrates that each region can provide at least one satisfactory site for the ILC. This is important, since it shows that any of the regions has the potential to be a host for the project.

- The cost of, and technical constraints on, the project could depend strongly on the site characteristics. Since the actual site is not yet known, it is important to assess a range of sites with a diverse set of site characteristics, to provide confidence that when the actual site is chosen, it will not present unexpected technical difficulties or major surprises in cost.

In addition to the three sample sites presented, a second European sample site near DESY in Hamburg, Germany, has also been developed. This site is significantly different from the other sites, both in geology and depth ($\sim$25 m deep), and requires further study.

The Joint Institute for Nuclear Research has also submitted a proposal to site the ILC in the neighborhood of Dubna, Russian Federation.

The three sites reported in detail here are all deep-tunnel solutions. The DESY and Dubna sites are both examples of shallow sites. A more complete study of a shallow site – either a shallow tunnel or a cut-and-cover site – will be made in the future as part of the Engineering and Design phase.

5.2 AMERICAS SITE

5.2.1 Location

The Americas sample site lies in Northern Illinois near the existing Fermi National Accelerator Laboratory. The site provides a range of locations to position the ILC in a north-south orientation. The range is bounded on the east by the Fermilab site, and extends some 30 km to the west. For the purpose of this document and the RDR estimate, a site alignment that is roughly centered on Fermilab was selected. While this site is more developed than an alignment to the west, there is a reasonable construction path and the location benefits more directly from the existing Fermilab site and facilities.

While the routing requires the tunnel to pass below residential areas, the shafts can be located in non-residential areas. It is highly possible that no homes will be physically affected by this project. Roughly one quarter of the alignment is on Fermilab property, including the ILC central campus and IR. The Fermilab site, is located approximately thirty-five miles west of downtown Chicago. The area surrounding Fermilab is comprised of residences, research facilities, light industry, commercial areas, and farmland. Higher population densities are found to the east with more rural and farm communities to the west. The towns and villages around Fermilab vary in population size from ten thousand to over one hundred thousand people. The surrounding communities have established schools, hospitals, infrastructure support functions and local governments.

The Fermilab site borders on a local railroad line with a railroad hub located within four kilometers to the south. Major roads connect Fermilab to the Illinois toll road system within two miles of its gates. Access to OHare International Airport and Midway Airport are via highways with travel times to these airports of less than one hour. Steel mills and other heavy industry are located both in Illinois and in neighboring states.

5.2.2 Land Features

The existing surface of northern Illinois is primarily flat, with surface elevations ranging from 200 meters to 275 meters above sea level. Much of the eastern half of northern Illinois is developed with Chicago suburban communities and municipalities including many commercial, residential and industrial complexes. Underdeveloped areas are currently used for agriculture. Major water bodies include Lake Michigan located approximately 65 kilometers east of Fermilab, the Illinois River approximately 30 kilometers southeast of Fermilab and the Fox River 3 kilometers west of Fermilab. An intricate highway system extends throughout the northeastern Illinois area.

The 2751 hectare (6800-acre) Fermilab site is also relatively flat with less than 15 meters of fall from northwest to southeast. Approximately one-third of the Fermilab site is developed with various high-energy physics accelerator complexes or related experimental areas. The remaining two thirds are equally split between leased agricultural uses and open space including prairies, wetlands and recreational areas. A series of paved roadways exist throughout Fermilab.

5.2.3 Climate

The climate is typical of the Midwestern United States which has four distinct seasons, and a wide variety of types and amounts of precipitation with moderate variations between

monthly and seasonal average values. In summer, temperatures ordinarily reach anywhere between 26°C to 33°C and humidity is moderate. Overnight temperatures in summer are usually around 17°C. Yearly precipitation averages 920 mm. Winter temperature averages -2°C during the daytime, and -10°C at night. T emperatures can be expected to drop below -18°C on 15 days throughout the winter season.

5.2.4   Geology
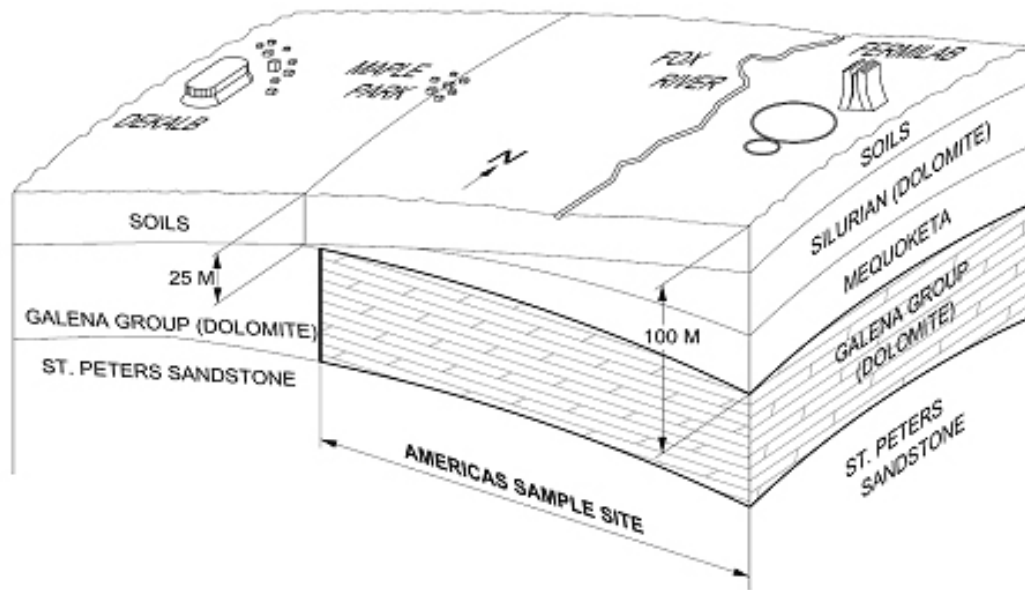
FIGURE 5.2-1. Geology of the Americas Sample Site

The tunnels are located in the Galena Platteville layer (Fig. 5.2-1), which is characterized as a fine to medium grained dolomite, that is cherty. The Maquoketa shales overlaying the dolomite have a low hydraulic conductivity that will act as a hydrogeologic barrier between upper overburden aquifers and the dolomite. At the proposed siting, the Galena Platteville varies from 100 to 125 meters in thickness, gently rising in datum elevation from the south to the north. The Galena is covered by 15 to 30 meters of shale, 15 to 25 meters of Silurian dolomite which in turn, is overlaid by 15 to 45 meters of overburden. The upper Silurian dolomite found at the Fermilab site disappears for alignments further to the west. These geologic conditions should provide a relatively dry tunnel, both during construction and during operations, but it is expected that some grouting will be required. The Galena is the most structurally sound rock in the area and, in general, should not require any extraordinary rock support methods.

5.2.5   Power Distribution

Electric power to the Northern Illinois area is provided by Exelon Generation with access to approximately 35,000 MW of electricity . Electrical power is generated by fossil fuel, hydroelectric, wind and nuclear power generating systems and distributed in Northern Illinois.

5.2.6   Construction Methods

Conventional un-shielded tunnel boring machines are used for the tunnels. No temporary support is required, permanent support can be pattern spaced rock bolts or dowels. Production rate is anticipated to be 30 m/day. Caverns are excavated using drill and blast methods. Temporary supports are required for the largest spans, permanent support is provided by rock bolts. Production rate for medium to large size caverns where mechanized equipment can be employed is estimated at 1,200 cm/wk. Shaft overburden is excavated using standard earth excavators and muck boxes, supported by ring beams and timber lagging, keyed into the underlying rock. Excavation through the limestone and shale to the final depth uses conventional Drill & Blast methods. Support is provided by resin encapsulated rockbolts and the shaft is reinforced and concrete lined.
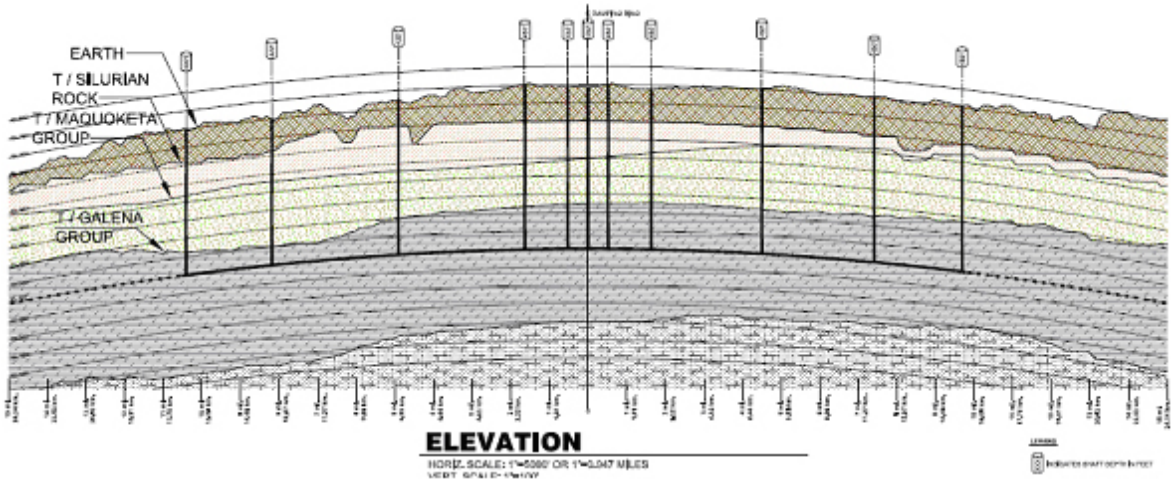
FIGURE 5.2-2. Longitudinal Profile of the Americas Site in Northern Illinois

5.3   ASIAN SITE

5.3.1   Location

A set of about 50 criteria have been used over the past decade to evaluate a large number of ILC candidate sites in Japan. Out of these candidates, a sample site was selected for the RDR with an endorsement by the ILC-Asia group at its 4th meeting in November 2005. It satisfies the following criteria, some overlapping with the criteria matrix developed by the CFS Global Group:

- Firm and uniform geology to ensure stable beam operation at the interaction region.
- Sufficient length to accommodate straight tunnels spanning over 50 km.
- Absence of any known, active faults in the neighborhood.
- Absence of epicenters of any known earthquakes exceeding M6 within 50 km from anywhere in the site since AD1500.
- Uniform altitude of the terrain so that the ILC tunnel depth is less than 600 m throughout.
- Availability of sufficient electrical power for ILC operation.
- Existence of a practical construction plan for the underground tunnels and caverns.
- Suitable environment, in terms of climate and access, for smooth operation.

The Asian site is located in a moderate plateau area (low mountains) in uniform solid rock. It is within 10 to 20 km of cities which provide a living environment with reasonable quality of life. The neighboring cities are connected to an international airport within several hours by both bullet train and highway.

5.3.2   Land Features

The site surface is dominated by woods and is partly occupied by an agricultural area which is crossed by occasional local paved roads. Only a few local residences exist along the tunnel route. There are no major high-ways or streets with heavy traffic and no large river systems which cross the tunnel route. Hence, very few sources of natural or human-made vibrations exist. An adequate flat surface area is available to accommodate surface facilities. Existing local roads can be utilized as access routes to entrances of the tunnel.

5.3.3   Climate

The climate is mild. There is snowfall in winter but only for a short period. It is not too hot in summer. There is no recorded history of major typhoons.

5.3.4   Geology and Tunnel Structure

The 31 km ILC tunnels for the first project phase can be constructed within solid hard rock. In the second project phase, when the tunnels are extended to 50 km, one side of the main linac tunnel will pass through an area with sedimentary rock, but this geology is also solid. The depth of the tunnels, which will be built in a low mountainous part of the site, is in the range between 40 m and 600 m. Most of the access to the tunnel is provided by sloped ramps

(Fig. 5.3-1). An exception is the access to the interaction region which has a vertical shaft approximately 112 m deep.

Past experience with Japanese construction projects indicates that the uniform granite has sufficient strength that the tunnels and caverns do not require reinforcement by rock bolts or concrete lining. Shotcrete is used to cover the inner surfaces of the tunnels. Excavation of very large caverns, such as the experimental hall, may require reinforcement by rock bolts.

5.3.5   Power Distribution System

The site is located in the neighborhood of an existing 275 kV power grid. It is considered to be reasonably straightforward to supply the power of 240 MW required for the 500 GeV ILC. Power failures in Japan are very rare, and even if they occur, the system average interruption duration index (SAIDI) [1] has been only 13 minutes, according to the statistics of the Ministry of Economy, Trade and Industry of Japan.

5.3.6   Construction Methods

The geology is uniform hard granite below 20 m of softer topsoil and weathered rock. The access shafts are sloped tunnels excavated by NATM (New Austrian Tunneling Method), except for the IR hall. These tunnels match the mountainous geography and allow vehicle transport of personnel and materials. They are 7.5 m x 7.0 m to accommodate access for the TBM. From the surface to a depth of 20 m, the tunnel is reinforced by rock bolts, a 15-20 cm thick shotcrete liner and steel supports. In the granite, the tunnel is reinforced by rock bolts and 5 cm thick shotcrete.

The IR vertical shafts are excavated by drill and blast, with metal supports and a concrete lining. Caverns are excavated by NATM. The top of the arch is excavated by advancing top drift method with drill and blast. Reinforcement is by rock bolt, pre-stressed bolt and sprayed concrete 20 mm thick with a metal mesh, overlaid by a 1.5 m thick cast concrete liner on the arch. The lower part of the cavern is excavated by drill and blast. After reinforcement in the same method as the top, the side wall is finished with 1.0 m thick concrete, and the concrete floor cast 2.0 m thick. Passageways are excavated manually and finished with sprayed mortar and pre-mixed fiber 20 mm thick.

---

[1] System average interruption duration index = sum of customer interruption durations normalized by the total number of customers served

FIGURE 5.3-1. Detail of an Access Ramp for the Asian Sample Site

FIGURE 5.3-2. Longitudinal profile of the Asian Sample Site in Japan

5.4   EUROPEAN SITE

5.4.1   Location

The European site for the ILC is located in the north-western part of the Geneva region near the existing CERN laboratory. The area is fairly well populated; the more than 30 km long path of the accelerator crosses the border between France and Switzerland three times and passes under several villages. The region around the accelerator path is mainly covered with agricultural lands and some forests. There are some biologically protected zones and historical places or memorials in the area but the site does not affect national parks.

The proposed site meets all the main requirements of the ILC Project. Colliders have been in operation in this area for more than three decades, including the new Large Hadron Collider (LHC) that will start operating soon. The geological characteristics allow construction of tunnels for the accelerator and its support equipment in a stable rock formation with little seismic activity at a depth of 80 - 110 meters.

CERN and the Geneva area have at their disposal all necessary infrastructure to accommodate specialists for the period of the accelerator construction, to store and assemble the equipment, and to provide for the project-production support during manufacturing of the special-purpose equipment. Due to the importance of Geneva as headquarters of many international organizations and to the existing colliders at CERN, all necessary modern network and information infrastructure is available.

The international airport of Geneva is situated only 5 km away from CERN and is served by Swiss Rail and connected to the European railway network. The highway connecting Switzerland and France (Northern Europe to Southern Europe) passes nearby. The access roads to CERN are suitable for all necessary transportation to deliver the equipment of the accelerator itself and its technical systems.

The governments of France and Switzerland have existing agreements concerning the support of particle accelerators in Geneva area, which make it very likely that the land for the accelerator location could be made available free of charge, as they did for previous CERN projects.

5.4.2   Land Features

The proposed location of the accelerator is situated within the Swiss midlands embedded between the high mountain chains of the Alps and the lower mountain chain of the Jura. CERN is situated at the feet of the Jura mountain chain in a plain slightly inclined towards the lake of Geneva. The surface was shaped by the Rhone glacier which extended once from the Alps to the valley o f the Rhone. The water of the area flows to the Mediterranean Sea. The absolute altitude of the surface, ranges from 430 to 500 m with respect to sea level.

5.4.3   Climate

The climate is warm-continental. The mean temperature of the air of the coldest month (January) is -0.2°C. The mean temperature of the air of the warmest month (July) is +18.4°C. The mean annual rainfall is 928 mm. Snow usually falls in the months of December to February. On the whole, the climate in the vicinity of Geneva is considered to be quite comfortable.

5.4.4 Geology

Most of the proposed path of the ILC is situated within the Molasse, an impermeable sedimentary rock of the Swiss midlands laying over the Jurassic Bedrock. The path crosses a fault at the valley of the Allondon river which is situated South-West of Geneva and filled with sands and gravels. In this valley, the tunnels are built below the groundwater level. For the 1 TeV extension of the projectd, the tunnel will cross a second valley at Gland, situated North-East of Geneva, and will just enter some Jurassic limestone.

. The alignment of the ILC accelerator is placed at a level of 370 m in the Molasse (Fig. 5.4-1). This makes it possible to excavate the tunnels with shielded tunnel boring machines (TBM-S) with a high penetration rate and simultaneous placement of precast concrete segments. For the crossing of the Allondon and Gland valleys, the shielded tunnel boring machines mustl be replaced by hydro mix-shield machines (SM) able to tunnel in closed mode through the sands and gravels below groundwater level and to work in open mode as a normal tunnel boring machine in the Molasse.

5.4.5 Power Distribution System

The European sample site provides sufficient electrical power for the accelerator complex. A nearby 400 kV substation of the French grid will serve as connection point. The availability of the network is considered adequate for the LHC and is thus likely to also be sufficient for the ILC.
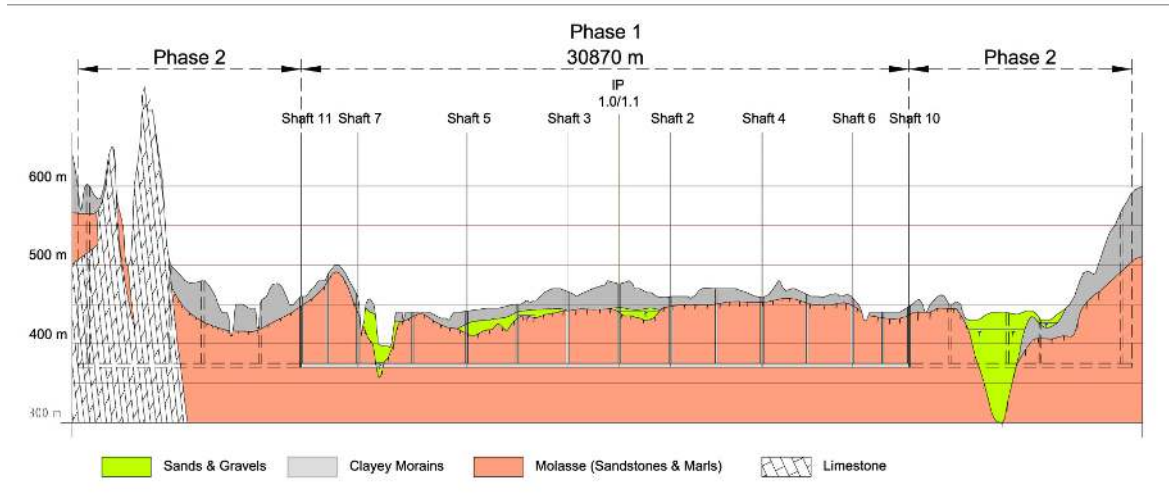
FIGURE 5.4-1. Longitudinal Profile of the European Sample Site near CERN.

5.4.6 Construction Methods

The upper parts of the shafts lie in dry moraines, with total thickness ranging from 0 to 50 m, depending on the situation. Traditional means can be used to excavate down to sound rock, except in water bearing sands and gravels where it will be necessary to use other techniques such as diaphragm walling to allow safe excavation of the shafts. Once in the rock (sandstone)

the shafts and caverns are excavated with the use of rock breakers and road headers, with blasting as a possible exceptional resort. After the temporary lining (rock bolts, mesh and shotcrete) is in place, the walls and vaults are sealed with waterproof membranes and covered with cast in-situ reinforced concrete.

Shielded Tunnel Boring Machines (TBM-S) with a prefabricated concrete segment lining are used for the long tunnels. An average daily advance of 25 m/day is assumed. The concrete tunnel floors are then cast in-situ. Short tunnel sections (less than 300 m) and passageways are excavated with road headers or small size rock breakers, then shotcreted. The penetrations between tunnels are excavated with small diameter boring machines, anchored in one of the two tunnels.

5.5   SUMMARY

Although the three sample sites have differences, they all meet the ILC design requirements and at comparable cost. Table 5.5-1 compares some of the salient features.

TABLE 5.5-1
Summary of notable features of the sample sites and construction methodology.

Subject	Americas Region	Asian Region	European Region
Sample site location	Northern Illinois – near FNAL.	Japan	Geneva Area – near CERN
Land features	200 ∼ 240m above sea level	120 ∼ 680 m above sea level	430 ∼ 480 m above sea level
Geology	Dolomite	Granite (sedimentary rock in phase-2 extension)	Molasse (sedimentary rock / sandstone)
Tunnel depth from surface	100 ∼ 150m	40 ∼ 600 m	95 ∼ 145m (except 1 valley 30 m)
Access paths to underground caverns	13 shafts 9m, 14m, 16m diam 100 ∼ 135 m deep	10 sloped tunnels (7.5m × 7m × 700 ∼ 2000m) and 3 shafts (for IR)	13 shafts 9m, 14m, 16m diam 100 ∼ 135m deep
Tunnel construction	TBM	TBM	TBM
Tunnel lining	20% of length shotcreted	100% of length shotcreted	100% of length precast concrete segments
Average tunnel excavation speed	30m/day/TBM (boring)	16m/day/TBM (boring + surface work)	25m/day/TBM (boring)
Number of TBMs	9	15 (6 out of 9 accesses have two TBMs starting in opposite directions)	9
Cavern construction	Drill and blast	Drill and blast (NATM)	Road breaker /header
Shaft construction	Earth excavation / Drill and blast	Drill and blast (step by step method)	Road breaker/header (Moroccan method)
New surface buildings	92	166	120
Distribution voltage	69/34 kV	66/6.6kV	36kV

DRAFT

CHAPTER 6

Value Estimate

6.1 VALUE ESTIMATING METHODOLOGY

6.1.1 Introduction

The ILC is an international scientific project to be funded by a collaboration of countries or regions around the world, each of which have different traditions and conventions for planning and estimating the cost of large projects. In order to equitably divide up contributions among the collaborators, one must develop a project estimate that is independent of any particular accounting system but compatible with all of them. The "VALUE" methodology has become the standard for such international projects. It was adopted by ITER (the international thermonuclear experimental reactor project) and by the LHC experiments, among others. Value is a particularly convenient concept for dealing with "in-kind" contributions, for which manufacturing costs and labor rates can vary widely between collaborators. Conversion of the value estimate to various national costing practices can only be done by each participating nation.

The ILC estimate consists of two important parts: VALUE (in terms of currency units) for items provided and LABOR (in terms of person-hours or person-years), which may be provided by the collaborating laboratories and institutions, or may be purchased from industrial firms. This is similar to what has been traditionally used for European project proposals. The value of a component is defined as the lowest reasonable estimate of the procurement cost in adequate quality, based on production costs in a major industrial nation. It is expressed in 2007 currency units (not escalated to the years in which the funds are projected to be spent) and does not include R&D, pre- or post-construction or operating costs, taxes or contingency. It is effectively the barest cost estimate that would be used by any of the funding agencies. Individual regions can then add to the base value any other items usually included in their own estimating system.

In this context, LABOR is defined as "explicit" labor, which may be provided by the collaborating laboratories and institutions, or may be purchased from industrial firms. This to be distinguished from a company's "implicit" labor associated with the industrial production of components and contained (hidden) within the purchase price. The implicit labor is included in the VALUE part of this estimate.

The ILC VALUE plus LABOR estimate is the basis on which contributions are apportioned among the collaborators. Each participant makes an agreement with the ILC man-

agement to provide a certain value of components and services. They are then responsible for providing the contracted items, independently of what they actually cost.

6.1.2 Scope of Estimate

The estimate is for a 500 GeV center-of-mass machine but includes some items sized for 1 TeV to enable a later energy upgrade, such as the beam dumps and the length of the Beam Delivery tunnel. The ILC estimate does not include the cost of the detectors. They are assumed to be funded by a separate agreement between the collaborating institutes, in the way the LEP and LHC detectors were built. The estimate does include civil engineering work for the detectors, e.g. assembly buildings, underground experimental halls, shafts, etc.

The estimate covers all aspects of construction, including tooling-up industry, final engineering designs and construction management. The estimate specifically does not include costs for any of the engineering, design, or preparation activities that can be accomplished before construction start. It does not include Research and Development, proof-of-principle or prototype systems tests, pre-construction (e.g. architectural engineering, conceptual and construction drawings, component and system designs and preparation of bid packages), commissioning, operation, decommissioning, land or underground easement acquisition costs. It also does not include items which are treated differently from region to region such as taxes, escalation, or contingency. Table 6.1-1 summarizes the items that are included in, or excluded from, the value and labor estimate.

The estimate assumes a seven-year construction period. The estimate for a given item covers the cost from the day the project obtains funding until that item is installed, tested, and ready for commissioning. Commissioning in one area may overlap with construction elsewhere. The construction period ends when the last component has been installed and tested.

6.1.3 Estimating Approach

The ILC estimate was developed by the RDR matrix of Area, Technical and Global System leaders working with the Cost Engineers. The Area Systems Leaders (AS) defined the requirements for their accelerator systems. The Technical (TS) and Global System (GS) Leaders provided the estimated value and explicit labor per component unit. Specialized components such as the polarized electron gun were estimated by the Area Systems themselves. The AS leaders then compiled the estimate for their areas. The estimates were iterated to optimize cost and performance.

The cost estimates were prepared using a Work Breakdown Structure (WBS) where each item included a description, basis of estimate, quantity required, materials and services estimate and implicit and explicit labor. These could then be summed to produce to an estimated total cost for the component, system, or section of the machine. There were 351 active WBS elements, where each element represented a roll-up of further detailed estimating information provided by the systems leaders. An example of the lower level of detail for one of these WBS elements provided by the Conventional Facilities and Siting group is presented in the Appendix.

TABLE 6.1-1
Summary of the items that are included in, or excluded from. the value and labor estimate.

Included	Excluded
Construction of a 500 GeV machine, including items sized to enable a later energy upgrade	
Tooling-up industry, final engineering designs and construction management	Engineering, design, or preparation activities that can be accomplished before construction start, such as, research & development, proof-of-principle or prototype systems tests, pre-construction
Construction of all conventional facilities, including the tunnels, surface buildings, access shafts and others	Surface land acquisition or underground easement acquisition costs
Construction of the detector assembly building, underground experimental halls and detector access shafts	Experimental detectors
	Commissioning, operations, decommissioning
Explicit labor, including that for management and administrative personnel.	Taxes, contingency and escalation

6.1.3.1 General Guidelines

The ILC estimate is given as the sum of VALUE (in currency units) and explicit LABOR (in person-hours).

Guidelines and Instructions for performing, preparing, and presenting the cost estimate are available at

http://www-ilcdcb.fnal.gov/RDR_costing_guidelines.pdf

http://www-ilcdcb.fnal.gov/RDR_Cost_Estimating_Instructions_23may06.pdf

Estimates are quoted as median or 50%-50% estimates, where, if a given item were to be independently purchased many times, taking the lowest world-wide bid each time, half of the purchases would be below the median estimate and half above.

6.1.3.2 Currency Rates and Raw Materials

Component estimates from all three regions were converted to a common cost basis, the ILC Unit, where one ILC Unit is set equal to $1 U.S. (January 2007 value) The conversion rates used were:

$$1 \text{ ILC Unit} = 1 \text{ US 2007\$} (= 0.83 \text{ Euro} = 117 \text{ Yen})$$

These currency exchange rates are an average of the exchange rates over the five years 2003 through 2007. The value estimates were developed during 2006 and then adjusted to January, 2007 using the official regional cost escalation indices.

Electricity and raw materials such as niobium, steel or copper are assigned fixed prices as of January 1, 2007, as summarized in Table 6.1-2.

TABLE 6.1-2
Assumed prices for electricity and representative raw materials

Resource	Jan 1, 2007 Price
Electricity:	$0.10 per kWh (including supply cost)
Copper:	$8 per kilogram
Black steel:	$0.6 per kilogram (up to three times higher price for stainless and magnet steel)
Niobium:	$70 per kilogram

6.1.3.3 Contingency and Risk

The ILC estimate does not contain contingency. Contingency is a quantitative measure of risk – the final number is set higher than the initial estimate to allow for unexpected or uncontrollable factors that may raise the ultimate price. The ILC project will avoid any future cost increases through R&D, industrial studies, vendor pre-qualifications, and competitive, global calls for tender. The risk analysis is being done and will be included in the final version of this RDR.

6.1.4 Component Estimates

Three different classes of items were identified and approached differently.

- *Site specific*: The costs for many aspects of conventional facilities are site specific and there are separate estimates for sample sites in all three regions: Asia, Europe, and the Americas. These costs are driven by real considerations, e.g. different geology and landscape, availability of electrical power and cooling water, etc. Site dependent costs due to formalities (such as local codes and ordinances) are not included. Common items such as internal power distribution, water and air handling, which are essentially identical across regions although the implementation details differ, have a single estimate. The sample sites have different geologies. Nevertheless, they use similar tunnel-boring machine technologies and the value estimates are very close. Because a site has not yet been chosen, the ILC value estimate is taken as the average of the three site-dependent estimates. Individual estimates for each of the three sites are also provided.

- *High technology*: Items such as cavities, cryomodules, and rf power sources, where there is interest in developing expertise in all three regions, have been estimated separately for manufacture by each region. Costs are provided for the total number of components along with parameters to specify the cost of less than the total number. The European estimate for the cavities and cryomodules is used for the ILC value as it is the most mature, in terms of R&D and industrial studies. Estimates from the other regions provide a crosscheck.

- *Conventional*: Estimates for components, such as conventional magnets and controls, which can be produced by many manufacturers in all regions, are based on a world-wide call for tender. They are the lowest reasonable cost available world-wide, for production in a major industrial nation.

Component estimates include the manufacturer's implicit labor, EDIA (engineering, design, inspection, and administration), quality control/assurance, and technical testing. A single supplier is assumed to be responsible for one deliverable, even though in practice, multiple suppliers may be chosen to reduce risk. The estimates quoted for mass-produced technical systems were generated either by detailed bottom-up industrial studies for the quantities required, or by assuming a learning curve [1] explicitly in an in-house engineering estimate. The basis of estimate and cost estimating methodology for each set of components are discussed in the individual Area System, Global System, and Technical System sections for this report.

6.1.5 Explicit Labor

Explicit labor is estimated separately from component costs, and is given in person-hours. It may be provided by the ILC collaborators as in-kind contributions, drawn from existing laboratories with their own personnel and budgets, or may be purchased from industrial firms. To convert person-hours to person-years, it was assumed that laboratory staff works an average of 1,700 hours per year. Only three classes of manpower are used: engineer/scientist, technical staff, and administrative staff.

6.2   ESTIMATE FOR CONSTRUCTION OF ILC

6.2.1   Value Estimate

The value and explicit labor estimates are current as of February 1, 2007, and will be updated in the final report. The preliminary value estimate presented here is for the cost of the ILC in its present design and at the present level of engineering and industrialization. The estimate contains three elements:

- 1.78 Billion (ILC Units) for site-dependent costs, such as the costs for tunneling in a specific region
- 4.87 Billion (ILC Units) for shared value of the high technology and conventional components
- 13,000 person-years for the required supporting manpower (=22 million person-hours)

For this value estimate: 1 ILC Unit = 1 US 2007\$ (= 0.83 Euro = 117 Yen)

A common estimate was used for all non site-specific technical components, regardless of region. The three regional site-specific estimates were based on local costs for civil engineering and the primary high voltage electrical power connections, feeds, substations and primary cooling water systems. All three site-dependent estimates are within a few percent of the average.

There are many possible models for dividing the responsibilities among the collaborating regions. The numbers below present one possible model where the estimates are divided into site-specific and shared parts. In this model, the host region is expected to provide the site-specific parts, because of the size, complexity, and specific nature of these elements. The site-specific elements include all the civil engineering (tunnels, shafts, underground halls and caverns, surface buildings, and site development work); the primary high-voltage electrical power equipment, main substations, medium voltage distribution, and transmission lines; and the primary water cooling towers, primary pumping stations, and piping. Responsibilities for the other parts of the conventional facilities: low-voltage electrical power distribution, emergency power, communications, HVAC, plumbing, fire suppression, secondary water-cooling systems, elevators, cranes, hoists, safety systems, and survey and alignment, along with the other technical components, could be shared between the host and non-host regions. Such a model may be summarized as shown in Table 6.2-1.

TABLE 6.2-1
Possible division of responsibilities for the 3 sample sites (ILC Units).

	Region	Site-Specific	Shared	Total
	Asia	1.61 B	4.86 B	6.47 B
	Americas	1.89 B	4.87 B	6.76 B
	Europe	1.85 B	4.86 B	6.71 B
and	Average	1.78 B	4.87 B	6.65 B
plus 13 K person-years of explicit labor				
or 22 M person-hours 1,700 hours/year				

The value estimates broken down by Area System are shown separately for both the conventional facilities and the components in Figure 6.2.1 and Table 6.2-2. Common refers to

infrastructure elements such as computing infrastructure, high-voltage transmission lines and main substation, common control system, general installation equipment, site-wide alignment monuments, temporary construction utilities, soil borings and site characterization, safety systems and communications.

The component value estimates for each of the Area (Accelerator) Systems include their respective RF sources and cryomodules, cryogenics, magnets and power supplies, vacuum system, beam stops and collimators, controls, Low Level RF, instrumentation, installation, etc.. The superconducting RF components represent about 65% of the estimate for all non-CF&S components.
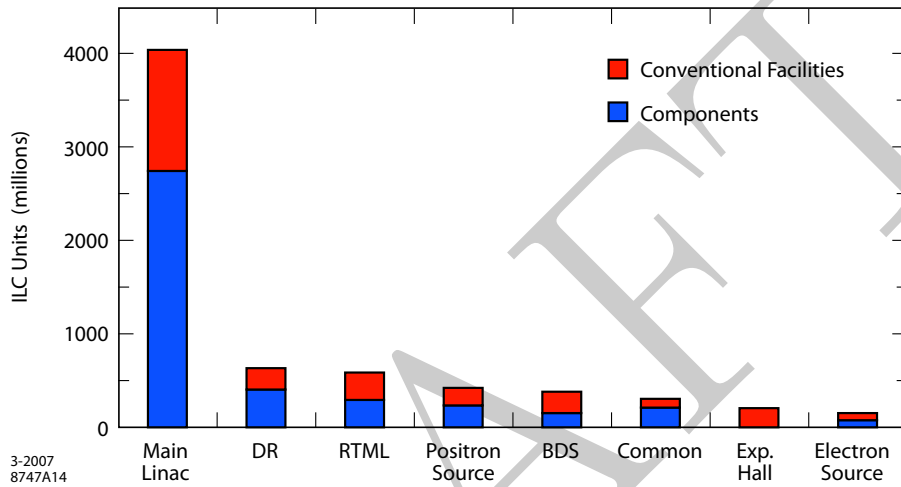
FIGURE 6.2-1. Distribution of the ILC value estimate by area system and common infrastructure. The estimate for the experimental detectors for particle physics is not included. (The Americas region estimate for Conventional Facilities has been used here as an example.)

TABLE 6.2-2
Distribution of the ILC Value Estimate by Area System and Common Infrastructure, in ILC Units. The estimate for the experimental detectors for particle physics is not included. (The Americas region estimate for Conventional Facilities has been used here as an example.)

Area - M	Total	Components	Conventional Facilities
Main Linac	4,038	2,762	1,275
DR	647	415	232
RTML	590	319	271
e^+ source	429	242	187
BDS	383	158	224
Common	323	228	95
Exp Hall	200	0	200
e^- source	151	94	57
Sum	6,760	4,219	2,540

6.2.2   Explicit Labor Estimate

The explicit labor for the Global Systems, Technical Systems, and specific specialty items for Electron Source, Positron Source, Damping Rings, and Ring to Main Linac, include the scientific, engineering, and technical staff needed to plan, execute, and manage those elements including specification, design, procurement oversight, vendor liaison, quality assurance, acceptance testing, integration, installation oversight, and preliminary check-out of the installed systems.

Installation is the largest fraction of explicit labor, about 39%. Management is the second largest fraction at about 18%. At this stage of the ILC design, it is too early for a complete analysis of installation requirements. Instead, the RDR estimate was based on scaled information from a variety of sources, including the actual manpower used for the installation of recent accelerator projects. There was also a bottoms-up study for installation of the cryomodules for the Main Linac done by two separate engineering teams, with comparable results. The estimates were reviewed by experts and crosschecked for reasonability.

In the present estimate, the installation task is characterized almost exclusively as explicit labor, with minimum costs for material-handling equipment. This is on the assumption that much of the installation and system check-out labor at the ILC site can be contributed by the staffs of collaborating institutions or laboratories. The validity of this assumption depends on the availability of the necessary skilled manpower and local labor regulations. Because of the size of the project, it is likely that many tasks like electrical and plumbing work will need to be outsourced to industry. Trade-offs and translations are likely between using in-house labor and external contracts. It is estimated that a minimum of 10% of the installation task must be management and supervision by in-house manpower.

The management model is similar to that of the construction phase of the Superconducting Super Collider (SSC), but without central computing staff which are included elsewhere. The
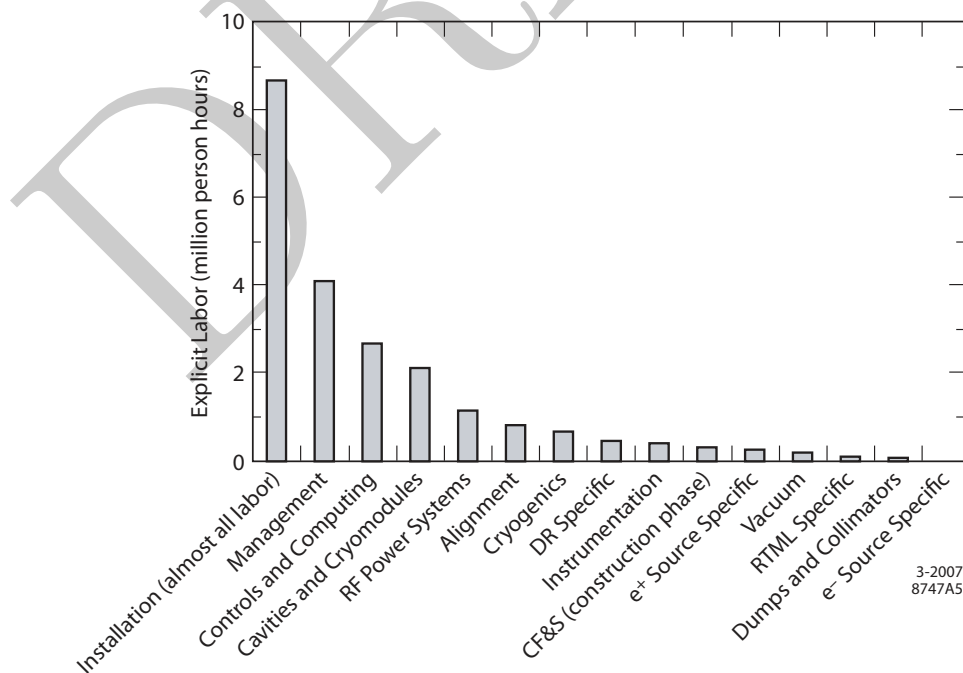
FIGURE 6.2-2.   Explicit labor, which may be supplied by collaborating laboratories or institutions, listed by Global, Technical, and some Area-specific Systems.

VALUE ESTIMATE

TABLE 6.2-3
Explicit labor, which may be supplied by collaborating laboratories or institutions, listed by Global, Technical, and some Area-specific Systems.

Explicit labor	M person-hours
Installation (all labor)	8.67
Management	4.09
Controls & computing	2.67
Cavities & cryomodules	2.16
RF Power Systems	1.14
Alignment	0.83
Cryogenics	0.69
DR specific	0.48
Instrumentation	0.44
CF&S (construction phase)	0.36
e^+ Source specific	0.30
Vacuum	0.18
RTML specific	0.09
Dumps & Collimators	0.06
e^- Source specific	0.04
Sum	22.21

management personnel is estimated to be half as large as in the SSC model. The ILC staff consists of 345 persons, divided as shown in Table 6.2-4. Personnel for the Area, Global, and Technical System groups are not included in the Project Management Division.

TABLE 6.2-4
Composition of the management structure at ILC.

Unit	Responsibilities
Directorate (30):	Directors Office, Planning, ES&H Oversight, Legal, External Affairs, Education, International Coordination, Technology Transfer;
Management Division (13):	Quality Assurance, ES&H;
Laboratory Technical Services (125):	Facilities Services, Engineering Support, Material and Logistical Services, Laboratory Fabrication Shops, Staff Services;
Administrative Services (94):	Personnel, Finance, Procurement, Minority Affairs;
Project Management Division (83):	Management, Administrative, Project Management Division Office.

It is the practice in some regions to apply general and administrative overheads to purchases and labor for projects. These overheads are applied as a multiplier on the underlying LABOR and VALUE, and cover the costs of the behind-the-scenes support personnel. In this estimate, such personnel are explicitly enumerated as labor under Directorate, Management Division, Laboratory Technical Service, and Administrative Services in Table 6.2-4. Therefore, the overheads are included as additional explicit LABOR, rather than as a multiplier on VALUE.

6.2.3   Risk Estimate

This February, 2007 estimate for the ILC is preliminary and does not yet include a complete analysis of the uncertainties and risks associated with the estimates for each cost element; there will be a risk analysis in the final RDR. There are uncertainties in the estimate of the costs of individual components that are simply due to the preliminary stage of the project. In addition, there are three major technical risks which affect the main cost drivers: attaining an economically acceptable performance yield for the superconducting RF cavities (a yield of 80% at a qualification gradient of 35 MV/m was assumed for this estimate); demonstrating adequate power and lifetime for the 10 MW klystrons; and minimizing both the geological and contractual (claims) uncertainties associated with the underground construction. There are additional technical risks to achieving the performance goals of the ILC, with little impact on the overall cost, e.g. the relatively inexpensive crab cavities are required to meet specifications in order to deliver the needed luminosity. Major R&D goals during the engineering design phase are to address and minimize these risks. Additional R&D goals are to reduce the cost estimate by incorporating improved technologies, such as alternative RF power modulators and higher gradient RF cavity geometries, and by cost-performance optimization through value engineering.

6.2.4   Operating Cost

Operating costs are not included in the estimate for the construction project, but a very preliminary estimate is given. It is also to be noted that spare components (those stored in warehouses and not the installed redundant components), although fabricated along with the installed components, are assumed to be financed through operating funds, and are not considered part of the construction projects. Major factors in the operating cost include personnel costs, electrical power, maintenance and repairs, helium and nitrogen consumables, and components that have a limited life expectancy and need continuous replacement or refurbishment, like klystrons.

The model assumes 9 months of machine operations per year at full power of about 200 MW, corresponding to 500 GeV at design luminosity, plus 3 months standby at reduced power (25 MW) with the superconducting cavities maintained at 4.5K, which is above their operating temperature. At the current electrical power rate of $0.1 per kW-hr, the operating costs for these materials and services are estimated to be approximately 150-180 M$ per year in 2007 Dollars. The continuing operations and administrative staff is expected to be comparable to that at existing facilities (not including support of the scientific program).

Commissioning activities and operating costs are anticipated to gradually increase over the fifth, sixth, and seventh years of construction from zero up to the full level of long-term operations at the end of the 7 year construction phase.

6.3 SCHEDULE

6.3.1 Example Construction Schedule

A detailed schedule for realization of the ILC depends on a variety of factors and milestones including: completion of crucial R&D, completion and review of the conceptual design of the machine (RDR) and detectors, and endorsement of the RDR and cost by international funding agencies so that critical R&D can be funded to completion. Site specific engineering and civil designs require international agreements on site selection which allow land acquisition, environmental assessments, etc. In addition agreements on cost sharing and spending profiles are required to plan the industrial production of components and the preparation of construction contracts.

In the absence of much of this information an attempt was made to construct a technically limited schedule for the construction of ILC assuming that these items have been completed prior to a physical construction start (T0). The RDR cost estimate has been based on this schedule.

6.3.2 Conventional Facilities Schedule

Conventional facilities include Civil Engineering of above and below ground structures, electrical infrastructure, cooling and ventilation, and buildings. In what follows, an assumption was made that a site was selected several years prior to the start of construction and that funding was available such that Architectural & Engineering (A&E) firms can be retained to design the conventional facilities and prepare bid packages prior to the start of construction. In the absence of other financial constraints, the construction schedule for conventional facilities is dominated by the required underground construction. ILC requires about 72 km of underground tunnel construction for the Main Linac, Beam Delivery and Damping Ring systems. For the purpose of this section it was assumed that the tunnel is deep, at a depth of ~100 m and located in dry rock such that standard tunnel boring machines can be employed. (Several possible ILC sites have different local underground conditions. However, these are believed to alter the conclusions in the section in only a minor fashion).

The layout of the ILC is shown in Figure 6.3-1. A possible construction schedule is shown in Figure 6.3-2 [108], where it is assumed that all shaft and underground construction can start simultaneously or optimally (i.e. no funding limits) and that at least 9 tunnel boring machines (TBM) of suitable diameter are available and employed simultaneously. Assuming 1 year for the shaft construction (based on LEP/LHC experience), 3 months for TBM setup, and 25 m/day boring speed/TBM, then the actual underground construction time for the ML and Damping Ring is about 3.5 years from ground breaking to beneficial occupancy.

For the purposes of this schedule it was assumed that the finished tunnel can be outfitted with services at the following rate:

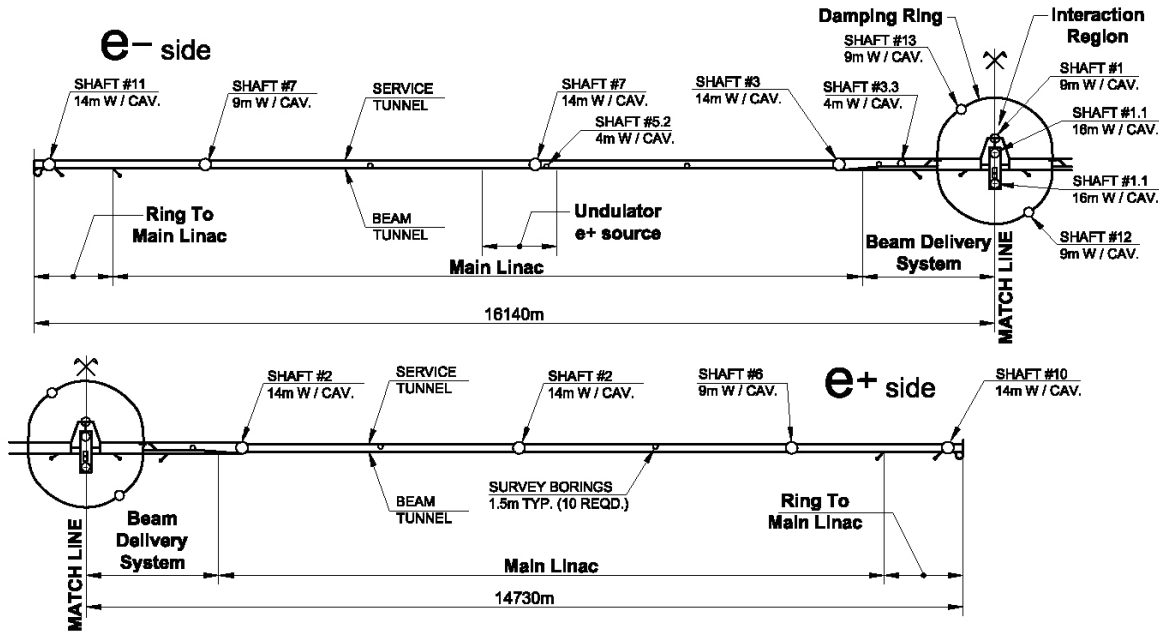|		
1	Installation of cable trays and pipes supports	4 weeks/km
2	Installation of cooling pipes	3 weeks/km
3	Installation of cables + connection	3 weeks/km
4	Installation of electrical equipment (transformers, switch gear)	4 weeks/km

FIGURE 6.3-1. Schematic Layout of the ILC.

These rates are based on experience at existing facilities, not independent analysis. It is assumed that these teams do not overlap in the tunnel at the same time, but that a sufficient quantity of trained personnel are available to form teams that can work in parallel at all available locations. The installation of services require about 1 year such that the tunnel is ready to accept technical components after about 3.5 to 4.5 years from the start of construction. (Some areas might be available for component installation a few months sooner, but the start of installation in these areas could disrupt the installation of services. As a result, this was not considered in the modeling.)

About one additional year is required to finish the underground detector enclosure so that detector installation can proceed about 4.5 years after the start of civil construction. It is assumed that detector assembly buildings and detector construction start at the earliest opportunity. Most of the detector assembly is assumed to take place above ground following the general scheme adopted for the CMS detector at CERN. This scheme allows detector construction and commissioning to occur in parallel with the underground construction. In the case of CMS the detector assembly and commissioning took 6 years. In the absence of more detailed information, we assume the same schedule for the ILC detectors.

6.3.3   Technical Component Schedule

It is assumed that the high volume technical components required for the Main Linac and Damping Ring are produced by industry. Components in this category include SCRF cavities, cryomodules, modulators, klystrons, SC and conventional magnets, cryogenic refrigerators, transfer line, cables, piping, etc. The production of even such complex components as klystrons, modulators and conventional magnets are well within the capability of industry. The sequence would probably involve industrial pre-series production by several vendors followed by tender for production quantities of components. The number of vendors and the region of production will largely be determined by decisions concerning "in-kind" contributions from the regions participating in the project. The required cryogenic plants are
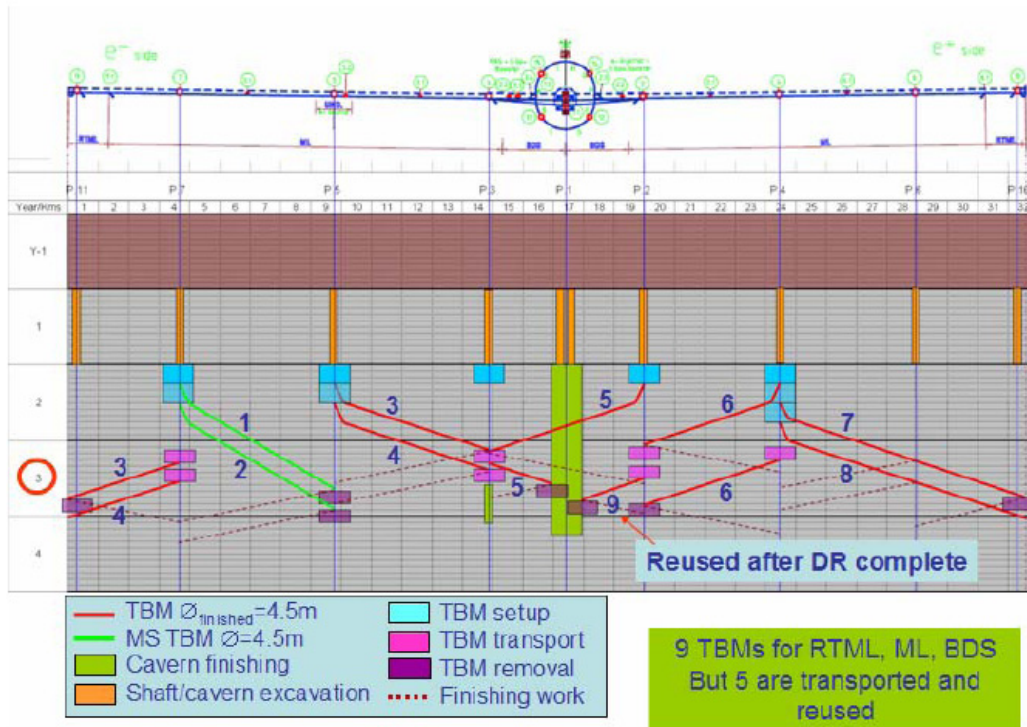
FIGURE 6.3-2. Schematic of an example of an ILC civil construction plan using TBMs. Note that TBM #9 is first used to excavate the tunnel for the damping ring (not shown). Five Tunnel Boring machines must be transported in this plan. (Analysis and figure is based upon LEP and LHC experience at CERN)

sufficiently similar to those recently acquired for the LHC that they can be procured from industry. Provided funding is available, these components do not determine a technically driven ILC schedule.

The SCRF cavities and cryomodules are the most technically challenging components and require the largest industrial infrastructure and technical ramp up. The overall cost of the cryomodules and associated infrastructure is likely to exceed any one regions production capacity. Regional interest in SCRF technology is also high. Both considerations suggest a model in which three regions of the world provide these cryomodules in equal quantity. Figure 6.3-3 shows one possible model for the ramp up of cryomodule production in one of three regions. Note that the five year production schedule shown in Figure 6.3-3 assumes funding is available prior to construction start so that infrastructure with long lead times can be purchased early. Different regions could have earlier start times and a flatter production schedule.

6.3.4   Technical Component Installation Schedule

The installation process follows the civil construction model with parallel ongoing activities in separate areas but planned to minimize interferences with other teams. The general schedule plan is based on experience with the LHC. Transportation of components from surface holding areas into their rough location in the underground tunnels takes place during the evening shift. This minimizes interference with all other activities above and below ground. These components are installed, aligned, interconnected etc. during the day shift.

**A Sample Cryomodule Production Schedule
for One Region**

**YEARS 1-2 are R&D, 3-4 are PRE-SERIES Production
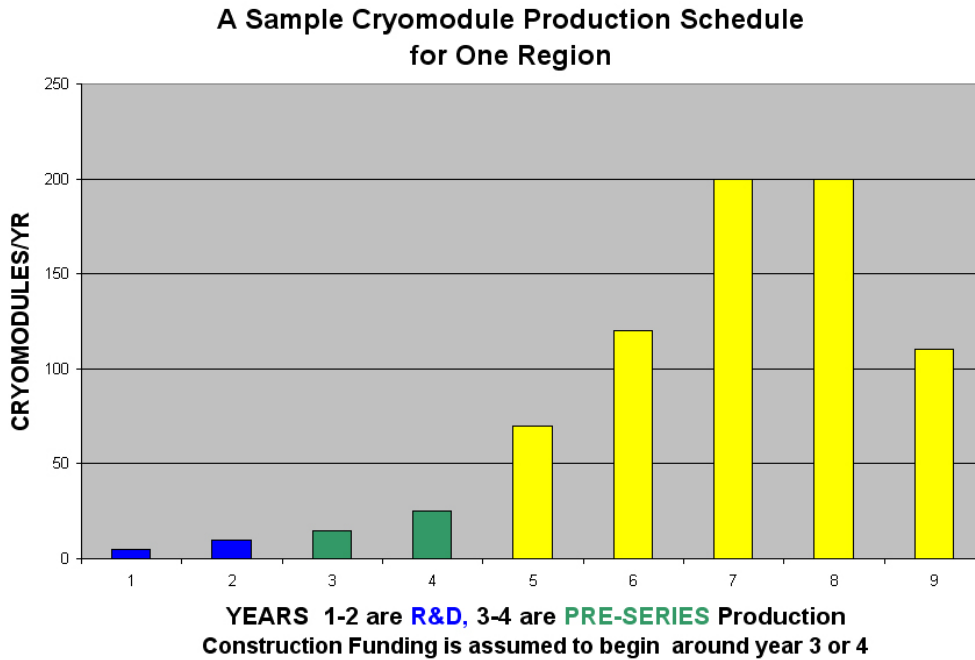Construction Funding is assumed to begin around year 3 or 4**

FIGURE 6.3-3. A possible model schedule for cryomodule production shows 1/3 of the required ILC cryomodules produced in one of three regions. R&D and pre-series devices lead to 5 years of series production (yellow). The position and magnitude of the peak of series production will vary with changes to the available construction and test infrastructure.

An example of this schedule for the main linac cryomodules is shown in section 4.9.5. This is accomplished with specialized crews which are appropriately trained and have all the required support from the technical systems. This manpower versus time profile for the linac installation is also shown in section 4.9.5. As with the civil construction schedule, installation in the central DR/INJ complex takes place in parallel and is 6 months to 1 year ahead of the main linac schedule.

6.3.5 Example Funding Profile

With the assumptions described above and with the value estimates, one can model a construction schedule with its required funding profile. This was done for a seven year construction project which is consistent with the construction, manufacturing and installation schedules. The civil construction of the underground facilities is concentrated in the first four years and the high technology cryomodules are spread throughout the seven years. The remaining civil construction and technical component manufacture and installation are spread throughout years three to seven.

This plausible plan shows the need for early funding of the two cost drivers, civil construction and the production of cavities and cryomodules. The civil construction schedule drives the overall schedule and therefore this funding, assumed to be mainly from the host country, is on the critical path. The more global distribution of funding of other systems allows flexibility in optimizing construction and installation. This funding profile is, of course, model dependent but it shows that there are no unusual or unattainable requirements in a seven year construction schedule. Operations funding would begin gradually starting in year
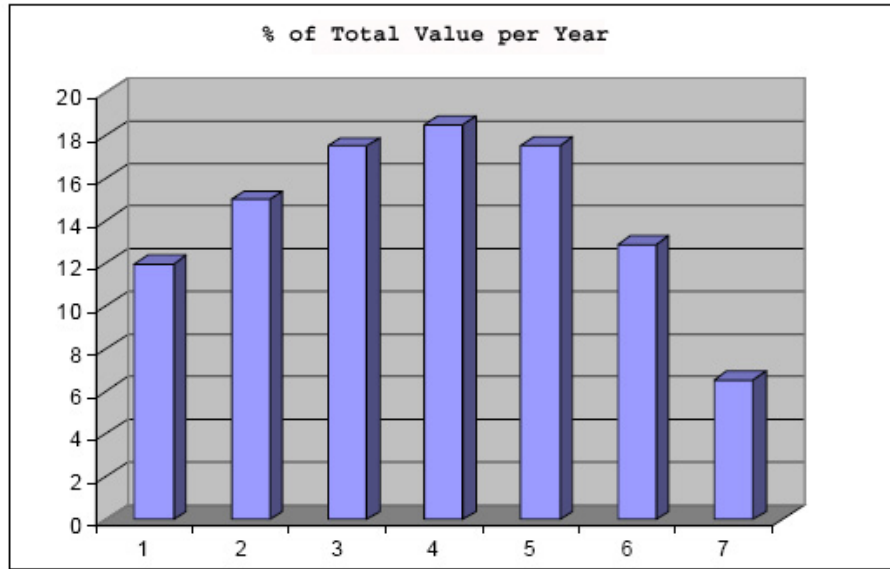
FIGURE 6.3-4. A funding profile for a model seven year construction schedule.

five and would be at full operating level in year eight.

Appendix: Example of the next level of WBS detail for Conventional Facilities and Siting for Civil Engineering for the Main Linac Area System for the Americas site.

TABLE 6.3-1: WBS detail for Conventional Facilities and Siting for Civil Engineering for the Main Linac Area System for the Americas site.

WBS #	WBS Title	Value	Unit
1.7	Conventional Facilities		
1.7.1	Civil Engineering		
1.7.1.1	Engineering, study work and documentation		
1.7.1.1.1	In-house Engineering		man-hr
	In-house Engineering	4%	%
1.7.1.1.2	Outsourced Consultancy Services		
	Outsourced Engineering	6%	%
1.7.1.2	Underground Facilities		
1.7.1.2.1	Shafts		
	e$^-$ ML 14m dia. Shafts @ Points 5,3 (2x425 vert ft)	259	vert m
	e$^-$ ML 9m dia. Shaft @ Point 7 (1x425 vert ft)	130	vert m
	e$^-$ ML 1500mm dia. Survey Shafts @ Points 3.1, 5.1 (2x425 vert ft)	259	vert m
	e$^+$ ML 14m dia. Shafts @ Points 2, 4 (2x425 vert ft)	259	vert m
	e$^+$ ML 9m dia. Shaft @ Point 6 (1x425 vert ft)	130	vert m
	e$^+$ ML 1500mm dia. Survey Shafts @ Points 2.1, 4.1 (2x425 vert ft)	259	vert m
	Surface Grouting of Points 2-5 14m dia. Shafts (4x425 vert ft)	4	ea.
	Surface Grouting of Points 6-7 9m dia. Shafts (2x425 vert ft)	2	ea.
	Surface Grouting of Points 2.1, 3.1, 4.1, 5.1 Survey Shafts (4x425 vert ft)	4	ea.
	Points 2,3,4,5,6,7 - 14&9m dia. Shafts, finishing (stairs, conc. wall, elev.#2)	777	vert m
	ML Underground Potable Water (1/2 of Points 2 & 3)	1	ea.
	ML Underground Potable Water (Points 4,5,6,7)	4	ea.
	ML Underground Sanitary Sewer (1/2 of Points 2 & 3)	1	ea.
	ML Underground Sanitary Sewer (Points 4,5,6,7)	4	ea.
1.7.1.2.2	Tunnels		

TABLE 6.3-1 – continued

WBS #	WBS Title	Value	Unit
	e$^-$ ML 4.5m dia. Beam Tunnel, TBM Excavation (37,162 lin ft)	11,327	lin m
	e$^-$ ML 4.5m dia. Service Tunnel, TBM Excavation (37,162 lin ft)	11,327	lin m
	e$^-$ ML 4.5m dia. Tunnels, Conc. Inv. (74,324 lin ft)	22,654	lin m
	e$^+$ ML 4.5m dia. Beam Tunnel, TBM Excavation (36,660 lin ft)	11,174	lin m
	e$^+$ ML 4.5m dia. Service Tunnel, TBM Excavation (36,660 lin ft)	11,174	lin m
	e$^+$ ML 4.5m dia. Tunnels, Conc. Inv. (73,320 lin ft)	22,348	lin m
	Provide Tunnel Construction Water Treatment Plant	4	ea.
	Maintain and Operate Tunnel Construction Water Treatment Plant	4	ea.
	Treatment of Tunnel Construction Water	4	ea.
1.7.1.2.3	Halls		
1.7.1.2.4	Caverns		
	e$^-$ ML Shaft Base Caverns D&B Excavation @ Points 3,5,7 (3x20,056 CY)	46,003	m^3
	e$^-$ ML Points 3,5,7 D&B Exc. for Shield Doors (in Base Caverns) (3x959 CY)	2,199	m^3
	e$^-$ ML Beam Dump Cavern D&B Excavation @ Point 3 (3,034 CY)	2,320	m^3
	e$^+$ ML Shaft Base Caverns D&B Excavation @ Points 2,4,6 (3x20,056 CY)	46,003	m^3
	e$^+$ ML Points 2,4,6 D&B Exc. for Shield Doors (in Base Caverns) (3x959 CY)	2,199	m^3
	e$^+$ ML Beam Dump Cavern D&B Excavation @ Point 2 (3,034 CY)	2,320	m^3
	Shield Doors @ Base Caverns @ Points 2-7	6	ea.
1.7.1	CIVIL ENGINEERING (continued)		
1.7.1.2.5	Miscellaneous works		
	e$^-$ ML Personnel Crossovers, D&B Excavation (23 X 295.5 CY)	5,196	m^3
	e$^-$ ML Waveguides, Drill Excavation (968)	968	ea.

TABLE 6.3-1 – continued

WBS #	WBS Title	Value	Unit
	e^+ ML Personnel Crossovers, D&B Excavation (23 X 295.5 CY)	5,196	m^3
	e^+ ML Waveguides, Drill Excavation (968)	968	ea.
1.7.1.3	Surface Structures		
1.7.1.3.1	Central Lab Buildings		
1.7.1.3.2	Detector Assembly Buildings		
1.7.1.3.3	Office Buildings		
	Points 4-7 Office Buildings (4 x 3,750 sq ft)	1,396	sq m
1.7.1.3.4	Service Buildings		
	Points 2-7 Electrical Service Buildings (6 x 1,500 sq ft)	836	sq m
	Points 2-7 Cooling Towers & Pump Stations Bldgs. (6 x 7,500 sq ft)	4,181	sq m
	Points 2-7 Cooling Ventilation Buildings (6 x 2,500 sq ft)	1,394	sq m
1.7.1.3.5	Cryo- Equipment Buildings		
	Points 2-7 Cryo - Warm Compressor Building (6 x 4,500 sq ft)	2,508	sq m
	Points 2-7 Cryo - Surface Cold Box Building (6 x 6,250 sq ft)	3,484	sq m
1.7.1.3.6	Control Buildings		
1.7.1.3.7	Workshops		
	Points 4-7 Workshop Bldg. - Machine & Detector (4 x 11,250 sq ft)	4,181	sq m
1.7.1.3.8	Site Access Control Buildings		
	Points 4-7 Site Access Buildings (4 x 750 sq ft)	279	sq m
1.7.1.3.9	Shaft Access Buildings		
	Points 2-7 Shaft Access Buildings (6 x 9,375 sq ft)	5,226	sq m
1.7.1.3.10	Miscellaneous Buildings		
1.7.1.3.11	User Facilities		
1.7.1.4	Site Development		
1.7.1.4.1	Off-site Site work		
1.7.1.4.2	Network of Monuments		
1.7.1.4.3	Construction Support		
1.7.1.4.4	Site Preparation		

TABLE 6.3-1 – continued

WBS #	WBS Title	Value	Unit
	Points 2 - 7, Clearing, Grubbing, and Initial Site Preparation (6 sites)	6	ea.
1.7.1.4.5	Utility Distribution		
	Points 2 - 7, Utility Corridors (Gas, DWS, San., Storm, Elec., Comm.)	6	ea.
	Points 2 - 7, Septic Field / Tank or Sanitary Sewer	6	ea.
	Points 2 - 7, Wells or DWS	6	ea.
	Points 4 - 7, Elevated Water Tank	4	ea.
	Points 4 - 7, Water Pump House	4	ea.
1.7.1.4.6	Road, Sidewalks & Parking Areas		
	Points 2 - 7, Service Roads (6 sites x 1250 lin ft / site)	2,286	lin m
	Points 2 - 7, Paved Areas (6 sites x 8750 sy / site)	43,896	sq m
	Points 2 - 7, Flatwork (6 sites x 2,500 sq ft / site)	1,394	sq m
1.7.1.4.7	Landscaping		
	Points 2 - 7, Landscaping	6	ea.
	Points 4 - 7, Security Fencing (4 sites x 5,000 lin ft / site)	6,097	lin m
1.7.1.4.8	Environmental		
	Points 2 - 7, Sediment & Erosion Control (6 sites)	6	ea.
1.7.1.4.9	Miscellaneous Site Works		

BIBLIOGRAPHY

[1] B. Barish, et al., "The International Technology Review Panel Final Report", `http://www.fnal.gov/directorate/icfa/ITRP_Report_Final.pdf` (2004).

[2] "TESLA Technical Design Report" `http://tesla.desy.de/new_pages/TESLA/TTFnot01.html` (2001).

[3] G. Dugan, et al., "US Linear Collider Technology Options Study", `http://www-project.slac.stanford.edu/ilc/techinfo/USLCTOS/` (2003).

[4] G. A. Loew, et al., "International Linear Collider Technology Review Committee Second Report", `http://www.slac.stanford.edu/xorg/ilc-trc/2002/index.html` (2002).

[5] R. Heuer, et al., "Parameters for the Linear Collider", `http://www.fnal.gov/directorate/icfa/LC_parameters.pdf` (2003).

[6] H. Ehrlichmann, S. Guiducci, K. Kubo, M. Kuriki, A. Wolski, "Recommendations for ILC Configuration Satisfying Timing Constraints", `http://www.linearcollider.org/wiki/lib/exe/fetch.php?cache&media=bcd:timingrecommendations-revapril17.pdf` (2006).

[7] T. Nishitani et al, "Highly polarized electrons from GaAsGaAsP and InGaAsAlGaAs strained-layer superlattice photocathodes", J. Appl. Phys. 97, 094907 (2005).

[8] T. Maruyama et al, "Systematic study of polarized electron emission from strained GaAs/GaAsP superlattice photocathodes", Appl. Phys. Lett. 85, 2640 (2004).

[9] Yu. A. Mamaev et al, "Improved Superlattices for Spin-Polarized Electron Sources", SLAC-Pub 12249 (2006).

[10] T. Maruyama et al, "Atomic hydrogen cleaning of polarized GaAs photocathodes", Appl. Phys. Lett. 82, 4184 (2003).

[11] R. Alley et al, "The Stanford linear accelerator polarized electron source", NIM A 365, 1-27 (1995).

[12] C.K. Sinclair et al, "Development of a high average current polarized electron source with long cathode operational lifetime", Phys. Rev. ST Accel. Beams 10, 023501 (2007).

[13] A. Curtoni and M. Jablonca, "Study of the TESLA preaccelerator for the polarised electron beam", TESLA 2001-22 (2001).

[14] F. Zhou et al, "Start-to-end transport design and multi-particle tracking for the ILC", SLAC-Pub 12240 (2007).

[15] K. Moffeit et al, "Spin Rotation Schemes at the ILC for Two Interaction Regions and Positron Polarization with Both Helicities", SLAC-TN-05-045 (2005).

[16] L. Young, Parmela Manual, LA-UR-96-1835 (2001).

[17] MAD 8.51, CERN.

[18] M. Borland, "Elegant: A Flexible SDDS-Compliant Code for Accelerator Simulation", Technical Report No. LS-287, ANL (2000).

[19] "ILC Baseline Configuration Document", DR Update (pg.5) (2006).

[20] Duncan Scott's paper

[21] F. Zhou, Y. Batygin, Y. Nosochkov, J. C. Sheppard, and M. D. Woodley, "Start-to-end beam optics development and multi-particle tracking for the ILC undulator-based positron source", SLAC-PUB-12239 (2007).

[22] Brechna, H, "150 kOe Liquid Nitrogen Cooled Pulsed Flux-Concentrator Magnet", Rev. Sci. Inst. (1965).

[23] J.W. Wang, et. al. "Studies of Room Temperature Accelerator Structures for the ILC Positron Source", PAC05, SLAC-PUB-11767 (2005).

[24] A. Wolski, J. Gao, S. Guiducci (eds.) "Configuration Studies and Recommendations for the ILC Damping Rings", LBNL-59449 (2006).

[25] G.V. Stupakov, T.O. Raubenheimer, F. Zimmermann, Phys. Rev. E 52, 5499-5504 (1995).

[26] T. O. Raubenheimer, private communications.

[27] A. Wolski, J. Gao, and S. Guiducci, LBNL-59449 (2006).

[28] K. Ohmi, F. Zimmermann, and E. Perevedentsev, Phys. Rev. E 65 , 016502 (2002).

[29] L. Wang, G. Stupakov, T. Raubenheimer, in *EPAC06*, Edinburgh (2006).

[30] L. Wang, H. Fukuma, S. Kurokawa, M. Pivi, and G. Xia, in *EPAC06*, Edinburgh (2006).

[31] D. Rice, et al., "Production and Testing Considerations for CESR-c Wiggler Magnets", *PAC03* , pp. 167-169 (2003).

[32] R. Boni, G. Cavallari, "Updated RF System for the ILC Damping Rings", ILC-LNF-003 (2006). `http://www.lnf.infn.it/acceleratori/ilclnf/T_Notes/ILC-LNF-003.pdf`

[33] A. Drago, "Fast Feedback System", ILC-LNF-002 (2006). `http://www.lnf.infn.it/acceleratori/ilclnf/T_Notes/ILC-LNF-002.pdf`

[34] L. Wang, private communication.

[35] F. Le Pimpec, et al., "Properties of TiN and TiZrV thin film as a remedy against electron cloud," NIM A 551, 187 (2005).

[36] T. Naito, H. Hayano, M. Kuriki, N. Terunuma, J. Urakawa, "Development of a 3 ns Rise and Fall Time Strip-Line Kicker, for the International Linear Collider", in preparation (2006).

[37] M. Pivi, T. O. Raubenheimer, L. Wang, K. Ohmi, *EPAC06*, Edinburgh (2006); submitted to PRSTAB.

[38] NLC Design Group, *Zeroth-Order Design Report for the Next Linear Collider*, 573-575 (1996).

[39] P. Emma, T.O. Raubenheimer, F. Zimmermann, "A Bunch Compressor for the Next Linear Collider," in *PAC05* (1995).

[40] R. Akre, L. Bentson, P. Emma, P. Krejcik, "Bunch Length Measurements Using a Transverse RF Deflecting Structure in the SLAC Linac," `http://accelconf.web.cern.ch/AccelConf/e02/PAPERS/THPRI097.pdf`, in *EPAC02* (2002).

[41] P.N. Burrows *et al*, "Tests of the FONT3 Linear Collider Intra-Train Beam Feedback System at the ATF," `http://accelconf.web.cern.ch/AccelConf/p05/PAPERS/RPPP013.PDF`, in *PAC05* (2005).

[42] J. Wu, private communication.

[43] K. Kubo, "Rough Estimation of Fast-Changing Stray Field in Long Transport of RTML", ILC-NOTE-2007-007, `http://ilcdoc.linearcollider.org/record/6900/files/` (2006).

[44] J. Frisch, T.O. Raubenheimer, P. Tenenbaum, "Sensitivity to Nano-Tesla Scale Stray Magnetic Fields", SLAC-TN-04-041, `http://www.slac.stanford.edu/cgi-wrap/getdoc/slac-tn-04-041.pdf` (2004).

[45] L. Wang, P. Tenenbaum, "Fast Ion Instability in the Long Transport Line of RTML," ILC-NOTE-2007-005, `http://ilcdoc.linearcollider.org/record/6841/files/` (2007).

[46] J. Smith, "Coupling Correction in the ILC Ring to Main Linac", ILC-NOTE-2007-006, `http://ilcdoc.linearcollider.org/record/6847/files/` (2007).

[47] P. Tenenbaum, "Application of Kick Minimization to the RTML 'Front End'," SLAC-TN-07-002, `http://www.slac.stanford.edu/cgi-wrap/getdoc/slac-tn-07-002.pdf` (2007).

[48] K. Kubo, "Simulation of Low Emittance Transport in Long Straight Line of ILC RTML", ILC-NOTE-2007-008, `http://ilcdoc.linearcollider.org/record/6901/files/` (2006).

[49] P. Tenenbaum, T.O. Raubenheimer, A. Wolski, "Multi-Stage Bunch Compressors for the International Linear Collider," in *PAC05*, `http://accelconf.web.cern.ch/AccelConf/p05/PAPERS/RPPP034.PDF` (2005).

[50] P. Tenenbaum, "Emittance Studies in the 2006 Bunch Compressor," ILC-NOTE-2007-003, `http://ilcdoc.linearcollider.org/record/6507/files/` (2007).

[51] M. Church, "Analysis of Phase and Amplitude Sensitivity for '300B' Bunch Compressor and Linac,"ILC-NOTE-2007-004, `http://ilcdoc.linearcollider.org/record/6508/files/` (2006).

[52] S.M. Seletskiy, "Thermal Photon and Residual Gas Scattering of the Electrons in the ILC RTML," SLAC-TN-06-007,`http://www.slac.stanford.edu/cgi-wrap/getdoc/slac-tn-06-007.pdf` (2006).

[53] P. Tenenbaum *et al*, "Direct Measurement of the Transverse Wakefield of Tapered Collimators," `http://prst-ab.aps.org/pdf/PRSTAB/v10/i3/e034401`, Phys. Rev. ST Accel. Beams **10**, 034401 (2007).

[54] P. Tenenbaum, "Collimator Wakefield Calculations for ILC-TRC Report," SLAC-TN-03-038,`http://www.slac.stanford.edu/cgi-wrap/getdoc/slac-tn-03-038.pdf` (2003).

[55] P. Raimondi and A. Seryi, "A novel final focus design for future linear colliders," Phys. Rev. Lett. **86**, 3779 (2001).

[56] P. Tenenbaum, "Collimator Wakefield Calculations for the ILC-TRC Report", LCC-0101, SLAC-TN-03-038 (2002).

[57] R. Brinkmann, P. Raimondi, A. Seryi, "Halo reduction by means of nonlinear optical elements in the NLC final focus system," SLAC-PUB-8896, *PAC01* (2001).

[58] Y. Nosochkov *et al.*, "ILC Extraction Line for 14 mrad Crossing Angle," SLAC–PUB–11591 (2005).

[59] A. Ferrari, Y. Nosochkov, "Beam losses in the extraction line of a TeV e+e- linear collider with a 20-mrad crossing angle", EUROTEV–REPORT–2005–025, SLAC–PUB–11791 (2005).

[60] Y. Nosochkov and A. Seryi, "Compensation of detector solenoid effects on the beam size in linear collider," Phys. Rev. ST Accel. Beams **8**, 021001 (2005).

[61] B. Parker and A. Seryi, "Compensation of the effects of a detector solenoid on the vertical beam orbit in a linear collider," Phys. Rev. ST Accel. Beams **8**, 041001 (2005).

[62] D. Schulte, "Study of Electromagnetic and Hadronic Background in the Interaction Region of the TESLA Collider," PhD. thesis, TESLA-97-08 (1996).

[63] J. D. Fuerst *et al.*, "An RF separated Kaon beam from the main injector : Superconducting aspects," FERMILAB-TM-2060, 1998; M. McAshan, R. Wanzenberg, "RF Design of a Transverse Mode Cavity for Kaon Separation", FERMILAB-TM-2144 (2001).

[64] G. Burt, A. Dexter , P. Goudket, "Effect and tolerances of phase and amplitude errors in the ILC Crab Cavity", EUROTeV Report (2006).

[65] M. Liepe, "Review on progress in RF control systems," SRF05, (2005).

[66] A. Dexter, et al., "The Cavity Loaded Waveguide and Beamloading", Cockcroft-07-01 (2007).

[67] C. Adolphsen, C. Beard, L. Bellantoni, G. Burt, et al., "Design of the ILC Crab Cavity", EUROTeV-Report-2007-010 (2007).

[68] G. Christian et al, "The electromagnetic background environment for the interaction-point beam feedback system at the International Linear Collider", *EPAC06*, Edinburgh (2006).

[69] P.N. Burrows et al, "Performance of the FONT3 fast analogue intra-train beam-based feedback system at ATF", *EPAC06*, Edinburgh; Eurotev-report-2006-063 (2006).

[70] P.N. Burrows et al, "Design of the ILC prototype FONT4 digital intra-train beam-based feedback system", *EPAC06*, Edinburgh; Eurotev-report-2006-062 (2006).

[71] K.C Moffeit, M. Woods, Y. Nosochkov , K.P. Schuler, K. Moenig, and W. Oliver, "Polarization Setup and Polarimetry for 2 IRs, and Status of Downstream Polarimeter Designs", SLAC-PUB-11322, IPBI_TN-2006-1 (2005).

[72] N. Meyners, V. Gharibyan, K.P. Schuler, "Upstream Polarimetry with 4-magnet Chicane", *LCWS05* (2005).

[73] K. Bane, "Resistive wall wake in the ILC IR", `http://www-project.slac.stanford.edu/lc/bdir/meetings_beamdelivery.asp` (2006).

[74] L. Keller, T. Maruyama, "Updates on Beam-gas effects in BDS and background", `http://ilcagenda.linearcollider.org/conferenceDisplay.py?confId=1277` (2006).

[75] J. Amann, "IR hall deflection study", http://ilcagenda.linearcollider.org/conferenceDisplay.py?confId=1225 (2006).

[76] R. Assmann, P. Raimondi, G. Roy and J. Wenninger, "Emittance optimization with dispersion free steering at LEP," Phys. Rev. ST Accel. Beams **3**, 121001 (2000).

[77] R. Assmann, et al., "Quadrupole alignment and trajectory correction for future linear colliders: SLC tests of a dispersion-free steering algorithm," *(IWAA 95)*, (1995).

[78] K. Kubo, ILC-Asia Note 2006-05 (2006).

[79] J. Frisch et al., SLAC-TN-04-041 (2004).

[80] P. Tenenbaum, A. Latina, K. Kubo, J. Smith, PAC07 (2007).

[81] A. Latina, to be published.

[82] N. Walker,. EUROTeV-Report-2005-017 (2005).

[83] A. Latina et al., EUROTeV-Report-2006-050 (2006).

[84] K. Ranjan et al., MOP064, LINAC 2006 (2006).

[85] K. Kubo, ILC-Asia Note 2005-25, ILC-Asia Note 2005-23 (2005).

[86] J. C. Smith, et al., "Benchmarking / Crosschecking DFS in the ILC Main Linac," SLAC-TN-06-035, FERMILAB-TM-2373-CD (2007).

[87] J. Smith, PhD thesis, To be published (2007).

[88] K. Kubo, ILC-Asia Note 2006-04 (2006).

[89] P. Eliasson and D. Schulte, EUROTeV-Report-2005-021 (2005).

[90] K. Kubo, ILC-Asia Note 2005-18, ILC-Asia Note 2005-17 (2005).

[91] R. Jones, et al., EPAC06 (2006).

[92] O. Napoly and D. Schulte, CERN-OPEN-2000-135 (2000).

[93] D. Schulte, Daresbury.

[94] D. Schulte, CLIC-Note 560 (2003).

[95] G. White, D. Schulte, N. Walker, SLAC-PUB-11340, EUROTEV-REPORT-2005-001 (2005).

[96] D. Schulte. EUROTeV-Memo-2006-010

[97] G. White, D. Schulte, N. Walker, "Design and Simulation of the ILC Intra-train Orbit and Luminosity Feedback Systems," EPAC06, EUROTeV-Report-2006-088 (2006).

[98] L. Hendricksen, A. Seryi, G. White, "Issues of Stability and Ground Motion in ILC," NANOBEAM 2005, SLAC-PUB-11661 (2005).

[99] R.M. Jones, et al, Linac06 (2006).

[100] L. Malysheva, EPAC06 (2006).

[101] Reichold et. al. "The LiCAS-RTRS – A Rapid and Cost Efficient Survey System for the ILC" in 9th International Workshop on Accelerator Alignment, `http://www.slac.stanford.edu/econf/C06092511/papers/WE008.PDF` (2006).

[102] P. Eliasson et al., "A Study of Failure Modes in the ILC Main Linac" , EUROTeV Report-2006-040, `http://www.eurotev.org/e158/e1365/e1378/e2250/EUROTeV-Report-2006-040.pdf` (2006).

[103] Mattison, T., "Thoughts on Fast Beam Aborts for ILC" , *NanoBeam 2005* `http://atfweb.kek.jp/nanobeam/files/presen//presen-WG2a-12.pdf` (2005).

[104] Ross, M. , et. al., "Single Pulse Damage in Copper" , `http://www.slac.stanford.edu/cgi-wrap/getdoc/slac-pub-8605.pdf`.

[105] M. Ross, "Some MPS Design Rules" , `http://www-project.slac.stanford.edu/ilc/MPS_design_rules.htm`.

[106] P. Tenenbaum, "Fast MPS for ILC" , *Snowmass 2005*, `http://alcpg2005.colorado.edu/alcpg2005/program/accelerator/GG3/peter_tenenbaum20050812215847.ppt` (2005).

[107] "LHC MPS Review Programme" , `http://lhc-mp-review.web.cern.ch/lhc-mp-review/Review-Programme.html`.

[108] M. Gastal, "Draft ILC Construction Schedule", `http://ilcagenda.linearcollider.org/materialdisplay.py?contribID=0$\&$amp;materialId=slides$\&$amp;confID=1144` (2006).

[109] L. Bertolini *et. al.*, "Design of the Linear Non-Evaporable Getter Pump for the PEP-II B Factory," *PAC98* (1998).

[110] C. Benvenuti *et. al.*, "A novel route to extreme vacua: the non-evaporable getters thin film coatings," *Vacuum* bf 53 (1999).

[111] S. Choroba, "The TESLA RF System", Snowmass 2005 (2005).

[112] H. Pfeffer, C. Jensen & D. Wolff, "The FERMI SMTF Modulators," (2005).

[113] C. Jensen, H. Pfeffer, D. Wolff, "ILC Modulator Talk", (2004).

[114] R. Boni and G. Cavallari, "RF System for the ILC Damping Ring", ILC-LNF-001 (2006).

[115] V. Vogel and S. Choroba, "Status Toshiba MBK" (2006).

[116] E. Wright, H. Bolen, S. Lenci, and A. Balkcum, "RF Source Selection for the ILC", Snowmass 2005 (2005).

[117] D. Sprehn, "MBK Testing at DESY - May 22 -June 2 2006" (2006).

[118] A. Beunas, G. Faillon, S. Choroba, A. Gamp, "A High Efficiency Long Pulse Multi Beam Klystron for the Tesla Linear Collider", *PAC01* (2001).

[119] G. Caryotakis, "ILC Klystron Design Options and Klystron Manufacturing", Snowmass 2005 (2005).

[120] TESLA Technical Design Report, March 2001.

[121] C. Adolphsen, T. Peterson, Table from a spreadsheet developed to calculate static and dynamic heat loads in an ILC cryomodule (2006).

[122] Cavity alignment documentation.

[123] FLASH User facility at DESY.

[124] M. Liepe, "Superconducting Multicell Cavities for Linear Colliders", DESY-THESIS-2001-045, PhD thesis (2001).

[125] M. Church, "Phase and Amplitude Tolerances for Crab Cavity" Internal document (2006).

[126] T. Schilcher, "Vector-sum Control of Pulsed Accelerating Fields in Lorentz-Force Detuned Superconducting Cavities", TESLA-Report, TESLA 98-05, PhD thesis (1998).

[127] S. Walston, et al., "Performance of a High Resolution Cavity Beam Position Monitor System"; submitted to NIM A (2007).

[128] S. Molloy, et al., "High precision superconducting cavity diagnostics with higher order mode measeruements"; Phys. Rev. ST Accel. Beams **9**, 112802 (2006).

[129] Z. Li, et al.; "Cavity BPM with Dipole-Mode-Selective Coupler", *PAC03*, SLAC-PUB-11913 (2003).

[130] M. Wendt, "Cold Cavity BPM R&D for the ILC", CARE ABI Workshop (2006).

[131] M.T. Price, et al, "Beam Profile Measurements wtih the 2-D Laser-Wire," EPAC06 (2006).

[132] S.T. Boogert, et al, "A laser-wire System at the ATF Extraction Line," EPAC06 (2006).

[133] Y Honda, et al, "Upgraded laser wire beam profile monitor," NIM A **538** (2005).

[134] O. H. Altenmueller, R. Larsen, G. Loew; "Investigations of Traveling-Wave Separators for the Stanford Two-Mile Linear Accelerator", Rev. Sci. Instr., Vol. 35(4) (1964).

[135] P.N. Burrows et al, "Design of the ILC prototype FONT4 digital intratrain beam-based feedback system", EUROTeV-Report-2006-62, *EPAC06*, (2006).

[136] Water Cooled Beam Dumps and Collimators for the Stanford Linear Accelerator. Dieter R. Walz, Joe Jurow, Edward L. Garwin (SLAC) . SLAC-PUB-0095, Mar 1965. 9pp. 1st IEEE Particle Accelerator Conference 10-12 Mar 1965, Washington, D.C. Published in IEEE Trans.Nucl.Sci.12:867-871,1965. (issue No.3)

[137] Beam Dumps, Energy Slits and Collimators at SLAC - - Their Final Versions and First Performance Data. Dieter R. Walz, L.R. Lucas, H.A. Weidner, R.J. Vetterlein, E.J. Seppi (SLAC) . SLAC-PUB-0279, Mar 1967. 5pp. 2nd IEEE Particle Accelerator Conference 1-3 Mar 1967, Washington, D.C. Published in IEEE Trans.Nucl.Sci.14:923-927,1967. (issue No.3)

[138] Radiolysis And Hydrogen Evolution In The A - Beam Dump Radioactive Water System. Dieter R. Walz, E.J. Seppi (SLAC) . SLAC-TN-67-029, Oct 1967. 11pp.

[139] The Sphere Dump - A New low-cost high-power beam dump concept and a catalytic hydrogen-oxygen recombiner for radioactive water systems. Dieter R. Walz, L.R. Lucas (SLAC) . SLAC-PUB-0555, C69-03-05.10, Mar 1969. 5pp. Presented at 3rd IEEE Particle Accelerator Conf., Washington, D.C., Mar 5-7, 1969. Published in IEEE Trans.Nucl.Sci.16:613-617,1969. (issue No.3)

[140] Projekt TESLA - Strahlabsorber, Erstellung des Basiskonzepts, Endbericht, Fichtner, Sarweystrasse 3 70191 Stuttgart, April 2003. 114pp.

[141] 18MW Beam Dump Project for TESLA;Studies under DESY Order No.29/430250122, Framatome ANP GmbH, Sept.4, 2002. 80pp.

[142] Marcus E., Stern H., "Blueprints for High Availability" Second Edition, Wiley Publishing Inc. (2003).

[143] Gotz A., Schmidt D., Clausen M., "Middleware in Accelerator and Telescope Control Systems" *ICALEPCS03* (2003).

[144] R.W. Downing, R.S. Larsen, "High Availability Instrumentation Packaging Standards for the ILC and Detectors" SLAC-PUB-12208 `http://www.slac.stanford.edu/cgi-wrap/pubpage?slac-pub-12208` (2006).

[145] Matlab, `http://www.mathworks.com/products/matlab/`.

[146] "Instrumentation – Timing", `http://docdb.fnal.gov/ILC-public/DocDB/ShowDocument?docid=107` (2001).

[147] Frisch, J., Bernstein D., Brown D., Cisneros E., "A High Stability, Low Noise RF Distribution System", *PAC01* `http://docdb.fnal.gov/ILC/DocDB/0000/000035/001/PhaseAndTiming.pdf` (2001).

[148] ILC Technical Note with details of CFS design, ILC-2007 (2007).

[149] RDR Costing Guidelines, `http://www-ilcdcb.fnal.gov/RDR_costing_guidelines.pdf` (2006).

[150] RDR Cost Estimating Instructions, `http://www-ilcdcb.fnal.gov/RDR_Cost_Estimating_Instructions_23may06.pdf` (2006).

[151] Department of Defense, United States of America, Joint Industry Government Parametric Estimating Handbook, Second Edition, (1999).